

This PDF was created from the British Library's microfilm copy of the original thesis. As such the images are greyscale and no colour was captured.

Due to the scanning process, an area greater than the page area is recorded and extraneous details can be captured.

This is the best available copy

D73375'87

Attention is drawn to the fact that the copyright of this thesis rests with its author.

This copy of the thesis has been supplied on condition that anyone who consults it is understood to recognise that its copyright rests with its author and that no quotation from the thesis and no information derived from it may be published without the author's prior written consent.

2

338



D 73375/87

BISHOP S.R.

Plates.

338

NORTH LONDON POLY
(CNA).

MATHEMATICAL AND COMPUTATIONAL MODELLING FOR THE
DESIGN OF PIPE BENDS AND COMPLIANT SYSTEMS

Steven Richard Bishop, B.Sc., M.Sc.

This thesis is submitted to the Council for National Academic Awards in partial fulfillment of the degree of Doctor of Philosophy. The research was carried out in the Mathematics Department, Polytechnic of North London and during the period of research the author was not registered as a candidate for any other award.

January 1987

ABSTRACT

This thesis is divided into three parts. In part I some theoretical and numerical processes are considered which arise when modelling the flow of a fluid through a pipe bend or deflector nozzle. These numerical processes include a new form of numerical integration and a finite element formulation which, it is suggested, could readily be extended to handle further realistic problems based on the pseudo three dimensional model chosen here. An introduction to nonlinear dynamics is included in part II leading towards a classification of bifurcational events in the light of recent advances in dynamics research. Most of the dynamical systems considered are dissipative such that the dynamic behaviour of the system decays onto a final steady state motion which may be modelled by a low order system of equations. In this way any resulting instability will adequately be described, qualitatively at least, by the low order bifurcations classified in part II. In part III the application of the geometrical theory of dynamical systems is used to study the wave driven motions of specified compliant offshore facilities with real data provided from structures currently in use in the offshore industry. In particular predictions are sought of any incipient jumps to resonance of the systems which might lead to potentially dangerous loads in the mooring lines or excessive displacements. Throughout the dynamics work stable steady state paths are closely followed and monitored so that any resulting bifurcation, including the possibility of chaotic behaviour, can be analysed with a view to its subsequent prediction.

ACKNOWLEDGEMENTS

I would like to thank my supervisor, Derek Payne, for his endless enthusiasm to discuss various problems that arose during the course of this research.

Heartfelt thanks must also go out to my family, friends, and colleagues for their constant encouragement and interest in my academic achievements. I am particularly grateful to Professor Michael Thompson FRS for inspiring the best part of this thesis and to Lawrence Virgin for many stimulating discussions. The contributions made by Farshid in the experimental work and the computational talents of Denis are also very much appreciated.

On a personal level I would like to thank my Mother and Jan, both of whose well meaning enquiries spurred me on to complete the reporting of this work. Lastly, but not least, I would like to offer Gill my sincere thanks for her patience and support over the last few years.

DEDICATION

"There is a tide in the affairs of men, which taken at the flood
leads to fortune. Omitted all the voyage of their life is bound
in shallows and miseries."

G.E.B. 1981

This thesis is dedicated to my father. If only I had his
vision..... and he mine.

CONTENTS

<u>PREFACE</u>	1
<u>NUMBERING SYSTEM</u>	4
<u>Part I : The Static Analysis of the Flow Through a Pipe Bend or Deflector Nozzle</u>	5
I.1 THE FLOW EQUATIONS AND THEIR SOLUTION	6
I.1.1 Motivation and Introduction	6
I.1.2 Flow Equations	10
I.1.3 Boundary Conditions	16
I.1.4 The Finite Element Method	20
Figures	29
I.2 TWO DIMENSIONAL FLOW	31
I.2.1 Test Cases	31
I.2.2 Calculation of L	33
I.2.3 Calculation of $\dot{\psi}$	35
Figure	41
Table	42
I.3 THREE DIMENSIONAL FLOW	43
I.3.1 Secondary Flow	43
I.3.2 Vorticity	46
I.3.3 Construction of a Three Dimensional Streamtube	49
<u>Part II : The Dynamic Analysis of Nonlinear Systems and Generic Instabilities</u>	51
II.1 AN INTRODUCTION TO NONLINEAR DYNAMICS	52
II.1.1 Background	52

II.1.2 Centre Manifold Theorem	54
II.1.3 Bifurcations of Steady State Attractors	55
II.1.4 The Analysis of Nonlinear Systems	60
Figures	64
II.2 AUTONOMOUS SYSTEMS	70
II.2.1 Introduction	70
II.2.2 Linearisation and the Stability of Equilibria	72
II.2.3 Instabilities of Equilibria	77
Figures	81
II.3 FORCED OSCILLATIONS	85
II.3.1 Introduction	85
II.3.2 The Poincaré Section	88
Figures	92
II.4 THE STABILITY AND BIFURCATIONS OF MAPS	95
II.4.1 Introduction	95
II.4.2 The Stability of a Two Dimensional Map	96
Figures	103
II.5 THE PREDICTION OF INCIPIENT DYNAMIC INSTABILITIES	105
II.5.1 Predictions of the Hopf Bifurcation	105
II.5.2 Determining the Eigenvalues of a Map	106
II.5.3 The Prediction of the Static Fold	111
II.5.4 The Prediction of the Cyclic Fold	113
II.5.5 Map Rotations and Orbit Numbers	115
II.5.6 Instability Predictions Near a Cyclic Fold	125
II.5.7 The Use of Orbit Numbers to Predict the Folding of a Periodic Oscillation	128
II.5.8 Conclusions	131
Figures	132

II.6 A ROUTE TO CHAOS	144
<u>Part III : Applications of the Geometrical Theory of</u> <u>Dynamical Systems to the Motions of</u> <u>Compliant Offshore Structures</u>	147
III.1 OFFSHORE TECHNOLOGY	148
Figures	154
III.2 EXPERIMENTAL INVESTIGATIONS INTO THE FISHTAILING OF A MOORED TANKER	156
III.2.1 Introduction	156
III.2.2 The Fishtailing Instability	157
III.2.3 The Experimental Model	158
Figures	163
III.3 A STUDY OF THE NEIMARK BIFURCATION WITH THEORETICAL APPLICATIONS TO THE INSTABILITY OF OF PERIODIC MOTIONS OF A BARGE	172
III.3.1 Introduction	172
III.3.2 The Delayed Logistic Map	173
III.3.3 The Neimark Bifurcation of Periodic Motions of a Barge	177
Figures	182
III.4 PREDICTING INCIPIENT JUMPS TO RESONANCE OF COMPLIANT MARINE STRUCTURES IN AN EVOLVING SEA-STATE	194
III.4.1 Introduction	194
III.4.2 Ship Roll Response Leading to Capsize	196
III.4.3 The Subharmonic Motions of an Articulated Mooring Tower	200
III.4.4 Conclusions	204
Figures	205

III.5 THE CHAOTIC MOTIONS OF A SHIP LEADING TO CAPSIZE	215
III.5.1 Introduction	215
III.5.2 Local Mathematical Models of Ship Roll	217
III.5.3 Chaotic Capsize	221
Figures	230
III.6 COMPLEX MOTIONS OF A MOORED SEMI-SUBMERSIBLE PLATFORM	248
III.6.1 Introduction	248
III.6.2 Mathematical Modelling	251
III.6.3 The Leeward Lines Slack Case	254
III.6.4 The Leeward Lines Active Case	261
III.6.5 Conclusions	267
Figures	270
III.7 SUBHARMONIC MOTIONS OF NONLINEAR MARINE STRUCTURES SUBJECTED TO RANDOM FORCING	283
III.7.1 Introduction	283
III.7.2 A Pilot Study of the Bilinear Oscillator	284
III.7.3 Types of Randomness	285
III.7.4 Numerical Studies	288
III.7.5 Conclusions	289
Figures	291
<u>REFERENCES</u>	298
PART I	298
PART II and PART III	302
 <u>APPENDIX</u>	 i
APPENDIX III.5 MELNIKOV'S METHOD	ii
III.5A.1 Theory	ii

III.5A.2 Applications of Melnikov's Method

vi

Figures

xii

PREFACE

Certain changes in the circumstances of the author meant that the intended research did not proceed as was originally proposed. As a consequence it was decided that a statement detailing the work reported within this thesis should be included in the form of a preface.

The work reported in this thesis was carried out under the supervision of Dr.D.Payne at the Polytechnic of North London. Much of the early research efforts in part I were directed towards the writing of finite element codes for the general solution of partial differential equations since no such software was available on the computing facilities at the time. The precise details of this programming and the subsequent flexibility and adaptability of the software produced will not be fully reported here; the interested reader may consult the internal reports written by the author [Bishop (1982)]. Similarly to employ a scheme of numerical interpolation and integration required during the design of a general pipe bend a suite of programs was written implementing popular interpolation routines and also a piecewise rational quadratic approximation, but again this shall only be mentioned briefly in this thesis [see Bishop (1983a,1983b,1984a)]. These programs formed part of a larger effort to model the steady flow of a fluid round a pipe bend and certain comparisons are favourably made with existing methods for a two dimensional approximation. The main motivation for a finite element/multigrid approach that is advocated within

this thesis was to present a method that could readily be extended to cover a fully three dimensional flow. This hopefully has been achieved but sadly constraints imposed by a change in the type and place of employment did not allow sufficient time or the necessary facilities to put into effect the ideas that shall be introduced.

On the positive side this enforced change in career has enabled the author to be aware of the need for a wider integrated approach to design in which dynamics must also play a vital role. As a consequence to this in parts II and III some aspects of dynamic modelling of certain offshore structures shall be reported, the study of which was carried out whilst the author was working at University College London in the Civil Engineering Department with Professor J.M.T.Thompson FRS.

The similarities between the introductory remarks in part II and the recent book by Thompson and Stewart (1986) is not coincidental. In fact the author of this thesis collaborated in the development and writing of the draft versions of several chapters of the book and is acknowledged as such.

No particular originality is therefore claimed for the work reported in chapters 1-4 of part II, but chapter II.5 does contain some new ideas. Similarly the nonlinear phenomenon of chaos is not new but its study until now has been restricted to those cases arising in Duffing type of equations or in simple maps. In part III several new areas of chaotic motions shall be

investigated which naturally arise when modelling the wave driven motions of certain offshore structures, chapter III.5 being particularly state of the art. The overall underlying new aspect of the dynamics work reported here is the classification and prediction of bifurcational events and, although not exhaustive within this thesis, this does provide a framework on which greater complexity may then be added.

Some of the work reported in part III was carried out in collaboration with Professor Thompson and colleagues at University College London; the author is particularly grateful and acknowledges their cooperation. Where such collaboration has occurred clear indication of the origin of the work is included throughout the text, some of the work has been published as cited but has not previously been submitted for any other degree at any other institution.

NUMBERING SYSTEM

The figures and equations within a "part" of this thesis are referred to sequentially within the chapter in which they appear; for example figure 2.3 refers to the third figure of chapter 2 or similarly equation (1.2) would be the second equation of chapter 1. Where a figure or equation is referred to which appears outside the current chapter then, to prevent any ambiguity, the "part" in which it appears is also stated; e.g. figure III.5.3 etc.. The figures themselves appear at the end of the chapter in which they are originally referred to.

Part I : The Static Analysis of the Flow Through a
Pipe Bend or Deflector Nozzle

CHAPTER I.1

THE FLOW EQUATIONS AND THEIR SOLUTION

I.1.1 Motivation and Introduction

The main motivation for this work stems from the necessity to design a deflector nozzle used in vectored thrust vertical take off aircraft. The modelling of the fluid flow through such a vaneless deflector nozzle is effectively the same as the flow that would have to be considered when modelling the passage of a fluid along any pipe undergoing a bend and thus the general applications of the ideas developed here may be much wider. The essential features of the deflector nozzle currently in use dictate the basic form of the nozzle; namely it should have a circular inlet to allow for rotation of the nozzle during flight, particularly take-off, and the outlet is usually elliptical in shape in order to reduce drag at high speeds.

Thus the purpose of this study is then to develop a method of mathematical construction of a pipe bend from a known two dimensional channel flow. The shape of the two dimensional channel is obtained by considering a prescribed distribution of the velocity along the channel walls, this channel then being embedded in a three dimensional stream tube. The flow in the stream tube is then known and choosing this as a first approximation to the rotational flow a method shall be discussed

to convect the upstream vorticity throughout the stream tube and the resulting vorticity distribution can then be used to provide a better understanding of the complete rotational flow.

The flow of a rotational fluid throughout a pipe bend is governed by the Navier-Stokes equations, but it is not feasible to solve these equations in a design environment. We therefore seek an approximate solution to the flow through a relatively low cost design method. One such approximation is to consider a potential or primary flow which, together with a boundary layer produce a parabolic profile in the pipe. This effectively means that we shall be considering an upstream rotational flow model in which the direction of the vorticity is orthogonal to the stream flow. The difference between a potential flow and the actual flow of the fluid is called the secondary flow which necessarily includes the effects due to viscosity and vorticity. Thus if we neglect any effects due to viscosity in the mainstream the secondary flow will consist of velocities perpendicular to the potential motion of the fluid.

The Helmholtz vorticity laws tell us that the direction and magnitude of the vorticity vector change in the same way as the direction and magnitude of a material line which was, at some instant, parallel to the local vorticity. That is a vortex tube moves with the fluid and furthermore the tube strength remains the same. Consequently the vorticity is finite and the inviscid flow together with the deformation, or drift, of material surfaces due to the primary flow may be carried downstream to

produce a streamwise vorticity component, the so called secondary vorticity. Thus the problem is then equivalent to a boundary value problem in an inviscid flow together with a bound vorticity. It should be said that flow past an isolated body presents certain paradoxes of drift surfaces; for example consider the flow past a cylinder given by $w=1-1/z^2$ which has singularities at $x=\pm 1$. A drift line approaching a cylinder in such a flow would become stretched around the cylinder, the stagnation points acting rather like a saddle point in dynamics with the drift line taking an infinite time to reach the leading stagnation point. However, in this work for the design of pipe bends and deflector nozzles no such problems arise in the absence of any stagnation points.

In a two dimensional approximation we are linearising a nonlinear mixed partial differential equation of plane compressible flow. This linearisation has been shown [Payne (1969)] to be valid in compressible flow for Mach numbers $M < 0.85$. The important aerodynamic features are the maximum speed and the maximum diffusion gradients, to prevent shock losses or cavitation, and the prediction of any boundary layer separation. The solution procedure is the so called prescribed velocity distribution (PVD) method and is used to design a nozzle shape by choosing an aerodynamically suitable variation of pressure and speed without any a priori knowledge of the actual shape of the nozzle. The implied flow directions determine the shape of the nozzle as we may consider the streamlines to be solid boundaries since no fluid may cross them. Thus the walls are

taken to be calculated streamlines making any adjustment to the prescribed velocity distribution during the construction stage for engineering demands whilst retaining the overall aerodynamic features.

A pseudo three dimensional model of a pipe bend or nozzle may then be generated by imbedding a circular streamtube in the known two dimensional channel flow upstream, from which it follows that streamlines will trace out a streamtube throughout the complete flow field, see figure 1.1. From these streamtubes a nozzle may be constructed such that all the points on the streamlines are elevated through a constant height above the design plane. This model will have a fully three dimensional appearance yet with the special feature that a uniform flow approaching it will proceed through the nozzle in a two dimensional manner and the flow conditions will remain constant along normals to the design plane. Alternatively the mass flow through planes normal to the channel flow may be analysed [see Dyer (1979)], the third dimension in this case may then be derived by ratios of the streamtube heights along streamlines to the upstream values maintaining continuity of mass flow.

Having obtained a two dimensional potential flow and constructed a three dimensional nozzle in the manner described above known velocity and vorticity distributions upstream may be used through the Helmholtz laws to give a first approximation to the complete vorticity distribution throughout the flow field.

After linearisation the equations of motion and continuity conditions together with the associated boundary conditions are formulated in the design space in which the nozzle is transformed into a circular tube or cylinder, see figure 1.2. The numerical process to approximate these equations will be based on the finite element method as introduced by Davies (1980) and put into practice by Bishop (1982). The nature of the shape of the tube in the design space allows for an automatic mesh generation algorithm to be applied which would enable the equations to be solved using a relatively simple discretisation scheme.

This work could then be extended to use the secondary flow as a first approximation in a quasi-iterative scheme which would be able to include the effects due to viscosity in the boundary layer. To efficiently perform these iterations a system of nested levels or grids of finite element spaces it is suggested could be set up in a manner similar to the multi-level adaptive technique of Brandt (1977).

I.1.2 Flow Equations

Initially we shall restrict our investigations to that of a fluid flow with a low viscosity then, according to Prandtl, the effect of the internal friction is only appreciable in a narrow region surrounding the boundary. From this hypothesis the flow outside this narrow region may be considered to act as an ideal

fluid. Thus if we consider adiabatic flow in which no heat is transferred then this boundary layer remains thin and the ideal fluid flow results may be used as an approximation to the true fluid flow. It should be said though that if the fluid undergoes a rapid deceleration the boundary layer may experience some separation.

Since we are for the time being considering a two dimensional flow then accordingly any velocity w can be written in terms of the separate components u and v in the x and y directions respectively. Steady flow occurs when conditions at each point does not change with time, i.e.

$$\frac{\delta w}{\delta t} = 0, \quad \frac{\delta \rho}{\delta t} = 0, \quad \frac{\delta p}{\delta t} = 0, \quad \frac{\delta T}{\delta t} = 0, \quad (1.1)$$

where ρ , p , and T are the density, pressure, and temperature respectively and t is the time. If we further make the substitutions

$$u = q \cos \vartheta \quad (1.2)$$

and

$$v = q \sin \vartheta \quad (1.3)$$

then it is possible to show that

$$\frac{\delta \vartheta}{\delta \psi} = \frac{\rho}{q} \frac{\delta q}{\delta \psi} \quad (1.4)$$

and

$$\frac{-1}{\rho^2 q} \frac{\delta(\rho q)}{\delta \varphi} = \frac{\delta \mathfrak{J}}{\delta \psi}, \quad (1.5)$$

where φ is the potential and ψ the stream function [as verified in the standard texts such as Batchelor (1967) or see Payne (1969)].

To simplify these equations still further we make the substitution

$$dL = -\frac{\rho}{q} dq. \quad (1.6)$$

Then equations (1.4) and (1.5) become

$$\frac{\delta \mathfrak{J}}{\delta \varphi} = -\frac{\delta L}{\delta \psi} \quad (1.7)$$

and

$$\frac{1}{\rho^3} \frac{\delta(\rho q)}{\delta q} \frac{\delta L}{\delta \varphi} = \frac{\delta \mathfrak{J}}{\delta \psi}. \quad (1.8)$$

Payne (1969) has shown that for subsonic flow this latter equation may be closely approximated by

$$\frac{\delta L}{\delta \varphi} = \frac{\delta \mathfrak{J}}{\delta \psi}. \quad (1.9)$$

This substitution in turn allows L to be written as an explicit

function of q since, for adiabatic flow, the density-speed relationship is given by

$$\rho = [1 - (\gamma - 1)q^2/2]^{1/(\gamma - 1)} \quad (1.10)$$

where for a hot gas the coefficient γ is taken to be $4/3$. That is

$$\rho = (1 - q^2/6)^3 \quad (1.11)$$

Therefore L may be explicitly written as

$$L = -\log q + q^2/4 - q^4/48 + q^6/1296 \quad (1.12)$$

Thus under these assumptions both L and ψ satisfy the Cauchy-Riemann equations and hence Laplace's equation. However for the problem under consideration here the speed q may be prescribed on part of the boundary walls so that L is also known there and we shall attempt to solve

$$\frac{\delta^2 L}{\delta \varphi^2} + \frac{\delta^2 L}{\delta \psi^2} = 0 \quad (1.13)$$

with the appropriate boundary conditions defined by this prescribed velocity distribution along the channel walls. In the physical (x, y) plane the velocity q is given together with the value ψ which is the difference between the average flow angle on inlet and outlet, see figure 1.1. The aim is thus to determine the shape of the channel walls and the internal flow

by solving equation (1.13) for L in the flow function plane, i.e. the (φ, ψ) plane, in which the flow field becomes a rectangle.

Having found L the corresponding values of the speed q can be found by inverting the L - q relationship such that

$$q = f(L) . \quad (1.14)$$

This can be achieved by approximating the inverse function f , and in particular here we use functions f_1 and f_2 in the form

$$f_1(L) = e^{\xi} \quad (1.15)$$

and

$$f_2(L) = \xi^k, \quad (1.16)$$

where k is a constant and the function ξ is given by

$$\xi = \sum_{j=0}^n a_j L^j . \quad (1.17)$$

Data was generated and the inverse functions were obtained by fitting the data in a least squares sense using the statistical package GLIM. After a thorough investigation for the range of values which arise in this particular problem it was ascertained that the best results were obtained by using the function $f_2(L)$ when $k=-1.7$, the least squares error being given

by $E=0.4 \times 10^{-8}$. The coefficients of the polynomial in this case are given, with $n=8$, by

$$\begin{aligned} a_0=0.35, a_1=2.91, a_2=-1.43, a_3=5.32, a_4=-3.80 \\ a_5=2.21, a_6=-0.45, a_7=0.12, a_8=0.01. \end{aligned} \quad (1.18)$$

If further restrictions are made on the variation of the speed then the GLIM package allows for a fast solution to find the best alternative function $f(L)$.

It is then possible to find the value of ψ at any point required by numerical integration of L with respect to first ψ and then φ using the Cauchy-Riemann equations.

This type of approach to the problem of nozzle design was used by Frost (1976) to calculate the flow for a two dimensional channel using a finite difference scheme but an extension to three dimensions using this method was not deemed to be viable due to the large amount of computational time necessary. Consequently in this thesis a finite element idealisation of the problem is proposed which will allow flexibility of the method to cover flow in general pipe bends by reducing the computer time with the application of efficient algorithms. This finite element approach, it is suggested, can readily be extended to cover a three dimensional flow in a way which could conceivably be feasible given modern computer technology.

I.1.3 Boundary Conditions

In the flow function plane the flow field is a rectangle and without any loss in generality we may choose ψ to lie within the range $\pi/2 > \psi > 0$. In the φ direction the flow is bounded by two equipotential lines at $\varphi=U$ and $\varphi=D$ denoting the upstream and downstream boundaries, The range of φ such that $A < \varphi < F$ is determined by the distribution of q on the channel walls and to distinguish between the two walls the subscripts p and s are used to denote the pressure and suction surfaces respectively, see figure 1.1.

Now since L and \mathcal{V} satisfy the Cauchy-Riemann equations if we consider the complex function $F(w) = L + i\mathcal{V}$, where $w = \varphi + i\psi$, then $F(w)$ is analytic and by Cauchy's theorem

$$\int_C F(w) dw = 0 \quad (1.19)$$

for any closed contour C taken to lie within the flow field. Then equating real parts of equation (1.19) gives

$$\int_C L d\varphi - \int_C \mathcal{V} d\psi = 0. \quad (1.20)$$

If we now consider C to be the contour round the flow domain this yields

$$\int_{\varphi_U}^{\varphi_D} L_s d\varphi - \int_{\varphi_U}^{\varphi_D} L_p d\varphi - \frac{\pi}{2} \mathcal{V}_U + \frac{\pi}{2} \mathcal{V}_D = 0, \quad (1.21)$$

where

$$L_s = L(\varphi, \psi) = L(\varphi, 0)$$

$$L_p = L(\varphi, \psi) = L(\varphi, \pi/2),$$

and where ϑ_U and ϑ_D represent the average flow angle on inlet and exit respectively. These integrals may be divided into separate integrals along the channel walls and since the velocity is prescribed for $A > \varphi > F$, q elsewhere chosen to be a constant such that the speed is continuous throughout, if we let

$$L_1 = L(\varphi, 0) - L(\varphi, \pi/2) \quad ; \quad 0 \leq \varphi \leq A$$

$$L_2 = L(\varphi, 0) - L(\varphi, \pi/2) \quad ; \quad F \leq \varphi \leq D$$

then it can be shown that

$$\int_{\varphi_A}^{\varphi_F} (L_s - L_p) d\varphi = \frac{\pi}{2} (\vartheta_U - \vartheta_D) - \varphi_A L_1 - (\varphi_D - \varphi_F) L_2,$$

Furthermore if we make the change of variable

$$\bar{\varphi} = (\varphi - \varphi_A) / (\varphi_F - \varphi_A) \tag{1.22}$$

then this leads to the expression

$$(\varphi_F - \varphi_A) \int_0^1 (L_s - L_p) d\bar{\varphi} = \frac{\pi}{2} (\vartheta_U - \vartheta_D) - \varphi_A L_1 - (\varphi_D - \varphi_F) L_2.$$

This last change of variable is performed since the velocity distribution is usually given in the form of a graph of q plotted against $\bar{\psi}$. For a given q the corresponding value of L may be found using the relationship of equation (1.5) and hence from this latter equation the interval $\psi_F - \psi_A$ may be calculated. Once the interval in which the speed has been prescribed has been found L may be calculated throughout the flow field by solving the boundary value problem by using the finite element method, ψ subsequently being evaluated by numerical differentiation and integration of the Cauchy-Riemann equation. Finally the L - q relationship can be inverted to give values for q throughout the flow field.

Now since it our intention to assume that the walls of the streamtube are in fact streamlines we need to be able to calculate their shape. The function ψ is such that

$$d\psi = q\cos\theta dx + q\sin\theta dy . \quad (1.23)$$

If we let s be the arc length measured along a streamline then

$$d\psi = qds , \quad (1.24)$$

and similarly if we let h represent the arc length measured along an equipotential line then

$$d\psi = \rho qdh . \quad (1.25)$$

At this point it is convenient to introduce the scaling factor k to account for the channel in the physical plane so that

$$d\phi = kqds \quad (1.26)$$

and

$$d\Psi = k\rho qdh . \quad (1.27)$$

This latter equation may be also written as

$$d\Psi = -k\rho qdx/\sin\vartheta = k\rho qdy/\cos\vartheta , \quad (1.28)$$

from which we see that

$$dx = -\sin\vartheta d\Psi / (k\rho q) \quad (1.29)$$

and

$$dy = \cos\vartheta d\Psi / (k\rho q) . \quad (1.30)$$

If in the physical plane the initial width of the channel is taken to be of unit width then integrating this last equation produces an expression from which k can be found, namely

$$\int_0^{\pi/2} \frac{\cos\vartheta d\Psi}{k\rho q} = 1 . \quad (1.31)$$

With the complete distribution of q and ψ now known it is possible to integrate the equations

$$dx = \cos\psi d\phi / (kq) \quad (1.32)$$

and

$$dy = \sin\psi d\phi / (kq) \quad (1.33)$$

along the streamlines to evaluate their shape in the physical plane.

I.1.4 The Finite Element Method

a) Introduction

The finite element method is now a standard numerical procedure for the solution of partial differential equations and is adequately detailed in any number of text books including Davies (1980), Bathe and Wilson (1976), with many programming hints given in such texts as Hinton and Owen (1977). As explained in the preface the finite element codes written for the specific purpose of the boundary value problem in this part of the thesis were in fact more general but this adaptability shall not be reported here, the interested reader should consult

the Reports by the author [Bishop (1982)]. However in this section some ideas shall be laid out in the light of the authors experience to clarify some of the points of interest that arise when creating any finite element software.

The idea of setting up a finite element package to solve any number of problems is a massive undertaking. At the outset it may be best to construct the program in modular form so that initially a simple case may be solved and thereafter subroutines added to increase the complexity of approximations possible. The following remarks are merely to be borne in mind when developing a program which might act as a general finite element solver.

For greater versatility the finite element codes should be based on a general weak formulation so that problems for which a variational does not exist may still be solved using the same method (the term 'weak' originates from the process of choosing an approximate finite dimensional subspace and does not indicate the numerical solutions inability to mirror the true solution). Since the completed code or package may be used by someone who may not be conversant with the finite element terminology it is preferable to require as little a priori information as is possible. Thus having input the differential equation to be solved and the geometry of the problem the code should automatically produce a mesh which gives optimal accuracy within a prescribed computational cost. If possible error estimates should be given, although it should be pointed out that the error of the complete solution must be sought since the error in

the numerical calculations may be small when compared with errors introduced by an oversimplistic model.

In order to solve many given problems it soon becomes necessary to develop a subroutine for the efficient solution of the resulting equations. This is mainly due to the storage restrictions of most computers and thus to reduce the storage the solution subroutine should only store the non-zero coefficients and the process of elimination should produce as little 'fill-in' as possible. If this is done then the method so produced will be of use to those small users who previously were unable to attempt such ambitious problems.

b) Solution Routine

The finite element method usually produces a set of linear equations whose matrix of coefficients is large and sparse. There are several solution routines, both direct and iterative, for such systems which attempt to minimise the amount of overall computation and storage required. Direct comparisons of the various methods is not straightforward due to the complexity of the algorithms and perhaps the only real test would be to compare CPU times for the different methods. The matrix involved is usually banded such that if a_{ij} is an element of the matrix then $a_{ij}=0$ when $|i-j|>M$, say. The position in the matrix corresponding to a particular point of the defined problem depends on the nodal ordering so that if D is the

maximum difference between any two such nodal numbers within the element discretisation chosen then the bandwidth M is given by $M=D+1$. Thus clearly nodal ordering is of prime importance and it is not a trivial problem to decide on a mesh for a particular problem.

Various methods of solution are discussed in Barker (1977) and one such method particularly efficient is the so called frontal solution method originated by Irons (1970). In this method the fact that the input of the coefficients to the system of equations is element by element is utilised so that the system need not be constructed explicitly but elemental coefficients are assembled into the system and modified as soon as is possible. If an equation is completely formed then the corresponding variable is eliminated and the reduced equation is then stored on a backup file until it is required in the backward substitution process. This method then uses less storage than typical banded solvers but it does involve a certain amount of programming details ('housekeeping'). At any particular time the core only contains the coefficients of any equations still being formed, this core being referred to as the 'front'. When a new element is to be considered its local stiffness matrix is read from a disc file of data and summed either into existing equations or forms a new equation if the node is appearing for the first time. If a node has appeared for the last time and the corresponding equation is fully formed then it may be eliminated and transferred to disc leaving space in the front for further equations. Thus the size of the front

changes during the process up to a maximum depending on the bandwidth M .

Clearly the actual elimination is not performed like straightforward Gaussian elimination, i.e. sequentially, equations are not physically swapped but instead pointer vectors are utilised. Furthermore if the matrix is symmetric savings are made by only storing the upper triangular portion in vector form. The interested reader should consult the work of Irons (1970) or perhaps see the book of Hinton and Owen (1977).

In the frontal solution method the last appearance of a nodal number in the front depends on the order in which the elements are summed. Thus the nodal numbering is of little consequence, an advantage here being that automatic mesh generators to give optimal elemental ordering take less time than optimal nodal ordering since the number of nodes may be considerably more than the number of elements. Also if a local mesh refinement is required there is no need to renumber the nodes. Despite the obvious tedious housekeeping required to implement this method those concerned with future developments should note that full indexing in the innermost loops of the method makes it possible that the method is capable of vectorisation.

It should also be noted that the routine need not necessarily be restricted to symmetric systems however for particularly large problems iterative schemes may have to be

employed.

c) Essential Boundary Conditions

When a boundary node has a Dirichlet or essential boundary condition at which the solution is given, i.e. $u(z_k) = p$ say, p known, then the global stiffness matrix becomes singular. This then requires the routine to either to enforce this condition and solve the resulting equations or it is also possible to calculate the reaction necessary to counterbalance this effect. For a typical problem

$$Lu = f \quad (1.34)$$

in which L is a symmetric, positive definite, linear operator, then after the essential boundary condition has been taken into account the resulting global stiffness matrix will also be symmetric and positive definite. These properties can lead to a more efficient solution routine but only if the k th row and column of the global stiffness matrix are not formed. Thus a certain amount of reordering is necessary but the final matrix will at least be of minimal size.

Alternatively the reaction at z_k can be calculated and the method can work with the full sized matrix, as does the frontal method. It is also possible to set the k th row and column to zero except the diagonal element which is set to unity, the

corresponding term in the load vector would be set to p . One further possibility is to multiply the diagonal element a_{kk} by a large number, 10^{20} say, and the load vector term would then be multiplied by $a_{kk} \times 10^{20} \times p$. It is then envisaged that with this procedure the rounding error during backward substitution remains small and the numerical solution gives $U(z_k) = u(z_k) = p$ (note though that this system will not be positive definite).

d) Mesh Generation and Multigrid Methods

With regards to the problem of the discretisation of any particular problem there are two questions that need to be answered. What is the best mesh for the problem at hand? and given such a mesh what is the best elemental or nodal ordering?. Various schemes have been developed to reduce the storage required in different ways; see Cuthill and Mckee (1969) for a minimal bandwidth algorithm, or Akin and Pardue (1976) for a minimal frontwidth algorithm, but the first question provides the most fundamental problem.

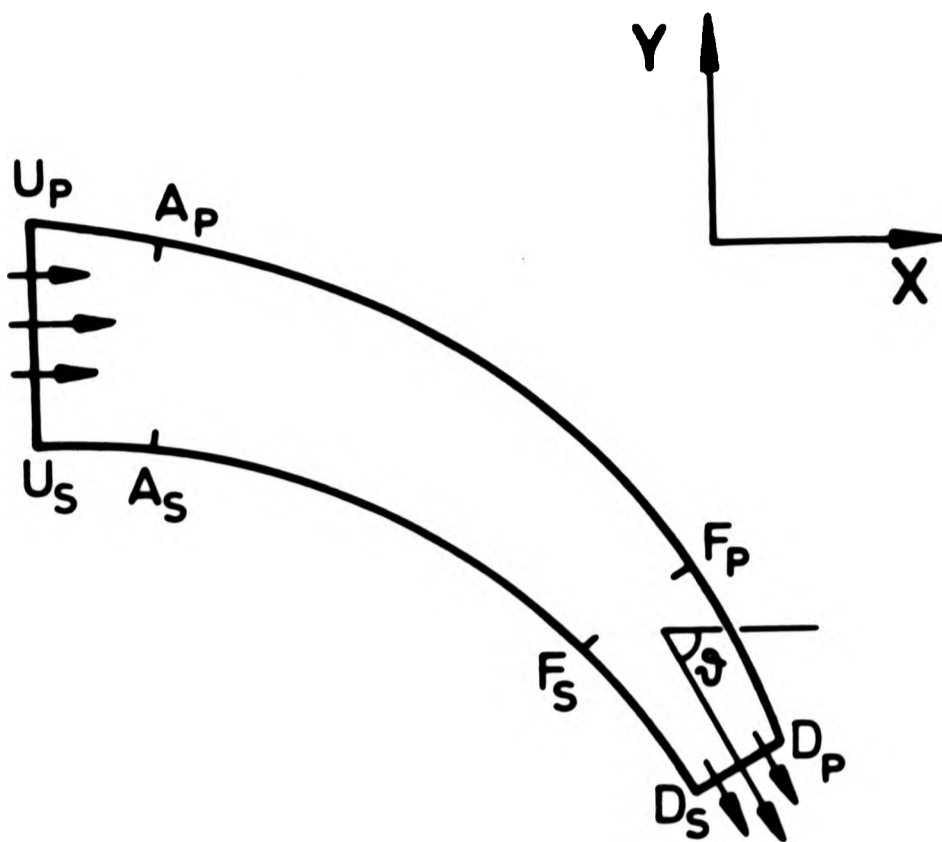
For certain problems an experienced finite element worker may be able to heuristically decide on a mesh needed to achieve a required accuracy. This is not always possible and the mesh description, being at the pre-processing stage, can very easily lead to gross inefficiencies. Either a mesh will be chosen which is too coarse and the approximations will be poor resulting in the need for a second discretisation, or too fine involving

excessive computational costs. Thus it would seem that the only realistic way of formulating a general purpose solver would be in terms of an adaptive scheme which requires little a priori information of the solution. In such an adaptive scheme, besides the basic geometry, the mesh would become an integral part of the numerical solution process producing optimal results within a prescribed computational cost (Achi Brandt's 'Golden Rule').

Multigrid methods are not an entirely new concept [see Southwell (1946)] but the application to the finite element method is not trivial and owes much to the pioneering work of Brandt (1977), and the work of Bank and Dupont (1978) is also worthy of mention. In most numerical procedures set up to solve continuous partial differential equations the region in which the solution is required is first discretised. Approximating algebraic equations are then expressed in a finite dimensional subspace and a numerical routine is then developed to solve the resulting system of equations. Usually no interplay between the discretisation and the solution routine is allowed leading to an inefficient overall method as previously explained. The main idea of a multi-level adaptive scheme is that an efficient discretisation depends on the solution which of course is not known. A smooth solution can be approximated by a coarse grid whereas an oscillatory solution, or one that contains singularities, can only be solved using a finer mesh or grid. It being quite conceivable that the solution varies considerably within the region which thus requires coarse and fine grids in different parts of the domain of flow. The problem can then best

be solved iteratively varying the mesh at relevant stages to try and match the solution. In fact the mesh need not be changed at each stage but relaxation schemes can be used to locally smooth out the error in the numerical solution. Hence a multigrid method uses a sequence of approximating levels with decreasing mesh size rather similar to standard mesh refinement. The difference being that new levels when introduced can interact with the previous coarser levels with relaxation sweeps and interpolations between levels. This not only forms an efficient fast solver but also forms a natural flexible way of producing a discretisation.

(a)



(b)

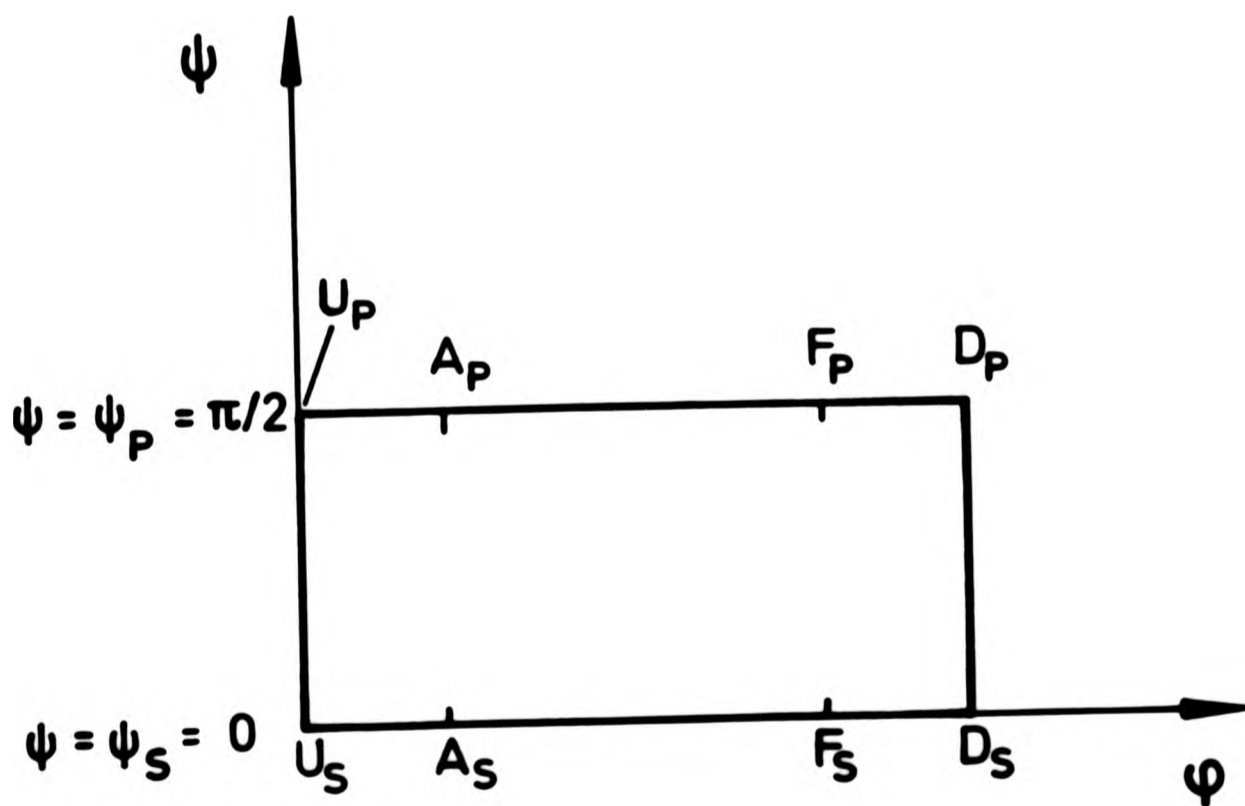
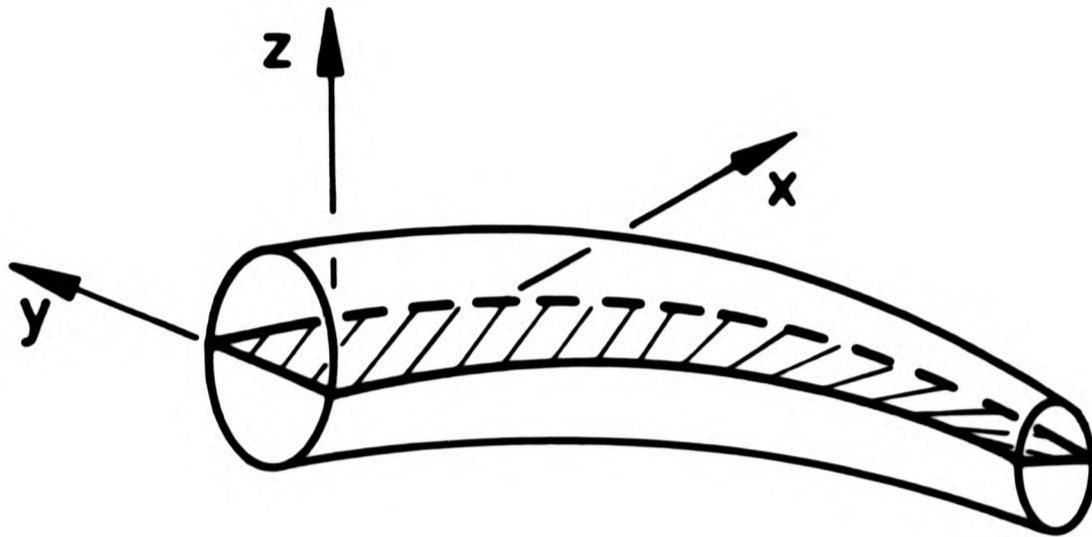


Figure 1.1 (a) Two dimensional channel flow in the (x,y) plane.
(b) Flow domain in the (ϕ,ψ) design plane.

(a)



(b)

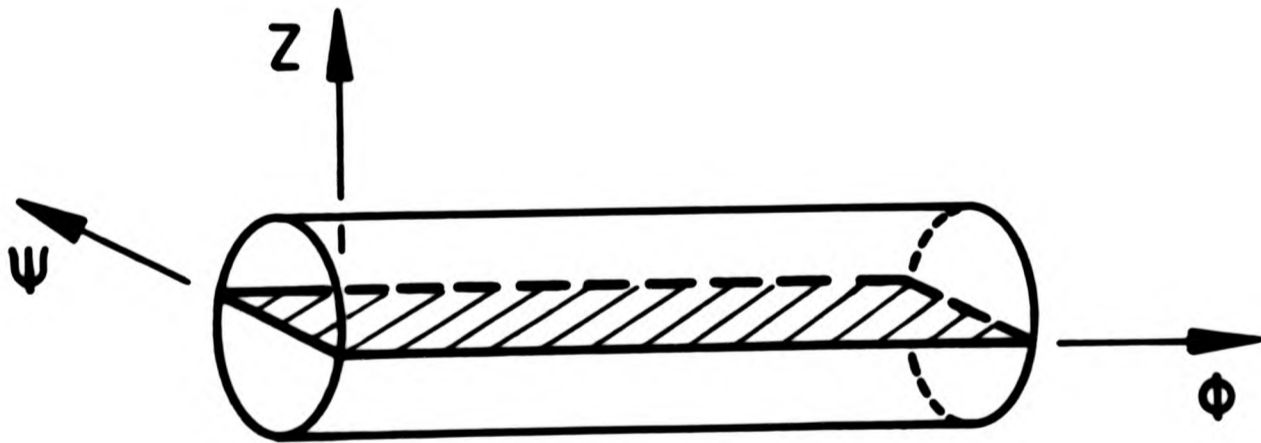


Figure 1.2 (a) Channel flow inbedded in a deflector nozzle
(b) Three dimensional streamtube.

CHAPTER 1.2

TWO DIMENSIONAL FLOW

I.2.1 Test Cases

In order to form a useful test for the proposed solution routine two test cases have been constructed based on the hyperbolic tangent which produce a suitable variation of parameters. The function $\tanh(\phi+i\psi)$ has singularities when $\phi=0$ and $\psi=(2n+1)\pi/2$; $n=0,+1,+2,\dots$ but to remove these singularities from the flow range $0<\psi<\pi/2$ the function is shifted by $\pi/4$. It is also worth noting that as $\phi\rightarrow\pm\infty$ the function $\tanh(\phi+i\psi-i\pi/4)$ tends to ± 1 independently of the value of ψ , thus in general we consider a function of the form

$$L+i\delta = A+iB+(C+iD)\tanh(\phi+i\psi-i\pi/4) \quad (2.1)$$

To ascertain the unknown constants we use the following boundary conditions to produce angles of deflection just over 57° and 80° respectively.

	Case 1	Case 2	
L at $\phi = -\infty$	1.5	2.0	
L at $\phi = \infty$	1.0	0.6	(2.2)

	Case 1	Case 2
ψ at $\phi = -\infty$	0.0	0.0
ψ at $\phi = \infty$	-1.0	-1.4

Now L and ψ are given explicitly by

$$L = A + \frac{C \sinh \phi \cosh \phi - D \sin \psi \cos \psi}{\cosh^2 \phi - \sin^2 \psi} \quad (2.3)$$

and

$$\psi = B + \frac{D \sinh \phi \cosh \phi + C \sin \psi \cos \psi}{\cosh^2 \phi - \sin^2 \psi} \quad (2.4)$$

Then if the pipe turns through an angle r radians during the flow passage and if we assume that the flow approaches parallel to the ϕ axis then

$$\lim_{\phi \rightarrow -\infty} \psi = B - D = 0, \quad (2.5)$$

so that $B=D$ and also, considering the value of ψ as $\phi \rightarrow \infty$, it can be seen that

$$B = D = -r/2. \quad (2.6)$$

If the approach and exit angle are further denoted by L_A and L_E respectively then by considering the limiting values of L yields

$$A = (L_E + L_A)/2 \quad (2.7)$$

and

$$C = (L_E - L_A) / 2 . \quad (2.8)$$

These conditions lead to the two following functions to be used as test cases

$$F_1 = 1.25 - 0.5i - (0.25 + 0.5i) \tanh(\phi + i\psi - i\pi/4) , \quad (2.9)$$

and

$$F_2 = 1.3 - 0.7i - (0.7 + 0.7i) \tanh(\phi + i\psi - i\pi/4) . \quad (2.10)$$

The range of ϕ may also be further restricted so that L on the upstream boundary is 99% of the value of L when $\phi = -\infty$, similarly for the downstream boundary. With this restriction the range can be limited such that $-2.5 < \phi < 2.5$.

Although alternative test functions can easily be defined these particular test cases have been set up to have typical variations of L , and hence the speed, along the boundaries $\psi = 0, \pi/2$ usually associated with channel flow see figure 2.1.

1.2.2 Calculation of L

Finite element programs were written to solve the boundary

value problem for the speed related variable L using a variety of elements, rectangular and triangular, as well as using differing approximating trial functions. The decision to use a particular element is often related to ones background; engineers choosing rectangular elements whilst mathematicians favour triangular elements. The actual numerical difference between the two shapes is small for the problem at hand since the region is regular but if this were not the case perhaps triangular elements have the edge being able to match a boundary more closely. Once the choice of element shape has been decided there still remains the question of what approximating function to use within the element. To provide a guide for the answer to this question the program was executed using three different trial functions with approximately the same number of unknowns in each case, the numerical results being given in table 2.1. As might have been envisaged the quadratic approximation produces a closer fit to the true solution than the linear trial functions. The choice between the 8 noded and the 9 noded quadratic elements is much harder to decide. Typically the 8 noded element gives a closer approximation, a surprising result perhaps and from whence it gets its name the 'serendipity' element with a Euclidean error norm calculated by evaluating the residuals at each node given by 4.9×10^{-4} . However, since for the particular problem at hand the values of L obtained by the finite element program will be subsequently used in further numerical processes the presence of the centre node will prove useful and prevent the need for interpolation at this point. Higher order elements were not utilised at this stage bearing in mind the overall need

for simplicity, and the proposed extension to three dimensional design.

The error in the approximation could naturally be reduced still further by increasing the number of unknowns, i.e. considering a smaller mesh, but if the number of unknowns exceeds 500 the frontal solution would have to be employed in the solution of the resulting equations. As is always the case in numerical work the gain in accuracy of the solution must always be compared with the extra work time and effort required to do so. In other words, except in certain one off calculations where accuracy is of vital importance, the amount of computational work should be proportional to the amount of real physical change in the computed system.

1.2.3 Calculation of δ

In order to determine shape of the channel walls the value of δ is required, and particularly the results along the streamlines $\psi=0$ and $\psi = \pi/2$. This then requires the integration of the Cauchy-Riemann equations. Firstly the derivative $\delta L/\delta \psi$ is calculated at each node using standard numerical differentiation schemes using the fact that L satisfies Laplaces equation on the boundary. The value of δ is then found by numerically integrating along the streamlines. Although there exists several schemes for numerical integration the input to any such program to perform this task depends on the mesh chosen

during the discretisation. This mesh may not be completely regular throughout the domain and hence subsequently discounts some of the integration routines which require equally spaced data etc.. For this reason a new scheme is proposed based on the interpolation to the data using piecewise rational quadratic functions.

The problem is thus how do we integrate a function given by a data set which might not be equally spaced?. The use of simple schemes, such as the trapezoidal and Simpson rules, may also prove to be oversimplistic especially as the function we are trying to integrate may contain rapid variations. To arrive at a more accurate solution it would seem appropriate, at first, to use an interpolation routine to produce an approximation to the function which is sufficiently accurate, in some sense. Clearly with no knowledge of the function itself the measure of error becomes somewhat heuristic but it is felt interpolation to any set of data provided by a piecewise rational quadratic function is particularly 'close', by eye at least, and so this will form the basis of the numerical integration routine.

We shall thus consider an interpolating polynomial which approximates the data (x_i, f_i) ; $i=1,2,\dots,n$ given by

$$s(x) = \begin{cases} P_i(y)/Q_i(y) & ; \Delta_i \neq 0 \\ f_i & ; \Delta_i = 0 \end{cases} \quad (2.11)$$

where

$$h_i = x_{i+1} - x_i$$

$$y = (x - x_i) / h_i$$

$$\Delta_i = (f_{i+1} - f_i) / h_i$$

and

$$P_i(y) / Q_i(y) = f_i + \frac{(f_{i+1} - f_i) [\Delta_i y^2 + d_i y(1-y)]}{\Delta_i + (d_{i+1} + d_i - 2\Delta_i) y(1-y)}, \quad (2.12)$$

in which d_i are approximations to the derivative of the function $f(x)$ at x_i . Full details of this method can be found in Gregory and Delbourgo (1981) or alternatively in the report by the author Bishop (1984b).

When integrating this approximating function there are initially two cases to be considered, either $\Delta_i = 0$ or not as the case may be. If $\Delta_i = 0$ then

$$\int_{x_i}^{x_{i+1}} s(x) dx = h_i f_i \quad (2.13)$$

and when $\Delta_i \neq 0$ we consider the integral

$$I = \int_{x_i}^{x_{i+1}} s(x) dx = h_i \int_0^1 \frac{P_i(y)}{Q_i(y)} dy. \quad (2.14)$$

Then from the definition of the interpolating polynomial we see

that

$$I = h_i f_i + h_i \int_0^1 \frac{Ry^2 + Ty}{A + 2By + Cy^2} dy, \quad (2.15)$$

where

$$R = (f_{i+1} - f_i)(\Delta_i - d_i)$$

$$T = (f_{i+1} - f_i)d_i$$

$$A = \Delta_i$$

$$C = 2\Delta_i - d_{i+1} - d_i$$

$$B = (d_{i+1} + d_i - 2\Delta_i)/2.$$

In which case there again two choices:

Case 1: C=0

If C=0 then the term B is zero and it is a simple matter to verify that

$$I = h_i f_i + h_i (R/3 + T/2)/A. \quad (2.16)$$

Case 2: C≠0

With C nonzero then the integral may be evaluated as follows

$$I = h_i f_i + h_i \int_0^1 \left(\frac{R}{C} + \frac{y(T - 2RB/C) - RA/C}{A + 2By + Cy^2} \right) dy, \quad (2.17)$$

i.e.

$$I = h_i f_i + h_i R/C + h_i \int_0^1 \frac{My + N}{A + 2By + Cy^2} dy, \quad (2.18)$$

where

$$M = T - 2RB/C$$

$$N = -RA/C.$$

There are then three different solutions depending on the value of the terms A, B and C as follows [see Gradstein and Ryzhik (1980)]:

AC > B²

$$I = h_i (f_i + R/C) + h_i \left(\frac{M}{2C} \log |(A + 2B + C)/A| \right) + h_i k (\tan^{-1} y_1 - \tan^{-1} y_2), \quad (2.19)$$

in which

$$S = \sqrt{AC - B^2}$$

$$k = (NC - MB) / (SC)$$

$$y = (C + B) / S$$

$$y = B / S.$$

AC < B²

$$I = h_i (f_i + R/C) + h_i \left(\frac{M}{2C} \log |(A + 2B + C)/A| \right) + h_i K \log \left| \frac{(C + B - S)(B + S)}{(C + B + S)(B - S)} \right|, \quad (2.20)$$

where

$$S = \sqrt{B^2 - AC}$$

$$K = (NC - MB) / (2CS) .$$

AC=B²

$$I = h_i (f_i + R/C) + h_i \left(\frac{M}{2C} \log |(A+2B+C)/A| \right) + h_i (NC - BM) / [B(B+C)] . \quad (2.21)$$

A program was written to employ this approximate integration scheme and various tests were performed comparing its performance with other forms of numerical integration schemes the results of which are reported in Bishop (1984b). Hence utilising this scheme of numerical integration ψ can be calculated at each point in the flow field producing results with comparable accuracy as those obtained for L , i.e. $O(10^{-4})$.

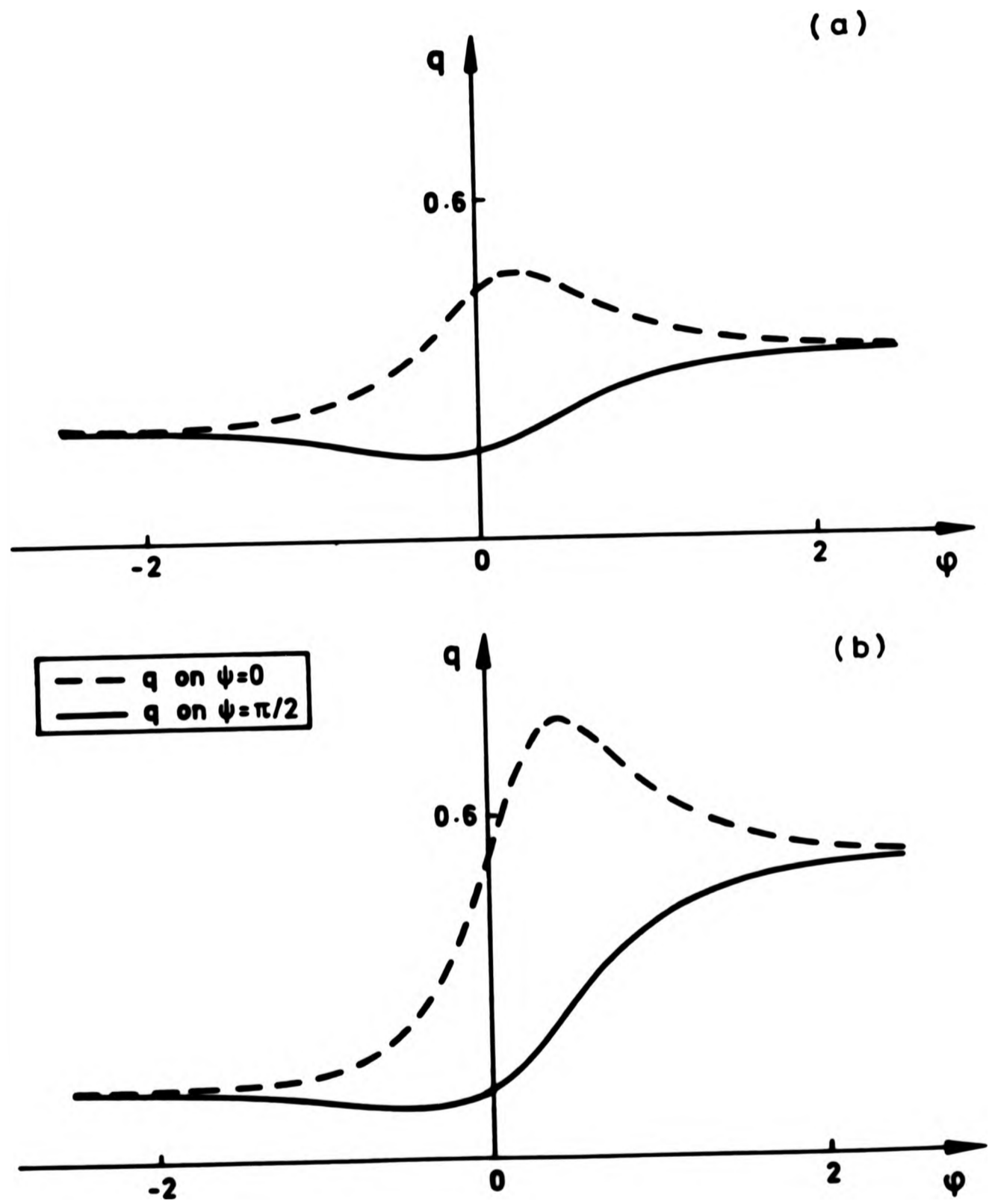


Figure 2.1 Speed variation along the channel walls in the design plane for the test functions (a) F_1 and (b) F_2 .

- A: 240 4 noded elements, 209 unknowns
- B: 60 9 noded elements, 209 unknowns
- C: 84 8 noded elements, 213 unknowns

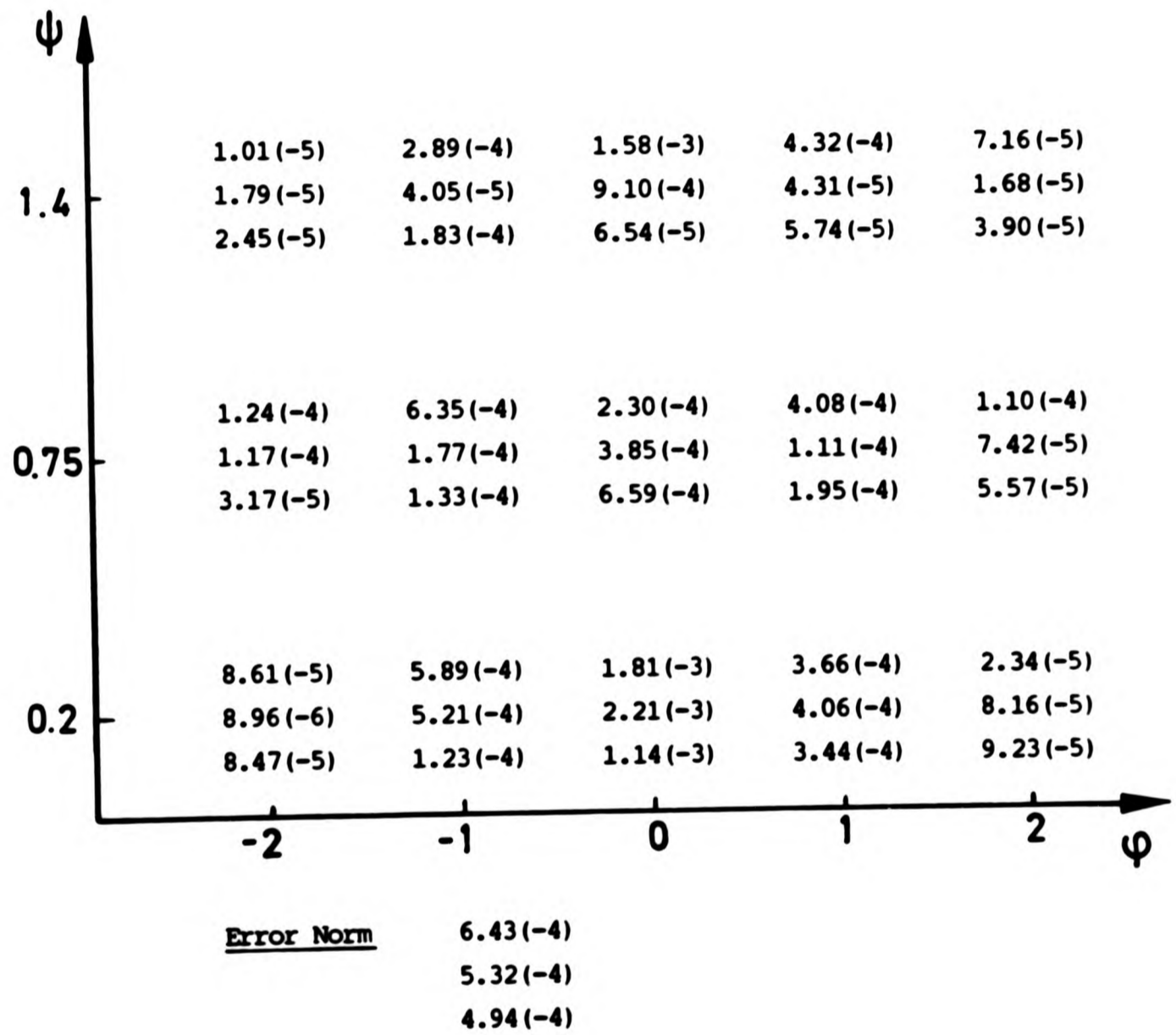


Table 2.1 Errors in the finite element approximation during the calculation of the function L. All error given in exponential form so that $1.52(-4) = 1.52 \times 10^{-4}$

CHAPTER 1.3

THREE DIMENSIONAL FLOW

I.3.1 Secondary Flow

To obtain a solution to the flow of a fluid in a pipe the flow passage is divided into a thin boundary layer near the wall and an inviscid potential flow outside this region. In some cases this division is not always possible and the effective boundary layer covers most of the flow region. For an inviscid fluid conditions when this separation is possible can be put into three categories; an irrotational potential flow, rotational flow but with a uniform stagnation pressure, and a flow with a non-uniform stagnation pressure.

If we assume an irrotational flow then the curl of the velocity vector is zero from which the potential function may be found. This irrotational assumption is equivalent to the stagnation pressure being the same along all streamlines but in practice this stagnation pressure varies from one streamline to another. We may define the secondary flow to be the difference between the actual flow and the potential flow and consequently the secondary flow must contain vorticity as well as including the effects due to viscosity.

Now since the vorticity is the curl of the velocity vector then this vorticity must arise from a velocity gradient. A non-uniform velocity distribution in a straight pipe will already contain vorticity in the flow and if this flow passes through a bend the vorticity will still be present, i.e. any vorticity need not necessarily be due to the bend itself. To study the effect of the bend on the flow we assume a small inlet vorticity and the secondary flow approximation is then found by considering the secondary flow to be a linear perturbation of the potential flow, neglecting any second order effects.

If we further assume the fluid to be continuous and homogeneous then the flow of the whole fluid is characterised by the flow of a small elemental volume. Each fluid particle cannot be treated as a solid body as it is continuously being deformed and influenced by neighbouring particles. However, as this element of volume passes round a curved path the force acting upon each particle within the element is proportional to its velocity squared and inversely proportional to the radius of the path of curvature. Hence the particles on the inside of the element, with respect to the bend, will experience a greater force than those on the outside, away from the bend, and these are consequently forced towards the outside so that particles with a higher stagnation pressure also migrate towards the outside of the bend. These forces act perpendicular to the longitudinal axis of the bend itself and create a motion in that plane. The presence of a secondary flow represents a loss of

energy since Kinetic energy of the axial fluid has been used to produce this perpendicular motion and a better understanding of this flow could be used to good effect in reducing any such energy losses.

Various authors have applied a secondary flow approximation to different situations and Hawthorne (1965) has produced an excellent summary of many of the relevant papers. However, for completeness and to put into perspective the new method introduced here we shall discuss some of these in more detail.

Squire and Winter (1951) used a approximation to calculate the secondary flow in a bend where the potential flow was approximated by a free vortex flow with outlet flow far downstream. In this paper and in the paper by Detra (1953) restrictions are placed on the ratio of the cross sectional width of the channel flow to the radius of curvature of the bend. Eichenberger (1953) applied similar techniques but used two coaxial cylinders to produce the required flow while Lighthill (1956) was the first to offer a more rigorous approach for the flow past an isolated obstacle. In the work by Lighthill he considered lines or surfaces of material, drift lines or drift surfaces, and applied the Helmholtz vorticity laws to establish how these lines might move with the fluid and hence calculated the convection of the upstream vorticity by the potential flow. A further assumption made was that the shear was small, hence the vorticity was small, so that the vorticity is convected by the potential flow. The secondary flow is then the

same order of magnitude as the shear and any change in vorticity due to a convection by the secondary flow will be of second order and hence may be neglected.

Thus in order to investigate the complete vorticity distribution for the design of a nozzle we shall use the Helmholtz vorticity laws and a method akin to that used by Lighthill.

I.3.2 Vorticity

For an inviscid fluid the vorticity can be thought of as being concentrated on sheets or along lines. Kelvin's Theorem states that

$$\frac{d}{dt} \Gamma = \frac{d}{dt} \int_C q \, d\lambda = 0, \quad (3.1)$$

where Γ is the circulation and d/dt is the material derivative which includes the change in position as well as the change in time. More precisely the value of the integral does not change during the motion if the curve C is composed of the same particles so that the circulation has a constant value for each curve. Thus the continuity equation, $\text{div}q=0$ for an incompressible fluid, together with Kelvin's Theorem describes the motion of a perfect fluid with pressures being evaluated by the use of Bernoulli's equation.

If we divide the area enclosed by the curve C into small elements then by Stokes' Theorem

$$\Gamma = \int_A \omega \, dA \quad , \quad (3.2)$$

where ω is the vorticity. This integral gives the relationship between the vector field of velocity, q , and the deduced vorticity field so that at each point in the fluid we have q and ω . A vortex line is defined to be a line such that at each point in the fluid its tangent line coincides with the vector ω at that point. All vortex lines through a closed curve C_1 , say, give a vortex tube.

Consider a curve C_1 on the surface of a vortex tube on which the local vorticity component normal to dA is zero so that $\Gamma = 0$. At some time later the vortex tube will be in a different position and the particles that formed the curve C_1 will now form a new curve C_2 , say. By Kelvin's Theorem $\Gamma = 0$ on C_2 and since C_1 was arbitrarily chosen this means that $\Gamma = 0$ and $\omega = 0$ at any point on the new tube surface implying that the new tube is also a vortex tube. Thus fluid particles coinciding with a vortex tube at any instant must do so permanently. By considering a cross sectional area of a tube that tends to zero we have also shown that a vortex line remains a vortex line.

The integral in equation (3.2) has the same value for any

cross section of the vortex tube; this fact leads to the second Theorem of Helmholtz, namely that the vorticity of any vortex tube is unchanged during any motion.

The proofs of both of the Helmholtz laws hold for steady and unsteady flow, compressible or incompressible, the only restriction being that the relationship between the density and the pressure is a simple one with the density independent of the temperature, i.e. barotropic.

A consequence of these Helmholtz laws is that if a material line coinciding with a vortex line is extended over a portion of its length the associated cross sectional area of the vortex tube must decrease to satisfy the conservation of mass and thus the vorticity must increase. The length of a line element and the magnitude of the local vorticity thus remains in the same ratio. The magnitude and the direction of ω in a material element change in the same way as that of the vector $\delta\lambda$ of a material line element which was coincident to the local vorticity at t_0 , say, and as $\delta\lambda \rightarrow 0$

$$\frac{\omega(t)}{|\omega(t_0)|} = \frac{\delta\lambda(t)}{|\delta\lambda(t_0)|} \quad (3.3)$$

This relationship links the vorticity at any point in the fluid to the vorticity on the upstream boundary. This introduces the concept of how a line or surface of particles moves through the fluid and how it changes with time. Similar ideas were first

introduced by Darwin (1953) and developed by Lighthill (1956) to calculate the vorticity distribution so that lines of constant time t can be described throughout the flow field and it is suggested here that a similar approach could be used in the design of a general pipe bend or nozzle.

I.3.3 The Construction of a Three Dimensional Flow Model

The mathematical construction of a streamtube may be achieved by imbedding the known two dimensional channel flow into a pseudo three dimensional model. We consider a flow with a circular inlet whose plane is perpendicular to the (x,y) upstream plane with the upstream boundary of the flow forming a diameter of the circle. The streamlines intersecting this circle will trace out a streamtube throughout which the complete flow is known. This mathematical construction results in a nozzle which has a general three dimensional appearance but it is peculiar in that a uniform flow approaching the tube will then proceed through it in a two dimensional manner with flow conditions constant along normals to the design plane. With this kind of construction if we let $Z = \pi/2z$ then the ordered triple (ϕ, ψ, Z) form a system of orthogonal curvilinear coordinates in which the flow tube is transformed into a cylinder. Thus any calculations performed in this new design space have the advantage that mesh generation for any finite element schemes will be able to utilise this simple geometry to produce optimal element or nodal ordering with only a relatively small

computational cost. Detailed evidence of these calculations shall not be produced here but it is thought that this integrated approach to the complete calculation of the flow within a general pipe could feasibly be achieved, particularly with the use of full multigrid finite element routines as suggested in the previous chapter.

Part II : The Dynamic Analysis of Nonlinear Systems and
Generic Instabilities

CHAPTER II.1

AN INTRODUCTION TO NONLINEAR DYNAMICS

II.1.1 Background

An n dimensional dynamical system is one which can be described by a system of n ordinary differential equations;

$$\dot{x}_i = F_i(x_1, x_2, \dots, x_n, t), \quad i=1, 2, \dots, n. \quad (1.1)$$

A dot denotes differentiation with respect to the time variable t and if t does not appear explicitly in the nonlinear functions F_i then the system is said to be autonomous. Many texts are available for the study of such systems [Jordan and Smith (1977) and Nayfeh and Mook (1979) to name but two] but it is the classification of bifurcations and the field of chaotic dynamics that are of most recent interest [see Abraham and Marsden (1978), Guckenheimer and Holmes (1983) and Thompson and Stewart (1986)].

Originally the use of such systems was restricted to the field of celestial mechanics but today the study of periodic processes and oscillations is of a wider importance to engineers and scientists alike, for instance to predict fluctuations in concentrations of white blood cells or to reduce destructive

vibrations of offshore platforms [Lighthill (1986)]. Following work by the early astronomer Poincaré applied his considerable intellectual weight to the subject with an abundance of papers [Poincaré (1892)] in the hope of answering such questions as

"Will one of the bodies (planets) always remain in the region (space) or can it escape to infinity?"

or more qualitatively

"Does the system (describing planetary motion) possess integral curves which form closed paths which perhaps correspond to a given equilibrium state, stable or unstable?"

Poincaré was particularly interested in the topological structure of dynamical trajectories in the phase plane described by the variables x_1, x_2, \dots, x_n and t .

For simple physical situations we may use a system of linear ordinary differential equations as a mathematical model, but for more complex arrangements nonlinearity is unavoidable. As a consequence the behaviour of such nonlinear systems can be extremely complicated and it is instructive to consider the typical instabilities that they might undergo or exhibit during the course of dynamic motions. It may also be that the problems of physical interest have parameters which appear in the defining system of equations and, as these control parameters are varied, changes occur in the qualitative structure of the

solutions, in which case the system is said to have undergone a bifurcation. It is our intention in this work to look at such typical or generic events by restricting our attention to the study of two dimensional phenomena.

II.1.2 Centre Manifold Theorem

Fortunately to help justify such a simplification to two dimensional systems the Centre Manifold Theorem provides a means of reducing the dimension of the state space which needs to be considered when analysing certain bifurcational events [Carr (1981)]. The theorem is akin to the method of reducing passive coordinates often used in the general concepts of catastrophe theory [Zeeman (1977), Thompson and Hunt (1984) or see Hunt (1986)]; the basic idea is to effectively isolate the complicated asymptotic behaviour of a system by locating an invariant manifold (space, surface or line) which characterises the eigenvalues of the system which are approaching a state of instability.

This idea can easily be viewed in dissipative systems in that the volume that the ensemble of states occupies decreases with time so that the topological structure of the trajectories in the phase space is much simplified. In other words the motion of a complex system sometimes settles down to a final motion which may be described by only a few dimensions and any subtle or drastic change in the qualitative behaviour of such a system

can be characterised by low order bifurcational theory.

II.1.3 Bifurcations of Steady State Attractors

Often a bifurcation in the flow of a dynamical system, or as we shall see later in the corresponding Poincaré map, can cause motions to increase in amplitude or alternatively the system may become unstable such that trajectories diverge. As a consequence of this latter fact the terms bifurcation and instability are sometimes used synonymously.

Now although it is well understood that certain high order bifurcations require the coupling of more than one mode or control parameter in order that they might occur, it is the goal of this work to investigate the simplest models that display typical bifurcations, in an engineering or physical sense. In this way it is hoped that our increased understanding of the way in which such simple, low order systems become unstable or bifurcate will prove a useful guide to the behaviour of more complex dynamical systems. With this newfound knowledge in part III we shall experimentally and computationally study the dynamic behaviour of certain physical compliant systems taken in the main from the offshore industry.

With the advent of current modern computer technology time integrated solutions can now be obtained to even the most complicated equations whereas previously only limited analytic

closed form solutions were available once a physical system had been modelled. The response or solution to such nonlinear systems depends intimately upon the initial conditions imparted to the system. For certain problems these initial conditions may be precisely defined however, in other more general fields encompassed by dynamical systems, such as atmospheric air flow or the roll motions of a ship, such precision is uncommon. Consequently when modelling such a system a study must be made of all the different possible starting conditions that the particular system can attain. Usually dissipative dynamical systems exhibit a transient motion due to these initial conditions after which the motion settles down to some form of long term recurrent behaviour, called an attractor. In simple terms if the motion developing from adjacent starts converges to a particular attractor then it is said to be stable. The simplest form of an attractor is the point attractor, otherwise known as a fixed point, at which all motion has ceased and the system is said to be in a state of equilibrium. A periodic attractor is one which characterises a steady state periodic oscillation of the system. Such periodic motion can be self induced, in which case it is often referred to as a limit cycle, or due to some external forcing of the system; in which case the motion might either be harmonic, i.e. at the same frequency as the excitation, subharmonic with a period that is a multiple of the forcing period, or superharmonic which repeats itself in a fraction of the forcing period. Chaotic motion is a form of stochastic motion which, despite the fact that it can develop from purely deterministic equations, produces 'random' responses

which have an underlying order described by a strange or chaotic attractor (termed 'strange' since originally the behaviour did indeed appear to be strange before both the term and the phenomenon chaos was universally accepted). Chaotic motions exhibit sensitive dependence on initial conditions so that two almost identical starts may eventually diverge from one another. Although the majority of research into chaos has so far been confined to simple mathematical models, experimental examples are becoming increasingly common [Moon].

Equations whose coefficients are linear possess unique solutions but the same is not true for nonlinear systems and thus the possibility arises of the existence of more than one attractor for given fixed values of the coefficients of an equation in such a way that the final motion of the system depends on the particular chosen initial conditions.

To put into perspective just how complicated the motions of nonlinear equations can be it is instructive at this point to consider a form of Duffing's equation and review its behaviour as examined by Hayashi (1964) and subsequently by Ueda (1980); namely

$$\ddot{x} + k\dot{x} + x^3 = B\cos t . \quad (1.2)$$

Despite the apparent simplicity of this equation the subsequent dynamical behaviour of the trajectories is far from trivial and as yet is not fully understood with new events even now only

just coming to light [see Abraham and Stewart (1986) or Ueda (1986)].

With B zero a stable equilibrium point exists at the origin and trajectories decay onto this point with a transient motion that depends on the level of the damping value k , see figure 1.1. Thus the origin is a point attractor for all trajectories in the phase plane, here given by (x, \dot{x}) . Likewise for different values of the coefficients stable periodic motions also attract nearby trajectories and shown here in figure 1.2 are five stable coexisting periodic motions of the system when $k=0.08$ and $B=0.2$. This figure shows the periodic steady state time history as well as the corresponding phase portrait which is the projection of the flow onto the (x, \dot{x}) plane. The points A, B, C marked on this figure are called Poincaré points characterising the motion, these will be explained in detail in chapter II.3.

The set of points in the phase plane that decay onto a particular attractor form the domain of attraction or the catchment region for that attractor. These regions need not be simply defined in fact the reverse is usually true; to appreciate this one only has to look at the figure drawn by Hayashi (1964) which maps out the domains of attraction for harmonic motion and subharmonic motion of order 3 (order $1/3$ in the notation of Hayashi) included here as figure 1.3.

Further to these periodic solutions, chaotic motions are

visible at a variety of values for the parameters k and B . One such motion is shown in figure 1.4 as a time history when $k=0.05$ and $B=7.5$; also shown in this figure in the bottom right hand corner is the chaotic attractor (often now referred to as Ueda's attractor following the pioneering work of Ueda). Although certain sections of the waveform of this figure are similar there is never exact repetition and the motion is truly non-periodic. It is the mixing and folding of the chaotic attractor as the phase angle of the Poincaré section is varied that leads to the divergence of adjacent starts as illustrated in figure 1.5.

Thus for each different set of values for the parameters k and B it is necessary to search the phase plane to establish the possible existence and whereabouts of the different stable attractors. For this particular equation, although quite simple, this study forms a mammoth investigation; the main part of which has been carried out by Ueda (1979) and is summarised here in figure 1.6. The five periodic solutions of figure 1.2 correspond to the region (a) in this diagram while the chaotic response considered is in the region (k).

This figure shows a wide variety of possible final motions of this so called 'simple equation' and alarmingly, after over 20 years of study of this particular equation, Professor Ueda still privately admits that some of the areas of this figure have not been thoroughly explored. It seems very likely that such rich complicated behaviour would exist in most nonlinear

equations and the large areas of chaotic solutions in this last figure indicate that this phenomenon is not an untypical event indigenous to this equation and consequently chaos should not be flippantly discarded as a purely pathological feature.

The type of motion that this equation (1.2) exhibits thus depends on the position in the (k,B) space that the parameters happen to lie, together with the initial conditions imparted to the system. If k and B are now allowed to vary, modelling some variability or evolution of the physical system, then the path taken by the parameters can cross one of the arcs in the (k,B) space delineating the regions of the particular solutions. If this were to happen then the motion of the system will settle down onto a qualitatively different behaviour; and such change is called a bifurcation (i.e. a more general definition than the word suggests).

II.1.4 The Analysis of Nonlinear Systems

The analysis of nonlinear systems is in some respects similar to that of linear systems [Luenberger (1979)], for example when approximating a nonlinear system by a linear system to establish the stability of a fixed point. Differences arise though in that new phenomena exist, like chaos, a jump to resonance or a limit cycle, that are not possible in a linear system.

The object of nonlinear analysis is not to be over rigorous in seeking detailed solutions but rather to discover certain events or phenomena that characterise the behaviour of the system. Generally we seek a summarizing function that suppresses detail providing a reflection of the broad outline of the critical aspects of the system. A summarizing function is a function of the state parameters x_1, x_2, \dots, x_n, t and as the system evolves this function takes on various values conveying certain information about the system. It may be that it is possible to write down simple low order equations that resemble this summarizing function so that an analysis of these simpler equations in some sense gives a summary of the analysis of the entire system. This idea was first systematically introduced by Lyapunov (1949) and as a consequence summarizing functions are often called Lyapunov functions.

The main criteria for a summarizing function is that the function must decrease continuously towards a minimum as the system evolves, though this minimum need not necessarily be zero. In general there is no easy way to find such a Lyapunov function, and it need not be unique, however often a function which has a significance within the physical situation can be taken to be a Lyapunov function.

Now in mechanical systems the dynamic behaviour of the system is governed by Newton's second law of motion and the work done by a force is the change in Kinetic energy. If the total

work done round any closed path is zero then the system is said to be conservative. When the force is conservative it is always possible to define a potential energy function V so that if V is set to zero at some point then the potential at any other point is defined as the negative work done in moving to that point. However in many physical situations a system is subjected to frictional or other non-conservative forces in such a manner that the total mechanical energy decreases with time and the system is dissipative. Thus because of this decreasing property the total mechanical energy can be considered as a Lyapunov function for that particular system.

A similar alternative approach is to consider the motion to be within a potential field governed by the potential V , thus equivalently we can use the governing potential energy of the system to summarise its behaviour [see Hunt (1986)].

We can check the robustness of the phase portrait of the system by perturbing the vector field $(x_1, x_2, \dots, x_n, t)$ via a perturbation of the defining differential system. A system is said to be structurally stable if for any sufficiently small alteration to the defining equations the resulting flow is topologically equivalent to the initial flow. Thus while Lyapunov functions may be used in the stability analysis related to the robustness of a single point in the phase space, structural stability relates to the robustness of a single point in the vector field. The mathematical study of structural stability was initiated by Andronov and Pontriagin (1937) but

the interested reader should also consult the work of Thom
(1975) or Arnold (1983).

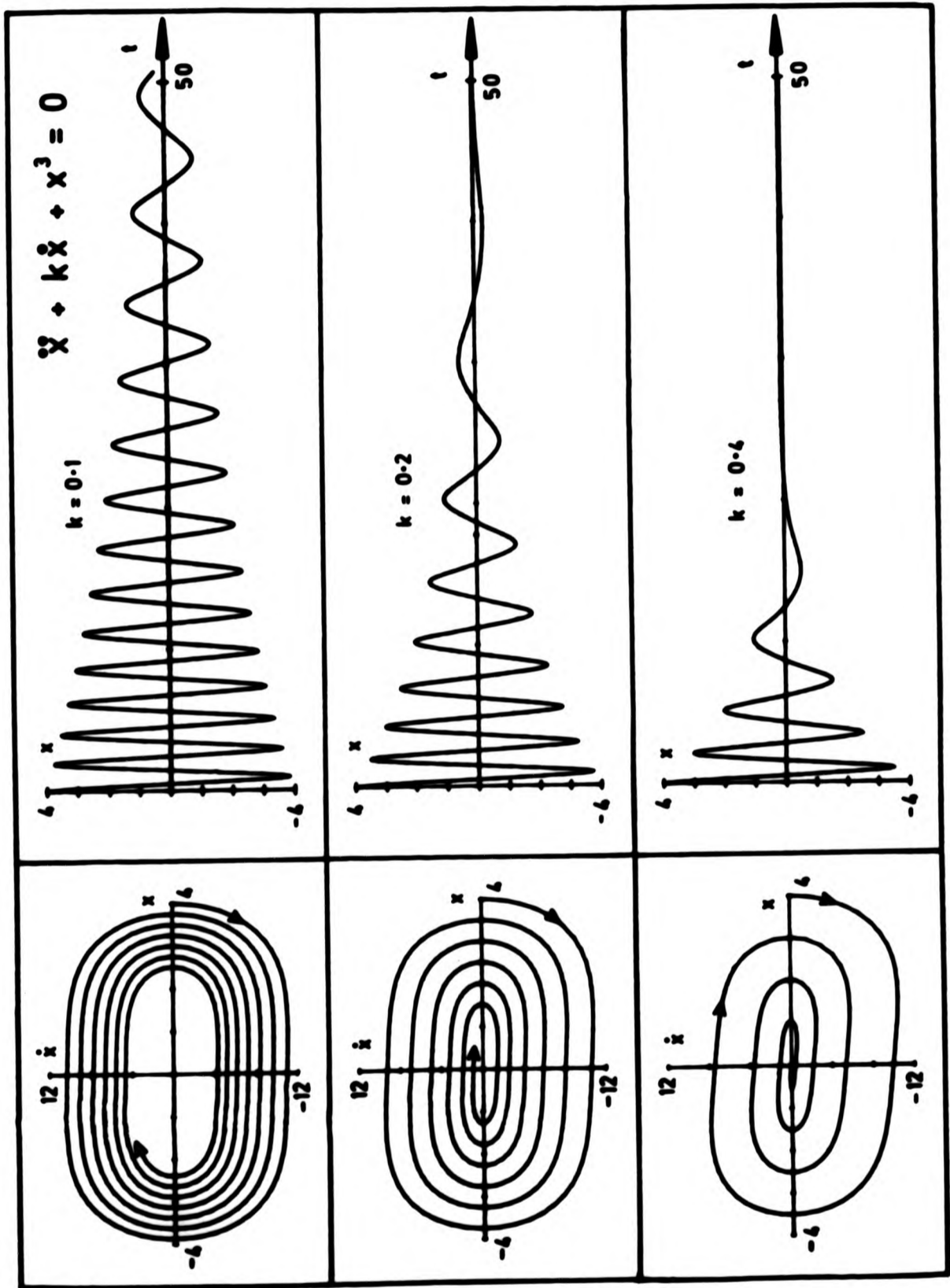


Figure 1.1.1 The decay of transient motions onto a point attractor for three different values of damping.

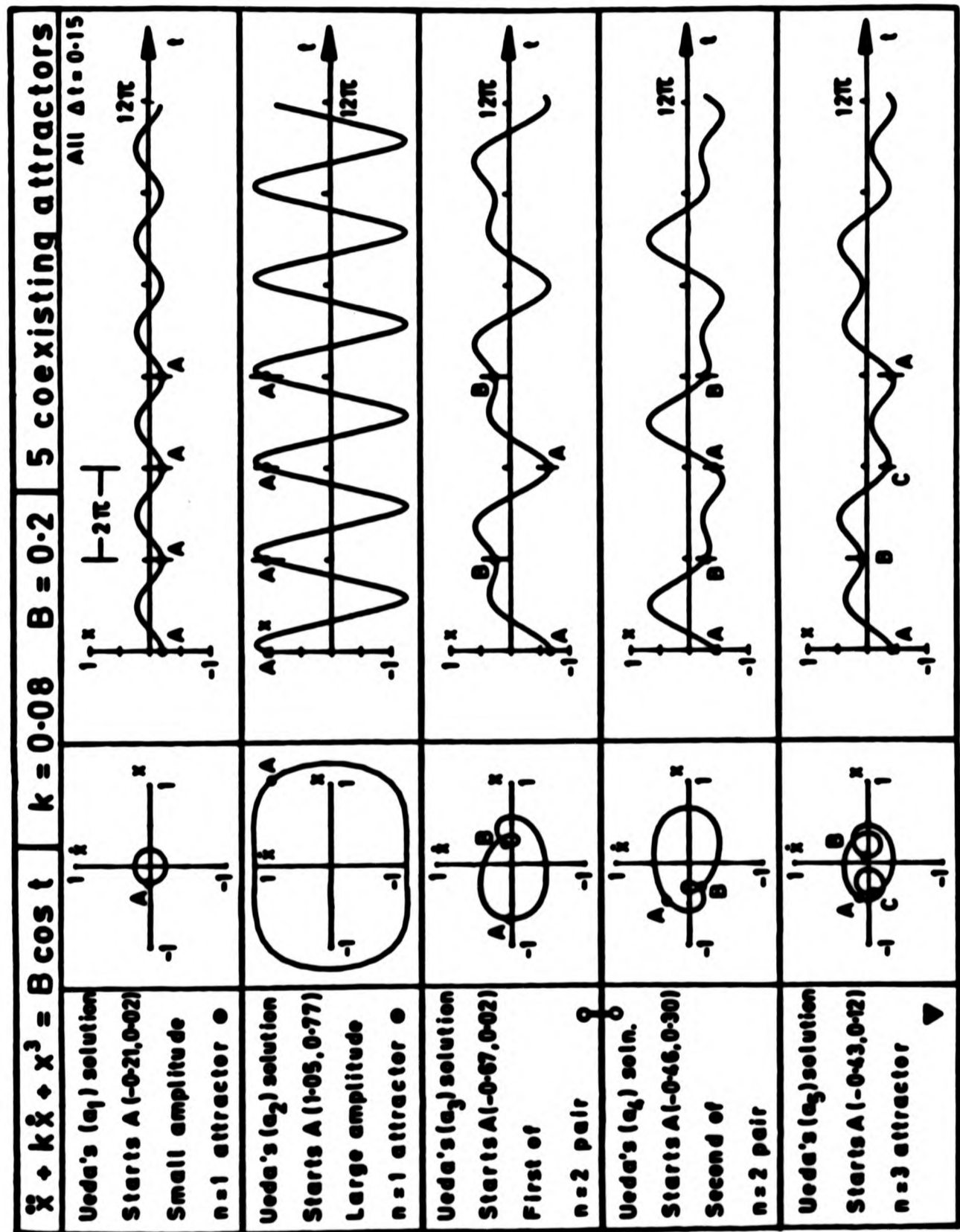


Figure 1.2 Five coexisting periodic steady states for Ueda's equation.

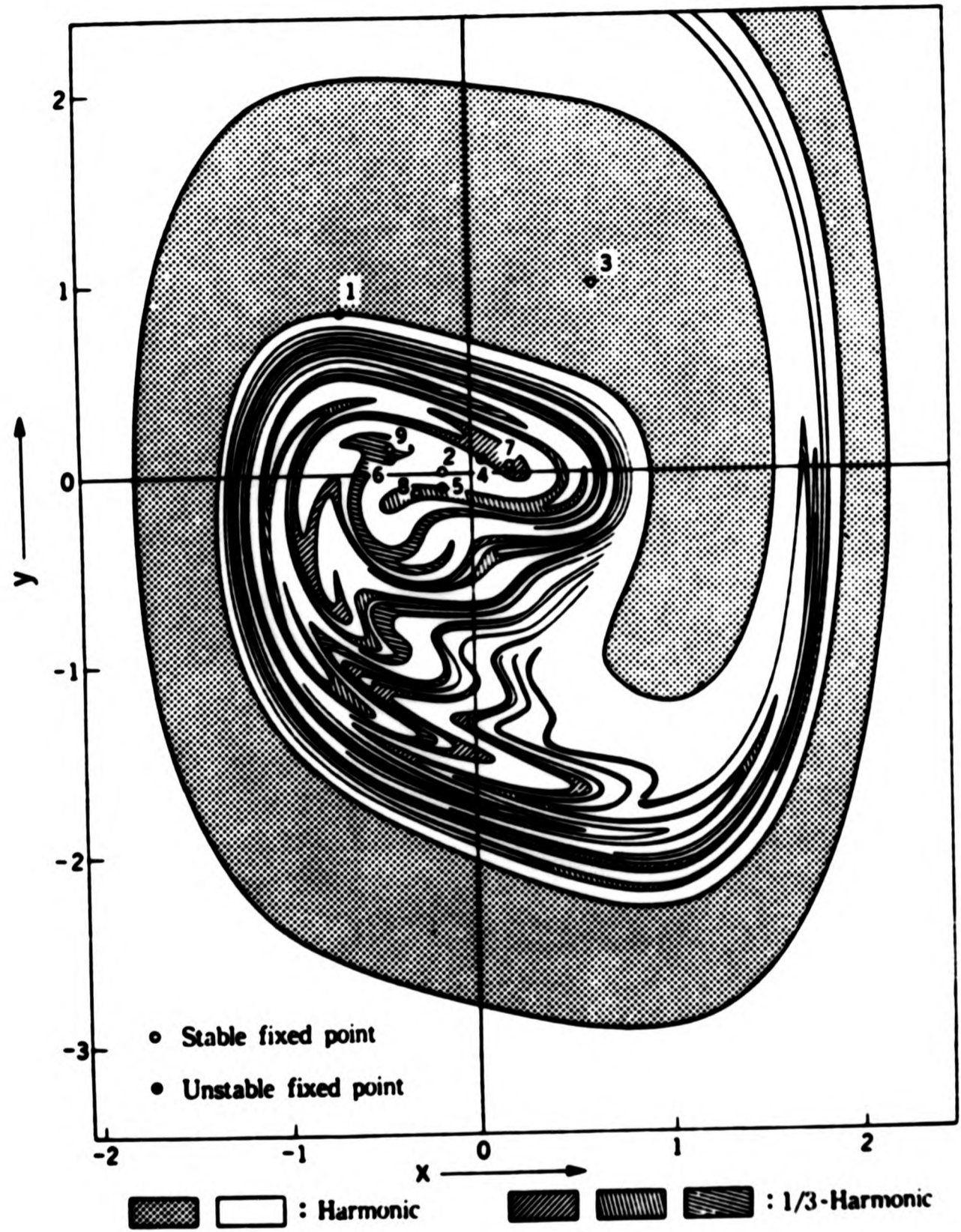


Figure 1.3 Catchment regions for harmonic and subharmonic motion of order 3 [due to Hayashi (1964)].

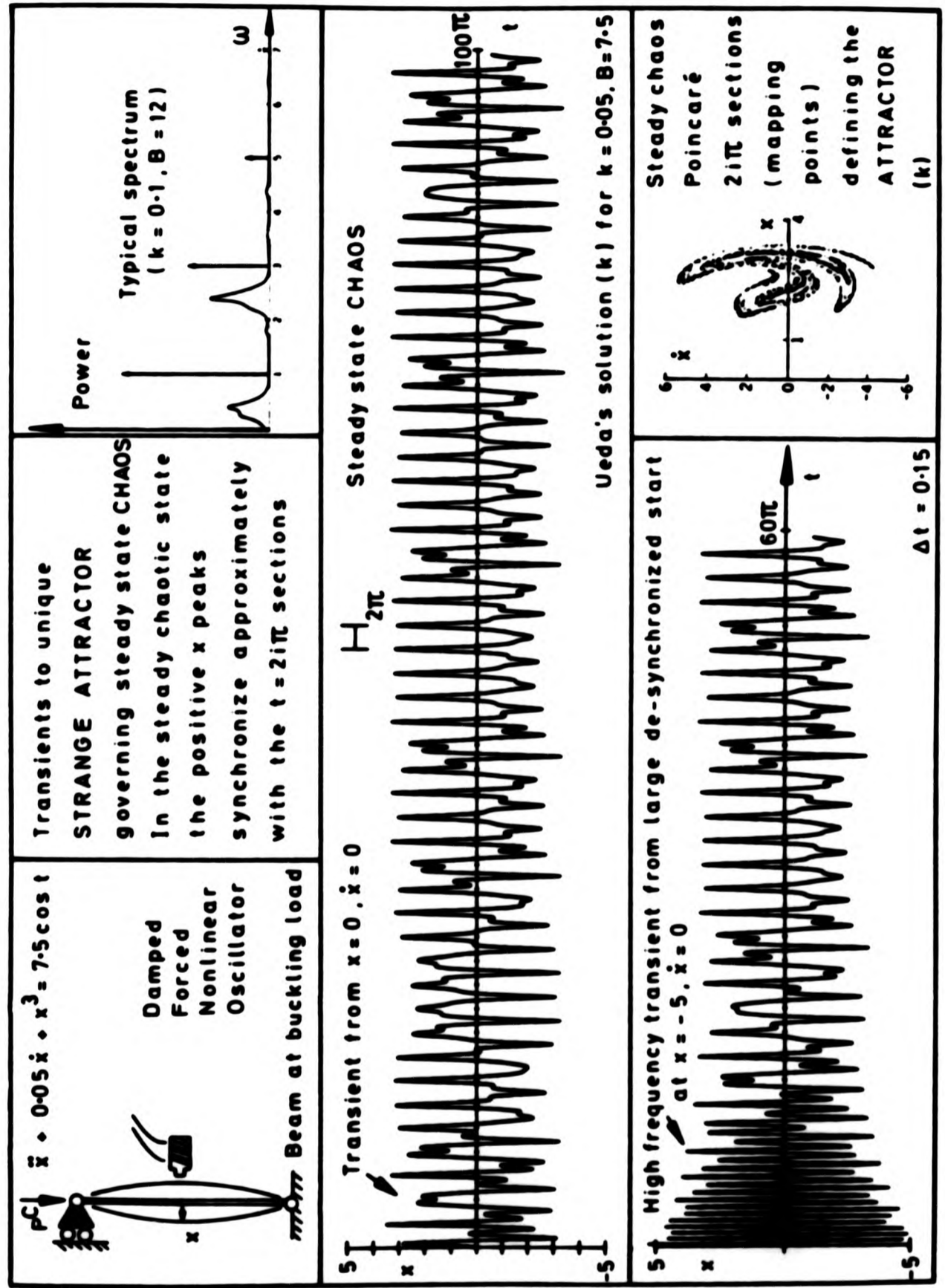


Figure 1.4 Chaotic motions of a nonlinear oscillator shown as a time history and associated chaotic attractor.

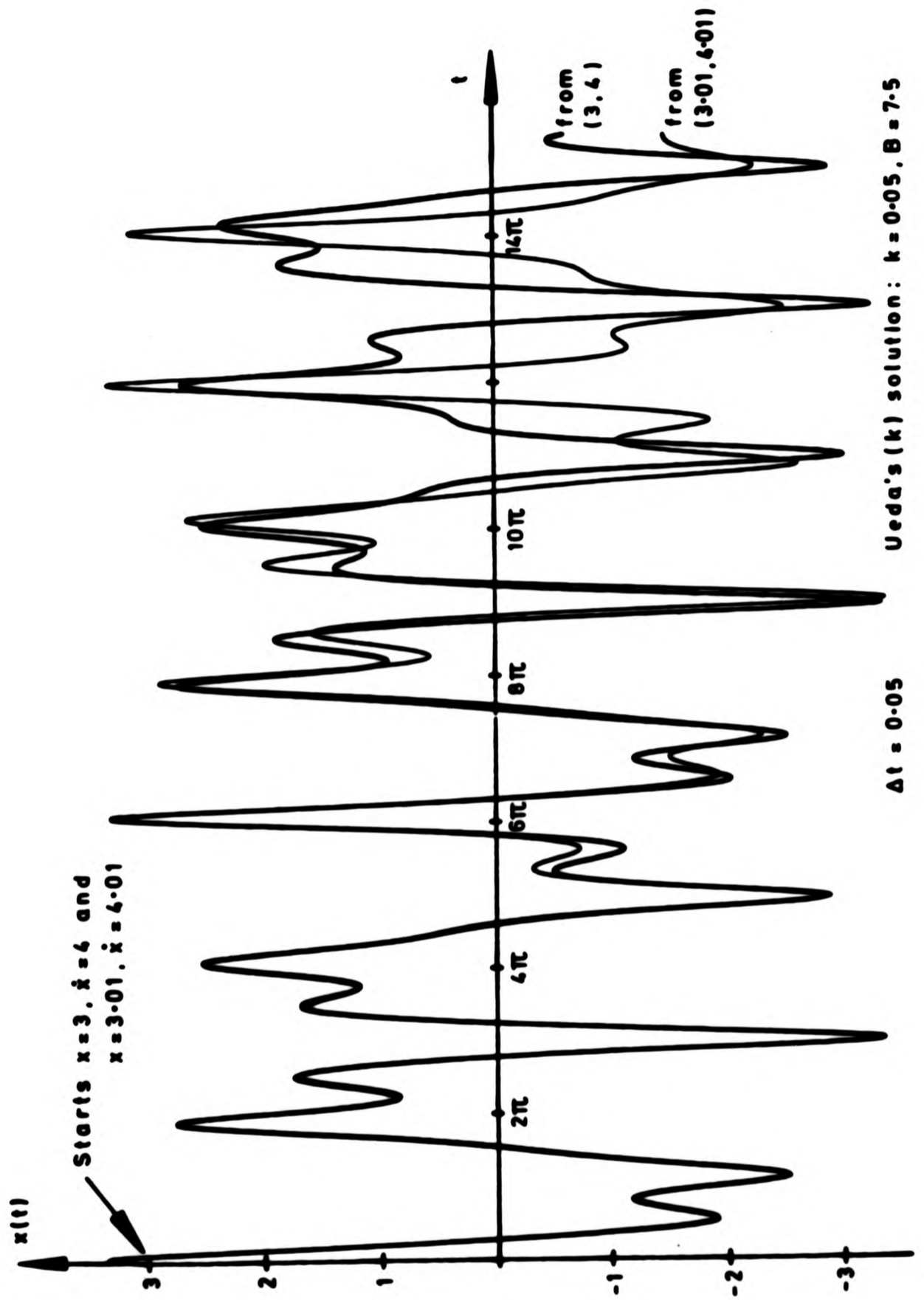


Figure 1.5 Divergence of adjacent starts on a chaotic attractor.

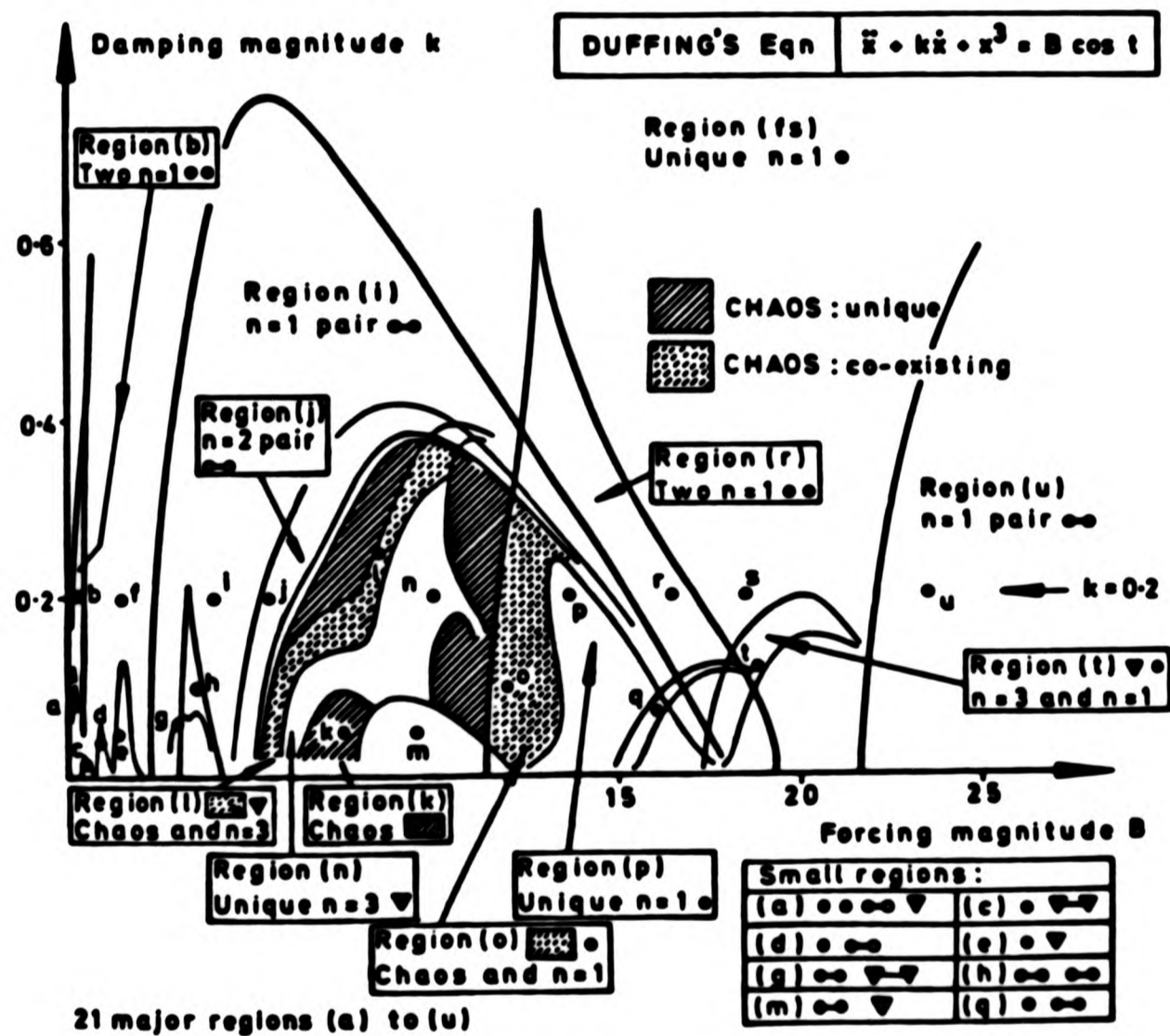


Figure 1.6 Regions of long term recurrent behaviour in Duffing's equation as determined by Ueda.

CHAPTER II.2

AUTONOMOUS SYSTEMS

II.2.1 Introduction

An autonomous system is one in which the time variable does not feature explicitly and following the discussion in the previous chapter regarding the use of the Centre Manifold theorem to reduce the number of dimensions necessary to describe the qualitative topological behaviour of a system approaching an instability, we shall restrict our attention here to two dimensional systems. Now given any second order ordinary differential equation, by the use of the substitution $\dot{x}=y$, it is always possible to write this equation in the more general form

$$\begin{aligned}\dot{x} &= F(x,y) \\ \dot{y} &= G(x,y) ,\end{aligned}\tag{2.1}$$

which is equivalent to the single first order equation

$$\frac{dy}{dx} = \frac{G(x,y)}{F(x,y)} .\tag{2.2}$$

[see Braun (1983)], where without loss of generality the fixed point is taken to be at the origin. The (x,\dot{x}) or (x,y) plane is

called the phase plane and solutions of equation (2.2) are called trajectories. Any point (x^e, y^e) such that

$$F(x^e, y^e) = G(x^e, y^e) = 0 \quad (2.3)$$

is called an equilibrium or fixed point (a singular point in the terminology of the more classical mathematical texts) corresponding to a point attractor. Any other point is termed an ordinary point through which must pass only one trajectory, thus for autonomous systems trajectories on the phase plane do not cross one another except at an attractor.

The differential system is said to be stable at a fixed point if every trajectory in a neighbourhood of the fixed point at $t=t_0$ remains near the point for all $t > t_0$. The system is said to be strictly or asymptotically stable if furthermore the trajectories approach the fixed point as time advances. If the system is neither stable nor strictly stable then it is said to be unstable.

Accordingly strictly stable systems ensure that all motion dies down, which generally occurs under damped motion and the system is called a dissipative system in which energy is lost.

II.2.2 Linearisation and the Stability of Equilibria

The linear analysis that shall follow is quite straightforward and explained in most texts on differential equations but is included here for two reasons; Firstly, the form of the solution gives a guide to the behaviour of the system approaching an equilibrium point and secondly it is useful here to introduce some of the new terminology either recently universally accepted or merely defined here by the author.

If we suppose that the functions F and G have Taylor series expansions in the form

$$\begin{aligned} F(x,y) &= ax + by + f(x,y) \\ G(x,y) &= cx + dy + g(x,y) \end{aligned} \quad (2.4)$$

where $f(x,y)$ and $g(x,y)$ are nonlinear containing terms of $x^m y^n$; $m+n \geq 2$, then Poincaré has shown that provided that $ad-bc \neq 0$ then the strict stability of the linear system

$$\begin{aligned} \dot{x} &= ax + by \\ \dot{y} &= cx + dy \end{aligned} \quad (2.5)$$

implies strict stability of the nonlinear system of equation (2.1). Thus we expect the solutions of the linear system to be geometrically similar to that of the nonlinear system. (In general this is true for a focus or saddle point to be defined later, but not necessarily true if the fixed point is a centre, i.e. we require strict stability; e.g. consider the system

$$\begin{aligned}\dot{x} &= -y - x\sqrt{x^2 + y^2} \\ \dot{y} &= x - y\sqrt{x^2 + y^2} .\end{aligned}$$

The linear system has a centre at the origin but the nonlinear system has a focus at this point. [Taken from Jordan and Smith (1977)].

For this reason we shall for the moment discuss the form of the solution and the stability of the linear system which may be written in the matrix form

$$\begin{bmatrix} \dot{x} \\ \dot{y} \end{bmatrix} = A \begin{bmatrix} x \\ y \end{bmatrix} , \quad A = \begin{bmatrix} a & b \\ c & d \end{bmatrix} . \quad (2.6)$$

The behaviour of the solution is now governed by the trace and determinant of the matrix A or its eigenvalues as given by the characteristic equation

$$\lambda^2 - T\lambda - D = 0 , \quad (2.7)$$

where the trace and the determinant are found by

$$T = a + d , \quad D = ad - bc .$$

For reasons that shall be explained later the eigenvalues are often referred to as the Lyapunov characteristic exponents.

Since later we shall assume that the coefficients of the matrix A are defined in terms of a control parameter μ that is allowed to vary and evolve, then accordingly it is necessary to consider the possible forms of the solution as T and D take on different values.

In the following discussions k and K are constants determined by the initial conditions given to the system, the behaviour of the trajectories being diagrammatically illustrated in figure 2.1.

(a) Case 1 : $D=0$

This case is of little importance with the solutions of the form

$$x = k + Ke^{Tt} \quad (2.8)$$

Thus for stability we require $T < 0$ so that solutions decay with time. Trajectories are given by straight lines with the limit point depending on the constant k , which need not necessarily be the origin, hence the system would be stable but not strictly stable.

(b) Case 2 : $T=0, D=\omega^2 > 0$

The solutions under these conditions are given in the form

$$x = k\cos\omega t + K\sin\omega t , \quad (2.9)$$

which are again stable but not strictly so as they are periodic and the equilibrium point is called a centre.

(c) Case 3 : $T=0, D=-\omega^2 < 0$

The solutions are in the form

$$x = k\cosh\omega t + K\sinh\omega t , \quad (2.10)$$

which are unstable corresponding to an unstable saddle point.

(d) Case 4 : $T \neq 0, T^2 > 4D$

If λ_1 and λ_2 are the eigenvalues of the system that satisfy the characteristic equation (2.7) then the solutions take the exponential form

$$x = k\exp(\lambda_1 t) + K\exp(\lambda_2 t) . \quad (2.11)$$

From this we can see that solutions are strictly stable if $\lambda_1 < 0$ and $\lambda_2 < 0$, i.e. $T < 0$ and $D < 0$ since $\lambda_1 + \lambda_2 = T$ and $\lambda_1 \lambda_2 = D$. The phase trajectories are 'quasi-parabolic' or 'quasi-hyperbolic' depending on whether the eigenvalues have the same or opposite sign. In this case the equilibrium point is either an unstable or a stable node respectively.

(e) Case 5 : $T \neq 0, T^2 < 4D$

This case corresponds to so called weak damping when the roots of the characteristic equation are now complex such that

$$\lambda = \alpha + i\beta, \quad (2.12)$$

where $2\alpha = T$ and $\alpha^2 + \beta^2 = D$. The solutions may be written in the form

$$x = e^{\alpha t} k \sin(\beta t + K), \quad (2.13)$$

and for stability of the fixed point we require $\alpha < 0$, i.e. $T < 0$. The phase trajectories will now spiral in towards the equilibrium point forming a stable focus.

(f) Case 6 : $T \neq 0, T^2 = 4D$

The system in this situation is said to have critical damping and the eigenvalues are now coincident, with $2\lambda = T$. The solutions of the linear system are now given by

$$x = (k + Kt)e^{\lambda t}. \quad (2.14)$$

For strict stability we again require $\lambda < 0$, i.e. $T < 0$ and here the trajectories in the phase plane would have a point of inflection with a common gradient at the fixed point which is referred to as a stable inflected node.

II.2.3 Instabilities of Equilibria

If we now imagine that the coefficients of this linear system, equation (2.6), are modelling a physical situation such that they depend on some control parameter μ , then as μ is varied the point in the (T,D) plane characterising the stability of the system moves. Furthermore if this movement was such that the point crosses one of the stability boundaries of the previous section then a bifurcation would result and an instability would have occurred. This instability is usually best seen as a bifurcation of an equilibrium path in the displacement control parameter space.

If this transition is such that the determinant becomes negative then the bifurcation is referred to as divergence (see figure 2.2 and also note the form of the solution in the previous section). This particular bifurcation is sometimes also called the static fold or saddle node bifurcation. This instability is basically a static event, examples of which can be seen when an elastic structure, such as a supported arch, is loaded to and beyond its critical load so as to induce buckling. During the instability the effective stiffness of the system changes from positive to negative as characterised by the movement of one of the eigenvalues of the linear system into the positive half of the complex plane along the real axis, as

viewed in the small inserted diagrams in figure 2.2. Since this instability mechanism is a static event it shall not be considered here in detail, the interested reader is advised to consult the paper of Virgin (1985).

Alternatively if the control parameter is varied so that the trace T changes sign and becomes positive then this corresponds to a dynamic instability as two complex conjugate eigenvalues attain positive real parts. This type of instability is called a Hopf bifurcation, also known as flutter.

This Hopf bifurcation occurs when an equilibrium point becomes unstable so that a trajectory started near the point spirals outwards with an oscillatory motion. In the case of a linear system the trajectory would merely diverge to infinity, however if the full nonlinear equation has certain nonlinear damping terms then for larger displacements these nonlinear terms dominate and the growth of the oscillations can terminate in a limit cycle, see figure 2.3. The simplest equation which displays this limit cycle characteristic is given by

$$m\ddot{x} + b\dot{x} + cx^3 + kx = 0, \quad (2.15)$$

in which the linear damping coefficient (b) is allowed to become negative. For small amplitudes the term cx^3 can be ignored yielding an unstable focus with b negative, while for larger displacements the dominance of this nonlinear term causes the motion to converge to a limit cycle.

This instability is the simplest dynamical instability under the variation of a single control parameter and gets its name following the work of Hopf (1942). In fact there are two forms of this instability, for both of these forms the linearisation process produces eigenvalues typified by the Hopf bifurcation as explained above. Under steady fluid loading an elastic structure can exhibit a unimodal version of this instability termed galloping or the bimodal instability called flutter. Typical examples of the former event include the galloping of ice coated transmission cables, or a bluff body in a steady flow [see Thompson and Lunn (1981)]. Examples of the bimodal form occurs in the flutter of aircraft panels at high speeds and, as we shall see later in chapter III.2, in the fishtailing oscillations of a moored vessel in a steady current.

In most cases these generic instabilities (typical in the engineering sense) possess unstable counterparts. A schematic diagram of the unstable Hopf bifurcation is shown here in figure 2.4 where the amplitude of oscillation is plotted against the control parameter μ representing some sort of fluid loading. A complete classification of the simplest low order bifurcations, both stable and unstable, is given in the text of Thompson and Stewart (1986), but in physical systems as indeed in numerical simulations the unstable steady state equilibria are by nature extremely difficult to locate. As a consequence to this, since the third part of this thesis will deal with instabilities of physical systems, the main emphasis here will be directed

towards the stable forms of the bifurcations.

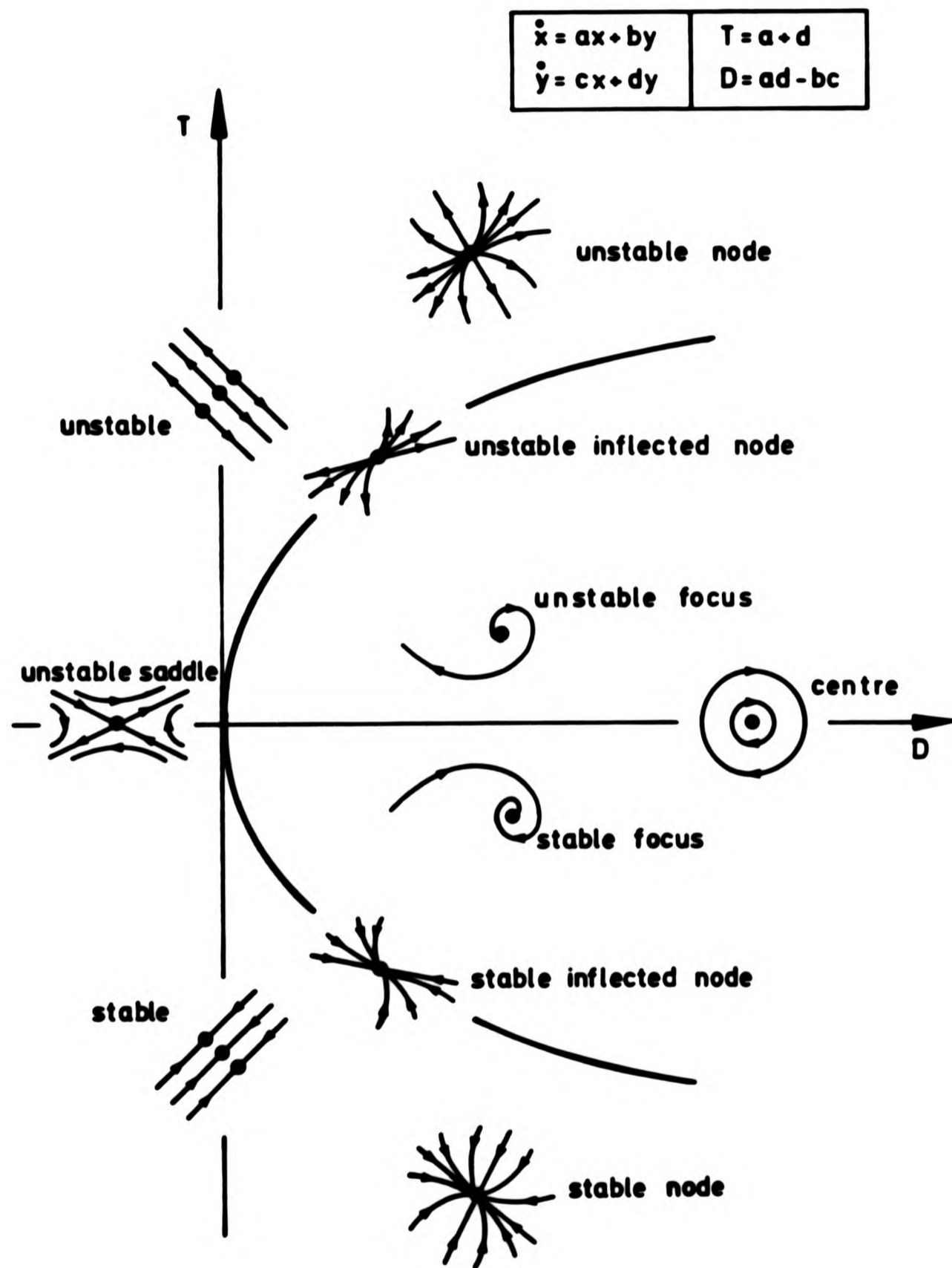


Figure 2.1 Behaviour of phase trajectories of a linear system.

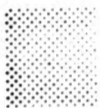
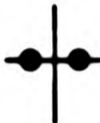

STABILITY OF A CONTINUOUS LINEAR SYSTEM

$$\dot{x} = ax + by$$

$$T = a + d$$

$$\dot{y} = cx + dy$$

$$D = ad - bc$$

-  Stable region
-  Position of eigenvalues
-  Coincident eigenvalues

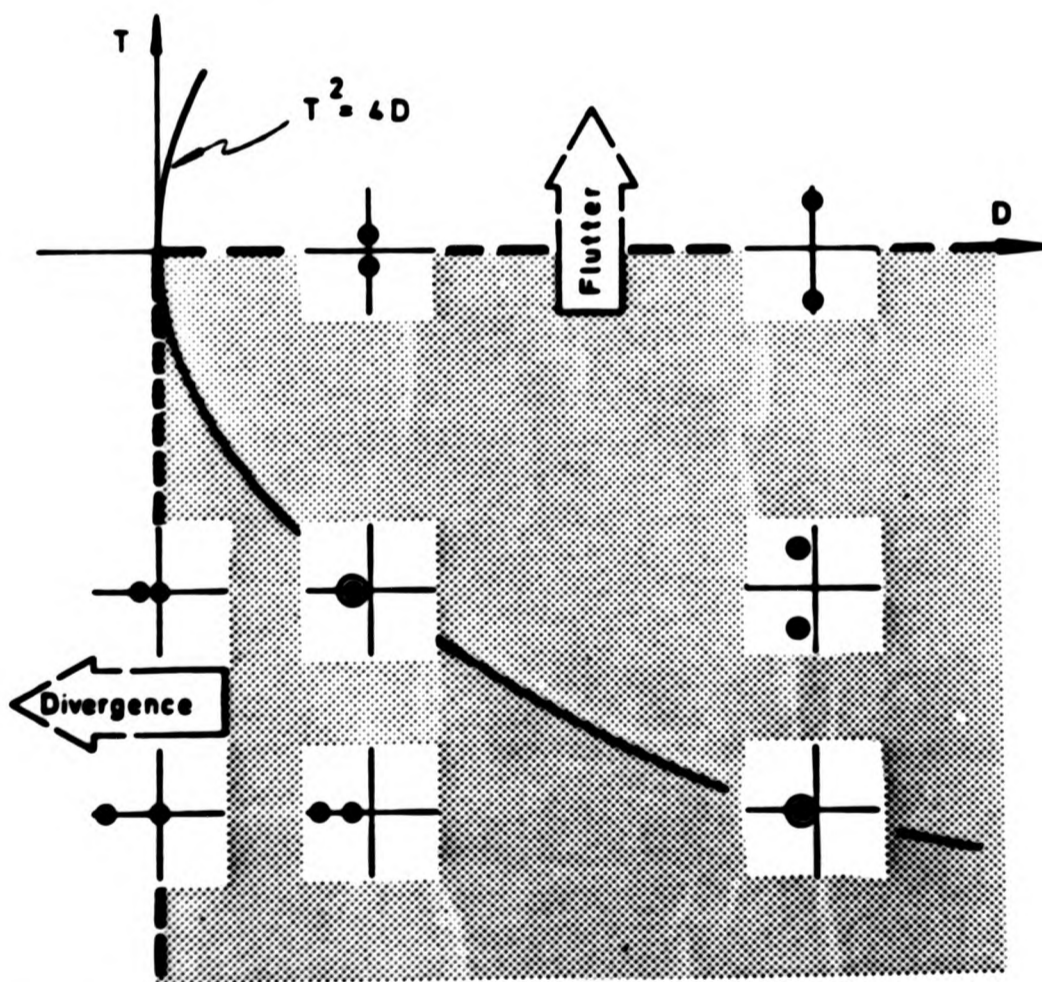


Figure 2.2 Stability region of a continuous linear system and associated bifurcations.

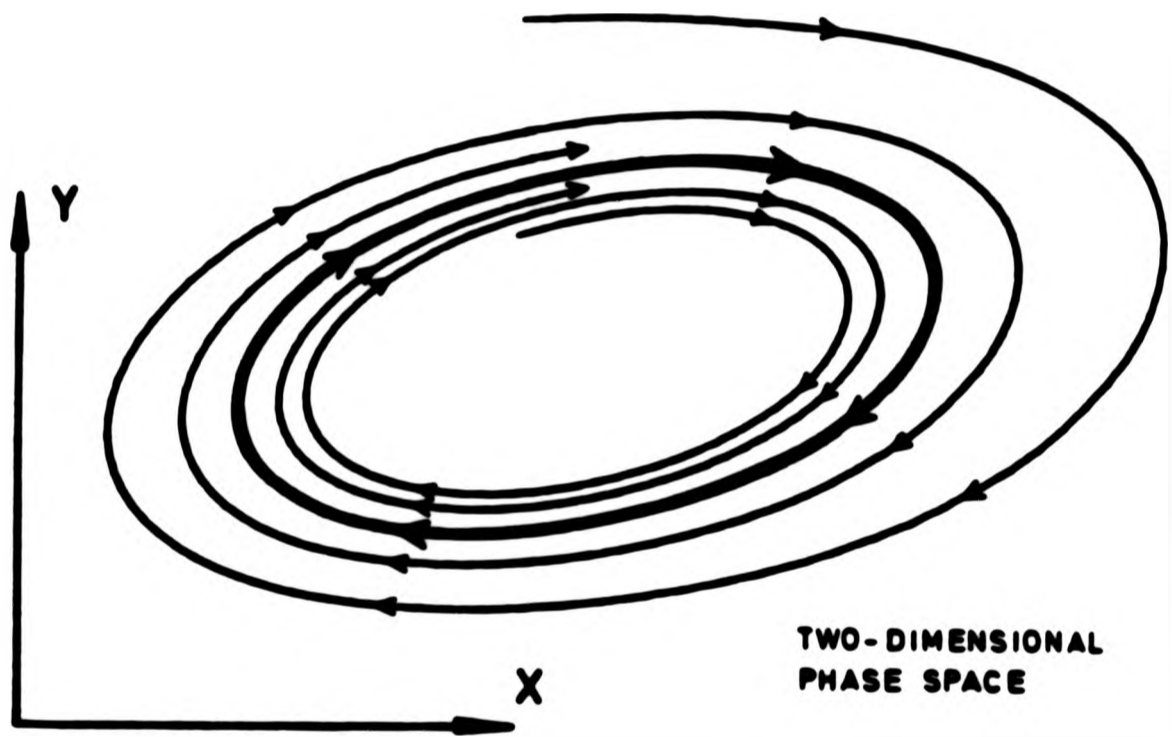
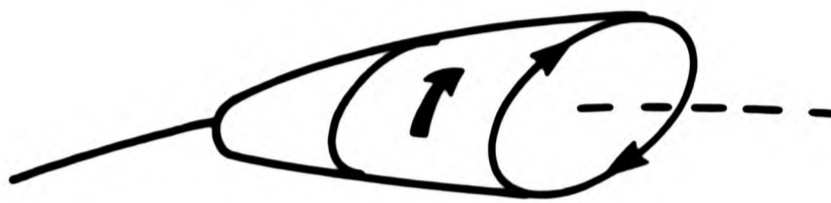
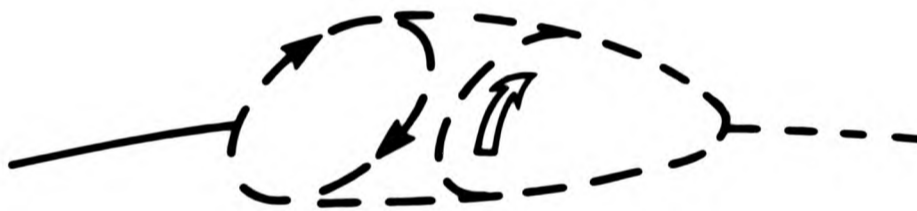


Figure 2.3 A stable limit cycle.

Stable Hopf



Unstable Hopf



— stable
- - - unstable

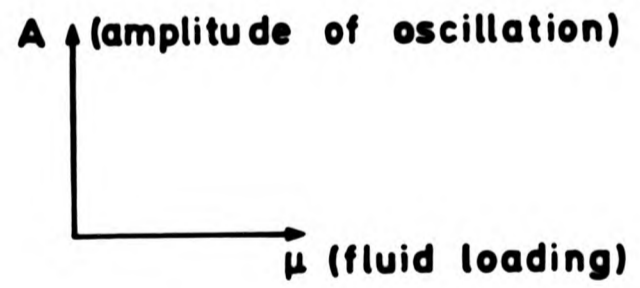


Figure 2.4 Schematic diagram of the stable and unstable Hopf bifurcations.

CHAPTER II.3

FORCED OSCILLATIONS

II.3.1 Introduction

In the previous chapter we considered autonomous systems typified by an unforced mechanical system whose phase space was two dimensional spanned by x and \dot{x} . If we now consider the forced non-autonomous counterpart to this equation, namely of the type

$$m\ddot{x} + f(x, \dot{x}) = F\sin\omega t, \quad (3.1)$$

then the phase space is now three dimensional spanned by x , \dot{x} and t . In this space trajectories of the flow do not cross one another but spiral round the t axis as time advances, however it is convenient to plot the phase projection of a trajectory onto the (x, \dot{x}) plane, on which the trajectory (or rather its projection) may now intersect itself.

Equilibrium points are not as a rule associated with non-autonomous equations though they can exist; for example the Mathieu equation given by

$$\ddot{x} + (\alpha + \beta \cos t)x = 0 \quad (3.2)$$

has a fixed point at the origin.

The main theme in part III of this thesis is to point out the inadequacies of standard linear vibration analysis in favour of nonlinear studies and so it is convenient at this point to briefly review some of the linear theory for forced systems [as in Thomson (1981) for instance].

The simplest forced equation for a general mechanical oscillator is defined by the equation

$$m\ddot{x} + b\dot{x} + kx = F\sin\omega t . \quad (3.3)$$

Since this equation is linear the structure of its solutions is relatively simple and formed by two parts. The complimentary function, or 'free oscillation', decays with time when damping is present ($b \neq 0$) and is dependent only upon the initial conditions. On the other hand the 'forced solution' (the particular integral) is proportional to the amplitude of forcing F . The independence of these two solutions allows only a restricted range of phenomena but nonetheless in certain situations can provide a useful guide to local behaviour.

The natural frequency of the undamped system is given by

$$\omega_n = \sqrt{k/m} \quad (3.4)$$

and the damping ratio ζ is defined by

$$\zeta = b/b_c , \quad (3.5)$$

where

$$b_c = 2m\omega_n . \quad (3.6)$$

Provided the damping ratio is such that $\zeta < 1$ then the complimentary function is given by

$$u(t) = Y \exp(-\zeta\omega_n t) \sin(\omega_n t / \sqrt{1-\zeta^2} + \phi_1) , \quad (3.7)$$

where Y and ϕ_1 are constants determined by the initial conditions. The amplitude of this solution decays with the frequency

$$\omega_d = \omega_n \sqrt{1-\zeta^2} .$$

The particular solution of equation (3.3) is given by the expression

$$v(t) = R \sin(\omega t + \phi) , \quad (3.8)$$

where the amplitude of oscillations (R) is found from the formula

$$R = \frac{F/k}{\sqrt{\left(1 - (\omega/\omega_n)^2\right)^2 + \left(2\zeta(\omega/\omega_n)\right)^2}} \quad (3.9)$$

and φ is the phase angle of the displacement with respect to that of the forcing.

In this linear system a plot of non-dimensionalised displacement against frequency ratio ω/ω_n yields a peak at $\omega/\omega_n = 1$ which decays monotonically on either side of the maximum. The height of the peak increases with decreasing damping producing a pair of asymptotes when $b=0$.

In a nonlinear system this peak bends over introducing a phenomenon known as the jump to resonance or the cyclic fold corresponding to the possibility of two alternative responses of different amplitudes for any one given value of the forcing frequency. This situation can be viewed in the small insert diagram at the top right hand side of figure 3.1 with the two alternative periodic steady states characterised by the points A and B.

II.3.2 The Poincaré Section

In classical texts the stability of periodic solutions of dynamical systems is usually discussed in terms of Floquet theory [Jordan and Smith (1977)]. A more general concept which has a heuristically geometric viewpoint is the Poincaré map [Pippard (1985)]. This map is obtained by periodically sampling

the three dimensional phase space (x, y, t) , where $y = \dot{x}$, of the driven oscillator, equation (3.1), and inspecting the projection onto the (x, \dot{x}) plane whenever t is a multiple of the forcing period, here $T = 2\pi/\omega$, see figure 3.2, in which case these samples are referred to as Poincaré sections. A complete set of starts would produce a bundle of trajectories which spiral round the t axis as time advances. However, as we have already seen with reference to the Duffing oscillator, steady state periodic solutions often exist in forced systems usually coexisting with several other periodic motions, so that among this bundle most trajectories will represent transient motions while a few will correspond to periodic solutions. The periodic path will appear to attract the transient trajectories and so is also termed an attractor. The simplest periodic attractor is a fundamental $n=1$ solution whose motion is harmonic, i.e. the motion repeats itself with exactly the same period as that of the forcing. Alternatively a trajectory may repeat itself after n samples such that its period is nT . This type of motion is said to be a subharmonic of order n [note that some authors refer to this type of motion as being of order $1/n$, see Hayashi (1964)]. A further type of periodic motion that is possible is when the trajectory repeats itself once or more within a time interval of the forcing period T , e.g. its period will be a fraction of T , $T/2$ say. Such a motion is called superharmonic but since this type of motion is not usually visible in most mechanical systems it will not be considered in the context of this thesis.

Inspecting the (x, \dot{x}) plane for a single trajectory by

taking Poincaré sections produces a sequence of points, Poincaré points (x_p, \dot{x}_p) , such that if a transient motion decays onto a fundamental harmonic solution then the sequence of points will eventually converge onto a single point. Similarly a subharmonic solution of order n will be represented by the sequence systematically jumping between n points. This situation is illustrated in figure 3.2 where the figure shows transients decaying onto an $n=2$ solution in the three dimensional phase space and also the two dimensional projection on the Poincaré plane. The relationship which governs the behaviour between successive Poincaré points belonging to a transient or steady state trajectory is called the Poincaré map.

Another important class of problems that can be usefully studied by the use of the Poincaré section is that which is governed by a differential equation with periodically varying coefficients [see Flashner and Hsu (1983)].

When considering an autonomous system which exhibits closed orbits or limit cycles then the Poincaré section is obtained by taking a surface such that the flow is everywhere transverse to it. The Poincaré map is then defined on this surface and links the flow to its first return point as illustrated in figure 3.3. These apparently distinct definitions of a Poincaré section can be made to coincide by reducing the non-autonomous system to an autonomous one by the introduction of the dummy cyclic variable $\dot{\psi}=1$, although of course this is at the expense of increasing the dimension of the system by one.

Hence studying the Poincaré map reflects the behaviour of the flow of differential equations which may have arisen from some physical situation. The stability of the discrete dynamical system defined by this Poincaré map is governed by the eigenvalues of the map, sometimes called Poincaré characteristic multipliers. However we note that in general the formulation of the Poincaré map relies on a knowledge of the flow of the system, i.e. the solution. This is clearly not always available and so the Poincaré map cannot usually explicitly be written down but the Poincaré section can be used to calculate successive points or iterations of the map and the stability is then examined via the transient response [Bishop et al. (1986)]. Before we move onto some examples which use this stroboscopic mapping technique we must first determine the stability criteria and bifurcations of a two dimensional map, since it is towards such low dimension systems that we focus our attention.

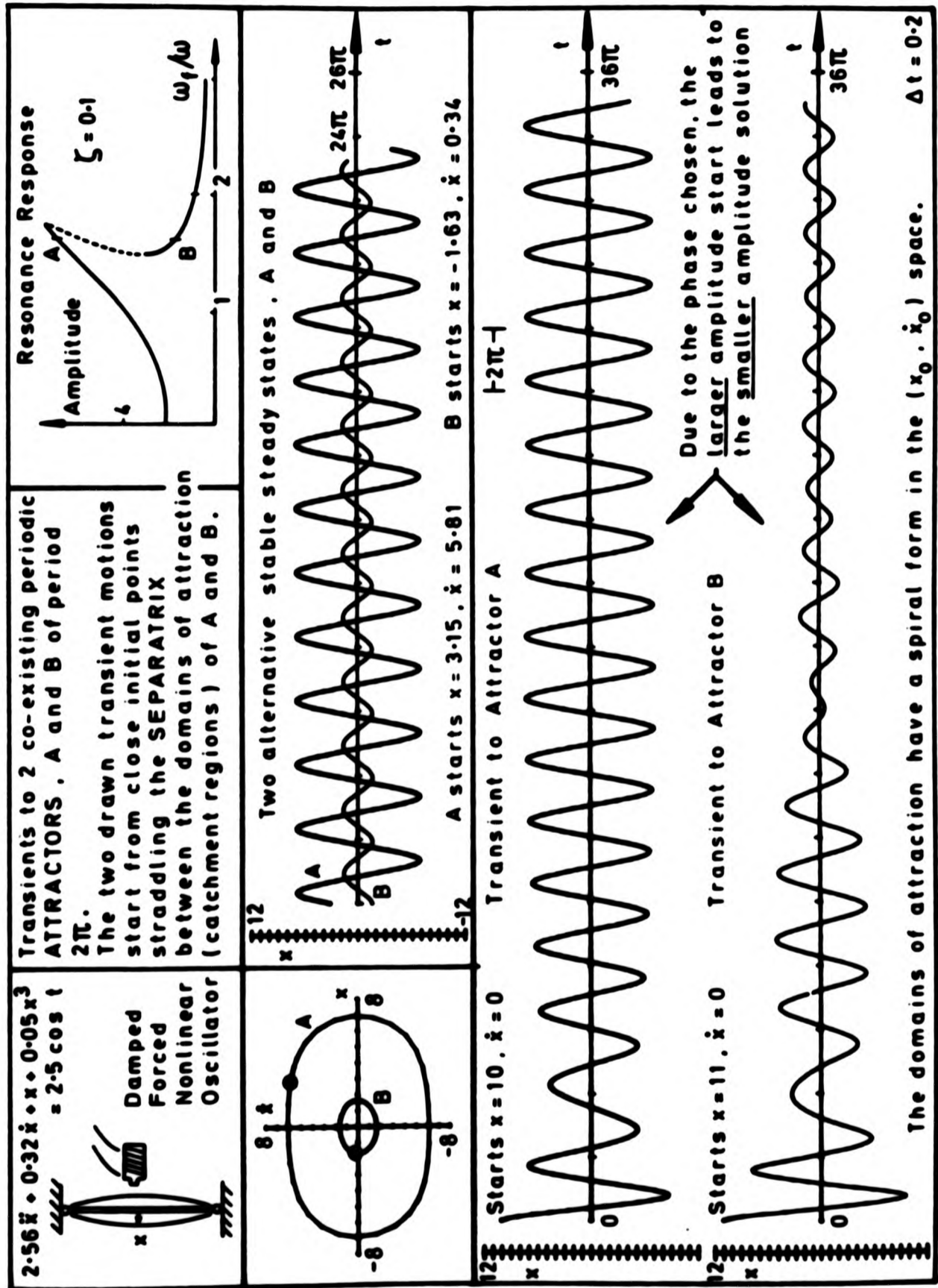


Figure 3.1 The nonlinear response of a Duffing oscillator.

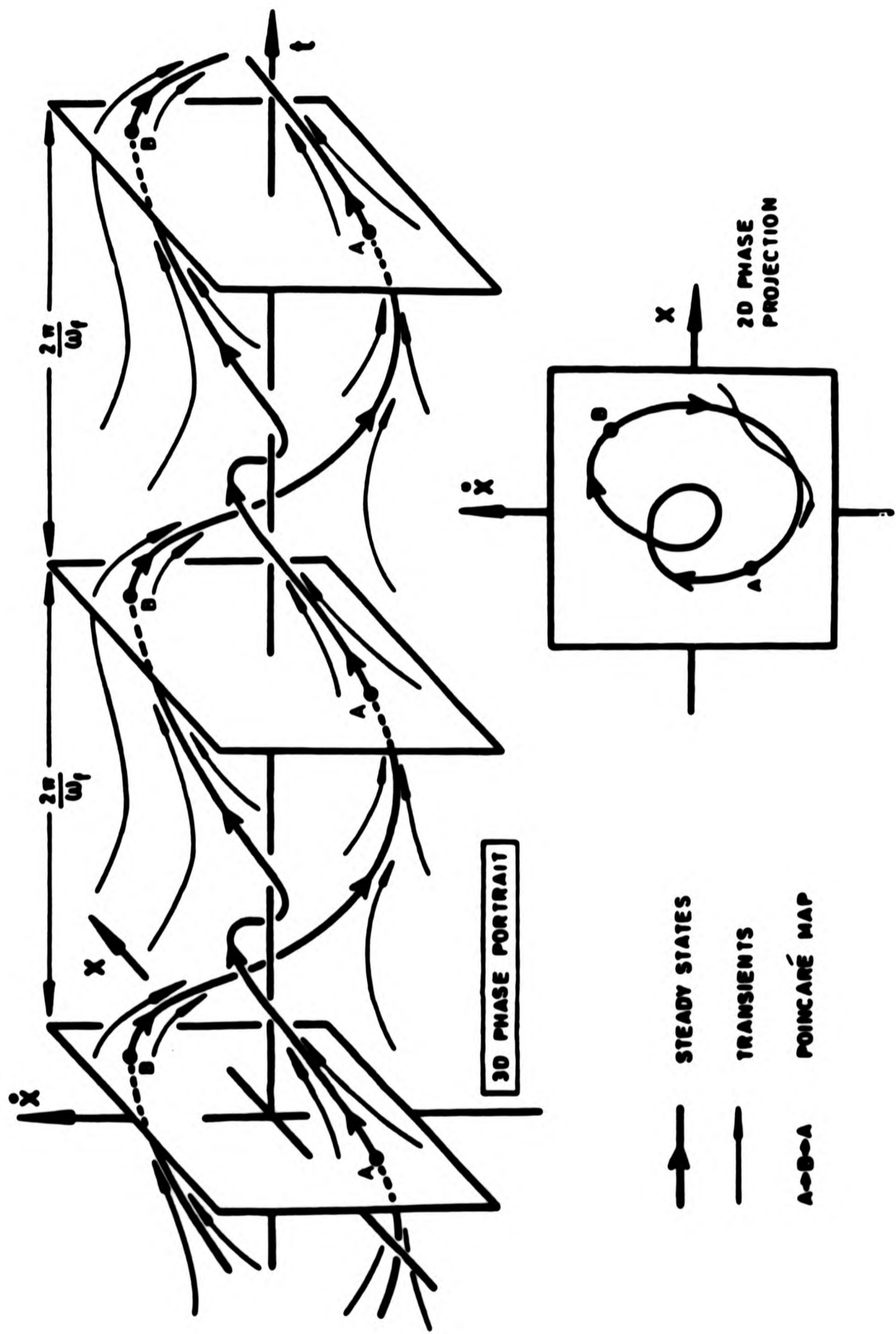


Figure 3.2 The Poincaré section of a three dimensional phase space and the two dimensional phase projection.

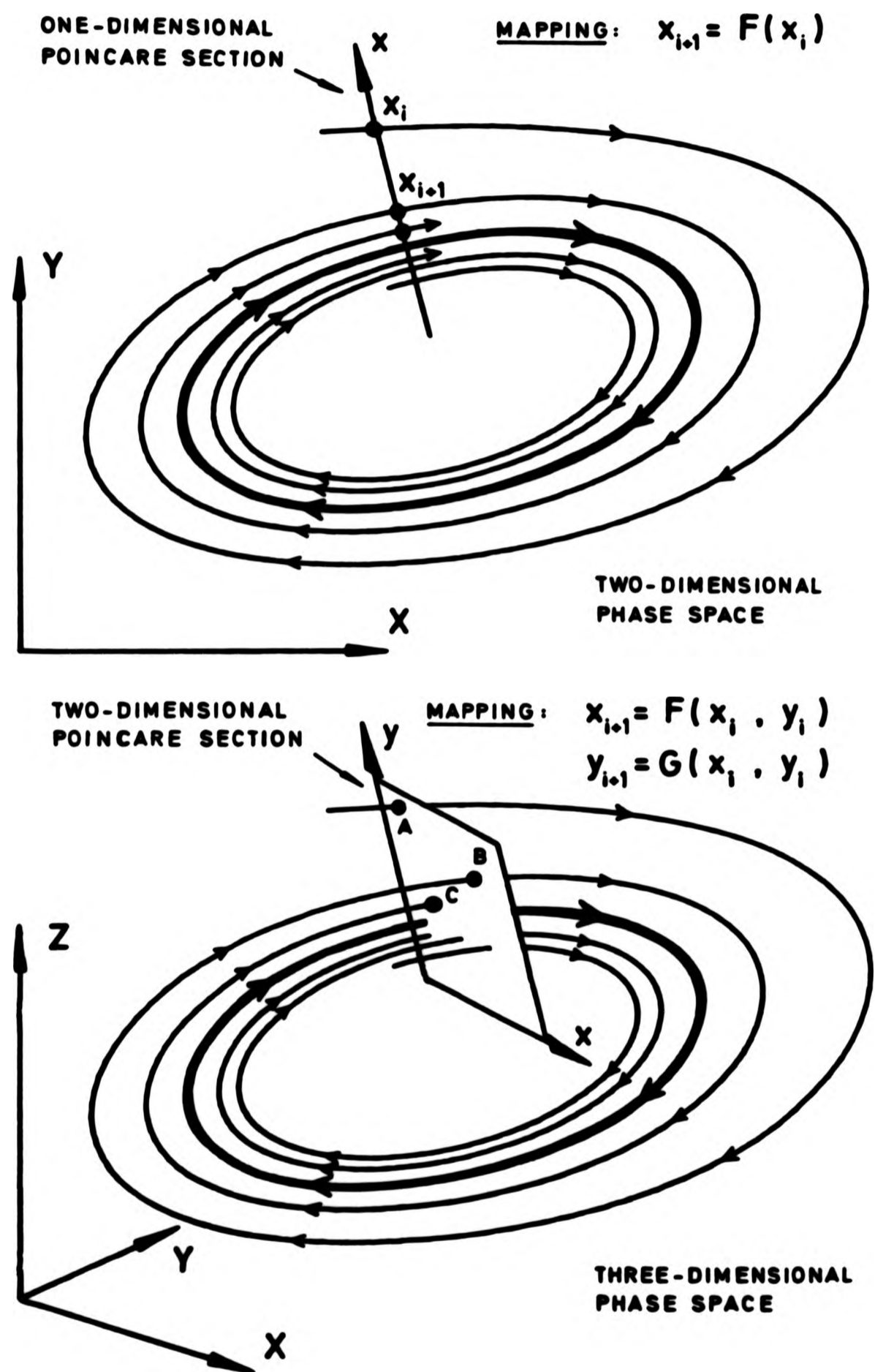


Figure 3.3 One and two dimensional Poincaré sections of an autonomous flow.

CHAPTER II.4

THE STABILITY AND BIFURCATIONS OF MAPS

II.4.1 Introduction

In this chapter we shall make a preliminary study of maps in their own right as discrete dynamical systems [Abraham and Robbin (1977)] which may be considered as Poincaré maps arising from a three dimensional flow or from a discrete model, such as census population dynamics, which involves discrete time steps [May (1976)].

The theoretical study of maps is largely due to the work of Poincaré (1881) and Birkhoff (1911,1913) with more recent contributions by Arnold (1963) and Smale (1963,1967). With improvements to computing facilities the emphasis has recently shifted to numerical investigations of particular maps, notably the map studied by Henon (1976) and the delayed logistic map as studied by May (1976), Aronson et al. (1982) and others.

As we have seen, by considering the representation of a periodic steady state on a Poincaré section, a one dimensional map

$$x_{i+1} = F(x_i) \quad (4.1)$$

can have fixed points at $x=x^e$. If we further consider the response of this map under the operation of a control parameter μ so that

$$x_{i+1} = F(x_i, \mu) , \quad (4.2)$$

then as μ is varied the steady states trace out equilibrium paths in the displacement control space (x, μ) . The local stability of these equilibrium points is guaranteed provided $|F'(x^e)| < 1$; the local bifurcations of an equilibrium path has been covered by various authors [Thompson and Stewart (1986)]. However in this work we are mainly interested in a three dimensional flow which produces a two dimensional map so thus we shall now review the stability criteria for such a map and define the local bifurcations.

II.4.2 The Stability of a Two Dimensional Map

A two dimensional invertible map may be regarded as a Poincaré map produced by a three dimensional flow or possibly as a transformation of a non-invertible one dimensional map [Ott (1981)]. We thus consider the nonlinear map

$$\begin{aligned} x_{i+1} &= F(x_i, y_i) \\ y_{i+1} &= G(x_i, y_i) , \end{aligned} \quad (4.3)$$

and then to examine the stability near an equilibrium point (x^e, y^e) , such that

$$\begin{aligned} x^e &= F(x^e, y^e) \\ y^e &= G(x^e, y^e) \end{aligned} \quad (4.4)$$

we introduce small disturbances ξ and η defined by $x_i = x^e + \xi_i$, and $y_i = y^e + \eta_i$ for all i . The map, equation (4.3), then becomes

$$\begin{aligned} x_{i+1} &= x^e + \xi_{i+1} = F(x^e + \xi_i, y^e + \eta_i) \\ y_{i+1} &= y^e + \eta_{i+1} = G(x^e + \xi_i, y^e + \eta_i) \end{aligned} \quad (4.5)$$

Expanding these functions in a Taylor series about the equilibrium and utilising the equilibrium condition equation (4.4) yields

$$\begin{aligned} \xi_{i+1} &= F_x \xi_i + F_y \eta_i + (F_{xx} \xi_i^2 + 2F_{xy} \xi_i \eta_i + F_{yy} \eta_i^2)/2 + \dots \\ \eta_{i+1} &= G_x \xi_i + G_y \eta_i + (G_{xx} \xi_i^2 + 2G_{xy} \xi_i \eta_i + G_{yy} \eta_i^2)/2 + \dots \end{aligned} \quad (4.6)$$

where all the derivatives are evaluated at the equilibrium point. Now for sufficiently small disturbances we may neglect higher order terms to obtain the variational equation

$$\begin{aligned} \xi_{i+1} &= F_x \xi_i + F_y \eta_i \\ \eta_{i+1} &= G_x \xi_i + G_y \eta_i \end{aligned} \quad (4.7)$$

which may be written in the matrix form

$$\zeta_{i+1} = H \zeta_i . \quad (4.8)$$

If this latter relationship is applied recursively we obtain

$$\zeta_{i+1} = H^{i+1} \zeta_0 , \quad (4.9)$$

for some non-zero initial error vector ζ_0 , from which we can see that the necessary and sufficient condition for the convergence of the map (corresponding to a strictly stable solution) is that H^{i+1} tends to the null matrix as i tends to infinity.

If the eigenvalues of H , denoted by λ say, are real then it is possible to use the Jordan canonical form to show that the requirement for stability of the map is when $|\lambda| < 1$ [see Hoffman and Kunze (1961)]. If in fact one of the eigenvalues lies on the unit circle with the other inside then the linear approximation is not sufficient to establish the stability condition of the fixed point.

If the eigenvalues happen to be complex conjugates then the canonical form can still be used to show that $|\lambda| < 1$ is needed for stability however it is instructive to consider the following theorem [Hirsch and Smale (1973)].

Theorem

Let the eigenvectors of the matrix H be given by $w, \bar{w} = u + iv$ corresponding to the eigenvalues $\lambda, \bar{\lambda} = \alpha + i\beta$, then there exist

a matrix Q such that

$$Q^{-1}HQ = \begin{bmatrix} \alpha & -\beta \\ \beta & \alpha \end{bmatrix} \quad (4.10)$$

In fact Q is given by the matrix $Q=[-v,u]$ and we may use the change of variable

$$\begin{bmatrix} \xi_i \\ \eta_i \end{bmatrix} = Q \begin{bmatrix} x_i \\ y_i \end{bmatrix}$$

so that

$$\begin{bmatrix} x_{i+1} \\ y_{i+1} \end{bmatrix} = Q^{-1}HQ \begin{bmatrix} x_i \\ y_i \end{bmatrix} = \begin{bmatrix} \alpha & -\beta \\ \beta & \alpha \end{bmatrix} \begin{bmatrix} x_i \\ y_i \end{bmatrix} . \quad (4.11)$$

At this point it is convenient to introduce the polar coordinates r and ϑ so that

$$\begin{aligned} x_i &= r_i \cos \vartheta_i \\ y_i &= r_i \sin \vartheta_i, \end{aligned} \quad (4.12)$$

and the eigenvalues may now be given by

$$\lambda = \rho e^{\pm i\vartheta} = \rho(\cos \vartheta \pm i \sin \vartheta) . \quad (4.13)$$

If we now apply the map forward recursively in these new coordinates it can be shown that in general

$$\begin{aligned} r_k \cos \vartheta_k &= r_0 \rho^k \cos(k\vartheta + \vartheta_0) \\ r_k \sin \vartheta_k &= r_0 \rho^k \sin(k\vartheta + \vartheta_0) , \end{aligned} \quad (4.14)$$

i.e.

$$r_k = r_0 \rho^k , \quad \vartheta_k = k\vartheta + \vartheta_0 . \quad (4.15)$$

The latter of these equations may be solved for k to yield

$$r_k = r_0 \rho^{(\vartheta_k - \vartheta_0)/\vartheta} , \quad (4.16)$$

from which it is easy to see that if $\rho < 1$ (i.e. $|\lambda| < 1$) then the trajectory spirals inwards and the equilibrium point is stable. If on the other hand $\rho > 1$ then the trajectory spirals out to infinity and the point is unstable. If $\rho = 1$ then the equilibrium point is a centre and again the linear approximation is no longer sufficient to establish the stability.

This exhausts the possibilities for the eigenvalues of the linear map and we see that the stability criterion is best discussed in the complex plane such that if both eigenvalues lie within the unit circle then the map is strictly (asymptotically) stable. If one or both of the eigenvalues lie outside the unit circle, which forms the stability boundary, then the map is unstable. Then for the map to become unstable the coefficients,

under the influence of a control parameter μ , must vary so that at least one eigenvalue moves outwards and crosses the stability boundary.

If both the eigenvalues are real then there are only two points at which they can cross the stability boundary, namely at $+1$ and -1 . When the critical eigenvalue, λ_1 say, is at $+1$, whilst the other eigenvalue remains inside the unit circle, the system is said to be in a state of incipient divergence. This bifurcation when $\lambda_1 = +1$ is termed the cyclic fold or saddle node bifurcation. If, on the other hand $\lambda_1 = -1$ then the system is in a state of incipient flip, where this flip bifurcation represents a change from a fundamental to a subharmonic motion of any underlying flow. These two instabilities both involve only one critical eigenvalue and are essentially thus one dimensional.

If the eigenvalues are complex they can cross the stability boundary at an angle $\pm \delta$ corresponding to the so called flutter or Neimark instability.

In figure 4.1 the stability transitions for equilibrium states for flows and for periodic orbits or cycles (studied via their Poincaré maps) are summarised in the complex plane. We note that the stability transition of a map when $\lambda_1 = -1$ does not have a counterpart for flows, and it can also be shown that the Neimark bifurcation of a map is more complex than the analogous Hopf bifurcation for equilibria, corresponding to a flow on a

two dimensional torus [Neimark (1949), Abraham and Marsden (1978) or see Iooss and Joseph (1977,1980)].

The movement of the eigenvalues of the matrix H as the control parameter is varied may also be discussed in terms of the trace and determinant of the matrix. If we consider H to be the matrix of coefficients

$$H = \begin{bmatrix} a & b \\ c & d \end{bmatrix}, \quad (4.17)$$

then the trace $T=a+d$ and the determinant $D=ad-bc$ are such that the eigenvalues satisfy the equation

$$\lambda^2 - T\lambda + D = 0. \quad (4.18)$$

The stability criterion and routes to instability as the coefficients of the matrix evolve can thus equivalently be viewed in the (T,D) plane as shown in figure 4.2. Divergence occurs along the line $T=D=1$, flip on the line $T+D=1$ while flutter (the Neimark instability) occurs on the line $D=1$ with points inside these lines representing a stable system.

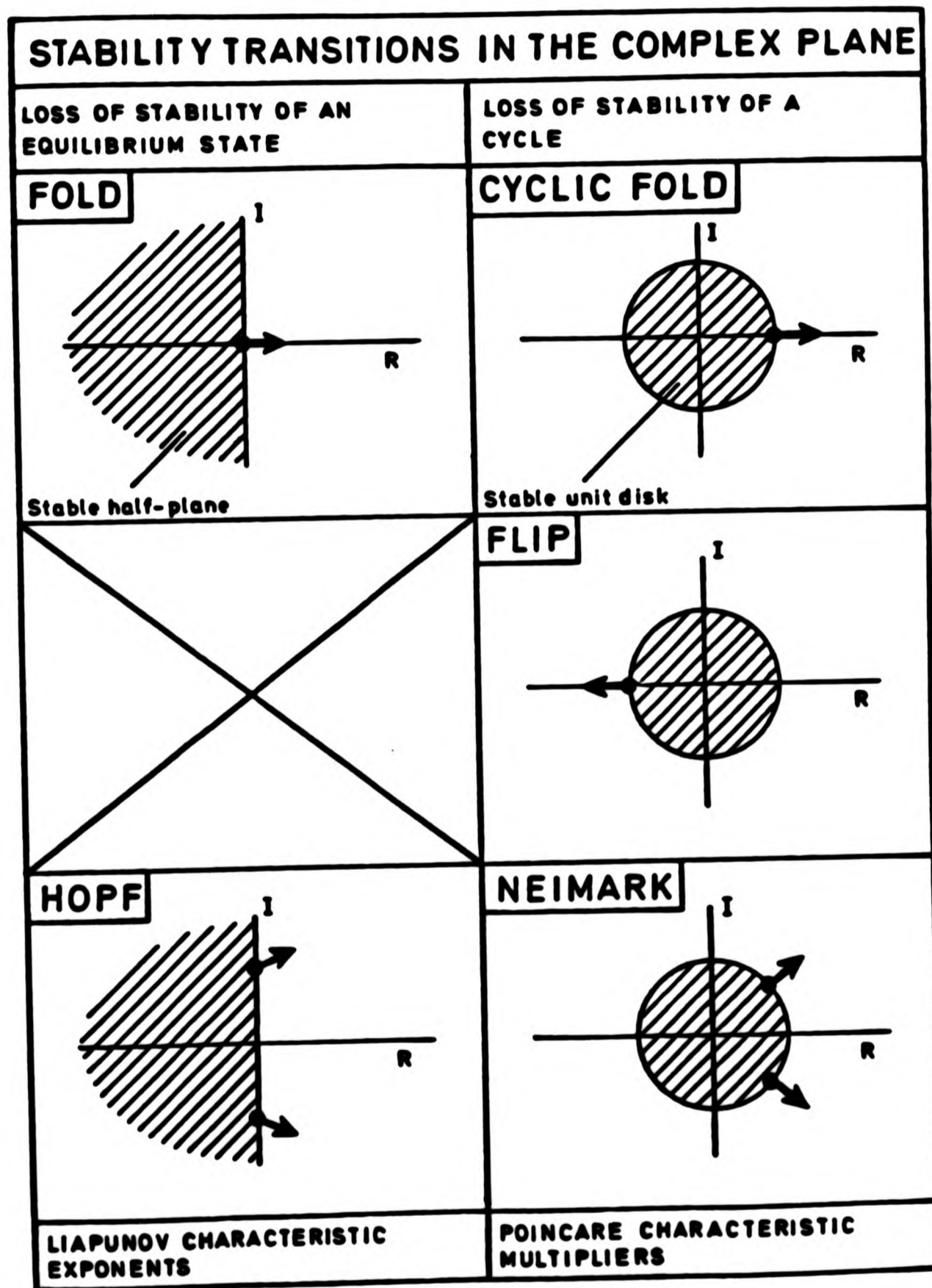


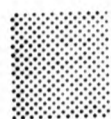
Figure 4.1 Instability transitions of an equilibrium state and the periodic counterparts.

$$x_{i+1} = a x_i + b y_i$$

$$T = a + d, \quad D = ad - bc$$

$$y_{i+1} = c x_i + d y_i$$

$$\lambda = (T \pm \sqrt{T^2 - 4D}) / 2$$



Stable region



Position of eigenvalues in complex plane

(● coincident)

unit circle

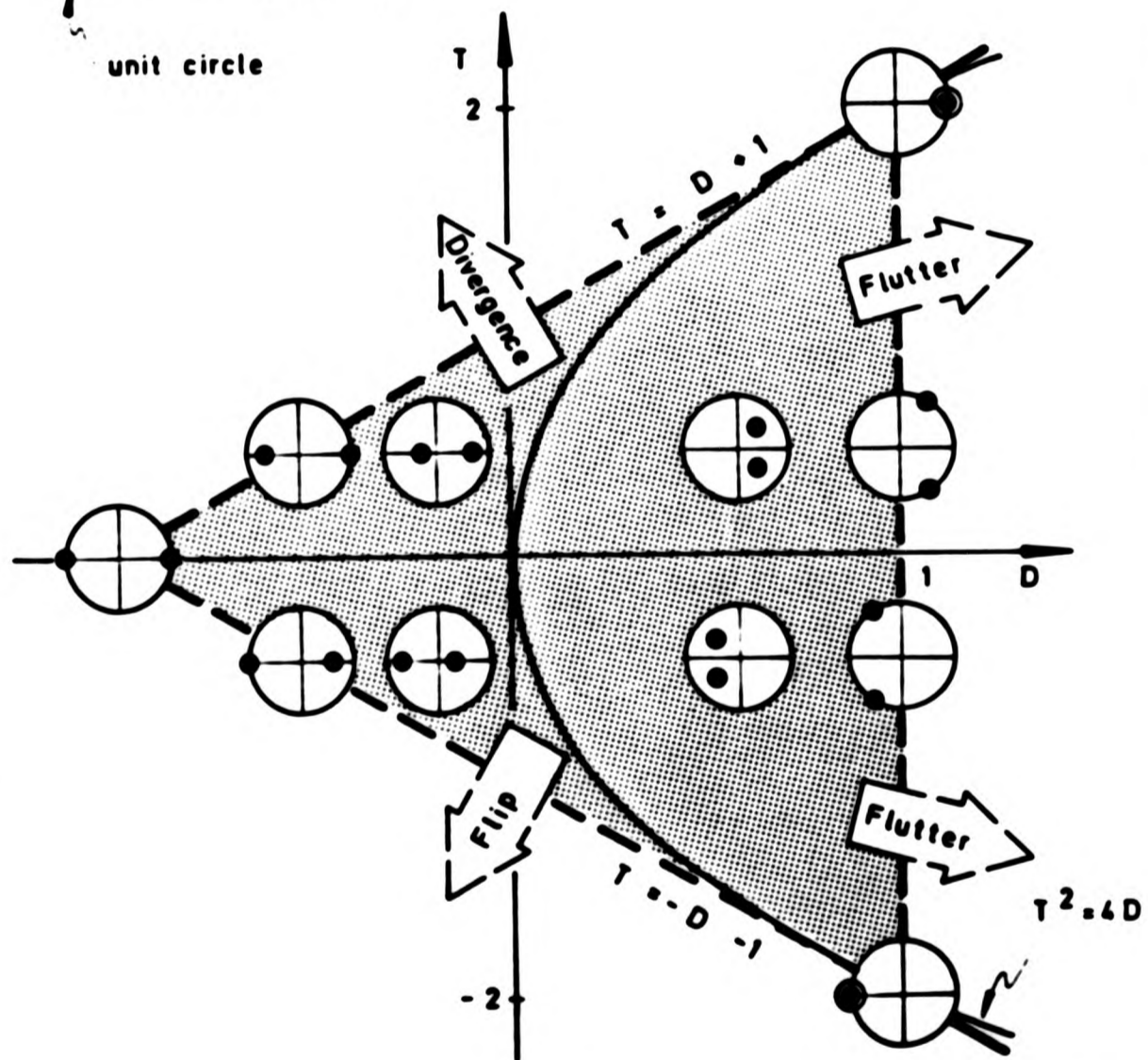


Figure 4.2 Stability region of a two dimensional linear map in the (T, D) plane and schematic inserts showing the position of the eigenvalues in the unit circle.

CHAPTER II.5

THE PREDICTION OF INCIPIENT DYNAMIC INSTABILITIES

II.5.1 Predictions of the Hopf Bifurcation

We have seen in chapter II.2 that the simplest equation which may undergo a Hopf bifurcation is given an autonomous equation that can equivalently be written as the system

$$\begin{aligned}\dot{x} &= y \\ \dot{y} &= -kx - by - cx^3.\end{aligned}\tag{5.1}$$

The trace of the linearised system is given by $-b$ and with determinant k (assumed to be positive). Then with reference to the form of the solution as given in chapter II.2 and referring to figure II.2.2 we see that for b positive trajectories will spiral inwards to form a focus with a solution in exponential form and exponential rate of decay given by $\alpha = -b/2$.

Now, since it is possible to represent any physical system undergoing a Hopf bifurcation locally by a model of the form equation (5.1), a first approach to the prediction of this instability would naturally be to estimate the rate of decay of any oscillations of the physical system and to determine the

point at which the damping becomes zero. The method of calculating this decay is often referred to as a calculation of the logarithmic decrement and, as we shall see in chapter III.2, this method can be used to predict the onset of the Hopf bifurcation in realistic situations. A further point to note is that since it is the linear damping that drops to zero, straight line extrapolations can be made to the point at which oscillations begin.

II.5.2 Determining the Eigenvalues of a Map

From the analysis of the preceding chapter it is clear that the eigenvalues of the linear approximation to a full nonlinear system, locally to an equilibrium point, determine the stability of the map; obtained by taking Poincaré samples. Consequently it is useful to evaluate these linear eigenvalues by considering successive points, or iterations, of the map as obtained from either a transient or a steady state response. As each new point of the map becomes available new estimates of the eigenvalues can be calculated, i.e. real-time updating [Bishop et al. (1986)].

If we assume that the points of the map are determined by a linear discrete system of the form

$$\begin{aligned}x_{i+1} &= ax_i + by_i \\y_{i+1} &= cx_i + dy_i\end{aligned}, \tag{5.2}$$

then given any three consecutive points

$$P_j = (x_j, y_j) , j=i, i+1, i+2 \quad (5.3)$$

it is always possible to solve a set of linear equations to calculate the coefficients of the map. More precisely if we define

$$\Delta = x_i y_{i+1} - x_{i+1} y_i \neq 0 \quad (5.4)$$

then

$$\begin{aligned} b &= (x_{i+2} x_i - x_{i+1}^2) / \Delta , \\ a &= (x_{i+1} - y_i b) / x_i , \\ d &= (x_i y_{i+2} - x_{i+1} y_{i+1}) / \Delta , \\ c &= (y_{i+1} - y_i d) / x_i . \end{aligned} \quad (5.5)$$

It is assumed that for this map the fixed point is at the origin however, if this is not the case, but the location of the equilibrium point is known then a simple transformation can be used to shift the origin accordingly.

Now if additional points of the map can be obtained that belong to a single transient response (i.e. before the influence of some further disturbance) then a sequence of linear maps can be calculated which, with increasing accuracy as the transient decays, approximate the Poincaré map of the system. This method

for tracking the eigenvalues of a transient response for convenience will be called the three-point method.

The above method is somewhat theoretical since it is unusual to know, a priori, the exact location of the fixed point. If this is the case then one additional iteration of the map, P_{i+3} , is required to obtain the appropriate number of linear equations for a unique solution for the unknown equilibrium point (x^e, y^e) as well as the coefficients of the system equation (5.2). This technique will thus be called the four-point method and might be used, for instance, in an evolving system.

Using either of the above methods for any particular set of points (either three or four) the stability of the system can be determined by calculating the trace and determinant of the map or equivalently the eigenvalues, since

$$\begin{aligned} T &= a + d \\ D &= ad - bc \end{aligned} \quad (5.6)$$

where

$$\lambda = (T \pm \sqrt{T^2 - 4D}) / 2 \quad (5.7)$$

In a changing physical system the eigenvalues can be tracked using either of the above methods by examining the transient response of the system since in most physical

situations of interest there is sufficient 'noise', or in the case of the North sea sufficient irregularity, to create a series of such transients as the system evolves in some way towards an instability. These eigenvalues can then be used to warn of any such incipient instability. Before we move on to describe some of these predictive techniques it is first of all worthwhile to consider local approximations for the flip and the fold instabilities.

From the previous chapter we note that the flip and fold bifurcations essentially involve the movement of only one eigenvalue. It would therefore seem sensible to seek a reduced system of one dimension that preserves all the qualitative structure of the full system as these instabilities are approached. This is the central theme of the centre manifold method, namely the idea that the system will exhibit its bifurcational behaviour on a manifold associated with the critical eigenvalue. This is of particular importance if the system is approaching a flip bifurcation where subharmonic motion is apparent and the corresponding Poincaré map is quickly attracted to and then oscillates close to the critical eigenvector (the centre manifold in this case). An example of this flipping motion can be seen in figure 5.1 where the Poincaré points are joined here by straight lines (this example is not that of just a simple two dimensional map but that of the flip bifurcation arising in the motion of a marine structure to be considered later in chapter III.4).

From a computational viewpoint no changes are necessary to either the three- or four-point methods to cope with a fold bifurcation but there are certain problems with approximating a system near a flip bifurcation. In particular if successive iterations of the map lie on the critical eigenvector then the equations for the solution of the system coefficients become singular such that as a transient motion approaches this flipping behaviour the system is ill-conditioned. However, since the manifold is here one dimensional, it would seem sensible to ignore the non-critical eigenvalue and approximate the system by a one dimensional Poincaré map and consider successive points of a transient response to be governed by a linear map of the form

$$x_{i+1} = \lambda x_i \quad (5.8)$$

If, as before, we are tracking a transient response then a sequence of estimates for this critical eigenvalue can be obtained which require $|\lambda| < 1$ for stability. We shall call this method the centre manifold method.

The three methods introduced here will be used in part III to monitor the stability of physical systems and used in conjunction with the information of the next section to predict the onset of typical instabilities of structures oscillating due to the action of ocean waves.

II.5.3 The Prediction of the Static Fold

Despite stating earlier that the static fold bifurcation will not be discussed in this thesis, it is nevertheless instructive to consider the prediction of such an event for a continuous system so that certain comparisons can be made with the corresponding bifurcation of a map, i.e. the cyclic fold.

If we consider the continuous system

$$\begin{aligned}\dot{x} &= jx + ky \\ \dot{y} &= lx + my \quad ,\end{aligned}\tag{5.9}$$

then the trace and determinant are given by

$$T = j + m \quad , \quad D = jm - kl \quad ,\tag{5.10}$$

with eigenvalues given by the characteristic equation

$$\lambda^2 - T\lambda + D = 0 \quad .\tag{5.11}$$

If we further imagine the system to be undamped (the term damping is usually only used for the decay characteristics of a single equation but here we consider the term to correspond to the more general definition of a conservative system) then the eigenvalues will lie on the imaginary axis such that

$$\lambda = \pm i\omega \quad .\tag{5.12}$$

We see that the only way in which the fold bifurcation can occur is if the two eigenvalues approach the origin along the imaginary axis, coalesce and then move apart with both eigenvalues real, and one positive. As this fold is approached the solution will take the general form

$$x = \sin \omega t , \quad (5.13)$$

and it has been shown that [Thompson (1982), also see Thompson and Virgin (1986)] if the coefficients of the linear system depend on a local coordinate (s) then as the eigenvalues near the origin this parameter varies according to the following relationship

$$\omega^2 \propto s . \quad (5.14)$$

In addition to this, since the equilibrium path itself is undergoing a fold whose universal canonical form is naturally quadratic, then s^2 is proportional to some global control parameter μ so that in fact

$$\omega^4 \propto \mu . \quad (5.15)$$

This relationship can be used to form a prediction of the point at which the equilibrium path folds resulting in the response jumping to a remote state of higher amplitude.

If we now consider a system which is lightly damped then the corresponding movement of the eigenvalues is shown in the left hand diagrams of figure 5.2. We note here that a predictor based on the relationship (5.15) actually predicts the point at which the eigenvalues meet, i.e. the point at which vibration ceases, but this itself being near to the fold point (in terms of μ) proves a useful predictor of the fold.

II.5.4 The Prediction of the Cyclic Fold

The cyclic fold bifurcation of a map occurs when the resonance response of a periodically oscillating system folds over producing a jump to resonance. The question that naturally arises is can the same type of argument used in the previous section be applied to predict this cyclic jump phenomenon?

If we refer back to the stable region for a map (figure II.4.2) then we see that for an undamped discrete dynamical system the only way in which a fold can occur is if the eigenvalues move around the unit circle, which forms the stability boundary for the eigenvalues, meet at +1 and then one eigenvalue passes outwards in a positive direction. The corresponding movement of the trace and determinant of this discrete system is given in the right hand diagrams of figure 5.2.

Taking, as an initial step, a first order approximation to the derivatives of the system equation (5.9) yields a discretisation

$$\begin{aligned}x_{i+1} &= (1 + \delta t j)x_i + ky_i \delta t \\y_{i+1} &= lx_i \delta t + (1 + \delta t m)y_i.\end{aligned}\tag{5.15}$$

The trace and determinant of this discrete system are found by

$$\begin{aligned}T &= 2 + (j+m) \delta t \\D &= (1 + \delta t j)(1 + \delta t m) - kl(\delta t)^2,\end{aligned}\tag{5.16}$$

and we see that as δt tends to zero, i.e. as the discrete system approximates the continuous system, T tends towards +2 and D towards +1. This is the region at the apex of the flutter and divergence boundaries and thus, heuristically, the result $\omega^2 \propto s$ for a discrete system is proved from the corresponding result from a continuous system.

Thus (heuristically) we have shown that if a stability analysis were performed at various points along an equilibrium path then ω^2 drops to zero linearly if plotted against some local control parameter s . Close to a fold in the response curve this local parameter varies parabolically with a global parameter describing some change in the system in such a way that ω^4 now drops linearly to zero as the fold is approached. Again though, for lightly damped systems the prediction is in fact the point at which the eigenvalues coincide, see the point

A marked on figure 5.3. In certain physical systems the folding of the resonance response curve may be very sharp so that the valid region of the ω^4 predictor may be quite local to the fold itself, see figure 5.4.

II.5.5 Map Rotations and Orbit Numbers

(a) Definitions

In this section we intend to continue an investigation of the prediction of the cyclic fold and shall study the local behaviour of the map in more detail. If we return to the movement of the eigenvalues as a cyclic fold is approached (figure 5.3) then we see that the position of the system in the (T,D) plane moves along the Neimark stability boundary. With the eigenvalues on the unit circle the map is in a condition of neutral stability and therefore local points produced by successive iterations rotate for an infinite number of times neither converging nor diverging. Furthermore, as the coefficients of the system are varied so that the eigenvalues move around the unit circle and towards confluence at +1, the number of iterations that are required for a complete rotation of 2π about the origin increases. In order to investigate this behaviour further it is possible to use the classical definition of the rotation number as follows:

Definition 1

If the $(k-1)$ th iteration of a map produces the point (x_k, y_k) , which may also be represented in polar coordinates by (r_k, ϑ_k) , then the rotation number R is defined by the expression

$$R = \lim_{k \rightarrow \infty} \frac{2\pi k}{(\vartheta_k - \vartheta_0)}, \quad (5.17)$$

where ϑ_k is defined on the real axis and not modulus 2π [see Aronson et al. (1982)]. This definition of the rotation number is valid for a general nonlinear map but if we consider the linear case then considerable simplifications are possible.

As we have seen in chapter II.4 when the eigenvalues are complex, as they are along the Neimark bounday, we may use a similarity transformation to produce a map in the form

$$\begin{aligned} x_{i+1} &= \alpha x_i - \beta y_i \\ y_{i+1} &= \beta x_i + \alpha y_i \end{aligned} \quad (5.18)$$

where the eigenvalues of the linear map are given by

$$\lambda = e^{\pm i\vartheta} \quad (5.19)$$

Then as we have seen

$$\vartheta_k = k\vartheta + \vartheta_0 \quad (5.20)$$

so that in fact the rotation number is given by

$$R = 2\pi/\delta . \quad (5.21)$$

This expression may be reduced still further if we let $\delta = 2\pi\varphi$ to give

$$R = 1/\varphi . \quad (5.22)$$

This definition is a function of the eigenvalues only and, since these are invariant under a similarity transformation, then this definition also holds for a general linear map whose eigenvalues are complex. The frequency of rotation of the map is given by

$$\omega = 1/R = \varphi . \quad (5.23)$$

We should note here though that the constant angular step implied by equation (5.20) only holds in the transformed coordinate system and will not hold necessarily in the original space in which we are obliged to perform our prediction measurements.

As an alternative to the above definition of rotation number, it is possible to use instead a first approximation to the period. Rather than consider the limiting behaviour of the rotations we calculate the number (n) of iterations of the map needed before a single rotation of 2π has been surpassed. It

is possible to see from figure 5.5 that an orbit number can be obtained by a simple geometric construction [see Bishop and Franciosi]. In fact it is given by n (defined above) plus the fractional part of the $(n+1)$ th iteration where it intersects the line from the origin to the starting point, see figure 5.5. This new definition can be written in precise analytical form as follows:

Definition 2

The orbit number N of a two dimensional map is given by

$$N = n + f , \quad (5.24)$$

where n is the least integer such that

$$|\arg(P_{n+1}) - \arg(P_n)| > 2\pi , \quad (5.25)$$

P_n being the point whose coordinates are (x_n, y_n) . The fractional part f is given by

$$f = \frac{\overline{P_n M}}{\overline{P_n P_{n+1}}} = \left(\frac{(x_m - x_n)^2 + (y_m - y_n)^2}{(x_{n+1} - x_n)^2 + (y_{n+1} - y_n)^2} \right)^{\frac{1}{2}} \quad (5.26)$$

where the coordinates of the point $M = (x_m, y_m)$ are found from

$$y_m = \frac{x_n y_{n+1} - x_{n+1} y_n}{(x_0/y_0)(y_{n+1} - y_n) + (x_n - x_{n+1})} , \quad (5.27)$$

and

$$x_m = x_0 y_m / y_0 .$$

To show that this new definition is well posed we must first prove the following theorem:

Theorem

The orbit number of a two dimensional linear map is a function of the invariants of the map and is independent of the initial start given to the iterations.

Proof

Consider a general two dimensional linear map

$$\begin{aligned} x_{n+1} &= ax_n + by_n \\ y_{n+1} &= cx_n + dy_n \end{aligned} \tag{5.28}$$

for $n=0,1,2,\dots$ and given the initial start $P_0=(x_0,y_0)$. It is easy to verify that successive points can alternatively be defined by the relationships

$$\begin{aligned} x_n &= R_n(a,b,c,d)x_0 + bS_{n-1}(a,b,c,d)y_0 \\ y_n &= cS_{n-1}(a,b,c,d)x_0 + R_n(d,b,c,a)y_0 \end{aligned} \tag{5.29}$$

If for ease of notation we define $Q_n(a,b,c,d)=R_n(d,b,c,a)$ then we may drop all the arguments of the polynomials R,S and Q to give

$$\begin{aligned}x_n &= R_n x_0 + b S_{n-1} y_0 \\y_n &= c S_{n-1} x_0 + Q_n y_0\end{aligned}\quad (5.30)$$

where the polynomials satisfy the following relationships

$$\begin{aligned}R_{n+1} &= a R_n + b c S_{n-1} \\S_n &= d S_{n-1} + R_n = a S_{n-1} + Q_n\end{aligned}\quad (5.31)$$

For $n > 1$ the polynomials S_n are given by the expression

$$S_n(a, b, c, d) = \sum_r^{n-r} C_r (a+d)^{n-2r} (bc-ad)^r, \quad (5.32)$$

where ${}^n C_r$ are the binomial coefficients and $r=0, 1, 2, \dots, (n-\delta)/2$; $\delta=0$ if n is even, or $\delta=1$ if n is odd. As a consequence S_n may be written in terms of the trace and determinant of the linear system, i.e. $S_n = S_n(T, D)$.

We may use equation (5.29) to substitute for x_n, y_n etc. to calculate y_m which yields

$$y_m = \frac{a_1 x_0^2 y_0 + a_2 x_0 y_0^2 + a_3 y_0^3}{b_1 x_0^2 + b_2 x_0 y_0 + b_3 y_0^2}, \quad (5.33)$$

where the coefficients are given by

$$\begin{aligned}a_1 &= c(R_n S_n - R_{n+1} S_{n-1}) \\a_2 &= R_n Q_{n+1} - Q_n R_{n+1}\end{aligned}$$

$$a_3 = b(Q_{n+1}S_{n-1} - Q_n S_n)$$

and

$$\begin{aligned} b_1 &= c(S_n - S_{n-1}) \\ b_2 &= (Q_{n+1} - Q_n) - (R_{n+1} - R_n) \\ b_3 &= -b(S_n - S_{n-1}) \end{aligned} \quad (5.34)$$

This latter expression may now be used in the equation for the fractional part to evaluate f in terms of x_0 and y_0 and the polynomials Q_n, S_n, R_n , etc.. Finally by comparing coefficients of x_0 and y_0 , and their powers, in the numerator and denominator of the resulting expression for f , after some algebra, it is possible to show that

$$f = \frac{S_n}{S_n - S_{n-1}} \quad (5.35)$$

That is f depends only upon n and the invariants of the matrix.

Q.E.D.

We emphasize that the perhaps more obvious definition of f based on the angular ratio

$$\frac{|\arg(P_0) - \arg(P_n)|}{|\arg(P_{n+1}) - \arg(P_n)|}$$

would be unsatisfactory since the independence from initial condition would be lost.

As previously stated, we wish for the moment to consider the behaviour of an area preserving map whose determinant is equal to +1, and whose eigenvalues move around the unit circle. It is useful to consider the simplest system that displays these characteristics, namely

$$\begin{aligned} x_{i+1} &= \mu x_i - y_i \\ y_{i+1} &= x_i \end{aligned} \quad (5.36)$$

In fact by the use of similarity transformations it is possible to transform any two dimensional linear area preserving map into a map of this form [see Bishop and Franciosi] therefore the following remarks are without loss in generality. This being the case we see that the determinant is equal to +1 and the requirement that the eigenvalues should move around the unit circle implies that μ must vary from -2 to +2. A point worth noting here is that with $D=1$ the polynomials are related to the Chebyshev polynomials^a of the second kind by

$$S_n(z) = U_n(z/2) \quad (5.37)$$

The properties of the map as we now move along the $D=1$ boundary are now recovered by the properties of the Chebyshev polynomials, particularly the occurrence of closed orbits of the map.

(b) Closed orbits

A closed orbit of the map occurs whenever the fractional part f is identically equal to zero but, since this itself is given in terms of the polynomials S_n , we see that closed orbits will occur at the zeros of the Chebyshev polynomials which are all real and lie in the range $(-2, +2)$.

When φ is a rational number, $\varphi = p/q$ say, the system performs exactly p rotations of 2π about the origin so that with $D=1$ its orbit is formed by q points. In this case we must have $S_{n-1} = 0$ and $S_n = 1$ and the value of the trace at which this occurs is given by the second zero of the Chebyshev polynomial, i.e.

$$\mu = 2\cos(2\pi p/q) . \quad (5.38)$$

With φ a rational number this corresponds to the eigenvalues being roots of unity so we see that the rotation number and the orbit number coincide at the integer numbers corresponding to closed orbits.

To act as a comparison between the two definitions of map rotation, and since we are expecting the frequency to drop to zero quadratically, we show here in figure 5.6 a computed graph

of $1/R^2$ plotted with $1/N^2$ for values of μ between -2 and +2. As we have seen, when N is an integer the two values must coincide but between two such points the curve of $1/N^2$ exhibits a 'scallop'. This behaviour is apparent for small integer values of the period but as we approach the fold at $\mu=2$ this characteristic becomes less critical and the two approximations closely agree. This scalloping behaviour can be examined if the continuity of the orbit number as a function is questioned since, although N and its first derivative are continuous, the second derivative is however discontinuous which may account for the discrepancy, it being subsequently accentuated by the square law.

(c) The area enclosed by three mapping points

If we consider the area, A_n , of the triangle enclosed by three consecutive mapping points, P_n , P_{n+1} and P_{n+2} say, then it can be shown that

$$2A_n = x_n y_{n+1} - x_{n+1} y_n + x_{n+1} y_{n+1} - x_{n+2} y_{n+1} + x_{n+2} y_n - x_n y_{n+2} \quad (5.39)$$

Equation (5.28) can be used to substitute for x, y etc. in this expression to give

$$2A_n = a_1(n)x_0^2 + a_2(n)x_0 y_0 + a_3(n)y_0^2, \quad (5.40)$$

where (neglecting arguments) the coefficients of this expression are given by

$$\begin{aligned} a_1 &= c(L_{n+1}z_{n+1} - L_n z_{n+2}) \\ a_2 &= bc(W_{n+2}z_{n+1} - W_{n+1}z_{n+2}) \\ a_3 &= -b(L_{n+1}W_{n+1} - L_n W_{n+2}) \end{aligned} \quad (5.41)$$

in which, following the earlier notation

$$\begin{aligned} L_{n+1} &= S_{n+1} - S_n \\ z_{n+1} &= R_{n+1} - R_n \\ W_{n+1} &= Q_{n+1} - Q_n \end{aligned} \quad (5.42)$$

If we now consider the ratio of successive areas obtained by further points of the same sequence it can be shown that

$$A_{n+1}/A_n = ad - bc = D. \quad (5.43)$$

This fact will be used later in chapter III.3 to predict the onset of the Neimark bifurcation .

II.5.6 Instability Predictions Near a Cyclic Fold

Near the folding of a resonance response curve, as shown in figure 5.3, the orbit number N may be approximated by the integer valued n , i.e. the fractional part is ignored and we are

approximating the orbit number by the period of rotation. In the neighbourhood of the fold bifurcation point the frequency $\omega = 1/N$ drops to zero and its square ω^2 varies linearly with the trace (μ or more generally T). Since the definition now coincides with the rotation number we see that in fact

$$\omega = \frac{1}{2\pi} \arctan \sqrt{(4-T^2)}/T \quad (5.44)$$

As T tends towards $+2$ this frequency may be expanded in a power series to obtain

$$\omega = \frac{1}{2\pi} \left(\frac{(4-T^2)^{1/2}}{T} + \frac{(4-T^2)^{3/2}}{3T^3} + \dots \right) \quad (5.45)$$

Hence a graph of ω^2 plotted against T will locally be given by

$$\omega^2 = \frac{4 - T^2}{4\pi^2 T^2} \quad (5.46)$$

Putting $\delta = 2-T$ and linearising with respect to δ we obtain

$$\omega^2 \sim \delta / (4\pi^2) \quad (5.47)$$

which shows that locally ω^2 varies linearly with the control δ as the trace tends towards $T=2$, confirming our earlier heuristic argument carried over from the static fold.

If the system is not area preserving but its determinant is constant, slightly less than 1, then the eigenvalues are constrained to move along a path of constant radius as illustrated in the right hand diagrams of figure 5.3. For such a lightly damped system the ω^2 relationship can now be used to predict the point at which the eigenvalues become coincident. Furthermore the definition of the orbit number, or the rotation number in terms of the angle ψ rather than the limit, do not require $D=1$, they are in fact quite general so consequently the vanishing of N (or R) may be used as a predictor of this point of confluence. Now if a system is lightly damped then this coincidence will be close and prior to the fold bifurcation and so predictions should be on the safe side.

It should be noted here that as the eigenvalues move around the unit circle towards the point at +1 the rate at which they do so as a function of the global parameter need not necessarily be a linear one. In the three dimensional diagram of figure 5.7 we see that the approach to the fold point is quadratic in nature and, as a consequence, for equal incremental increases in the control parameter μ the eigenvalues at first steadily move around the unit circle or just inside it. Near the fold this quadratic approach causes the movement of the eigenvalues to speed up considerably, a point illustrated later in chapter III.4.

II.5.7 The Use of Orbit Numbers to Predict the Folding of a Periodic Oscillation

(a) Duffing's equation

As an example of how the orbit number may be used to predict a fold bifurcation in the resonance response of a periodically oscillating system we shall first consider a computational application to Duffing's equation in the form

$$\eta^2 \ddot{x} + 2\zeta\eta \dot{x} + x + \alpha x^3 = F_0 \cos t \quad (5.48)$$

If we choose η to be our control parameter and fix the variables $\zeta=0.1$, $\alpha=0.005$ and $F_0=2.5$ then the equation exhibits a jump to resonance at a cyclic fold near $\eta=1.46$. Some computed Poincaré maps are shown in figure 5.8 for various values of the control parameter in the neighbourhood of the critical point. The orbit number was calculated for a series of values of η using the earlier definition and used to produce prediction curves as shown in figure 5.9.

The concave nature of the ω^4 prediction curve in this system allows straight line predictions to be always on the safe side while those predictions based on the ω^2 curve may, in this particular case, overestimate the fold unless local extrapolation are used.

The scalloping behaviour of the prediction curves is

clearly evident in the top two diagrams, it being possible to reduce the extent of the scallops by calculating the orbit number after more than a single rotation of 2π about the origin as shown in the lower diagrams of figure 5.9. However, one of the advantages gained by taking the orbit number from one rotation is that it is a quick method of determining the frequency so there must be a trade off between speed and accuracy, particularly bearing in mind that either for systems with relatively heavy damping or for systems whose period is large an estimation based on only one rotation might be unavoidable.

(b) An experimental beam

The rotation of a map will manifest itself as a low frequency beat on top of a steady state periodic response and this beat can be used in exactly the same way as the frequency of a map. This fact is clarified in the diagrams of figure 5.10 which show a three dimensional phase space of a periodically driven oscillator where the Poincaré section defined by $x=0$ will produce as mapping variables the amplitude of response (A) and the time t , the latter being replaceable by the phase. Then the rotation of the amplitude-phase map will manifest itself in the $x(t)$ time history as a beat on the amplitude as illustrated. A computational study of this beat phenomenon has been made by Thompson and Virgin (1985) and included here is a figure taken from their paper which shows the beats produced by the

oscillator (see figure 5.11)

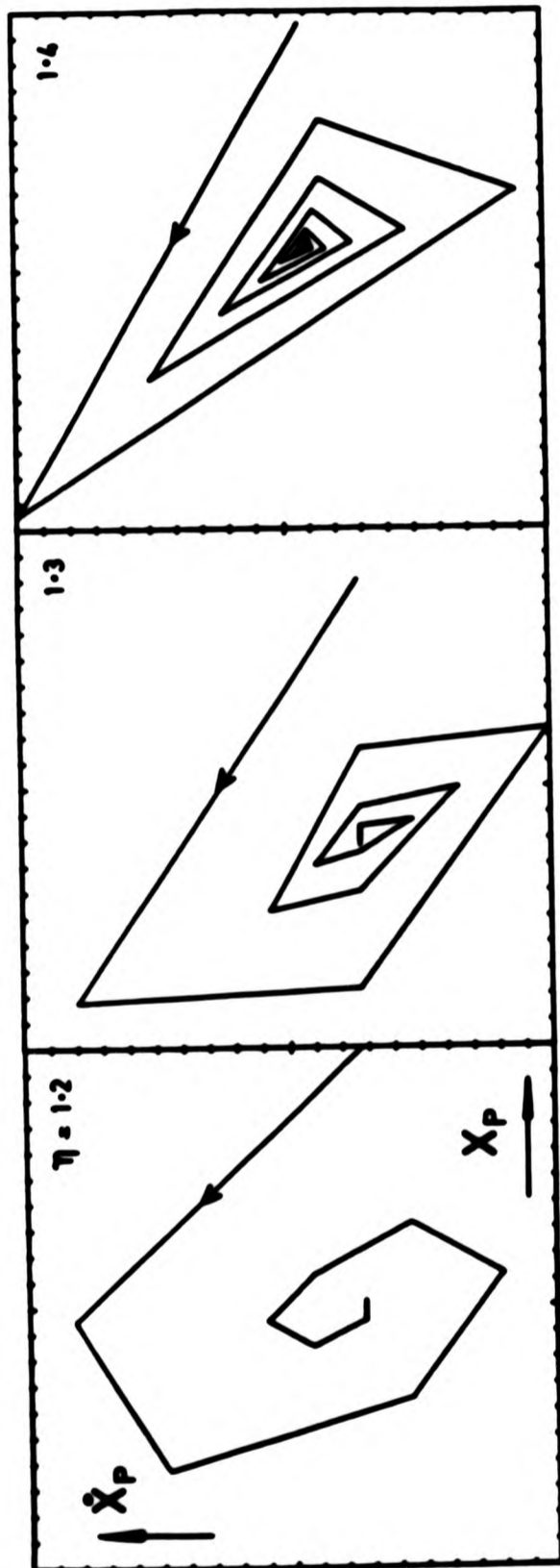
$$\ddot{x} + x^3 = B \cos t \quad (5.49)$$

for various values of the forcing amplitude B . Also shown in this figure is a successful use of the ω^4 predictor (here denoted by p^{-4}), estimating the point at which a fold occurs.

To conclude this study of the prediction of the cyclic fold we consider an experimental study of a thin steel beam clamped between two rigid supports and driven to resonance by an electromagnet [see Bishop and Franciosi]. The results are briefly summarised in figure 5.12 where the top diagram shows the experimentally determined response curve with a jump to a large amplitude resonance at a value of the forcing frequency just below 58Hz. The lower diagram shows the two beat frequency predictors, the beats in this case being measured manually off a trace produced by a u/v recorder. In this physical system the ω^2 curve is clearly the best predictor with the ω^4 curve approaching the axis in a most undesirable way. This was perhaps as to be expected since if we look at the resonance response curve in figure 5.12 the folding of the response is very rapid so that its parabolic nature will not be significant over the wide range of forcing frequency considered here.

II.5.8 Conclusions

In overall conclusion then we have shown that either by estimating the decay rate of transients or by evaluating the eigenvalues of the map of the governing periodic behaviour we can, theoretically at least, predict the onset of low dimension bifurcations of continuous and discrete systems. In part III we shall apply these predictive techniques to physical situations and, as we shall see, with certain limitations the methods prove to be successful in a variety of 'real' problems.



Sample Poincaré maps (all to the same arbitrary scale)

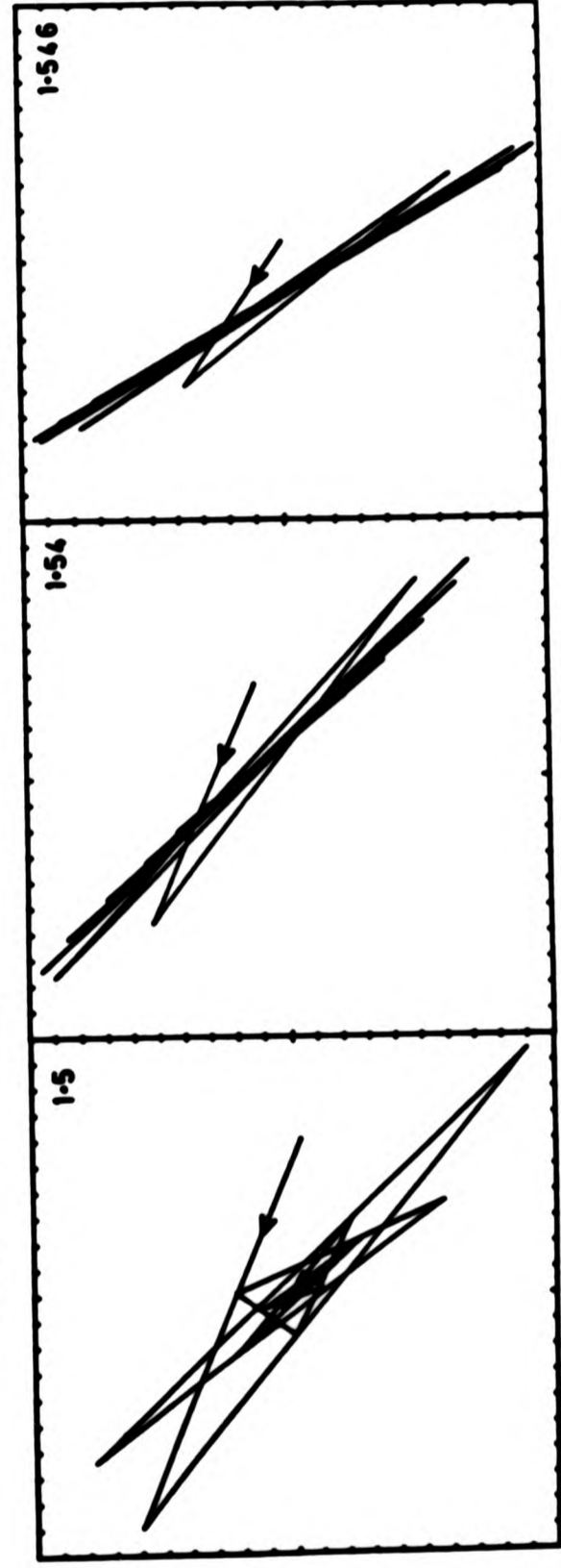


Figure 5.1 Poincaré maps approaching a flip bifurcation.

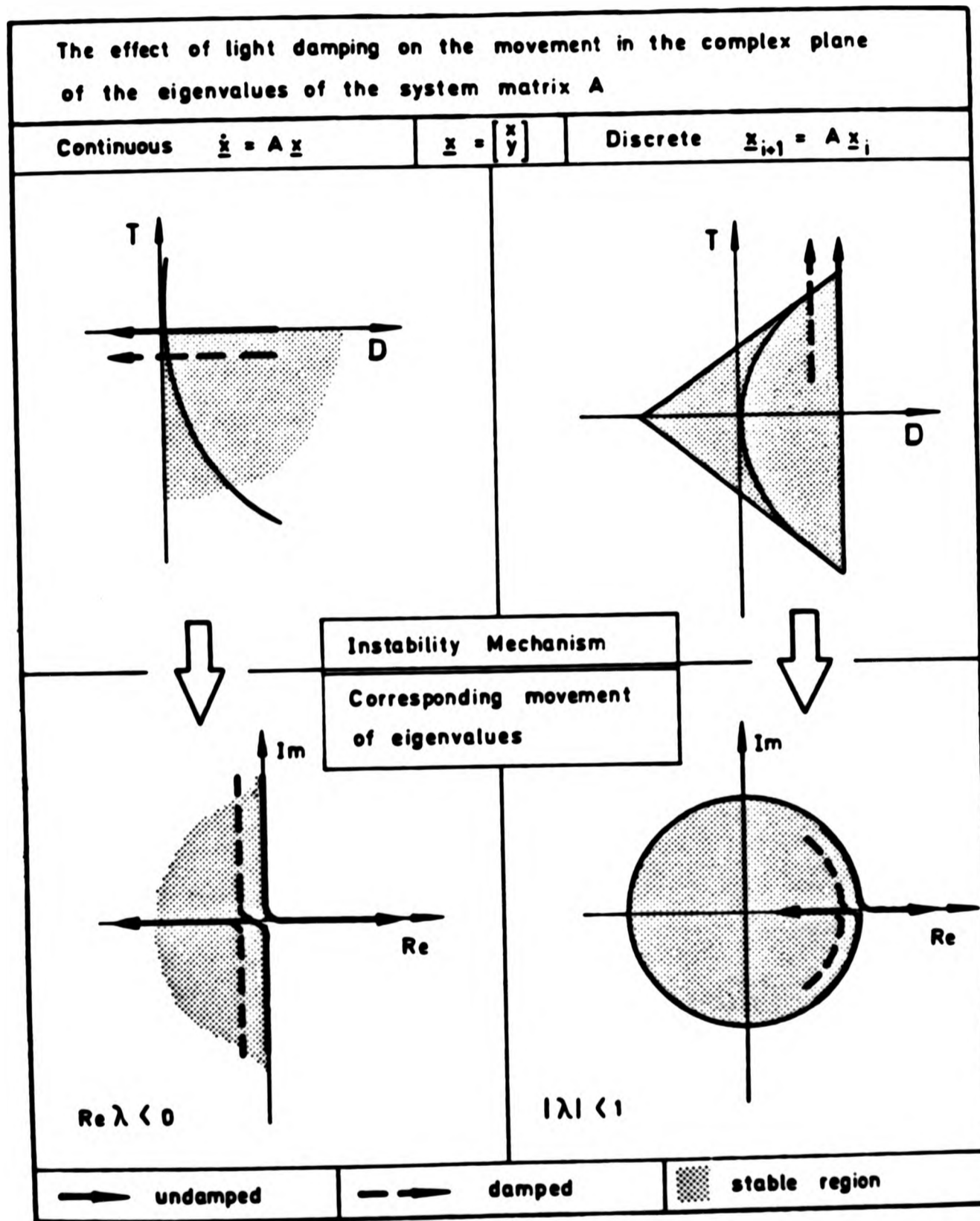


Figure 5.2 The effect of light damping on the movement of the eigenvalues of continuous and discrete linear systems.

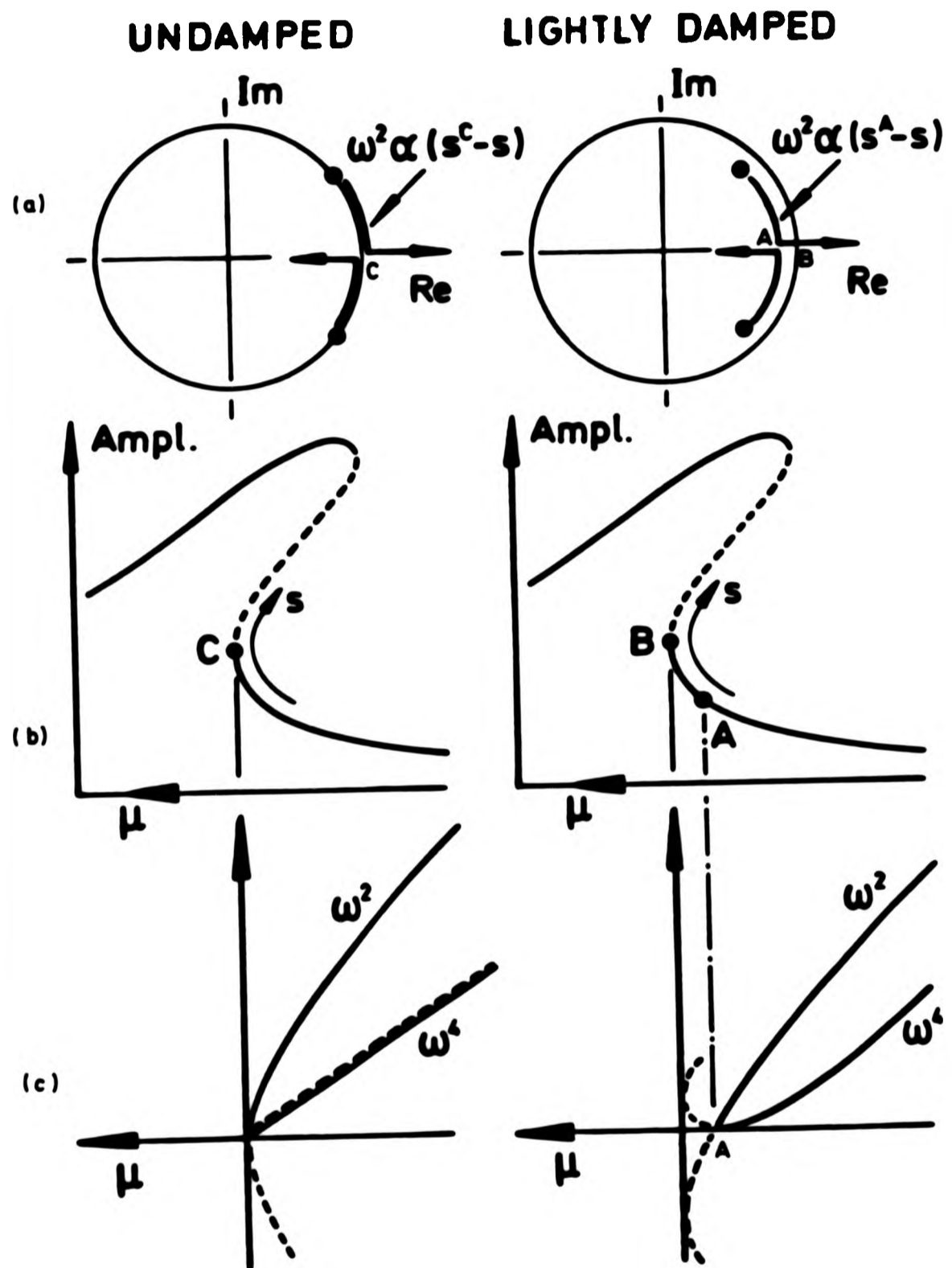


Figure 5.3 ω^2 and ω^4 predictors for the cyclic fold for undamped and lightly damped systems.

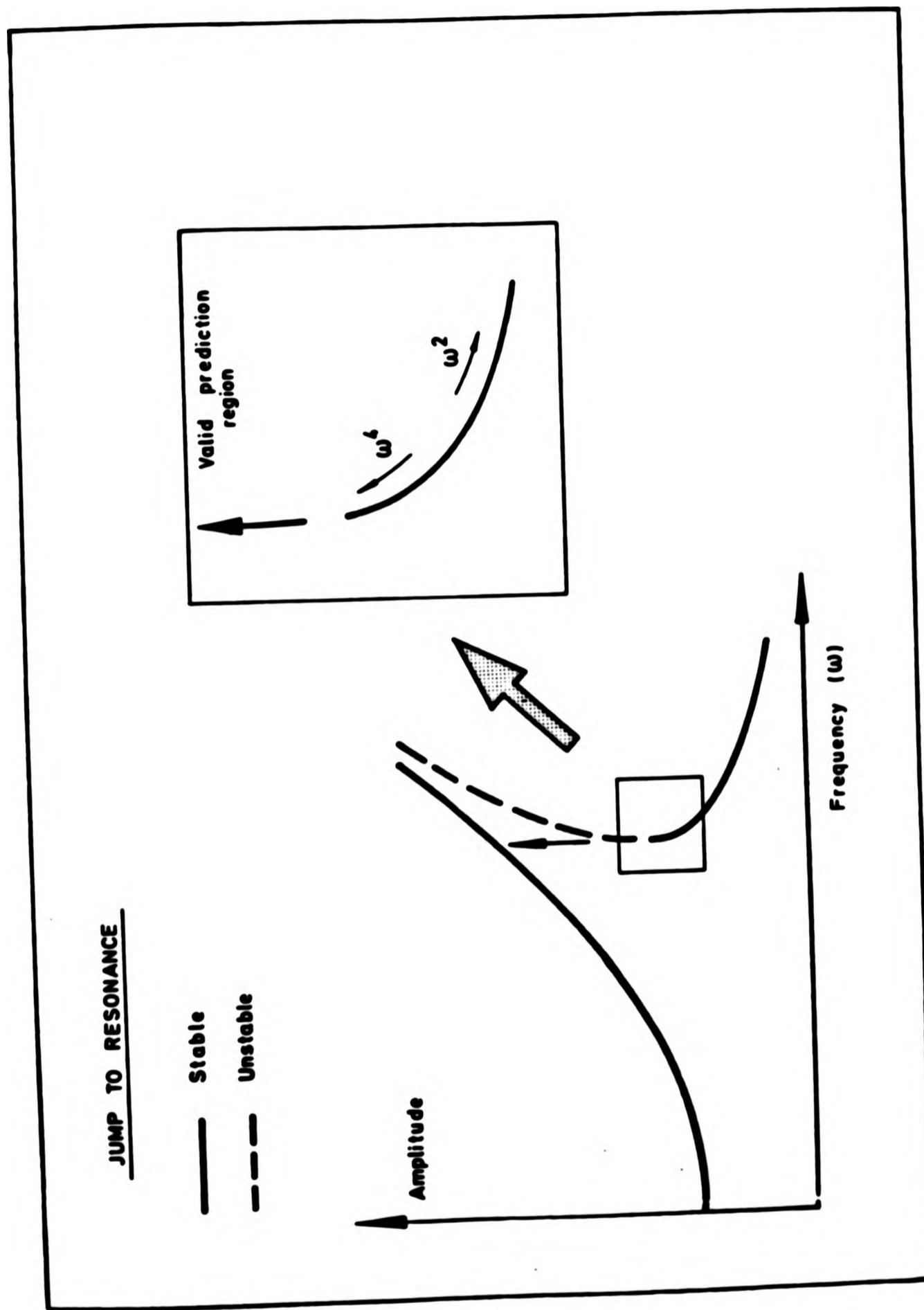


Figure 5.4 Region of valid prediction of the cyclic fold.

DEFINITION OF ORBIT NUMBER N

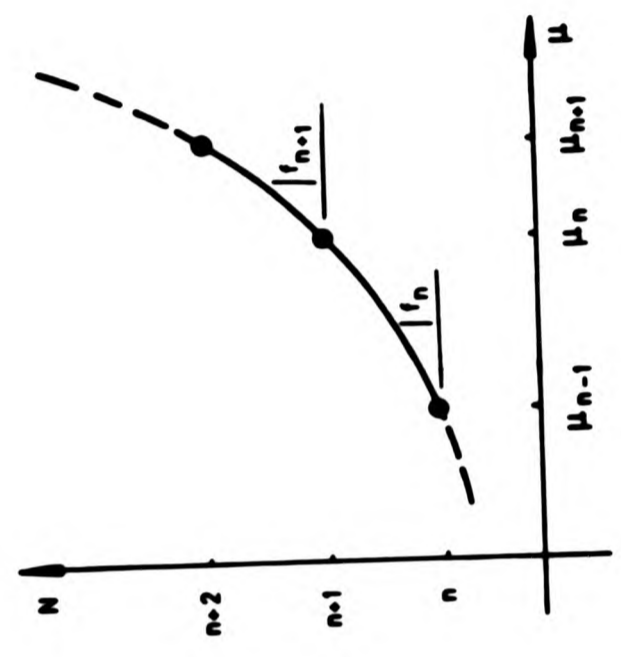
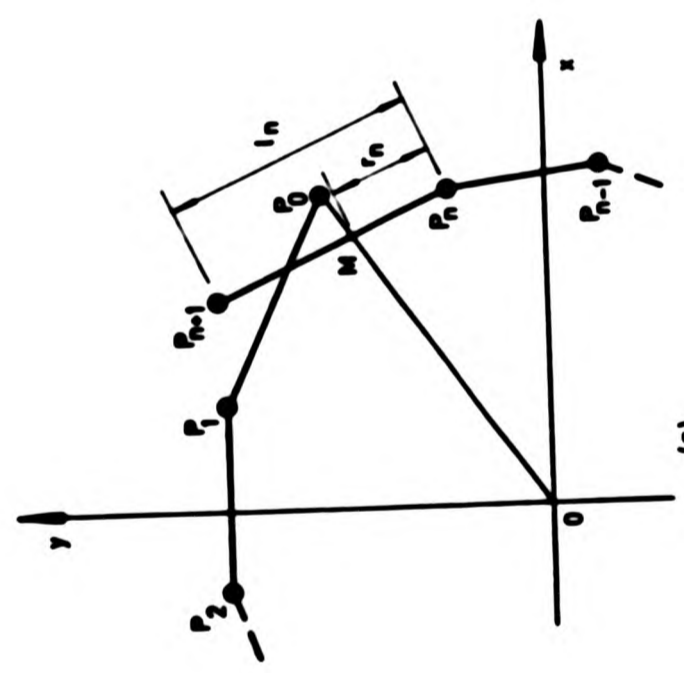
$$x_{i+1} = a x_i + b y_i$$

$$y_{i+1} = c x_i + d y_i$$

$$P_i = (x_i, y_i)$$

$$f_n = r_n / l_n$$

$$N = n \circ f_n$$



(b)

(a)

Figure 5.5 The definition of the orbit number of a map.

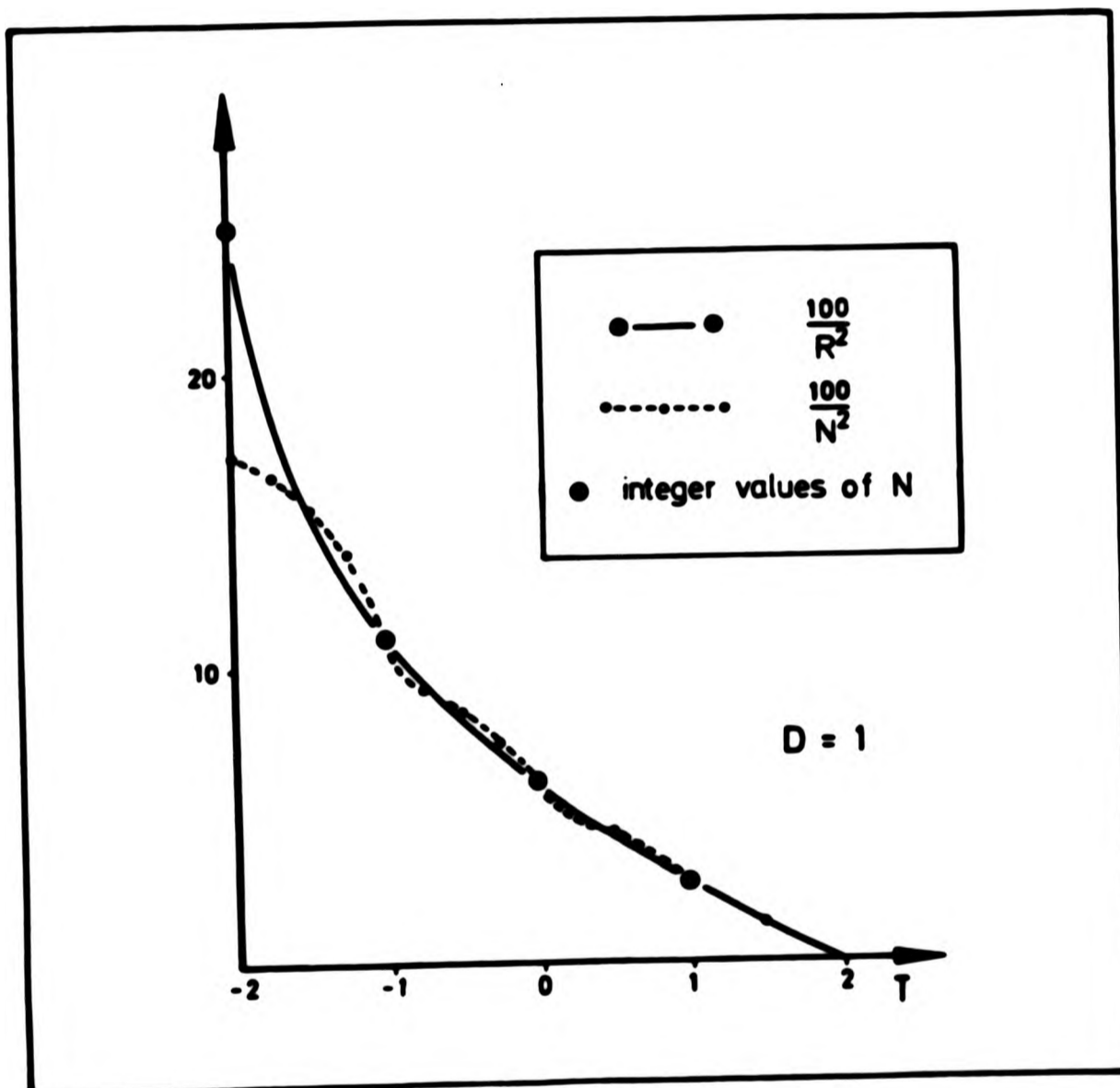
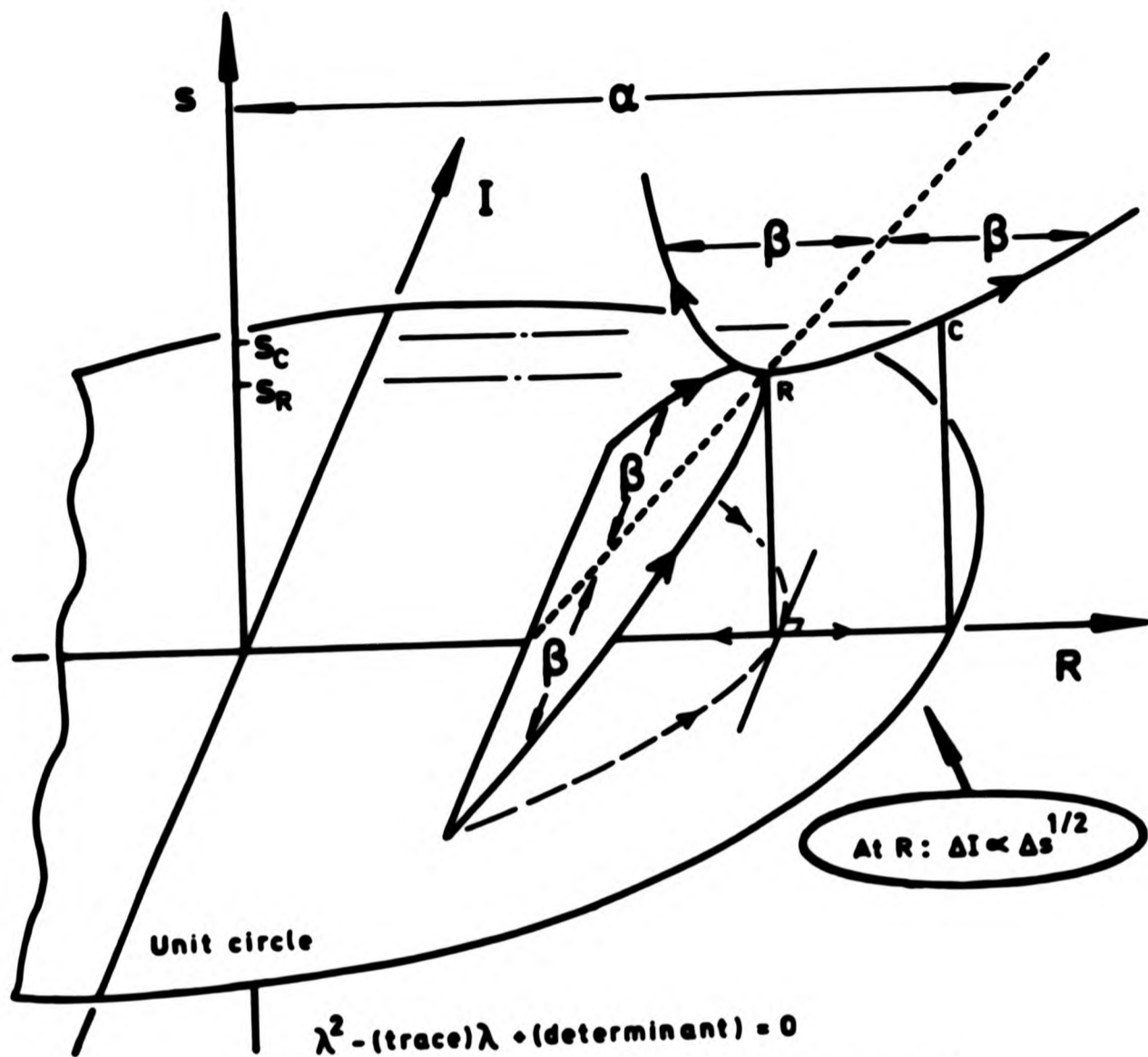


figure 5.6 Comparison between the rotation number and the orbit number of a map.



$$\lambda^2 - (\text{trace})\lambda + (\text{determinant}) = 0$$

$$\text{Discriminant} = (\text{trace})^2 - 4(\text{determinant})$$

$$\alpha(s) = \frac{1}{2}(\text{trace}) \quad \beta(s) = \frac{1}{2}\sqrt{|\text{discriminant}|}$$

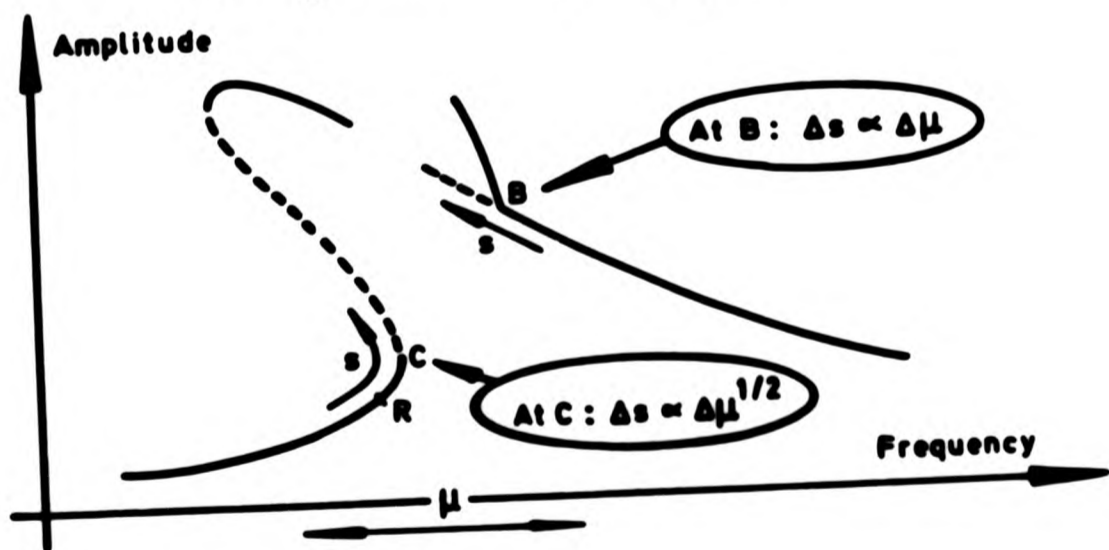


Figure 5.7 Explanation of the rapid movement of the eigenvalues as they approach a fold.

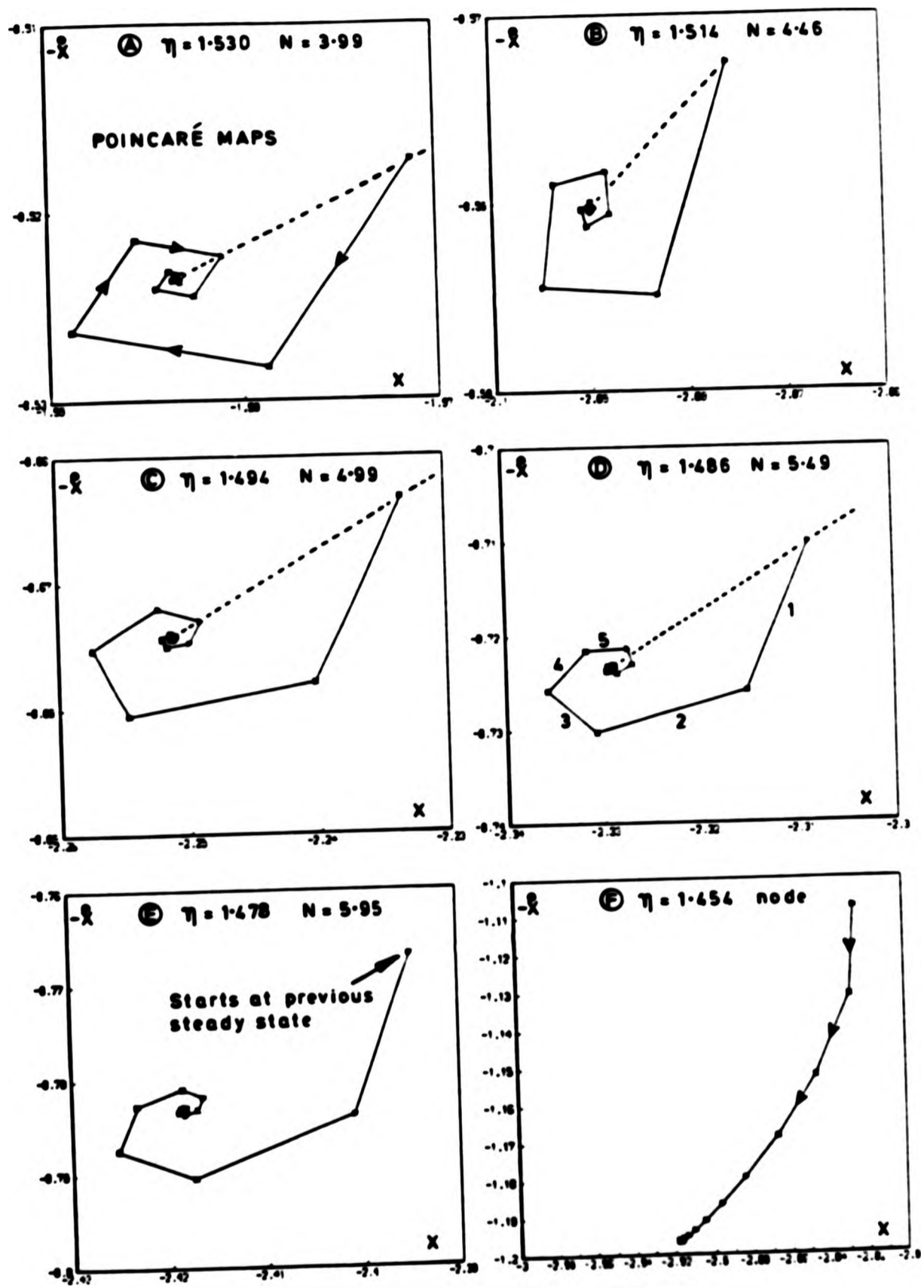


Figure 5.8 Some computed Poincaré maps for Duffing's equation.

$$\eta^2 \ddot{x} + 2\eta[\lambda - x + \alpha x^3] = F_0 \cos t$$

$$\zeta = 0.1, \alpha = 0.05, F_0 = 2.5$$

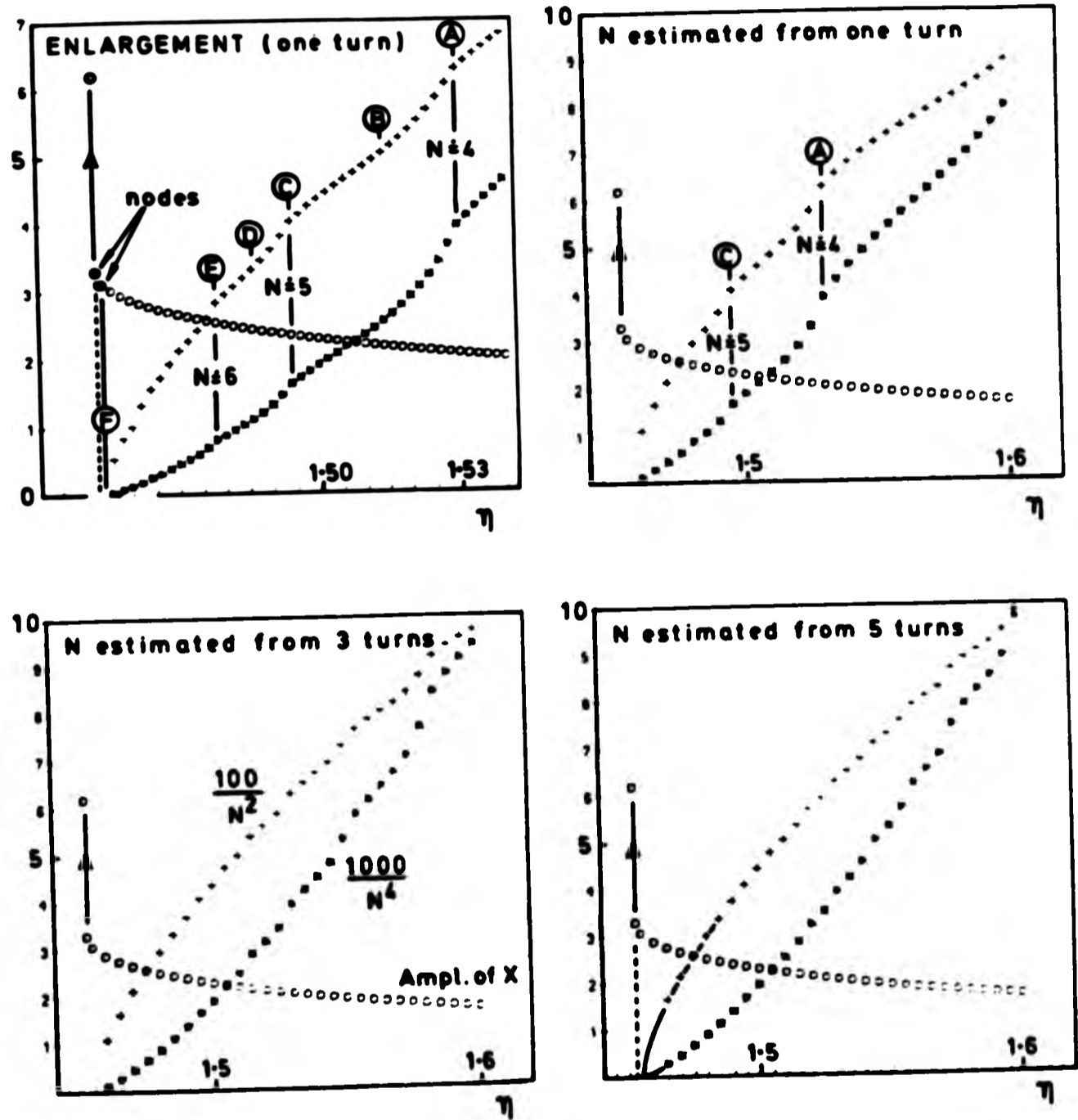


Figure 5.9 Predictions of the fold in Duffing's equation using the orbit number of the Poincaré map.

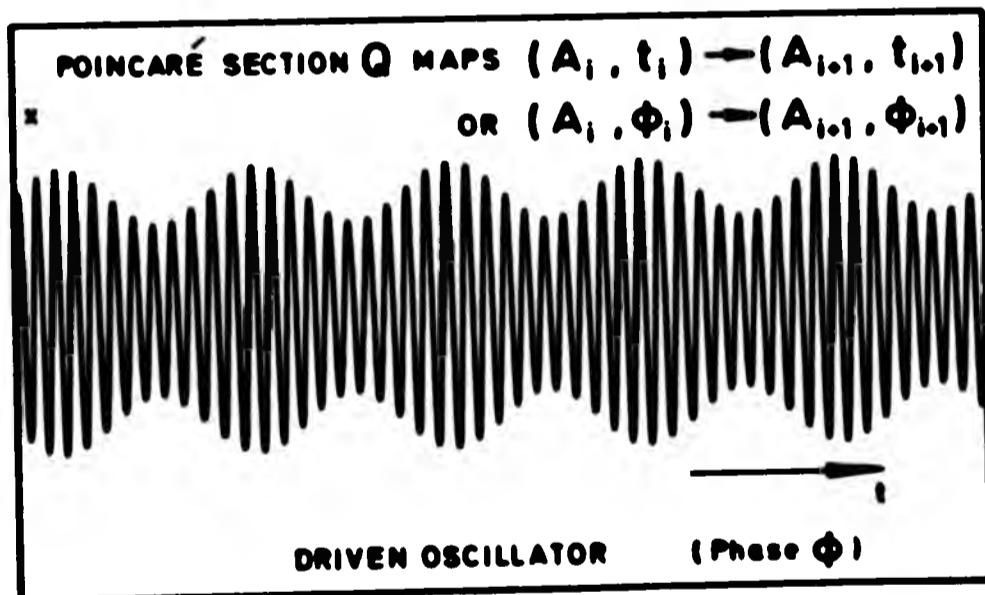
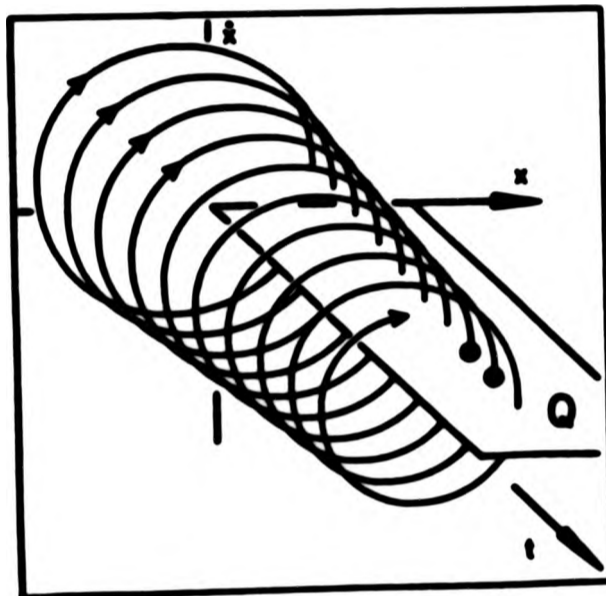


Figure 5.10 The equivalence of the map rotation to the beat frequency.

QUARTIC BEAT PREDICTOR

$$\ddot{x} + x^3 = B \cos t$$

$$B = 0.40 \text{ to } 0.45$$

$$P = \text{Beat period} / 2\pi$$

All integrations

$$\text{start } x = -\frac{2}{3} \quad \dot{x} = 0$$

$$\Delta t = \pi / 10$$

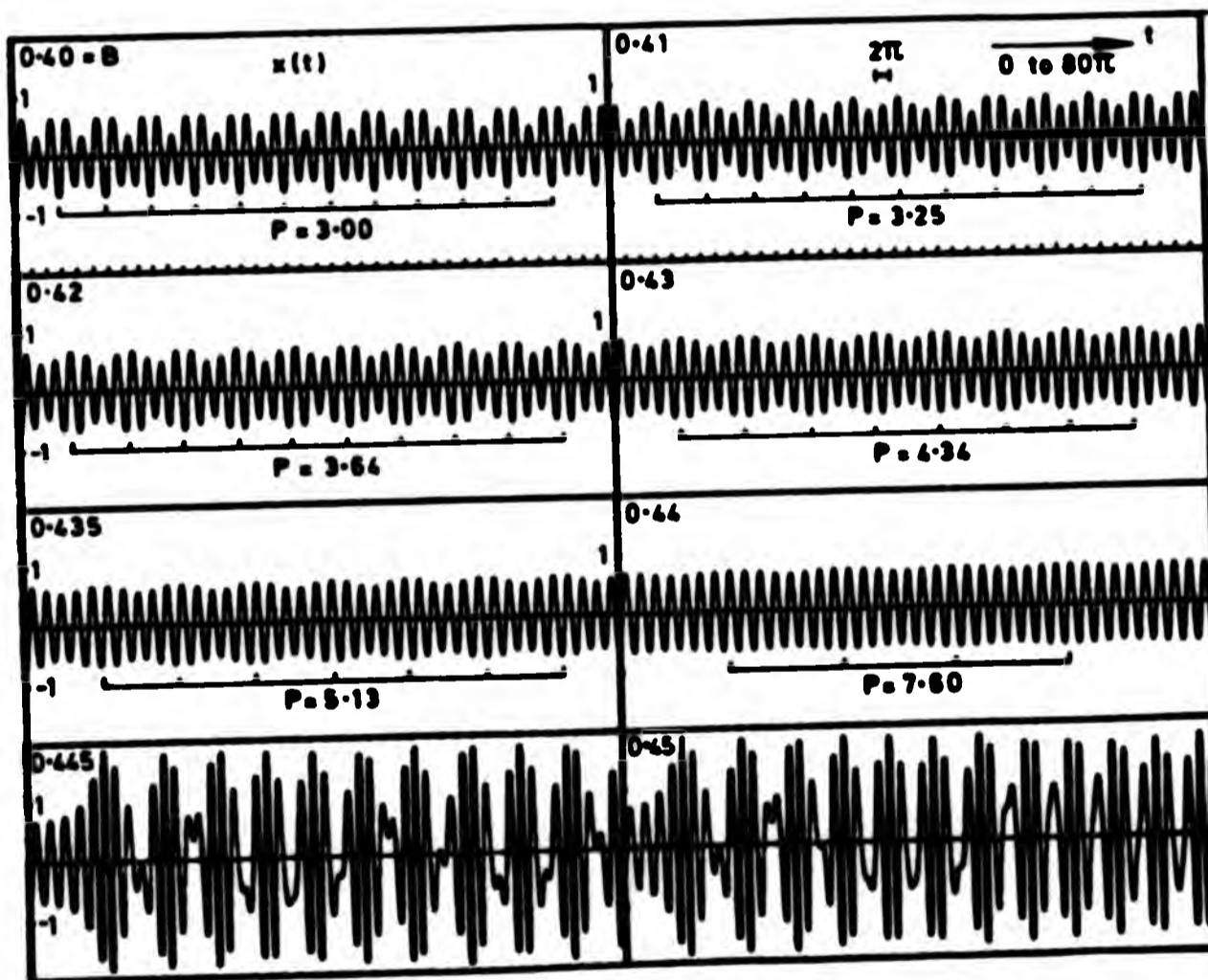
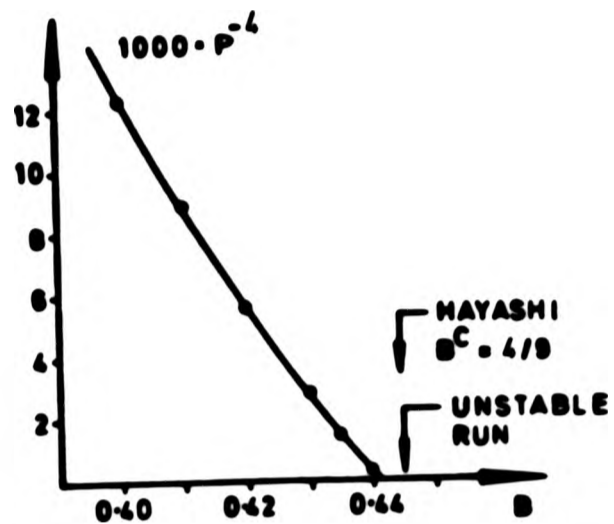


Figure 5.11 Beat frequency of a nonlinear oscillator used as a predictor of the cyclic fold.

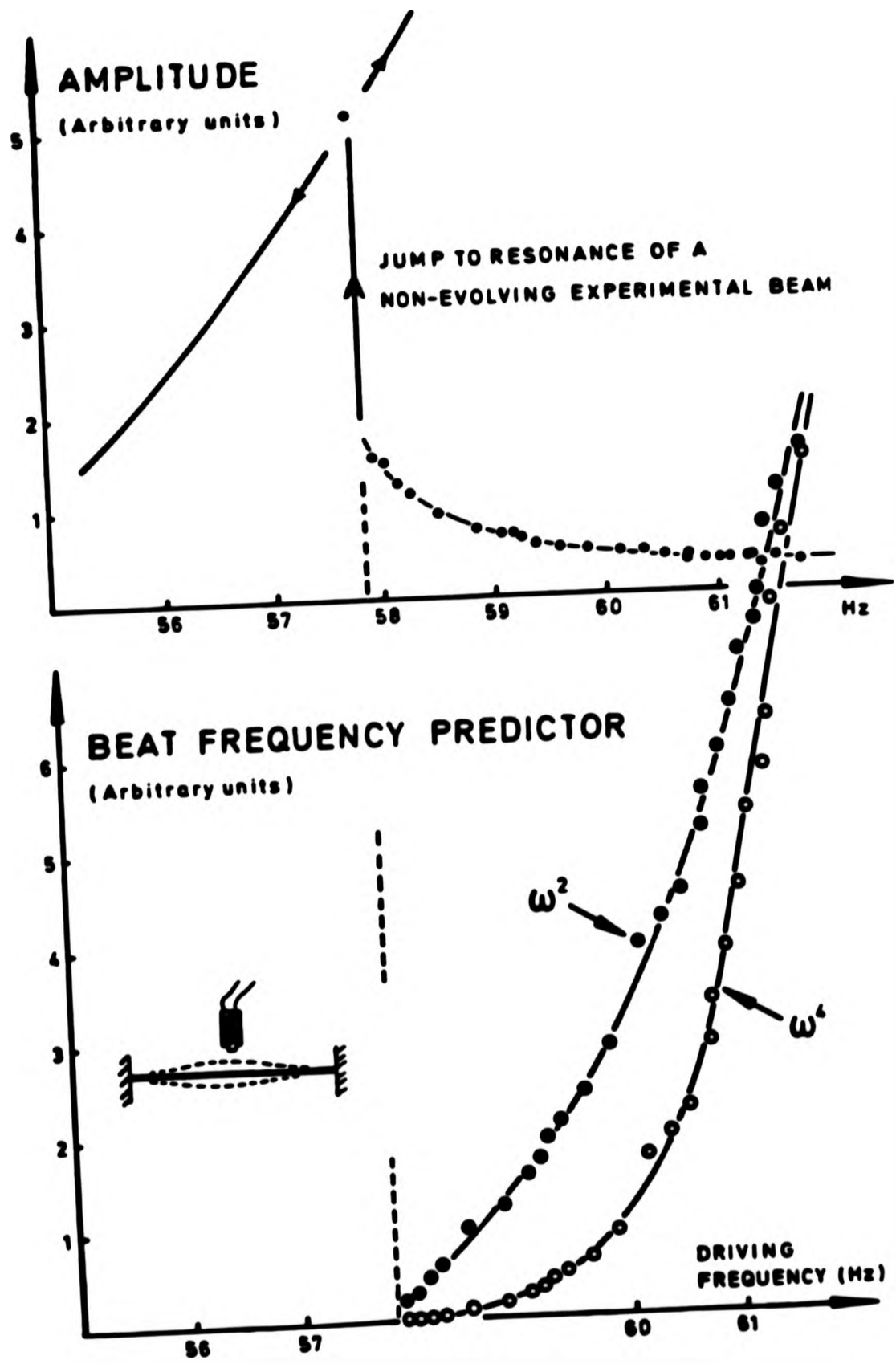


Figure 5.12 Summary of the predictions of the jump to resonance (fold) of an experimentally driven beam.

CHAPTER II.6

A ROUTE TO CHAOS

Some early remarks have already been made in chapter II.1 about chaotic motions and the underlying governing chaotic attractor with specific reference to the work of Ueda. There are now many texts that record in detail the theory of chaos since its first discovery by Lorenz (1963,1964) or, as some argue, by the early work of Ueda; Cvitanović (1984), Holden (1986) or Thompson and Stewart (1986) to name but a few. The text of Guckenheimer and Holmes (1983) is also an invaluable addition to the literature of chaos but such a global study of the subject shall not be attempted here. The appearance of chaotic motions reported in this thesis in part III will mainly come about via a cascade of period doubling bifurcations although other routes to chaos do exist [Kadanoff (1983)].

This route to chaos occurs when a periodic attractor representing a fundamental harmonic response, for instance, initially bifurcates at $\mu = \mu_1$ say into a subharmonic periodic motion of order 2. This periodic orbit itself bifurcates as the control parameter μ is gradually increased. The second flip bifurcation at $\mu = \mu_2$ leads to a subharmonic of order $n=4$ solution. As μ is increased still further, bifurcations to higher orders of subharmonic oscillation will continue with ever

decreasing values of the control parameter such that an accumulation point μ_∞ will exist just after which chaotic motion occurs which has an infinite period.

Universal features of this scenario in maps were discovered by Feigenbaum (1978) and later proved by Collet (1980) and Lanford (1982). The ratios

$$\delta_i = \frac{\mu_{i+1} - \mu_i}{\mu_{i+2} - \mu_{i+1}} \quad (6.1)$$

were shown to converge to the universal number $\delta_\infty = 4.66920\dots$, universal referring here to the fact that this result holds generally for all maps. The same result has not been proved for the maps which are produced by stroboscopically sampling a trajectory of a flow, i.e. a Poincaré map, but as we shall see later in experiments [Shaw (1984)] and in numerical simulations [Bishop and Virgin (1986)] it does appear that the result can indeed be carried over to flows.

As the period doubling (flip) bifurcations occur they each leave behind (in the control-phase space) an unstable orbit so that at the accumulation point there is in fact an infinite number of such unstable orbits, it has been suggested that the subsequent chaos is thus merely the computer jumping about between different unstable periodic solutions. However due to the heavy weight of mathematical rigour now being applied to the study of chaos it seems that the subject is on a much stronger

footing than this suggests.

The cascade of period doubling bifurcations is the only continuous route to chaos from a periodic orbit (see the table of bifurcations, figure III.5.11). The other possible routes to chaos are via an intermittency explosion or a chaotic explosion, both of which are discontinuous bifurcations in which a gradual change in the control parameter produces a sudden jump in the response and the appearance of a chaotic attractor. These latter bifurcations can both be seen within the period doubling sequence in chapter III.5 but shall not be considered in depth. The interested reader should consult the work of Frisch (1980) or the studies of Grebogi et al. (1980).

Part III : Applications of the Geometrical Theory of
Dynamical Systems to the Motions of
Compliant Offshore Structures

CHAPTER III.1

OFFSHORE TECHNOLOGY

In the offshore industry modelling the complex motions of vessels, whether they are powered or moored, and production or drilling facilities is an extremely engaging task. In contrast, the aircraft industry has many advantages in that scale models can be constructed and tested, in wind tunnels for example, to produce meaningful results. Even full scale prototypes can be thoroughly evaluated before the production of a new design model is implemented in the fabrication of a particular aircraft (note here that there were several prototype Concorde aeroplanes before commercial operations began). On the other hand, in the offshore industry fluid forces cannot be scaled with any certainty to give confident calculations of any great accuracy. More importantly perhaps the cost of a full scale experimental model of a new design for oil and gas production platform is so immense as to be prohibitive (Conoco's Tension Leg Platform (TLP) cost £1 billion to design and construct) and even the testing of individual components has certain drawbacks since interaction is of paramount importance. The sheer size of these production facilities is staggering; the Hutton TLP shown here in figure 1.1 weighs almost 50,000 tonnes and its deck structure outflanks a football pitch. Thus the smallest improvement in dynamic efficiency of such a massive system as

this can lead to huge savings in terms of cost. It must also be remembered that, unlike aircraft which can regularly be taken out of service and thoroughly checked and maintained in a 'dry' situation, an oil platform has to remain in place enduring up to 100 m.p.h. winds and at times waves of over 100 feet, and do so continuously for over 20 years. Though it is true that certain components can be replaced from time to time the above mentioned problems create a need for mathematical and engineering skills on a mammoth scale.

In this part of the thesis some specific examples shall be considered in which the geometrical theory of dynamical systems is applied to the motions of compliant structures. The particular models chosen are necessarily of simplistic form, but nevertheless they do capture the fundamental behaviour of the real situation. Indeed, in some cases that shall be described in the following chapters the models that shall be investigated were actually developed and tested in a design process and here are merely analysed in more detail with the insight of nonlinear dynamics theory.

It is clear that the modelling of the dynamics of highly complex systems, such as barges, tankers and offshore platforms, is a daunting challenge. The models selected for study in this section are not intended to cater for 'microscopic' events (fluid forces, differing keel shapes etc.) even though they may play a considerable role in determining the final dynamics of the system, but rather to investigate the possible qualitative

behaviour of the dynamic motions of time evolution systems. In particular we shall examine any generic instabilities that such systems might undergo in the light of the knowledge gained from the earlier part II of this thesis.

Although it is well understood that the wave forces present in the North Sea are highly irregular, for the main part of the investigations reported here deterministic forcing of the mathematical models shall be considered. This is not quite so worthless as it may first seem since during the working life span of these typical structures and vessels it is readily conceivable that at some time there will be a train of waves which are in fact extremely regular (for instance waves emerging from a distant storm tend to be inherently periodic in nature as the fastest waves, of longer period, reach the structure before being infiltrated by shorter waves of varying frequencies), thus vindicating these studies, although clearly they form only a small section of an investigation of which a large part must be random excitation. It should also be borne in mind that there are many physical situations in which the external excitation or force is predominantly unimodal, such as for example in the rotation of machine tools, the motion of vessels in a harbour, etc. for which the methods developed here can easily be carried over. However, to give an insight into the behaviour of offshore structures in random sea-state conditions, and in particular to see whether nonlinear effects remain visible, in chapter III.7 we shall consider the effects of the introduction of a 'random element' superimposed onto the otherwise deterministic forcing.

Until recently most theoretical dynamical investigations carried out by design and consultant engineers were mainly of linear or quasi-linear systems so that closed form solutions were obtainable. The preceding discussions only indicate some of the complicated characteristics of compliant systems that produce a truly nonlinear system from which little analytic information can be recovered. The theoretical tools still available in this situation, e.g. perturbation methods [Jordan and Smith (1977)], the method of slowly varying amplitude and phase [Hayashi (1964)] and the describing function method [see Mees (1973,1981)], only allows the evaluation of solutions of certain types (modes) with sometimes quite considerable limitations. The fact that large regimes of chaotic motions have been identified in the Duffing oscillator [Ueda (1980), Holmes (1979)] emphasises the shortcomings of these traditional methods of analysis for ordinary differential equations. Hence the only recourse is then to direct time simulations. With the advancement of computer technology more elaborate mathematical models are being developed to account for physical processes. However, partly due to the high costs of commercial computer time and partly due to the sheer weight of data so produced, little effort is placed on the actual amount of simulations performed once a model has been achieved. One should remember that most designers and engineers, being traditionally trained, are used to linear systems in which unique solutions prevail so normally only a single or at most a few time domain simulations are envisaged during the complete design procedure. The

topological approach to dynamical systems increasingly becoming popular [see for instance Stewart and Thompson (1986) and Abraham and Shaw (1982,1983,1985)], and which is advocated here, is a method by which the qualitative behaviour of a system can be gleaned from this mass of results. The generality of this approach means that it is equally applicable in many areas of mathematics, engineering and in the social and biological sciences.

One aspect of nonlinear phenomena that shall often be referred to in this section of the thesis is the possibility of subharmonic oscillations. In the construction of offshore facilities the main concern is to design the structures so as to have a natural period of vibration that is clearly distinct from the period of expected waves [Langewis (1986)] so that fundamental excitation is excluded; illustrated in figure 1.2(a) are the natural sway periods of the main designs of platforms currently in use. Obviously this is a clear enough design criterion but heed must also be taken to the possibility of subharmonic resonances, perhaps of large amplitudes, at a fraction of the natural period, be it sway, surge or pitch. In turbomachinery design in the aircraft industry this problem does not arise since, although subharmonic resonances would clearly exist, the machine is advanced rapidly to its operating speed so that sufficient power at the relevant frequencies is not available to excite extreme vibrations. The North Sea does not always behave in such an ordered, controlled manner and subharmonics must therefore not be ignored.

As the oilfields currently under production become exhausted the move into deeper water results in further complications with increased static and dynamic loads. The choice of a particular design of platform in this situation is largely determined by weight considerations in the course of manufacture. Figure 1.2(b) shows the percentage increase in weight of the different structures for a move into 1500 feet of water and gives a clear justification for the use of compliant platforms. However the subsequent dynamic motion, bearing in mind the fact that the natural periods of oscillation of fixed structures increases with such a move into deep water edging ever closer to the wave periods and vice versa for the compliant platforms, plays a vital role in future design work. In addition for the need to move into deeper waters the exploitation of marginal fields gives rise to the concept of transportable production facilities and so for these reasons the main emphasis of the work that shall be reported here shall be towards the dynamic modelling of compliant systems.

In the chapters that shall follow all the time domain simulations were carried out using the Runge-Kutta routines of numerical integration. In each case the usual stephalving checks were made to ensure the long term stability of the numerical solution as well as checks of the overall solution of the equations by other routines run on different computers (particularly to show that the chaotic solutions are not machine dependent).

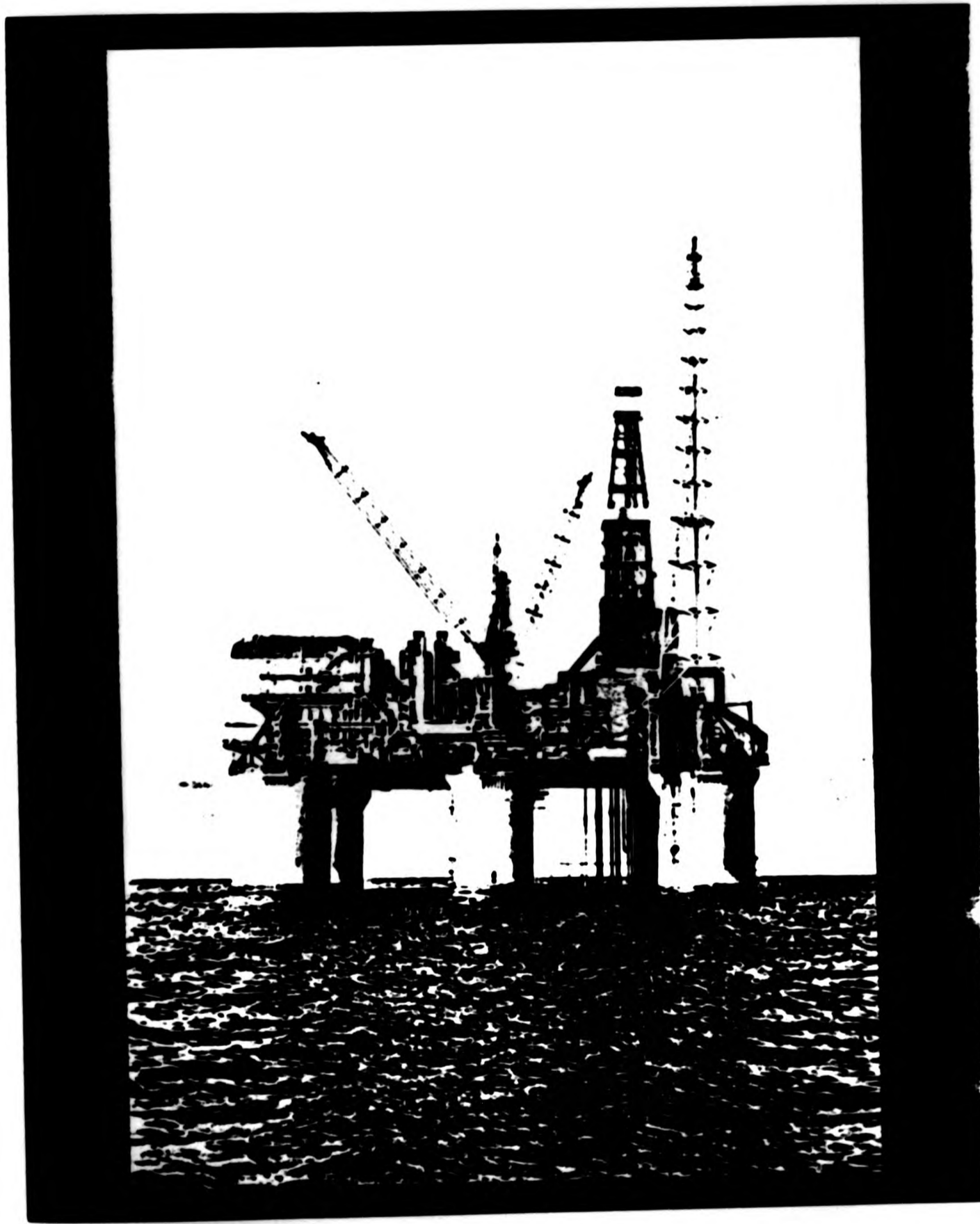


Figure 1.1 Conoco's Hutton Tension Leg Platform (TLP).
reproduced here with kind permission from
Conoco UK Ltd.

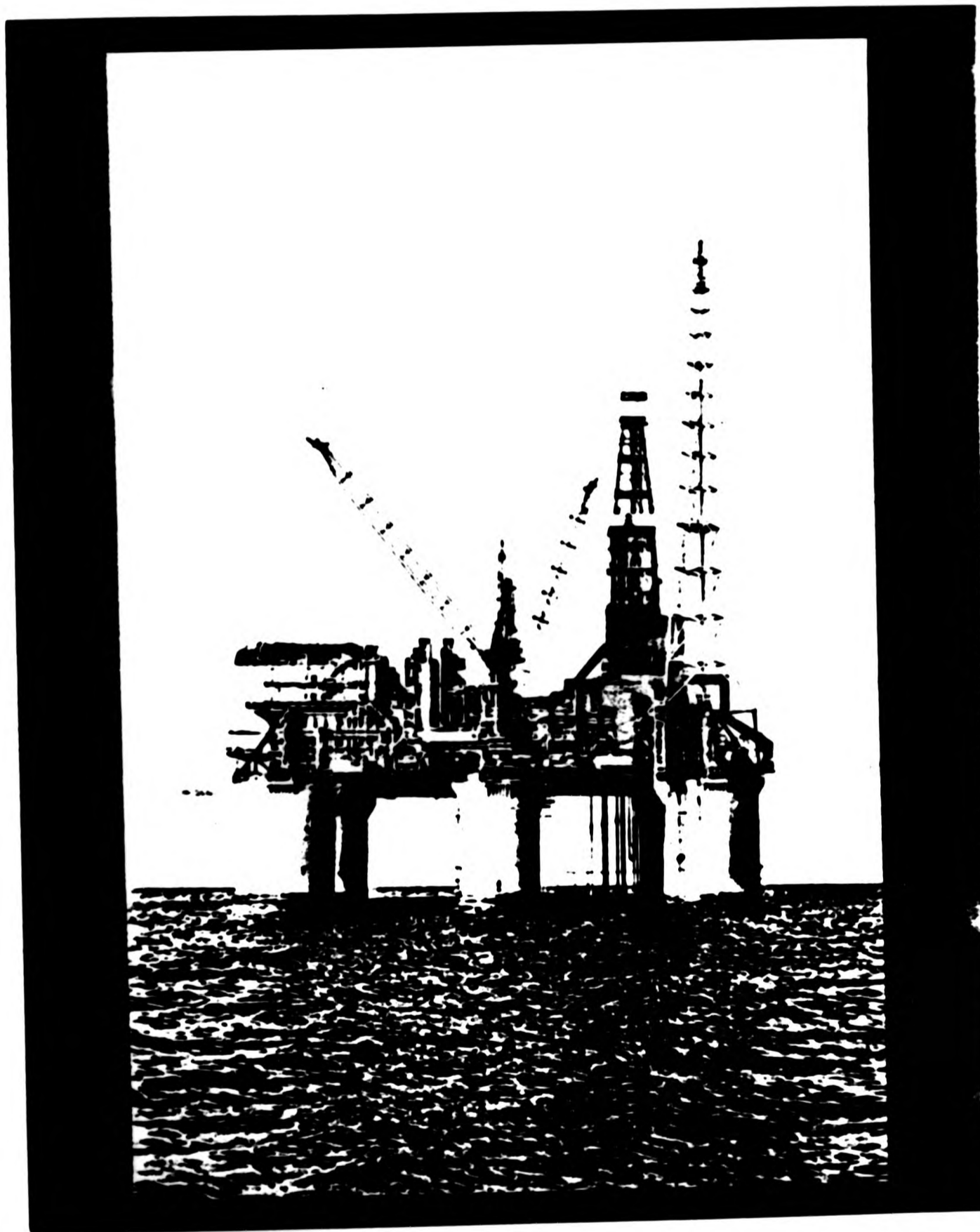


Figure 1.1 Conoco's Hutton Tension Leg Platform (TLP).

reproduced here with kind permission from

Conoco UK Ltd.

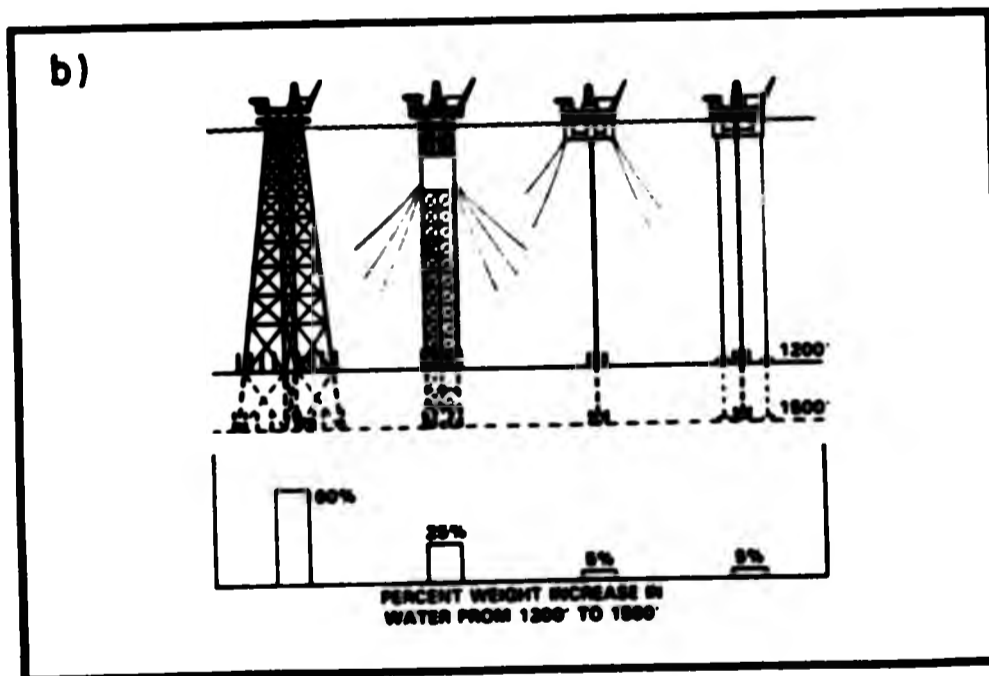
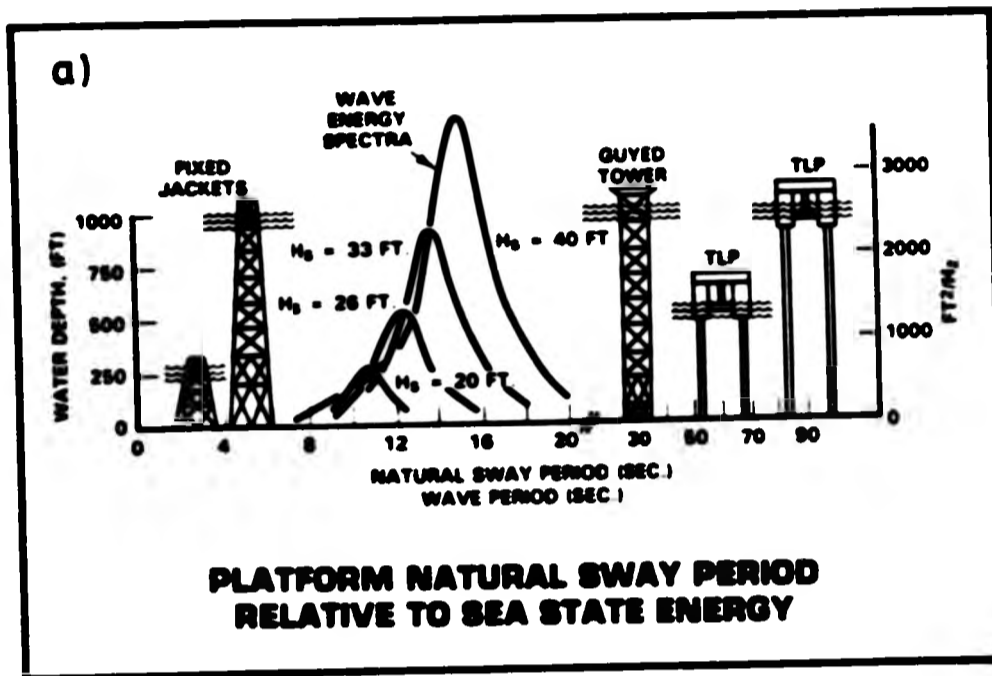


Figure 1.2 a) Natural sway periods of typical offshore platforms and wave energy spectra.
b) Percentage increase in weight for a move from 1200' to 1500' water depth.

CHAPTER III.2

EXPERIMENTAL INVESTIGATIONS INTO THE FISHTAILING OF A MOORED TANKER

III.2.1 Introduction

In deep water fields the offtake of oil and gas can either be conducted by means of a pipeline or by the use of a shuttle tanker. Each of these methods has its individual merits depending on the environmental conditions but the final choice of which of the two methods should be employed for a particular field is most probably dictated by economic factors. While the laying of pipelines in shallow waters is a well established and feasible activity, in deep waters the costs make it a less than obvious choice. Specifically one mile of finished pipeline in deep water can currently cost as much as £50,000 per inch diameter mile; so that a 50 mile, 20 inch pipeline can cost up to £50 million [see Langewis (1986)], and costs are on the increase. Besides this economic constraint there are many technical complexities of pipeline technology which may give rise to shorter fatigue life and even lead to failure.

An alternative approach commonly adopted is the use of shuttle tankers for the offload of oil; in which case insitu storage facilities are required or the possibility of an

intermittant production. When using such tankers in deep waters the main technical difficulty is the mooring system and it is necessary to consider the structural and seakeeping characteristics of the vessel to reduce the amount of disconnect time as much as is possible.

III.2.2 The Fishtailing Instability

The Hopf bifurcation is a feature found in many fields of engineering and mathematics [see Hopf (1942) or Marsden and McCracken (1976)] in which periodic oscillations occur in a system when some control parameter is varied. Classic examples include the galloping of bridges and transmission cables, the aeroelastic flutter of aircraft panels [Dowell (1975)], limit cycles in chemical reactions [Vidal (1980)] and biological systems [May (1976)], and, in particular, the fishtailing oscillations of moored vessels. If the vessel happens to be one of the huge crude oil transporter then it is imperative to avoid any large scale oscillations to protect neighbouring installations and to reduce the risk of a mooring line breaking due to excess tensions. As explained earlier, when offshore developments move into deeper waters pipelines to shore based plants become impracticable, hence it is important that we should have a thorough understanding of the basic instability phenomena that may arise in single point mooring (SPM) systems, commonly used to moor vessels whilst loading is underway.

The motions of such a moored vessel are obviously affected by many external and internal sources; wave, wind and current actions, size, and distribution of the payload of the vessel as well as the subsequent effects of the SPM system and any dynamic positioning of the ship. However the purpose of this study is to construct and examine the simplest experimental model which exhibits the fishtailing instability so that our understanding of this mechanism can be advanced. With this newfound knowledge it is hoped that further factors could later be considered, such as a more realistic marine environment, to give a complete picture of the fishtailing problem so that predictions can ^{then} be made of the onset of such large such periodic motions in sufficient time to enable active control of dynamic positioning and station keeping thrusters to prevent the onset of the fishtailing instability.

III.2.3 The Experimental Model

For the purpose of these experimental investigations obvious simplifications were necessarily made to the model of a moored vessel and a SPM system, the single control parameter was chosen to be the length of the rigid mooring arm. However, for convenience, we shall equivalently use the variable μ which is taken to be the length of the rigid arm beyond the adjustable pivot, see figure 2.1. All experiments were conducted in a flume approximately 0.5 metres wide, 0.25 metres high, and 6 metres long with a constant current provided by a head tank. The model

itself was mounted as close as possible to the upstream end of the flume following tests to check velocity profiles.

A vertical flexible cantilever was used to simulate a mooring tower which allowed lateral movements only, these motions being recorded and subsequently converted to actual displacements at the pivot point, see figure 2.1. With the mooring arm length set at a particular value such that the control parameter, μ , is less than the critical value at which the bifurcation occurs, μ_c , a static equilibrium state exists. If μ is increased past this point the system becomes dynamically unstable and periodic oscillations occur terminating in a limit cycle due to a combination of nonlinear terms, schematically viewed by the tanker in the positions 1-5 in figure 2.2. To examine the incipient nature of the system as the bifurcation is approached displacement/time histories were obtained in two distinct ways. Firstly the vessel was positioned on the equilibrium position and then released. Secondly the vessel was given a finite displacement just before records of displacements were made. Thus if the system were stable the vessel would either remain or decay onto the equilibrium position, with the exception of minor deviations due to fluctuations in the flow. Whereas if the system were unstable oscillations would be evident culminating in a limit cycle of periodic oscillations. Sample traces can be seen in figure 2.3 both with and without an initial disturbance. The corresponding phase portraits are shown in figure 2.4, where for $\mu=30$ and $\mu=90$ only the phase portrait from trajectories with an initial

disturbance or kick are visible; while for $\mu=115$ and $\mu=140$ after the bifurcation the diagrams on the left hand side correspond to the trajectory given an initial kick, those on the right hand side are those started on the equilibrium point.

The Hopf bifurcation in its simplest mathematical form can be represented by the equation

$$m\ddot{x} + b\dot{x} + cx^3 + kx = 0 \quad , \quad (2.1)$$

[see Thompson (1982)] in which the linear damping coefficient (b) drops to zero. The presence of the cubic damping term causes any ensuing oscillations to terminate in a limit cycle instead of diverging to infinity. Consequently a first approach to be considered as a possible prediction technique of the fishtailing instability was to monitor any induced transient motions and evaluate the logarithmic decrement in order to estimate the effective damping of the system. When this procedure is carried out over a range of the control parameter, before μ_c , a least squares fit can be used to provide a linear approximation to the data. A plot of the amplitude of oscillations against the control parameter is given in figure 2.5(a) and as can be seen from the lower diagram, figure 2.5(b) the aforementioned straight line provides a good extrapolated estimate of the value of the control parameter at which oscillations first occur. It should be said that care has been taken here as to when to evaluate the decrement, firstly since it is the linear damping coefficient that we are trying to approximate then early

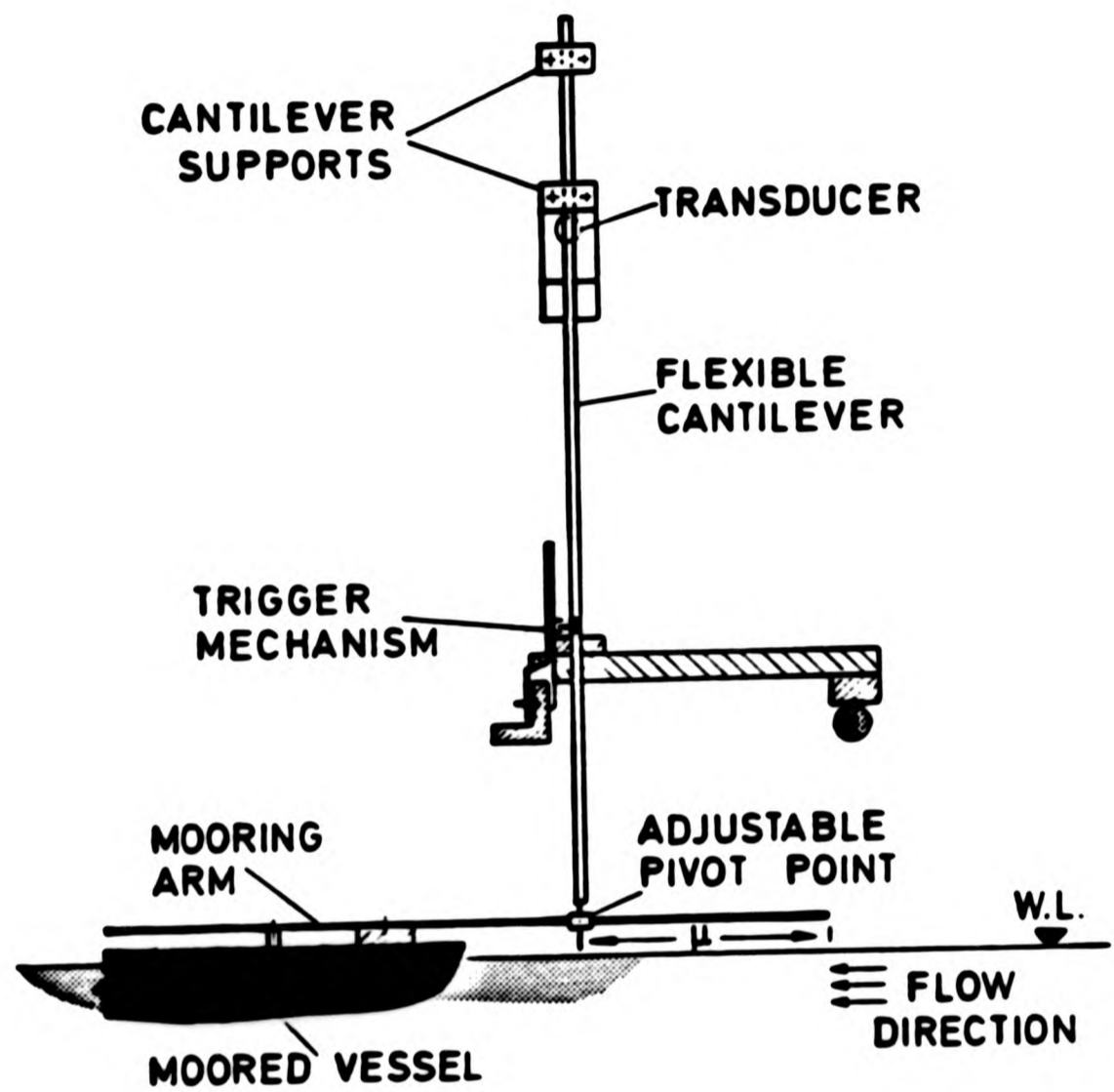
readings should be discounted, and secondly since small amplitude motions will be greatly effected by any fluctuations in the flow so then latter readings are also ignored.

Experiments were carried out for a variety of vessel profiles and current speeds, a further example being illustrated in figure 2.6 with an alternative approach to analysing the oscillations as a power spectrum of the output signal shown in figure 2.7.

In addition to these investigations a motor arrangement was attached to the vessel so that the length of the mooring arm could be evolved. Experiments were carried out with this set up in an attempt to isolate combinations of variables which lead to the occurence of an unstable Hopf bifurcation in conjunction with a cyclic fold as illustrated in figure 2.8 (see also chapter II.2) which is potentially more dangerous containing the possibility of a rapid jump from a stable steady state equilibrium to a periodic large amplitude solution. Although this particular type of bifurcation has not as yet been identified a particular case has been studied in which an apparent cyclic fold of the periodic path occurs, see figure 2.9.

It should be noted that in this experimental system the damping in sway is provided by a coupling between the fluid damping, which is always present, and the effective damping provided by the rigid mooring arm. It was not the intention here

to study this damping mechanism in detail but instead to investigate the instability more from a global qualitative viewpoint.



SIDE VIEW (not to scale)

Figure 2.1 Experimental set up of a moored vessel.

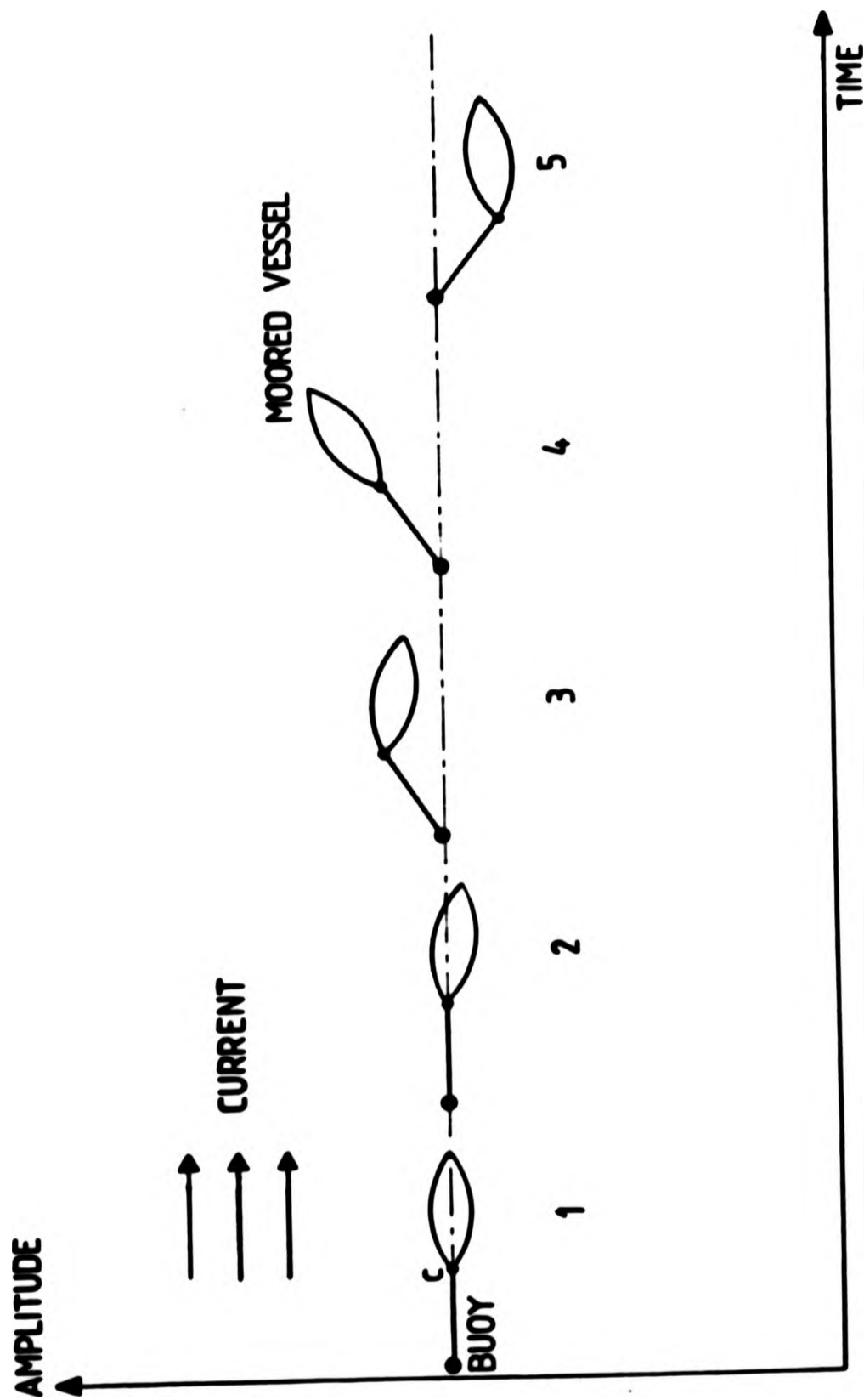


Figure 2.2 Positions of a moored tanker during fishtailing oscillations.

(b)

(a)

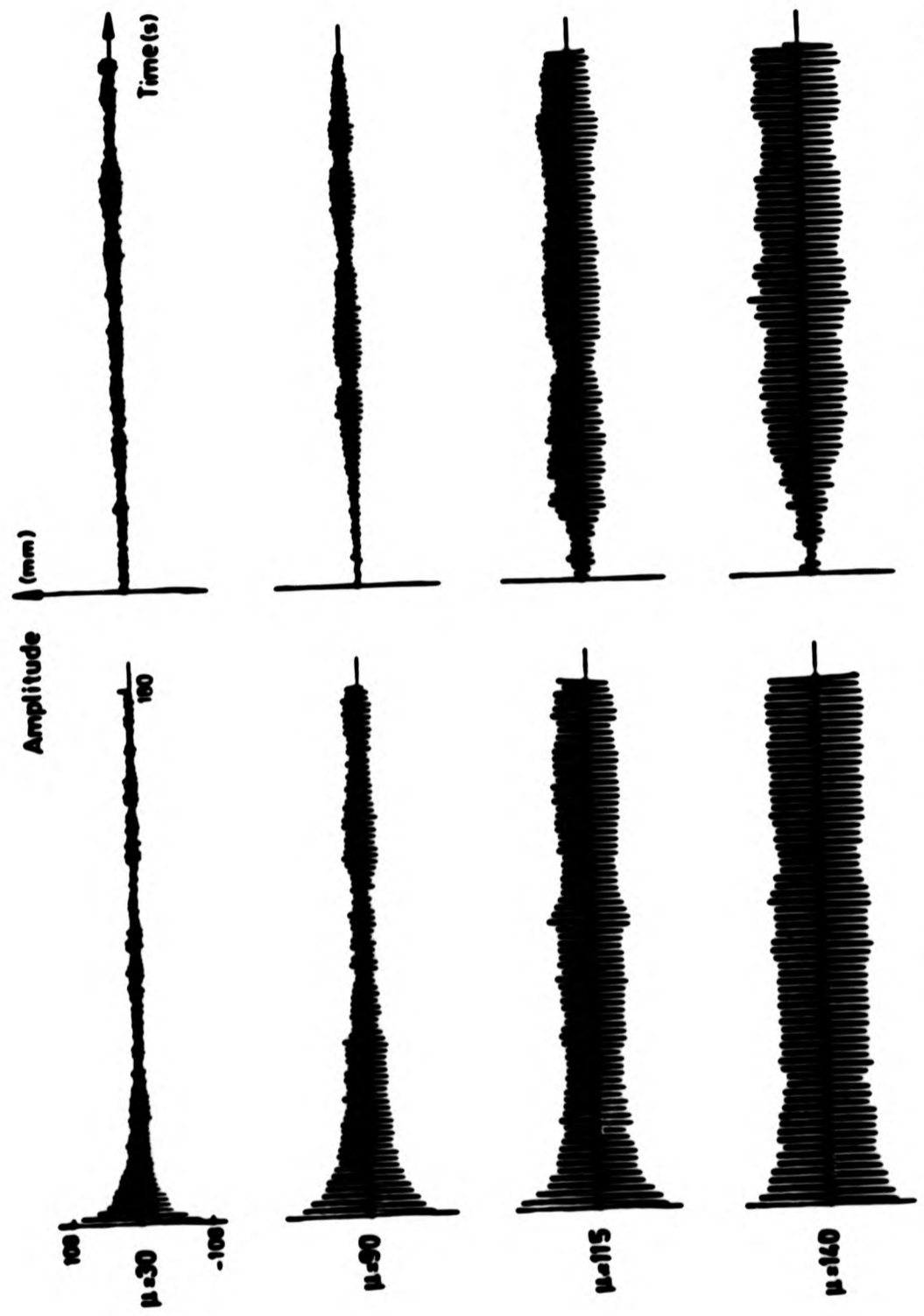


Figure 2.3 Time histories of a moored vessel before and after the Hopf bifurcation (a) given an initial displacement and (b) started from the equilibrium.

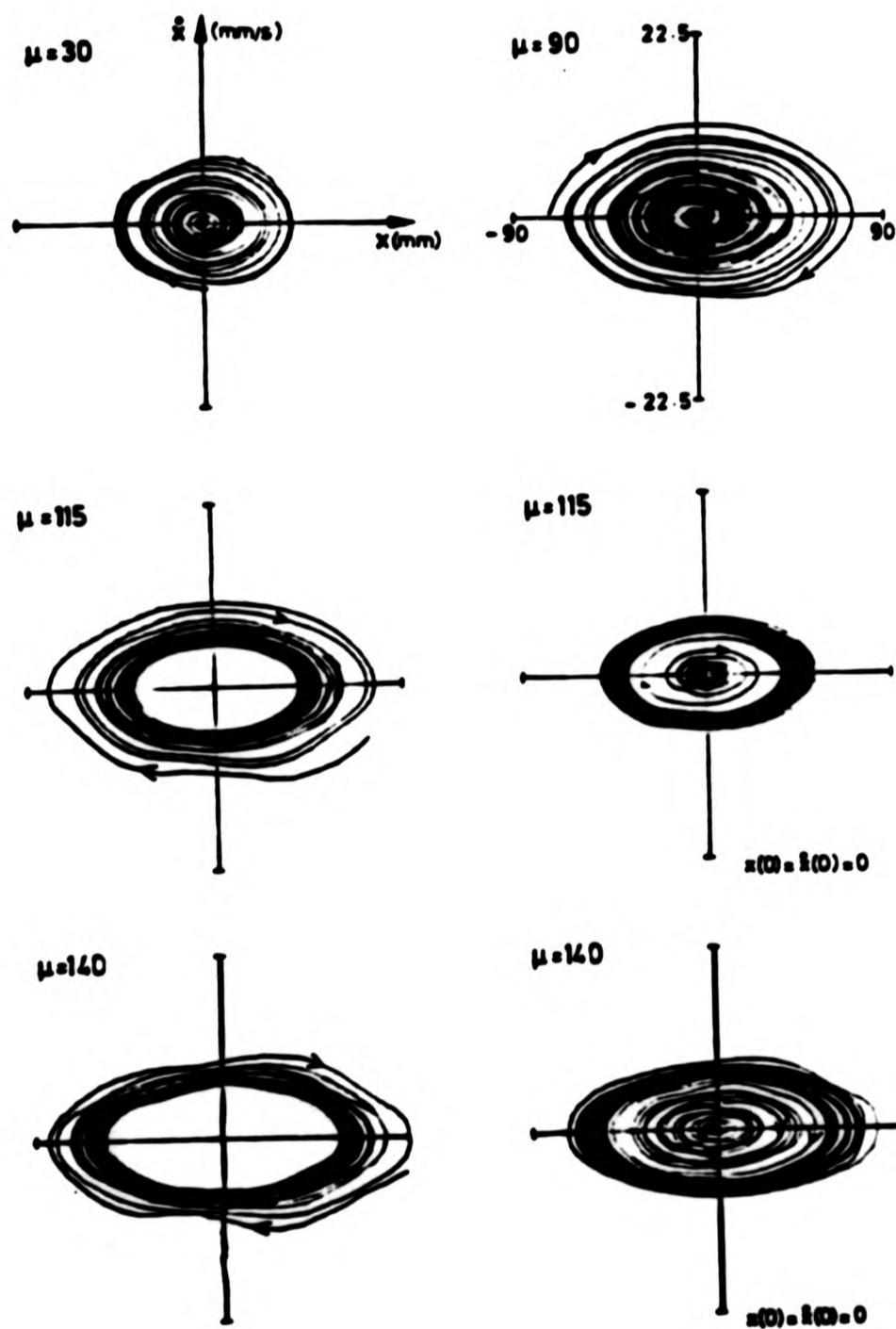


Figure 2.4 Phase portraits of typical trajectories before and after the Hopf bifurcation.

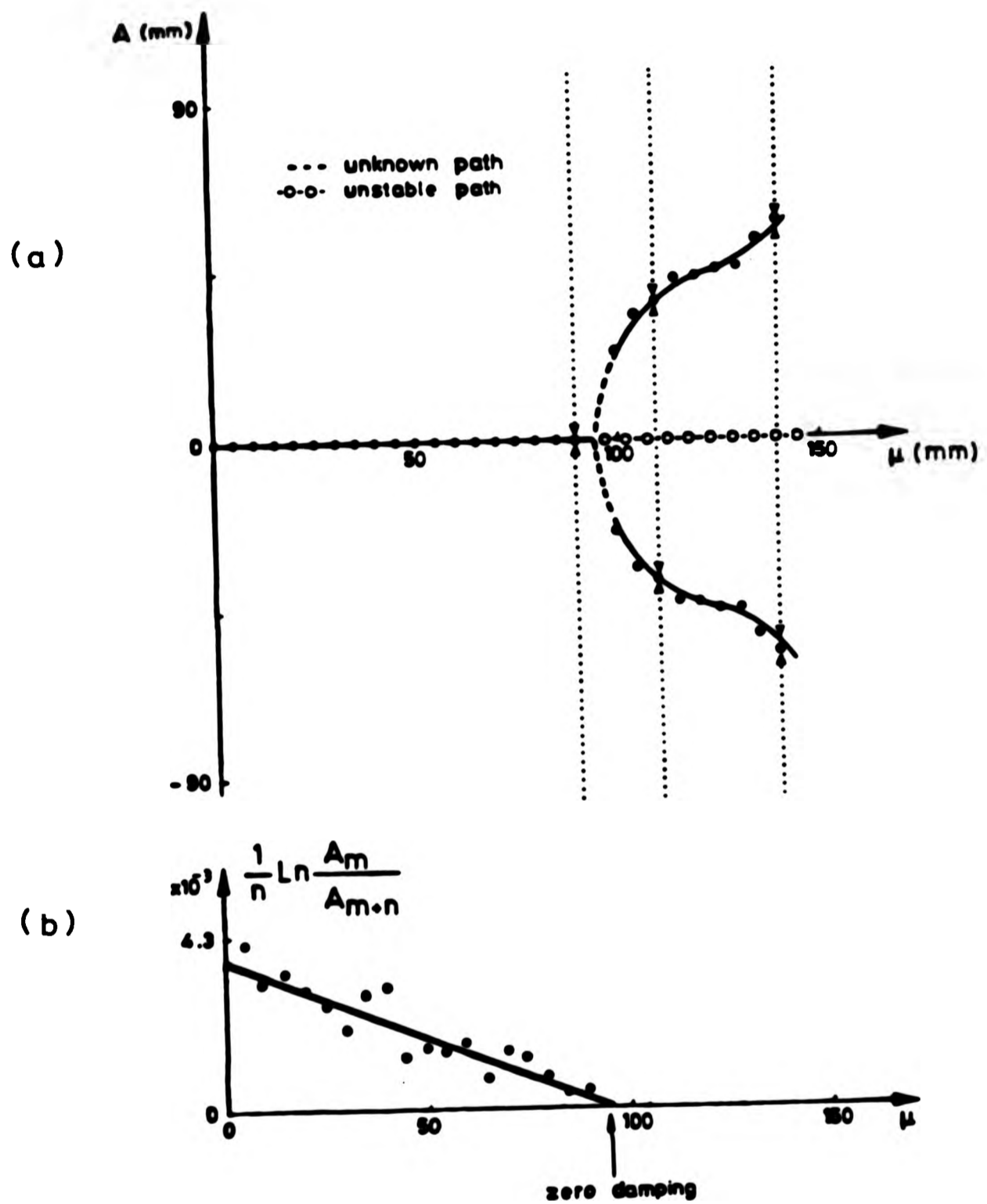


Figure 2.5 (a) Steady state amplitudes plotted against the control parameter.
 (b) Logarithmic decrement approximation to the effective damping and straight line prediction of zero damping.

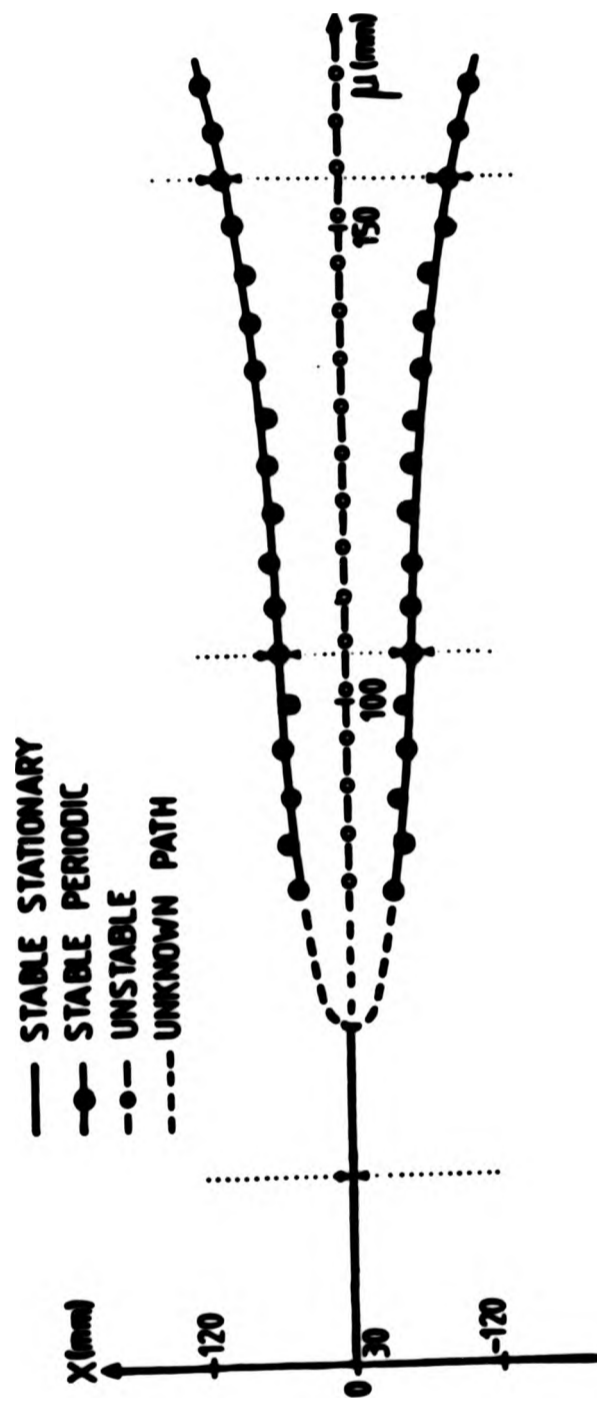


Figure 2.6 Experimental results of fishtailing using model 2.

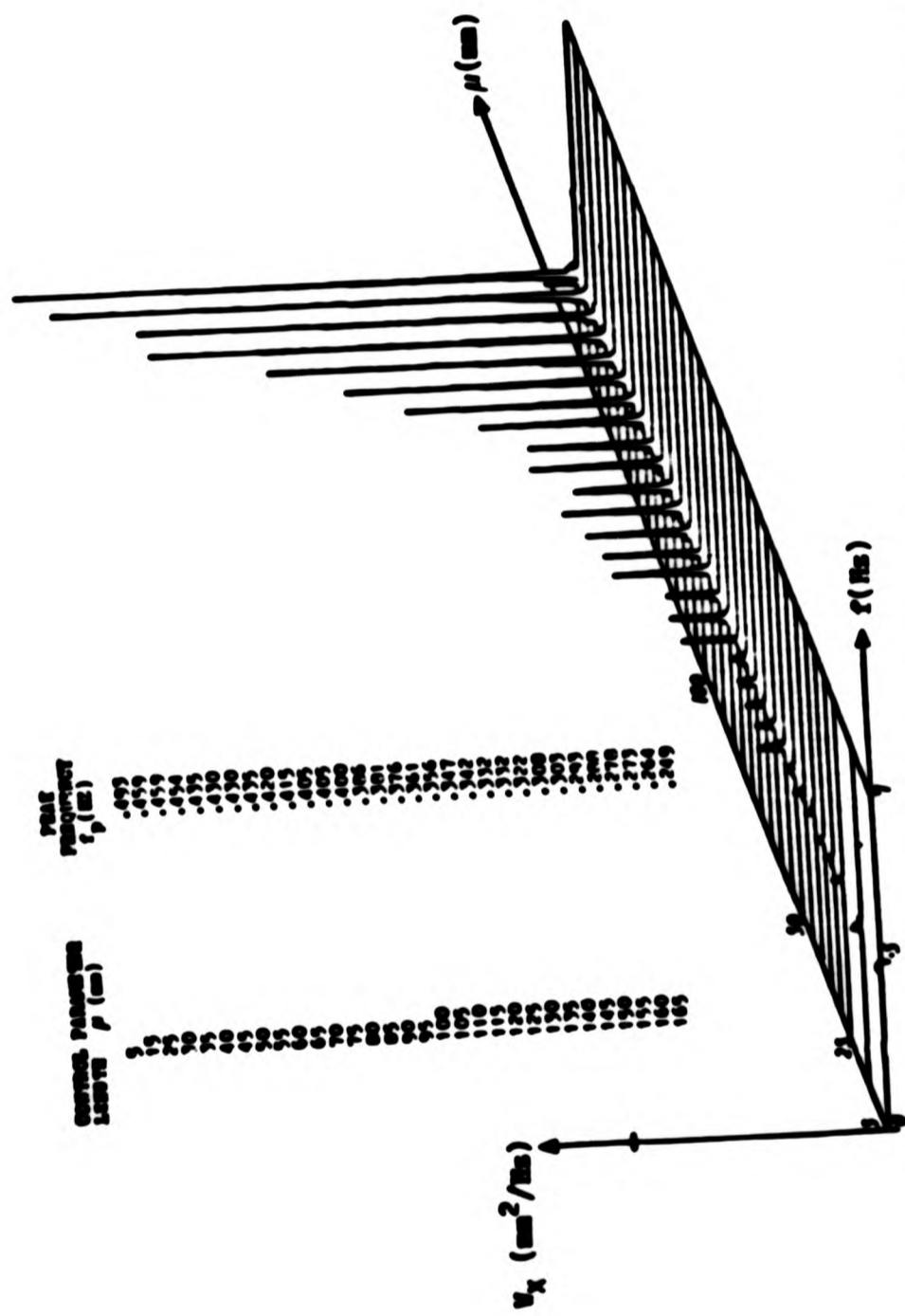


Figure 2.7 Power spectrum of output during fishtailing experiments with model 2.

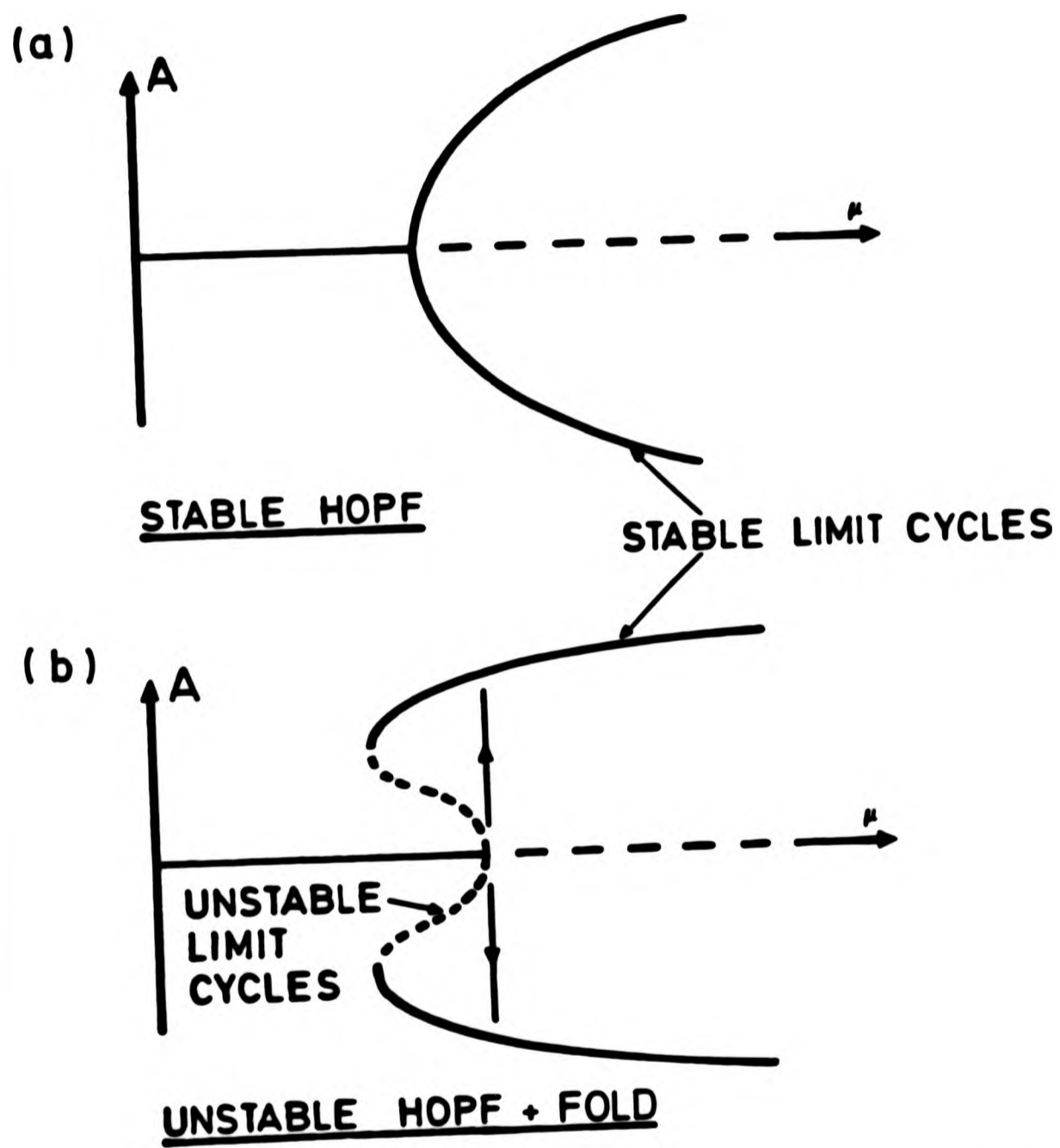


Figure 2.8 Schematic diagrams of stable limit cycles produced by (a) a stable Hopf and (b) an unstable Hopf bifurcation followed by a cyclic fold.

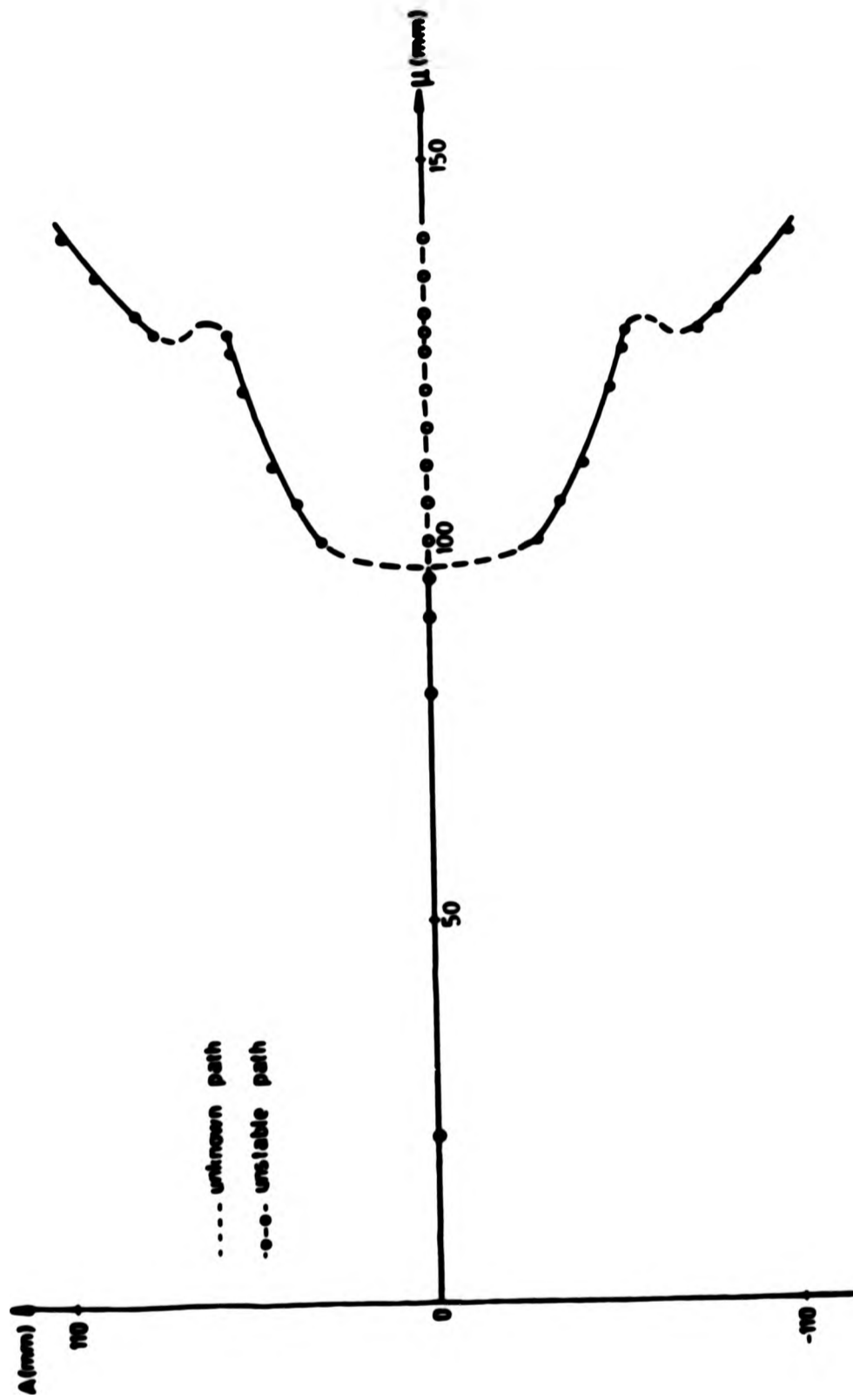


Figure 2.9 Amplitude versus control parameter plot for model 3 tests which displays a jump in response.

CHAPTER III.3

A STUDY OF THE NEIMARK BIFURCATION WITH THEORETICAL APPLICATIONS TO THE INSTABILITY OF PERIODIC MOTIONS OF A BARGE

III.3.1 Introduction

In the previous chapter we have seen an example of the Hopf bifurcation in which a stable fixed point loses its stability and the resulting motion terminates in a limit cycle due to the presence of further nonlinear terms. The counterpart of this bifurcation for a periodic orbit is referred to as a secondary Hopf or Neimark bifurcation [following Abraham and Marsden (1978)], in which a periodic motion becomes unstable and an attracting torus is borne [Neimark (1959), Sacker (1964), Ruelle and Takens (1971) and Iooss and Joseph (1977,1980)]. In order to detect a Neimark bifurcation it is necessary to consider a system with a three dimensional phase space and perhaps for this reason simple examples of the instability from a flow are not as apparent as are those examples of the flip and fold bifurcations. One possible source of the bifurcation is in the flow of fluid between two concentric cylinders which rotate independently, known as Taylor-Couette flow [see Gorman et al. (1980) or Andereck et al. (1983)], producing a variety of flow patterns. In this thesis for the sake of completeness a theoretical example shall be considered of the occurrence of the

Neimark instability relating to the roll motions of a barge and although experimental evidence shall not be reproduced here to support the model, it does nonetheless provide a simplistic description of the real situation.

III.3.2 The Delayed Logistic Map

Despite its apparent lack of simplicity from a flow the Neimark bifurcation is readily visible as an instability of a map viewed either as a two dimensional Poincaré map extracted from a three dimensional flow or merely as a map arising from a pair of discrete difference equations. One such example of a map is the so called delayed logistic map described by the pair of equations

$$\begin{aligned}x_{i+1} &= y_i \\ y_{i+1} &= \mu y_i (1-x_i) , \quad i=0,1,2\dots ,\end{aligned}\tag{3.1}$$

which arises in population biology and ecological systems [see May (1976)]. This two dimensional map, which includes the control parameter μ , has been studied in detail by Aronson et al. (1982) and several other authors including Guckenheimer and Holmes (1983). The system has a non-trivial path of fixed points given by

$$x = y = (\mu - 1)/\mu ,\tag{3.2}$$

which loses its stability at a supercritical (i.e. stable) Neimark bifurcation at $\mu = 2$, illustrated in figure 3.1. In the region just after the bifurcation the mapping points form a limit cycle rotating about the now unstable equilibrium path under the influence of a pair of complex conjugate eigenvalues, the sixth roots of unity in this instance. Figure 3.2 shows iterations of the map for various values of the control parameter before and after the bifurcation. For $\mu < 2$ we see that the mapping points spiral onto the equilibrium path from the starting conditions $x=y=0.01$ (initial conditions given in brackets), similar to the behaviour of a trajectory of a flow in towards a stable node, whilst for values of μ just greater than 2 an attracting limit cycle is formed and iterations either spiral out from the approximate centre of the limit cycle away from the unstable fixed point, or converge onto the periodic orbit from outside for larger values of initial conditions. When $\mu = 2.27$ the limit cycle collides with the unstable path along $x=y=0$ and in doing so sees the end of the attractor.

To investigate the possibility of using the techniques developed in chapter II.5 to predict the onset of a Neimark bifurcation of a flow as a first approach we shall assume that the delayed logistic map is in fact the Poincaré map of a hyperthetical flow.

If we consider a linear approximation of the delayed logistic map in the form

$$\begin{aligned}x_{n+1} &= ax_n + by_n \\y_{n+1} &= cx_n + dy_n,\end{aligned}\tag{3.3}$$

then for consecutive points of the nonlinear map corresponding linear approximations can be determined by either the three- or four-point methods as described in chapter II.5 producing a linear system in which the coefficients depend on the iteration points, i.e. $a=a_n$ etc.. The invariants of the Jacobian matrix, T and D , can be approximated by

$$\begin{aligned}T_n &= a_n + d_n \\D_n &= a_n d_n - b_n c_n.\end{aligned}\tag{3.4}$$

Figures 3.3 and 3.4 show the first 16 values of these approximations for three typical values of the control parameter as the bifurcation is approached. In each case the initial conditions used for the iterations of the map was $x=y=0.01$ with the values of T_n and D_n for $n=0$ corresponding to the third mapping point, since in this particular exercise the equilibrium point is known then the three-point method can be applied. The figures show that well before the bifurcation at $\mu=2$ the approximations rapidly converge to the correct value of the trace or the determinant. However, as the instability is approached estimates take longer to settle down to a fixed value and more iterations of the map would be required for a confident estimate to be evaluated. This particular fact is of less consequence that might at first be imagined since, unlike predictions for the fold bifurcation which are known to only

hold locally to the critical value, predictions can be made by extrapolation using values of the trace (determinant) well away from the bifurcation. Secondly the fact that successive estimates are not quickly settling down to a limiting value could itself be taken as a precursor to the onset of a Neimark instability.

Hence estimates for the trace and determinant of the nonlinear system can be obtained as the control parameter is varied and a parametric study can be made and used to follow their movement in the (T,D) plane, or equivalently the movement of the eigenvalues in the complex plane, as illustrated in figure 3.5.

For the particular nonlinear map under consideration here the Jacobian matrix is given by

$$J = \begin{bmatrix} 0 & 1 \\ 1-\mu & 1 \end{bmatrix} \quad (3.5)$$

so that a linear relationship between the determinant and the control parameter μ can be used as a predictor for the critical bifurcation point when $D=1$.

It should be noted that the mapping points of the delayed logistic map have a periodic motion of order six due to the fact that the eigenvalues are the sixth roots of unity when $T=D=1$ such that

$$\lambda = e^{i42\pi\psi}, \quad \psi = 6. \quad (3.6)$$

An additional tool which can be used when analysing transient maps which rotate near a Neimark bifurcation is the variation of the area A_n enclosed by three consecutive points of the map. Clearly, prior to the bifurcation a transient mapping sequence will converge to the fixed point and thus in this case A_n tends towards zero. Figure 3.6 shows values of the area enclosed by three successive points of the delayed logistic map prior to bifurcation. After the critical value of the control parameter has been passed transient maps will now converge to the limit cycle and so the area does not diminish without end. As a transient map now decays onto the periodic orbit A_n will initially decrease, if the start is outside the limit cycle, or initially increase if the start is close to the unstable centre. As pointed out in part II chapter 5, the ratio of successive areas A_{n+1} and A_n of the linear map is equal to the determinant D_n of the linear system and so once again a linear relationship can be used in this case to predict the onset of the Neimark bifurcation using this ratio. The complete prediction process is summarised in figure 3.7.

III.3.3 The Neimark Bifurcation of Periodic motions of a Barge

A thorough investigation of the Neimark instability from a continuous flow situation has not as yet been undertaken but it

would seem clear that the techniques previously described for a map could also be applied to a flow problem. Complete theoretical and experimental justification for the model to be used in this section shall not be examined rigorously, but it is useful and instructive to form a complete study of low dimension bifurcations by considering a mathematical model rather similar to the fishtailing problem in the previous chapter but with certain added complexities.

The physical situation we shall model is that of a flat bottomed barge fishtailing and rolling under the influence of a steady current. It is known that typical flat bottomed barges can shed vortices from bilges or keels that are constructed to provide extra restoring moment in roll [see for instance Robinson and Stoddart (1986)]. The increased lateral force produced as these vortices are shed can induce a sway motion and this force can be represented by a sinusoidal term due to the regularity at which they are shed. The equation of motion of such a system can be described, in non-dimensional form, by an equation of the Van der Pol type, namely

$$\ddot{x} + b\dot{x} + (x^2 + \dot{x}^2)\dot{x} + x = f\sin\omega t, \quad (3.7)$$

where x is the displacement of the vessel in the sway direction. Further details of the non-dimensionalisation process and properties of this equation can be found in Thompson and Lunn (1981), also see Thompson (1982).

With $f=0$ the system is autonomous such that if the linear damping coefficient, b , is allowed to change from being positive to become negative then the system will experience a stable Hopf bifurcation at $b=0$ similar to the fishtailing model of the previous chapter. This situation is schematically viewed in the top diagram in figure 3.8 with some typical trajectories both before and after the bifurcation being included in figure 3.9.

When f is nonzero, while b is still positive, the system (3.7) can sustain periodic oscillations which are harmonic due to the forcing term. As explained, this motion is a direct consequence of the vortices shed during roll motions (possibly caused by the excitation of the barge by additional head waves), but we assume that these two motions can be uncoupled so that we shall only consider lateral sway displacements. If we now consider the further possibility that during these small amplitude sway oscillations the mooring length between the barge and its load is altered, similar to the approach of chapter III.2, such that the effective linear damping coefficient of the system changes from being positive to become negative then a bifurcation will occur when $b=0$. This instability will be a Neimark bifurcation and the subsequent motion will be on an invariant torus and not, as previously, a simple limit cycle. This scenario can be seen in the lower diagram of figure 3.8, with the small amplitude harmonic motion prior to the bifurcation marked by a faint circular path; this in turn being characterised by a single repeating Poincaré point.

The projection of trajectories in the (x, \dot{x}) phase plane can now cross one another, since the system is now non-autonomous, as can be seen in the diagrams in figure 3.10 calculated at the same control parameter values as used in figure 3.9. As is usually the case for a forced system it is now more convenient to examine the motion via its Poincaré map sampling the trajectories at multiples of the forcing period (i.e. 2π). The control-phase plane will now have a structure similar to that of the delayed logistic map (figure 3.1) which will include a Neimark bifurcation at $b=0$. A variety of Poincaré maps for control values before and after the bifurcation can be seen in figure 3.11 which have the same structure (node followed by a limit cycle) as in figure 3.2, the equivalent situation for the map. The top left hand diagram of figure 3.11 shows the position of the Poincaré points on the trajectory, though a record of the trajectory itself is not usually retained.

A final point to note here is that the rate of rotation of the Poincaré points is directly governed by the frequency at which the vortices are shed. This relationship can be most clearly visualised when considering the path of trajectories converging onto the attracting invariant torus from a starting condition close to the centre of the torus. Some trajectories and corresponding Poincaré maps for a range of values of the frequency ω are given in figure 3.12. Reference should be made here to the definition of the orbit number given in chapter II.5 and the use of the variation of the speed of rotation to predict the folding of a periodic orbit in the next chapter.

In conclusion, although this investigation of the Neimark bifurcation is somewhat hypothetical using as it does a heuristic model, it does appear likely that predictions of the onset of this instability could be made by using the same techniques as applied to the delayed logistic map as previously detailed.

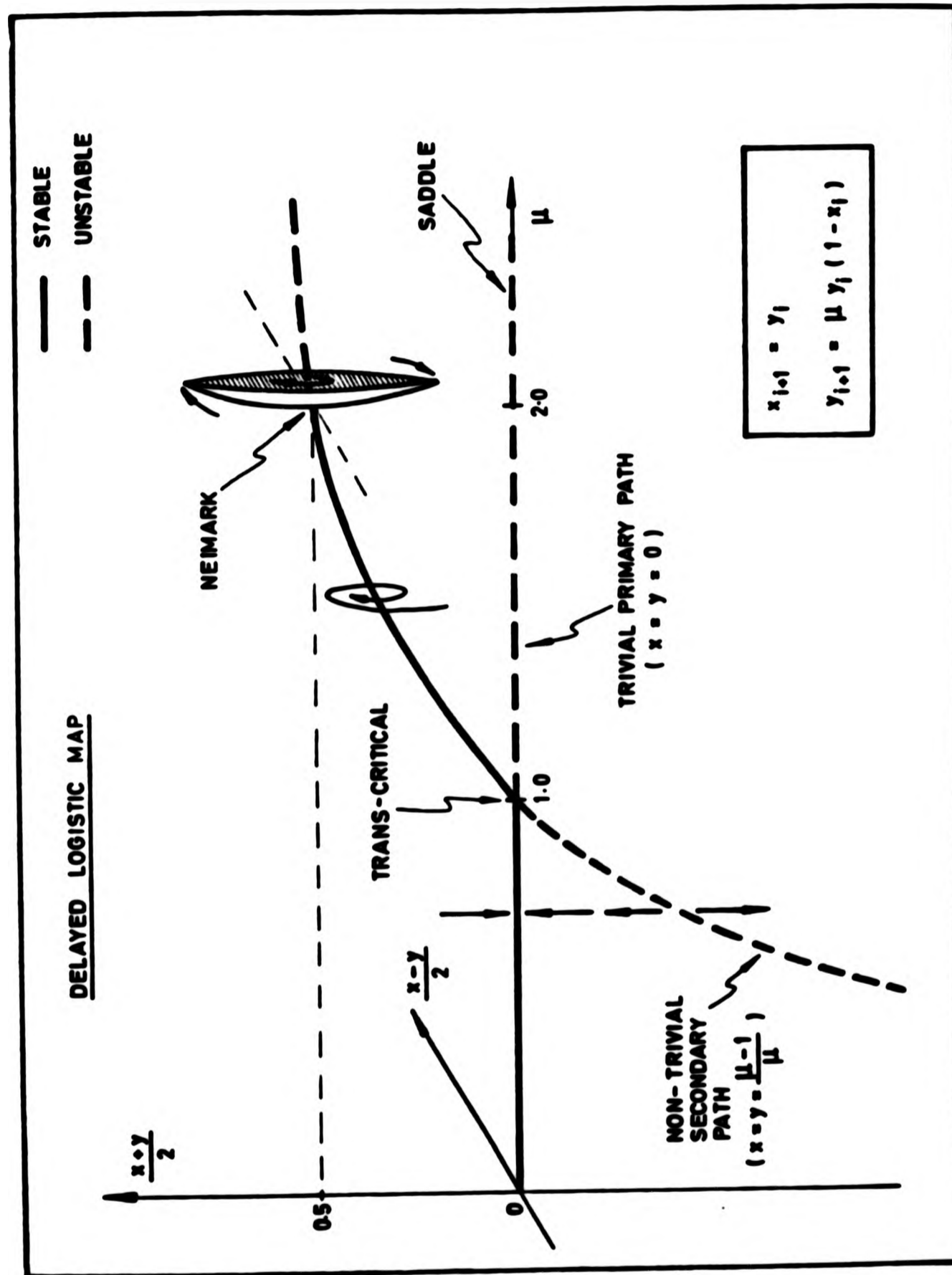
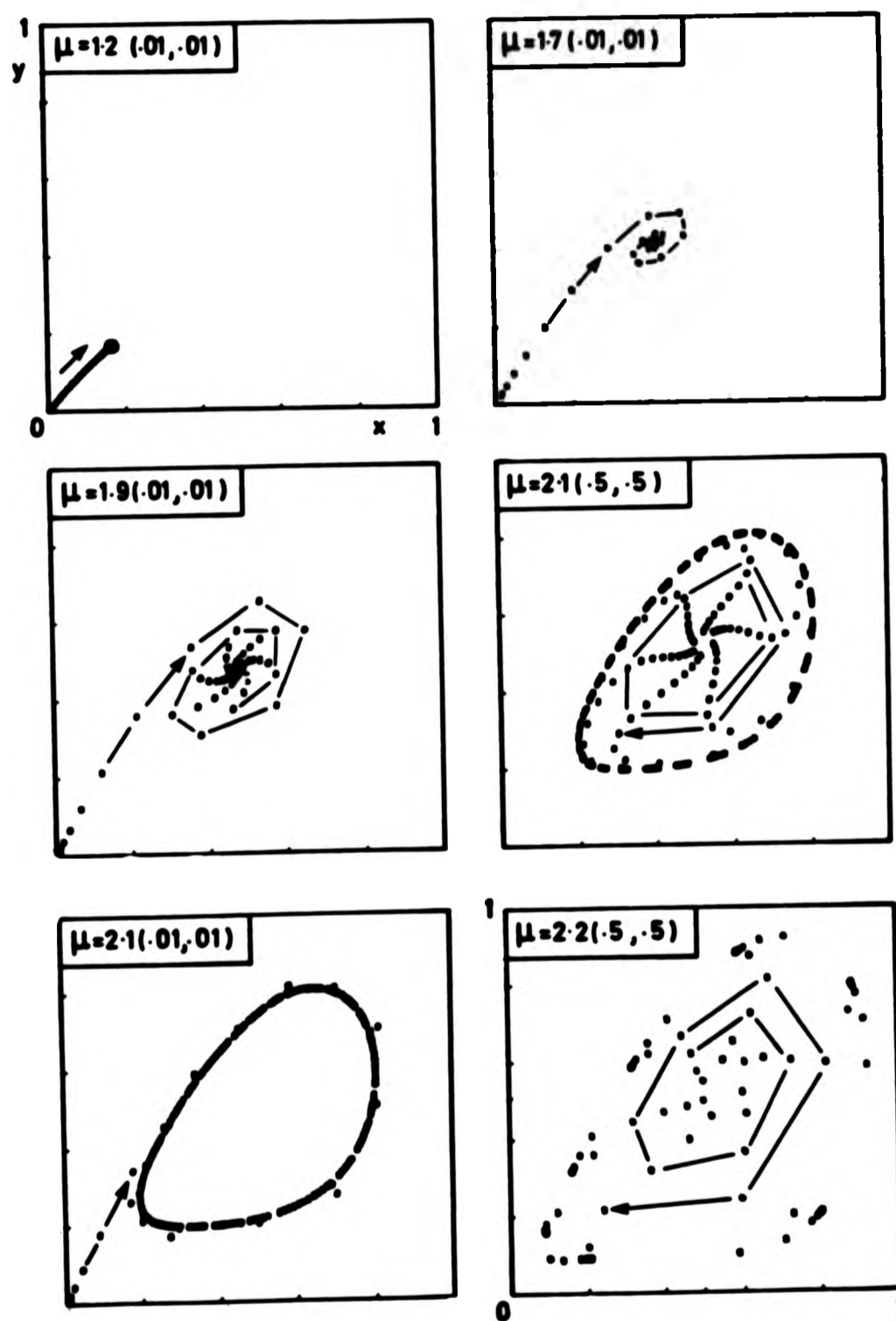


Figure 3.1 The equilibrium paths of the delayed logistic map with a Neimark bifurcation at $\mu = 2$.

DELAYED LOGISTIC MAP



NEIMARK BIFURCATION :

$$x_{i+1} = y_i \quad y_{i+1} = \mu y_i (1 - x_i)$$

Figure 3.2 Iterations of the delayed logistic map
(initial conditions given in brackets).

TRACE

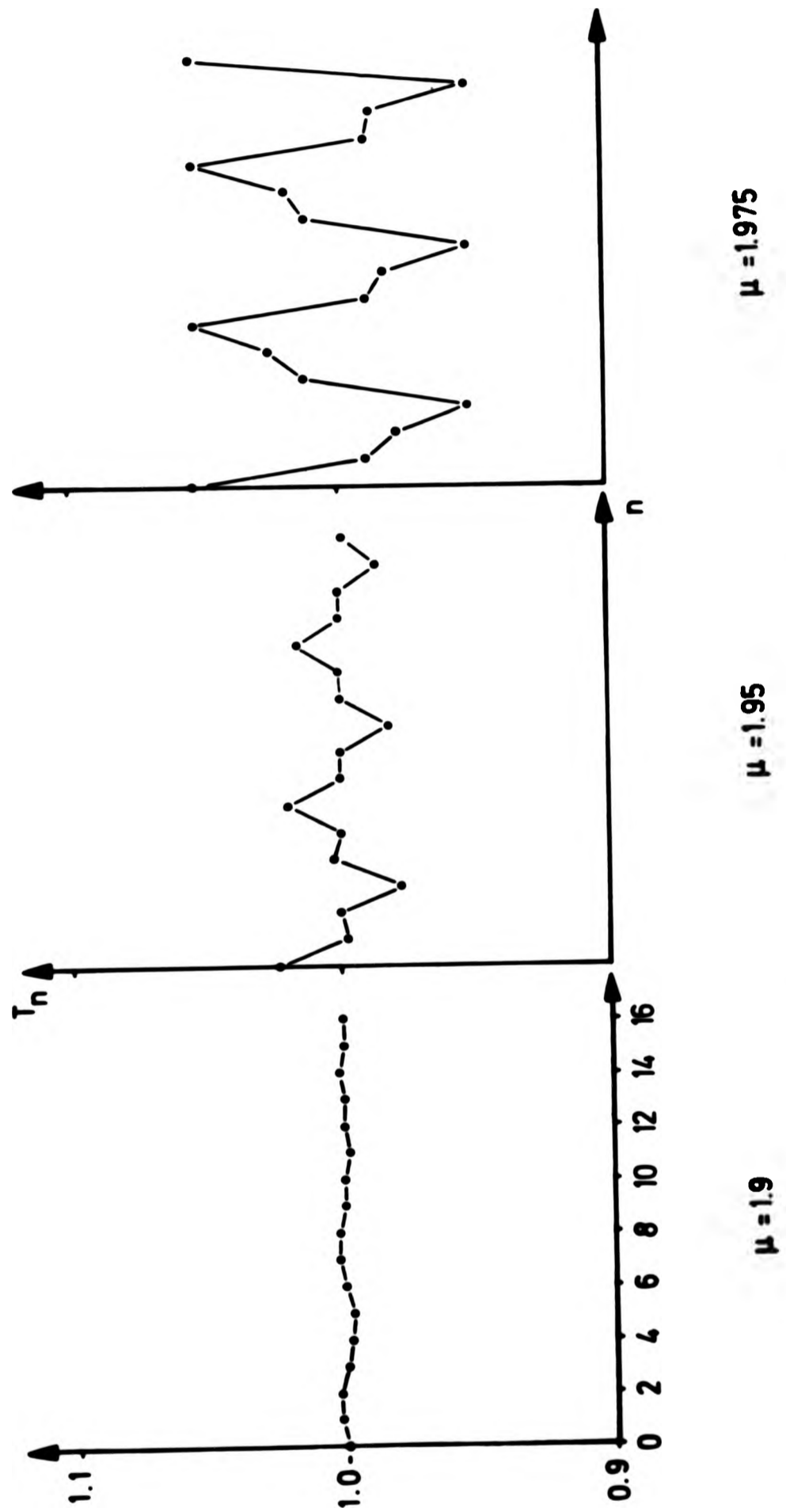


Figure 3.3 Linear approximations to the trace of the delayed logistic map.

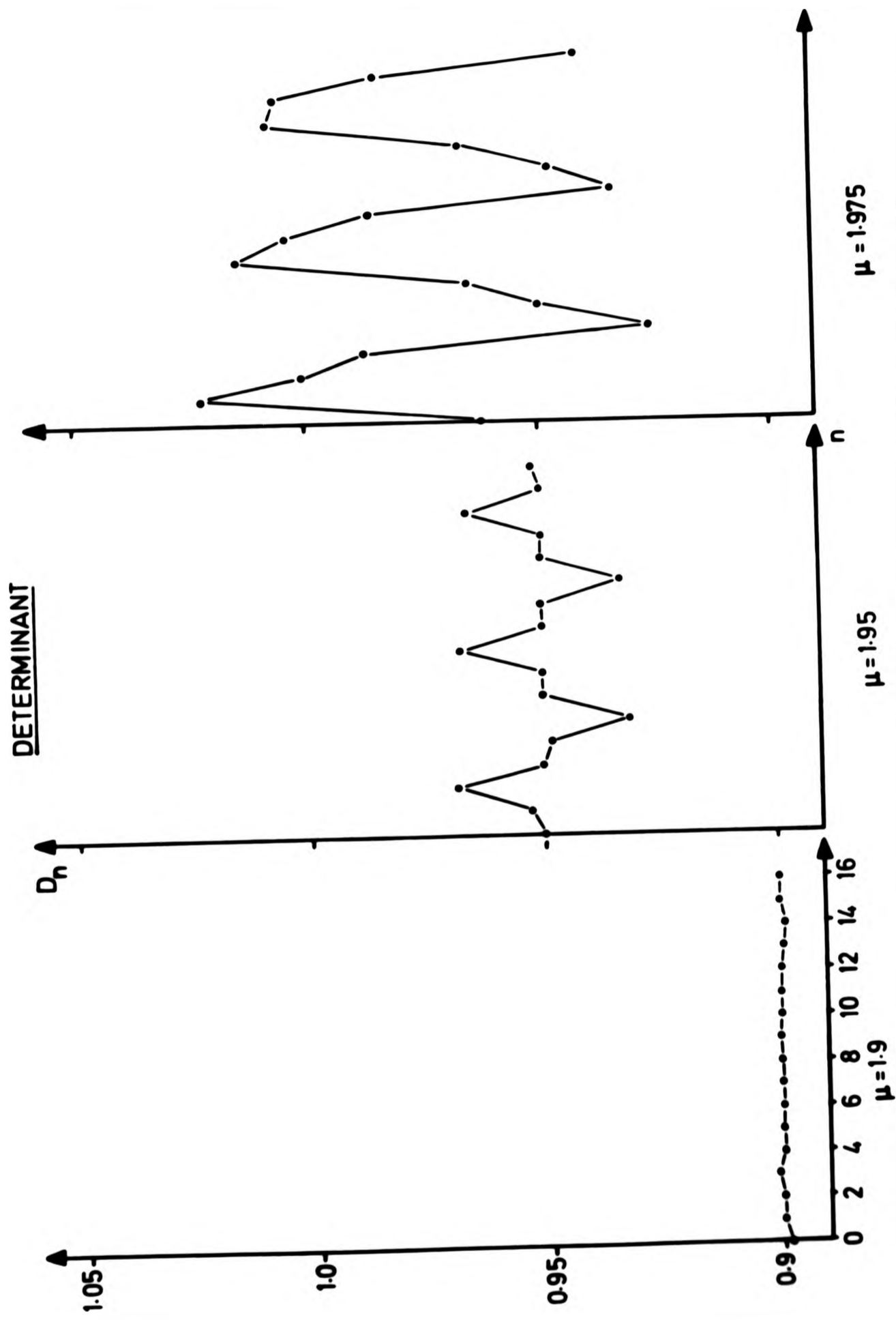


Figure 3.4 Linear approximations to the determinant of the delayed logistic map.

NEIMARK BIFURCATION

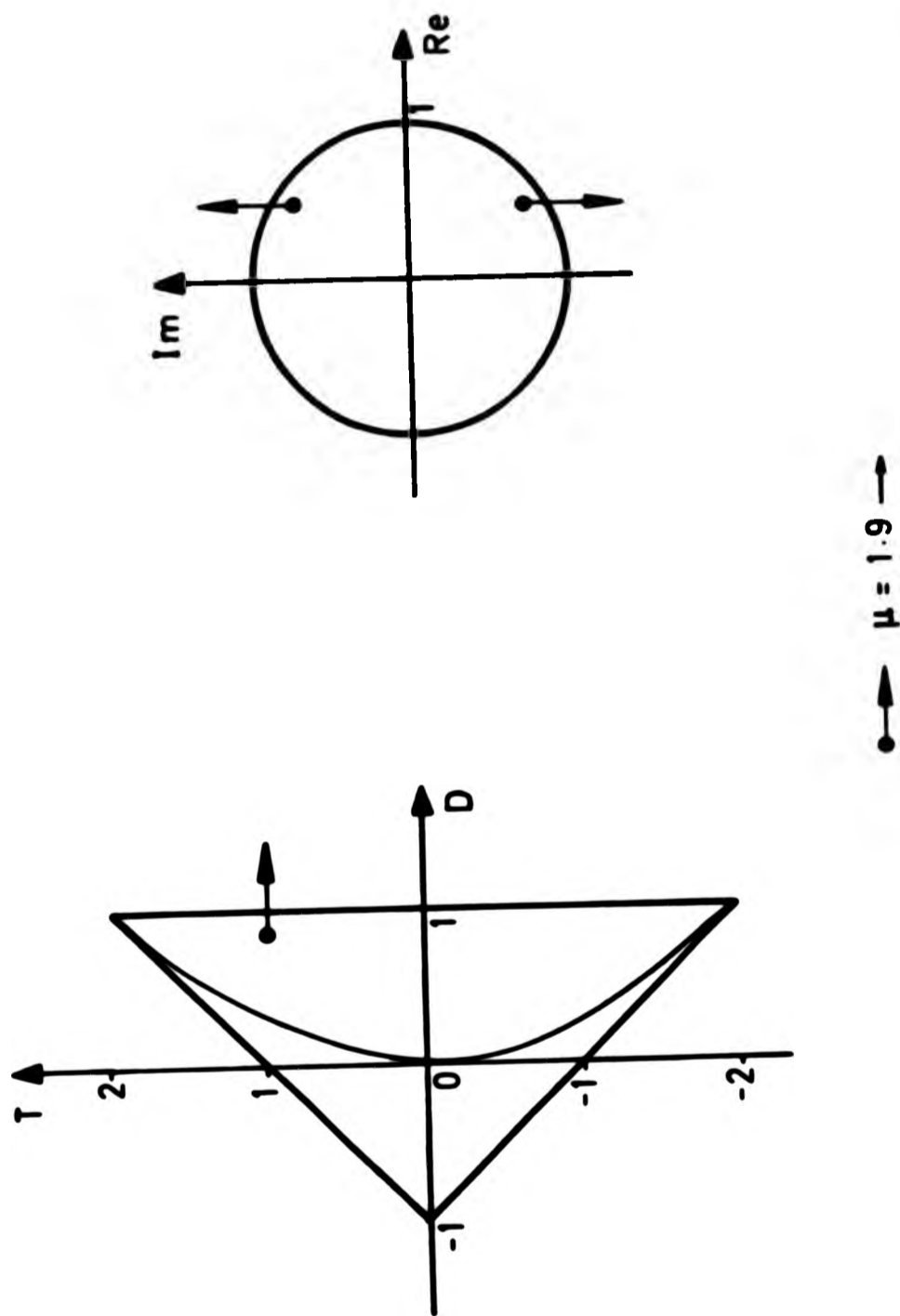


Figure 3.5 Parametric study of the Neimark bifurcation as portrayed by the movement in the (T,D) plane or as the movement of the eigenvalues in the complex plane.

AREA

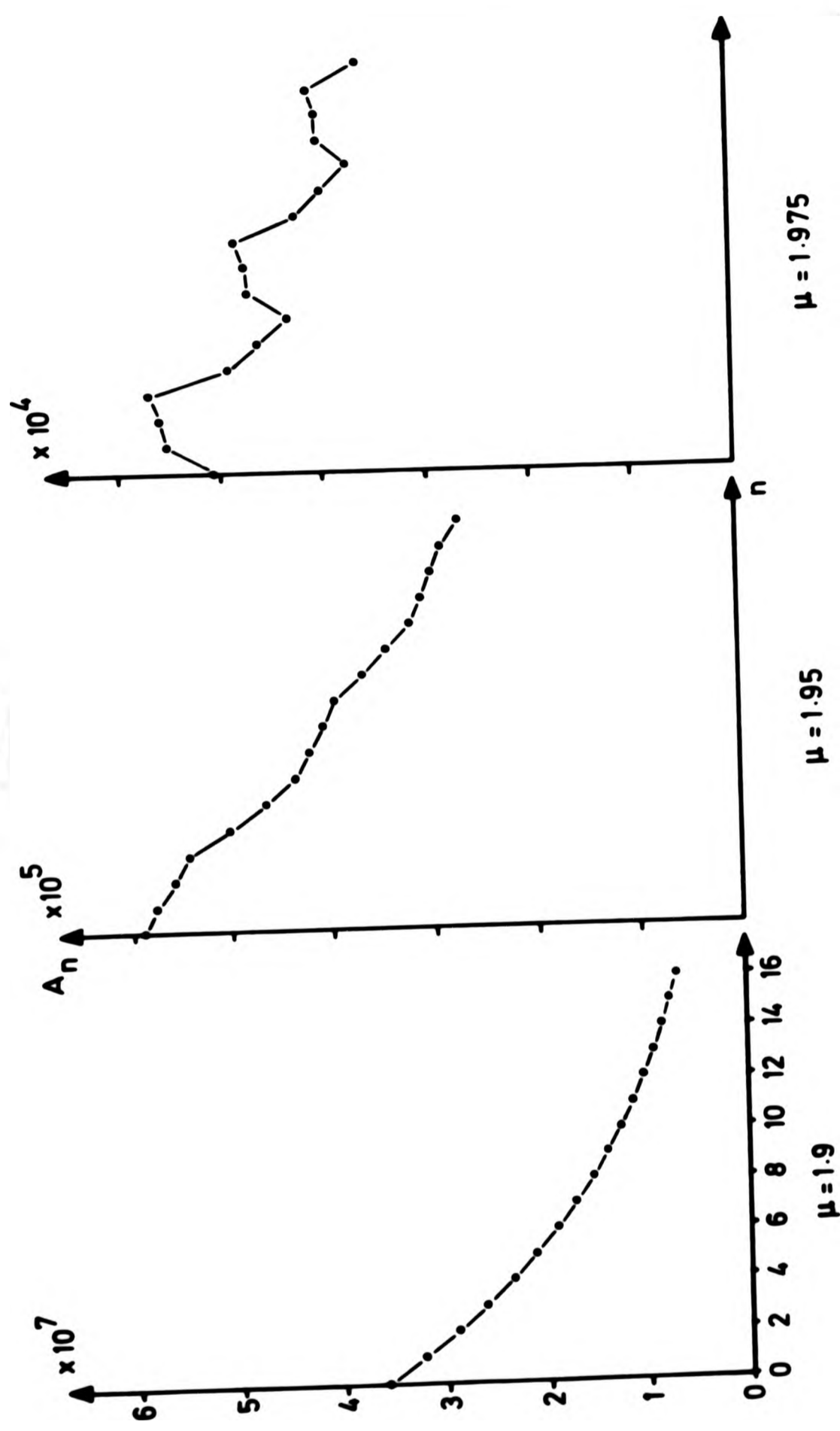
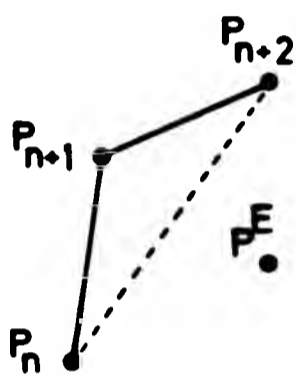


Figure 3.6 Area (A_n) enclosed by successive points as the Neimark bifurcation is approached.

DELAYED LOGISTIC MAP

$$\left. \begin{aligned} x_{n+1} &= y_n \\ y_{n+1} &= \mu y_n (1 - x_n) \end{aligned} \right\} n=0,1,2,\dots$$



$$P_n = (x_n, y_n)$$

$$P^E = (x^E, y^E)$$

$A_n = \text{area enclosed by } P_n, P_{n+1}, P_{n+2}$

linear approximation

$$x_{n+1} = a_n x_n + b_n y_n$$

$$y_{n+1} = c_n x_n + d_n y_n$$

$$T_n = a_n + d_n$$

$$D_n = a_n d_n - b_n c_n$$

$$\frac{A_{n+1}}{A_n} = D_n$$

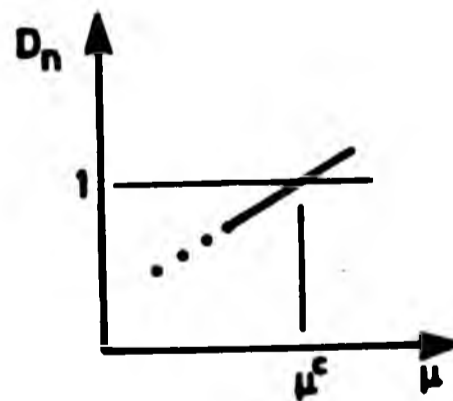


Figure 3.7 Prediction procedure for the Neimark bifurcation.

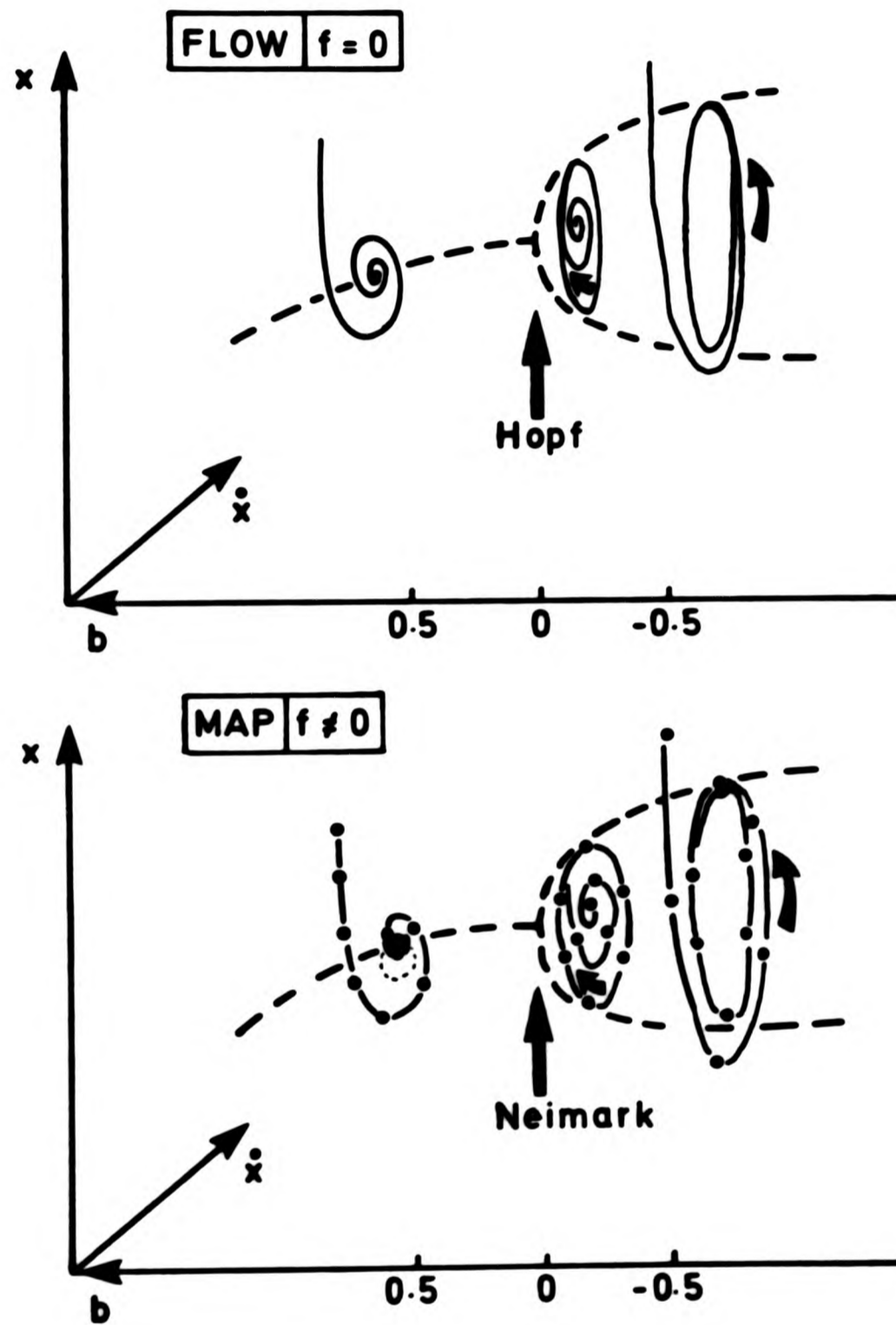


Figure 3.8 Idealisation of the Hopf and Neimark bifurcations.

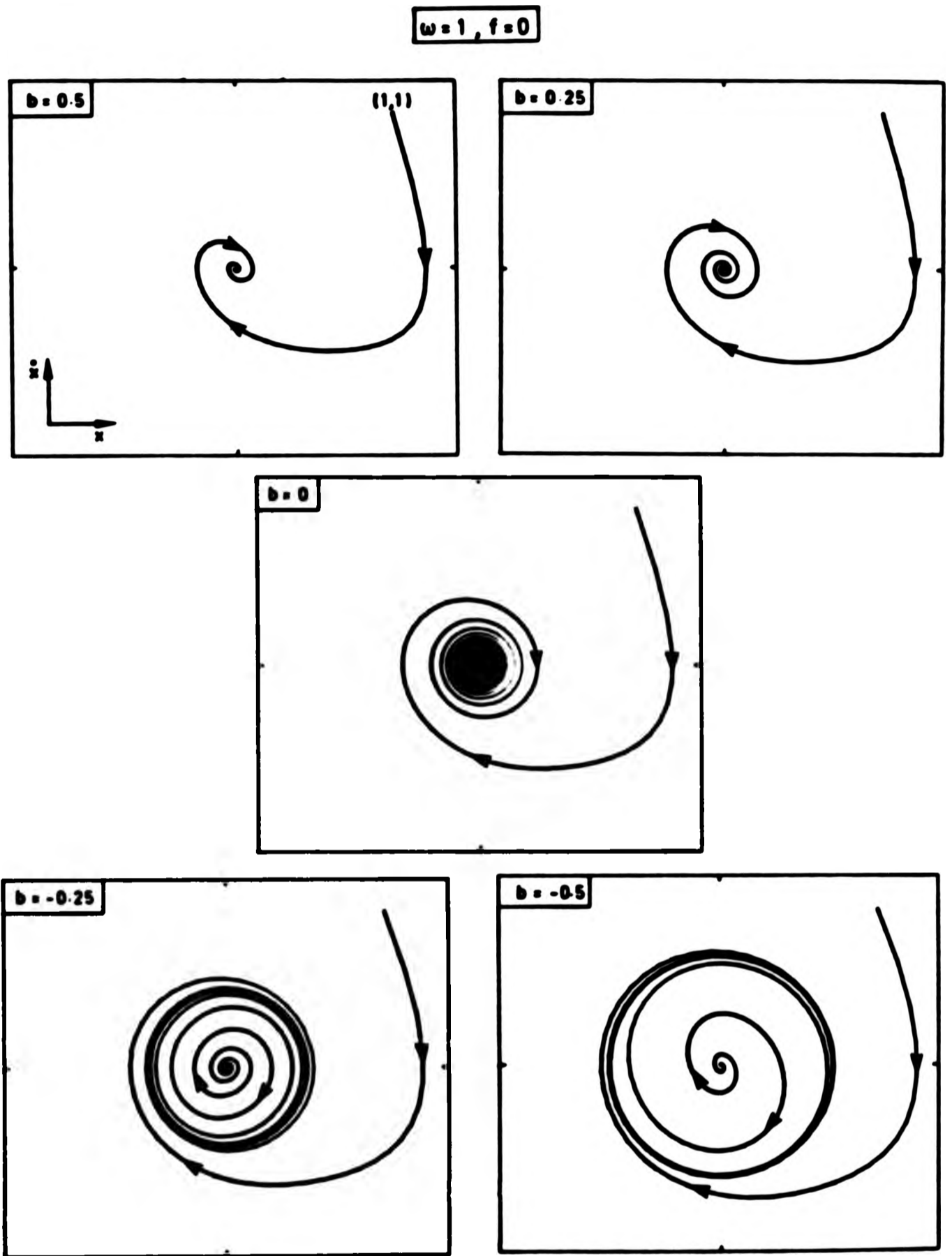


Figure 3.9 Typical trajectories for a system undergoing a Hopf bifurcation, the lower diagrams include a limit cycle with starts both inside and outside the limit cycle.

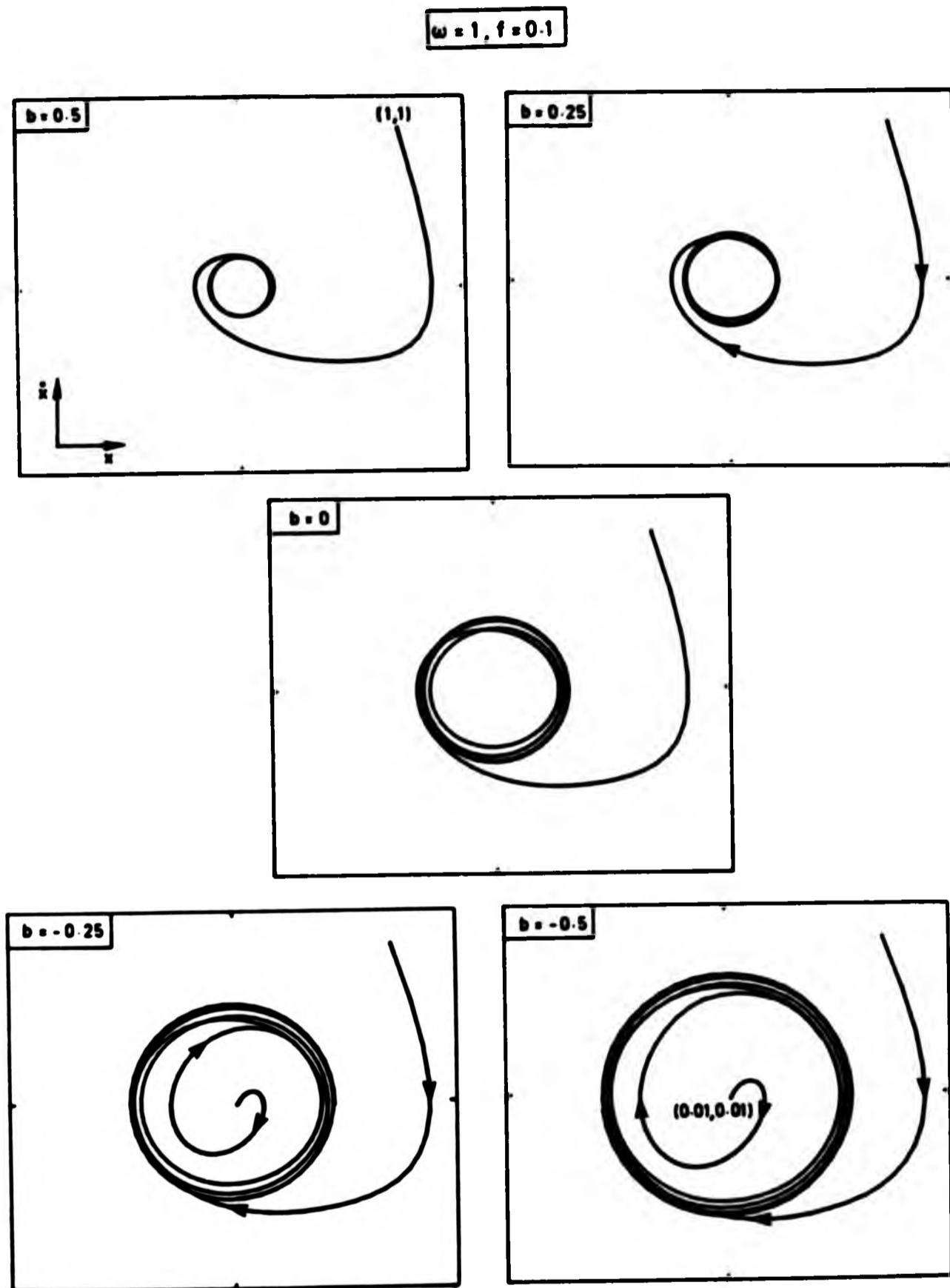


Figure 3.10 Typical trajectories of a system undergoing a Neimark bifurcation.

$$\omega = 4, f = 0.1$$

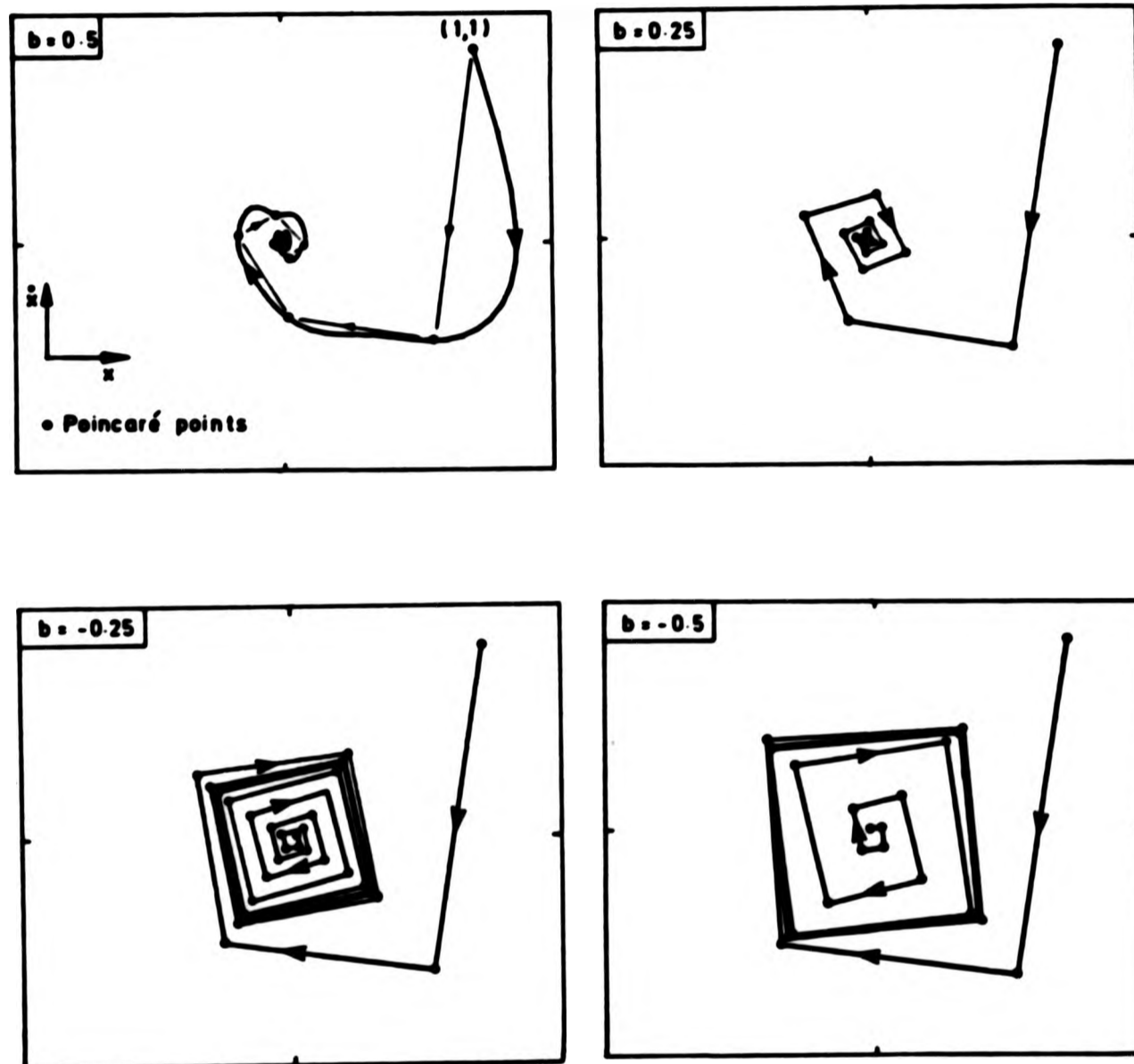


Figure 3.11 Poincaré maps of a forced system during a Neimark bifurcation inducing a limit cycle in the map.

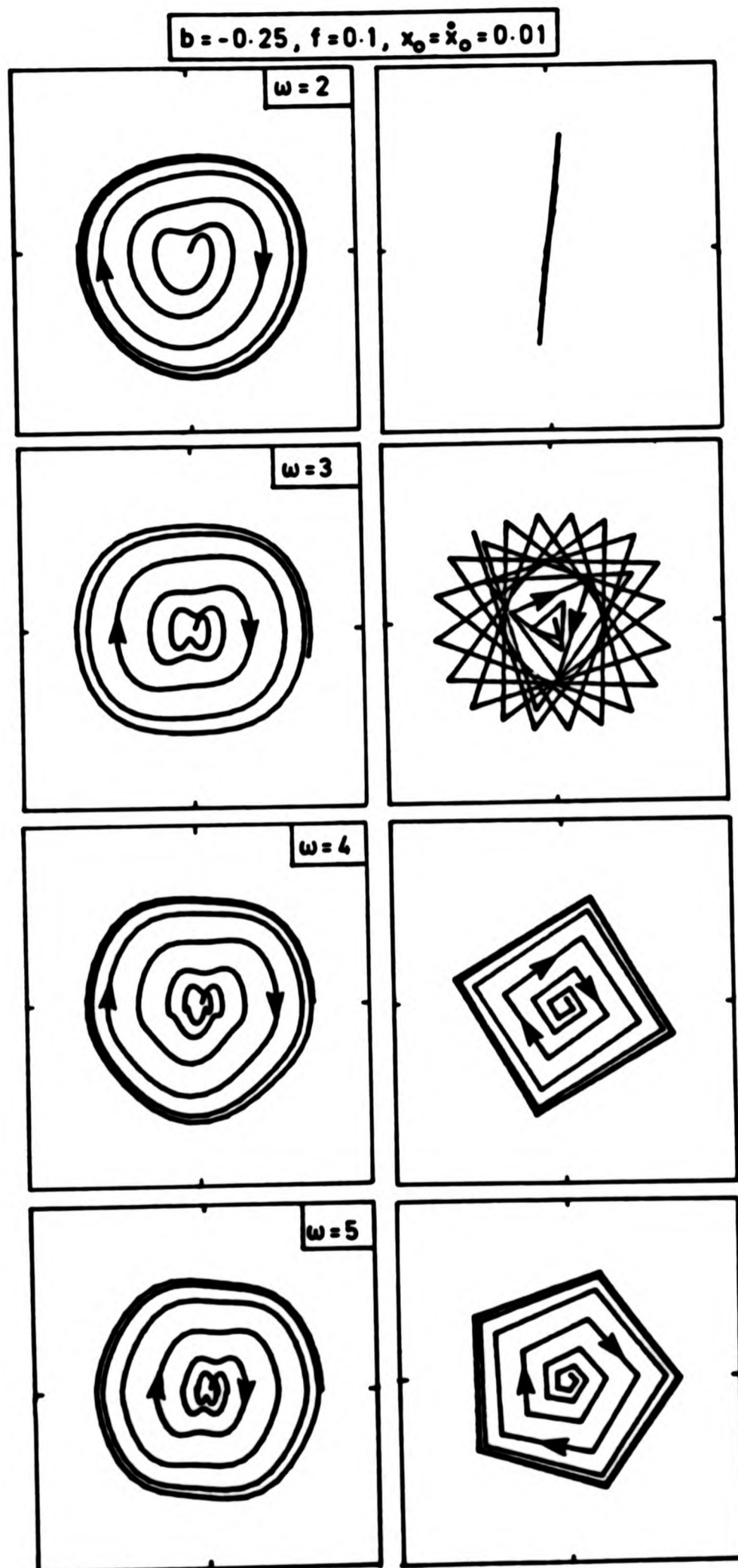


Figure 3.12 Trajectories and corresponding Poincaré maps for various values of the frequency of forcing.

CHAPTER III.4

PREDICTING INCIPIENT JUMPS TO RESONANCE OF COMPLIANT MARINE STRUCTURES IN AN EVOLVING SEA-STATE

III.4.1 Introduction

When monitoring the wave driven motions of a compliant offshore facility, be it a vessel, a platform or an articulated mooring tower, the engineer would like to be able to predict, in real-time, any incipient jump to resonance that might be imminent due to a slowly evolving sea-state. We explore in this chapter the use of some possible predictions introduced earlier for both a jump to fundamental resonance and a flip to subharmonic resonance. Stroboscopic mapping techniques based on discrete time sampling are used to give information about the approach to instability. The first application of these techniques is in the prediction of the jump to resonance and consequent capsize at a cyclic fold in the roll response of a vessel in regular beam seas. Secondly, the techniques are shown to work well in a variety of computational situations when applied to the simulation of the motions of an articulated mooring tower during the approach to the potentially dangerous oscillations produced by the onset of subharmonic resonance at a flip bifurcation, both in regular and irregular ocean waves.

The study of the behaviour of compliant offshore structures is well suited to stroboscopic mapping techniques since ocean waves tend to be inherently periodic in nature. Many offshore facilities can be modelled by nonlinear oscillators and in such problems the response of the system can be sampled at multiples of the predominant period of the waves. In a realistic sea-state ocean waves are not entirely regular but prone to some large amplitude slam or irregular waves, caused for example naturally by wind action or wake interaction from a neighbouring vessel. Any impulsive or slam loading of a compliant system in an otherwise regular sea causes a perturbation from an equilibrium state and will produce a transient motion. Given a single or even a random sequence of such transients what information can we retrieve about the imminent behaviour of the structure and in particular can we predict at what point, if any, the system will become unstable?

In order to attempt to answer this question we shall utilise the Poincaré mapping ideas as introduced in part II of this thesis and apply the prediction methods based on the monitoring of the eigenvalues of the system using the Centre Manifold, three- and four-point methods.

Obviously at this stage it is not intended that these techniques should form a design method but should be considered as tools to assist in the analysis of behaviour, monitor and predict instabilities, and add to our overall understanding of compliant structures in ocean waves. To illustrate these

techniques we shall consider two practical problems currently of great interest in the offshore industry, namely the modelling of the capsize of a ship in a regular sea, and the behaviour of an articulated mooring tower in a changing sea-state.

III.4.2 Ship Roll Response Leading to Capsize

In this section we consider the roll response of a ship, or vessel driven by regular beam seas. The capsize of ships is obviously a complicated mechanism with little data recorded about the displacement time histories of such vessels just prior to capsize. It is certainly true that a number of the ships that capsize each year do so in seas in relatively mild environmental conditions not in conditions thought at the time to be harsh or dangerous [see the Lloyds Register], and this is verified to some extent by the experimental model studies conducted by the Admiralty [see Marshfield (1978) or Wright and Marshfield (1980)]. For clarity at this stage we shall consider periodic beam seas (i.e. deterministic and non-evolving) so that the essential features of the problem can be modelled by a relatively simple equation. This type of analysis can then be extended to include a more irregular sea as in the section that shall immediately follow this work.

We start by introducing a semi-empirical nonlinear oscillator with a single degree of freedom. Assuming that the wave length is long compared to the ship's beam, the roll motion

of the vessel can be sufficiently modelled by the equation

$$\ddot{\vartheta} + G(\dot{\vartheta}) + F(\vartheta) = \alpha \sin \omega t, \quad (4.1)$$

where a dot denotes differentiation with respect to time t , ϑ is the relative roll angle, α is the effective wave slope amplitude, ω is the forcing frequency (taken here to be the control parameter). $G(\dot{\vartheta})$ and $F(\vartheta)$ are odd polynomials of order 3 and 15 which represent the damping and restoring forces respectively, the coefficients of which were obtained from laboratory experiments [Marshfield (1978)]. An extensive experimental investigation of this problem has been made by Wright and Marshfield (1980) and figure 4.1 gives some details of the model used and approximate steady state solutions of equation (4.1) as obtained by Wright and Marshfield using the perturbation method and Floquet theory [for a similar study see Cardo et al. (1984)]. Equation (4.1) was shown to give reasonably close agreement with the experimental results of the laboratory tests under various fluid loading conditions. For more details and a more elaborate roll motion analysis the interested reader should consult the papers of Marshfield, and Wright and Marshfield.

The approach here is to study the transient behaviour of equation (4.1) as the forcing frequency is increased and the system nears a jump in resonance [similar to the jump in resonance of a driven beam as modelled by a Duffing type of equation, see Bishop and Franciosi]. Physically this is

modelling a changing sea-state in which the frequency of the exciting waves is slowly increasing. Simulations of the system using this mathematical model were carried out using a time integration routine on a digital computer, the results of which are indicated in the lower diagram of figure 4.1 by a small circles. Due to the form of the righting lever, also referred to as the GZ curve, solutions past the fold point of the resonance response curve can lead to capsize rather than picking up the larger amplitude steady state. Transient motions, caused by random kicks superimposed on the periodicity of the waves (simulated by setting the initial conditions of the system away from the stable steady state) are tracked by the Poincaré sampling methods as they decay onto the equilibrium state.

The stability region shown shaded in figure 4.2 implies that oscillations will start to grow locally if the approximating two dimensional linear map evolves so that the path representing the trace and determinant of the system passes through the divergence boundary associated with the cyclic fold instability. This path in the (T,D) plane for the roll motion of a vessel for increasing frequency is shown in figure 4.3. As the path, which represents the stability of the system, crosses the parabola $T^2=4D$ the transient motion changes from an oscillatory to an asymptotic behaviour corresponding to a coalescence of the eigenvalues in the complex plane as seen in figure 4.3. The coalescence, which occurs within the unit circle because of the positive damping which gives the ship overall stability, is rapidly followed by one of the (now real)

eigenvalues crossing the unit circle at the cyclic fold resulting either in a jump to a resonant state or, as in this case, capsize. The movement of these eigenvalues can be used to predict the incipient instability of the periodic motion and a linear relation of a power of the argument of the eigenvalues plotted against frequency of forcing can be established analogous to the quartic beat predictor in Bishop and Franciosi [also see Thompson and Virgin (1986)]. This prediction curve is shown in figure 4.4. As pointed out in chapter II.5 the prediction will be of the point at which critical damping occurs but as a function of the control parameter the fold appears very close to the point of critical damping. Thus in practical situations a knowledge of the critical damping would prove a useful, conservative estimate of the point of folding.

Returning to figure 4.3 it is worthwhile to note that the rapid movement of the eigenvalues, as argued in chapter II.5, can be seen from the fact that the points, corresponding to values obtained from simulations, are initially evenly distributed, yet after meeting the next point already represents an unstable system with eigenvalues outside the unit circle. It is of practical interest to note that the route to the fold in either of the diagrams in figure 4.3 is not straightforward, in fact at one point it appeared that the system was heading towards a flip bifurcation. This would seem to imply that the practicalities of using these methods as a black box prediction routine might be a little hopeful, nonetheless for systems which evolve slowly the methods may

prove more successful.

This brief study shows a relatively simple application of the numerical techniques earlier introduced. Mathematical models in the form of equation (4.1) have been used to model a variety of floating vessel situations and as we shall see in the following chapters the roll response can exhibit a wide range of nonlinear behaviour including chaotic motions. We shall now concentrate on a second and more elaborate application of the methods including a random sea-state which is allowed to evolve with time.

III.4.3 The Subharmonic Motions of an Articulated Mooring Tower

The articulated mooring tower is used in the offshore industry for loading crude oil into tankers [for more details of this set up see Dumazy and Leturcq (1983)]. Essentially it is an inverted pendulum pinned at the sea bed which stands vertically due to its own buoyancy, see figure 4.5. A tanker moored to this tower behaves like a fixed object in comparison to the local oscillations of the tower. Due to a discontinuity in the stiffness of the system, corresponding to whether the mooring line is slack or not, the system is inherently nonlinear. It has been shown [Thompson et al. (1984)] that the motions of the column can adequately be modelled as the nondimensional bilinear oscillator

$$\ddot{X} + 2\frac{\zeta}{\eta}\dot{X} + kX = \frac{1}{\eta^2} \sin t + r(t) , \quad (4.2)$$

where a dot denotes differentiation with respect to the time (t), X represents the displacement, ζ is the damping factor, η the frequency ratio, k is the stiffness term (non-constant) which has a discontinuity at the origin. The function r(t) is a series of scaled random delta functions modelling any impulsive slam loads. This dynamical system can be shown to exhibit complex behaviour including chaotic motions [Thompson et al. (1984)], but we wish to focus our attention here on the transition from fundamental to subharmonic resonance via a flip bifurcation. With this purpose in mind we fix the stiffness and damping terms and choose η to be our control parameter so that from this previous work we know the critical value at which the flip bifurcation occurs.

Figure 4.6 shows two typical time histories and their associated Poincaré maps in the phase plane of a transient response after an impulsive loading perhaps due to a freak wave. Successive Poincaré points are joined by straight lines to indicate the movement of the map. With a particular value of the control parameter far away from the flip bifurcation, the Poincaré map spirals in towards an equilibrium point, corresponding to a harmonic periodic oscillation, and the eigenvalues of the approximating linear map are complex conjugate. For values of η closer to the critical point the eigenvalues become real and negative as the map oscillates along the centre manifold (eigenvector) as it slowly converges.

As before we shall monitor the transient responses and determine the stability of the system by approximating the nonlinear Poincaré map by a linear map as previously described. In the vicinity of the flip bifurcation the transient is rapidly attracted to the centre manifold and so estimates for the eigenvalues using the three-point method cannot be obtained. Of course when this happens we are now only interested in the critical eigenvalue and so the centre manifold method can be used which approximates the system by a one dimensional map. Figure 4.7 shows estimates of the eigenvalues using both the three-point and centre manifold methods for two chosen representative values of the control parameter. A peculiarity of the equations used in the three-point method means that, close to the centre manifold, after initial divergence estimates restabilise and lock onto the same solution as obtained using the centre manifold method. Similar problems also occur when applying the four-point method.

If we now consider applying these tracking methods to the idealisation of the articulated mooring tower which is subjected to a sequence of random impulses, i.e. of varying amplitude and frequency, then, far away from the bifurcation point, it will be possible to easily detect both eigenvalues. Relatively close to the bifurcation it may prove difficult to evaluate the non-critical eigenvalue λ_2 , but it may still be possible to derive some knowledge of its location by using only the initial estimates which correspond to mapping points which have not as

yet converged onto the centre manifold, see figure 4.8.

Thus using a combination of these methods it will be possible to compute the eigenvalues which determine the state of the stability of the system for increasing increments of the control parameter as it approaches the critical point $\eta = \eta^C$, where the fundamental $n=1$ path bifurcates into the $n=2$ subharmonic path depicting a periodic motion with two distinct amplitudes. This process is viewed in figure 4.9 and included is the equivalent movement of successive maps leading to a path in the (T,D) plane. It is worth noting at this point that the region of the eigenvalues which we are considering here is a local one after the eigenvalues have approached one another and coalesced, a similar local study of the ship roll problem in the previous section could have also been performed provided the sea-state were to evolve at a sufficiently slow rate.

To successfully model a realistic sea-state it is necessary to consider an evolving system in which the frequency is a function of time. To analyse such a model we must now use the four-point method since the precise location of the instantaneous steady state is not known. Figure 4.10 shows some of the results from this type of study at two different rates of evolution, where $\eta = \eta_0 + \beta t$. Clearly estimates are severely effected by the occurrence of a slam load causing a rapid discontinuous divergence followed by a return to the true value of the respective eigenvalue.

If such a system as is modelled here were closely monitored then we have seen that it will be possible to predict the point at which subharmonic motion begins in which one of the two positive amplitudes of the motion can become large, hopefully in time to take preventative action.

III.4.4 Conclusions

The techniques applied in this section form the early stages of research into the application of dynamical systems theory to the problems encountered in modern compliant offshore structures. The methods are intended to provide the offshore analyst with a means of extracting useful information from the transient behaviour so that the onset of potentially dangerous oscillations can be predicted and hence prevented. Obviously in a real situation improved sophisticated monitoring devices and software will have to be developed in order to obtain real-time information about the underlying stability of the dynamic motions of the system. More immediately these theoretical tools can be extremely useful when, for example, guiding laboratory tests or computer simulations or in defining stability criteria.

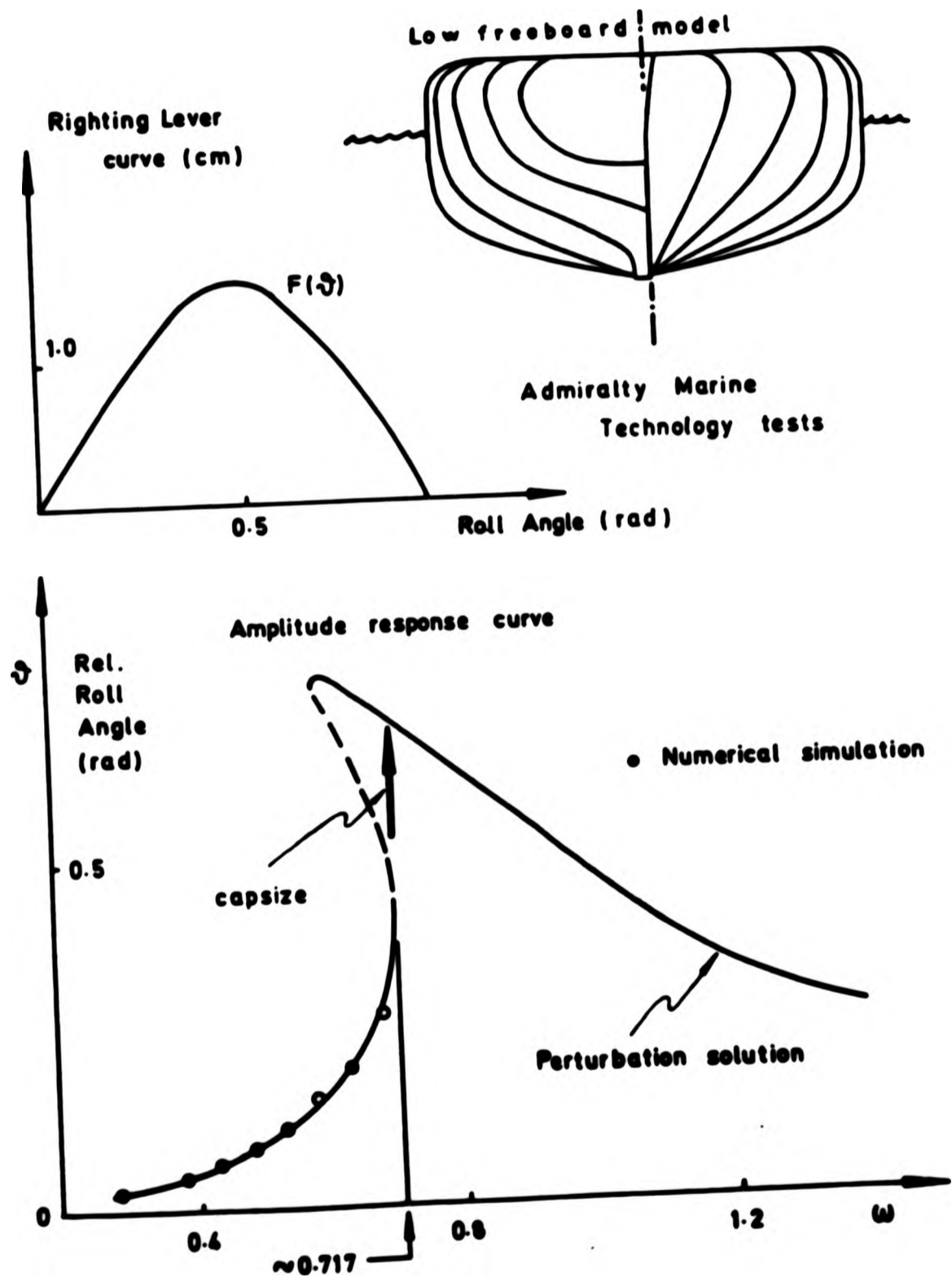


Figure 4.1 Model details and analytical solution of the roll response of a ship.

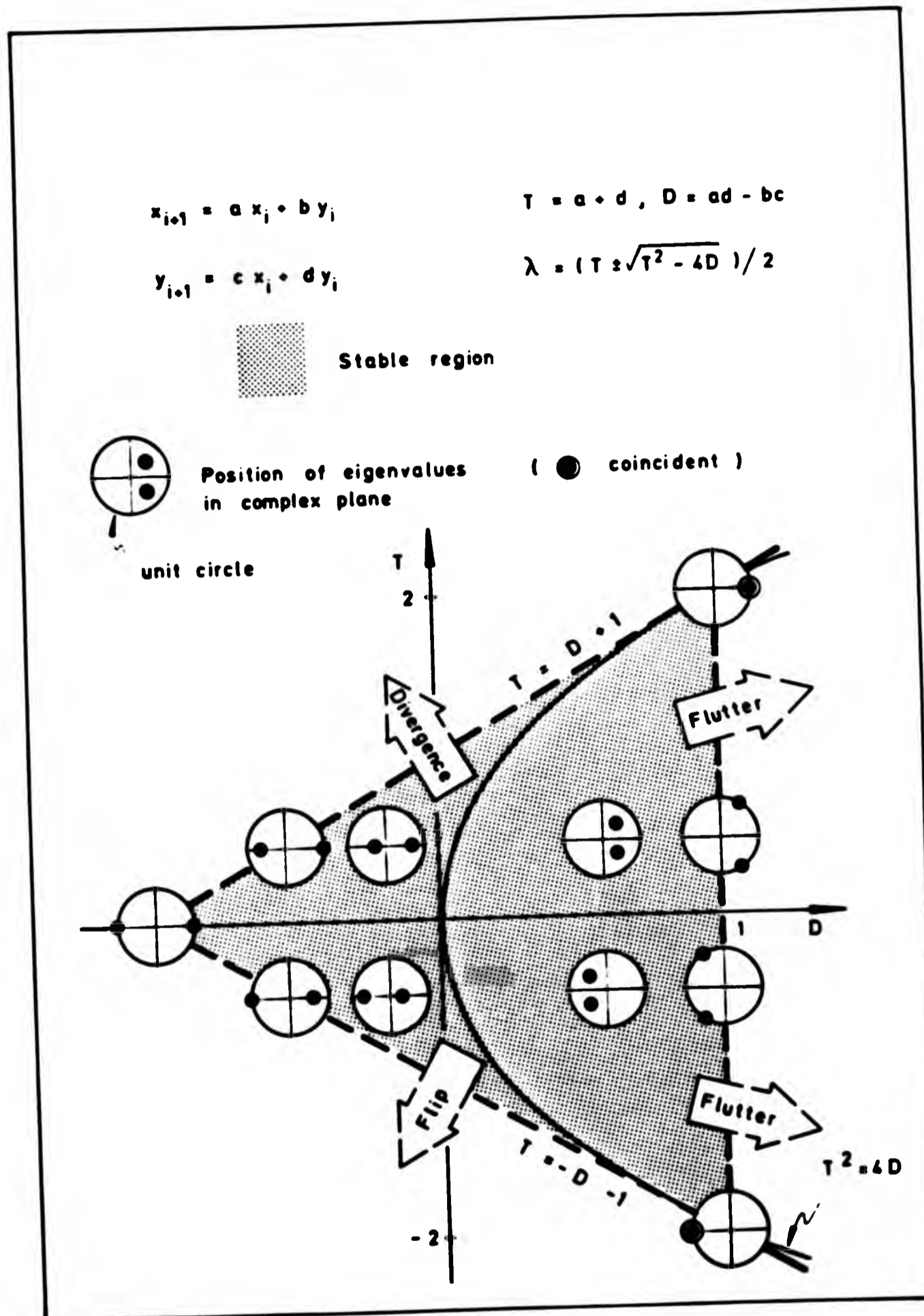


Figure 4.2 Stability regions in the (T,D) plane of a two dimensional map indicating the movement of the eigenvalues.

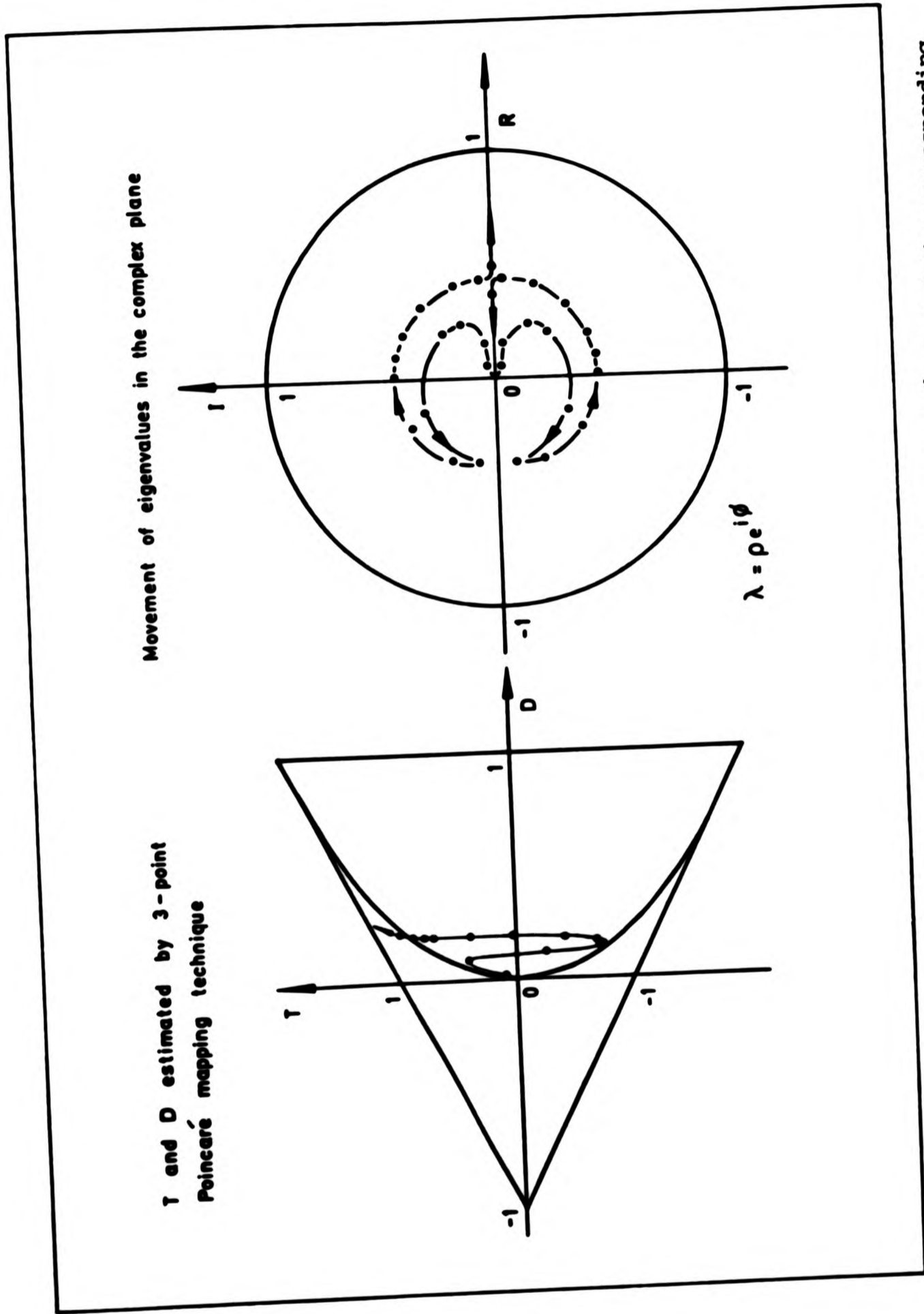


Figure 4.3 Paths traced out in the (T,D) plane by the Poincaré map and the corresponding movement of the eigenvalues as the jump to resonance is approached.

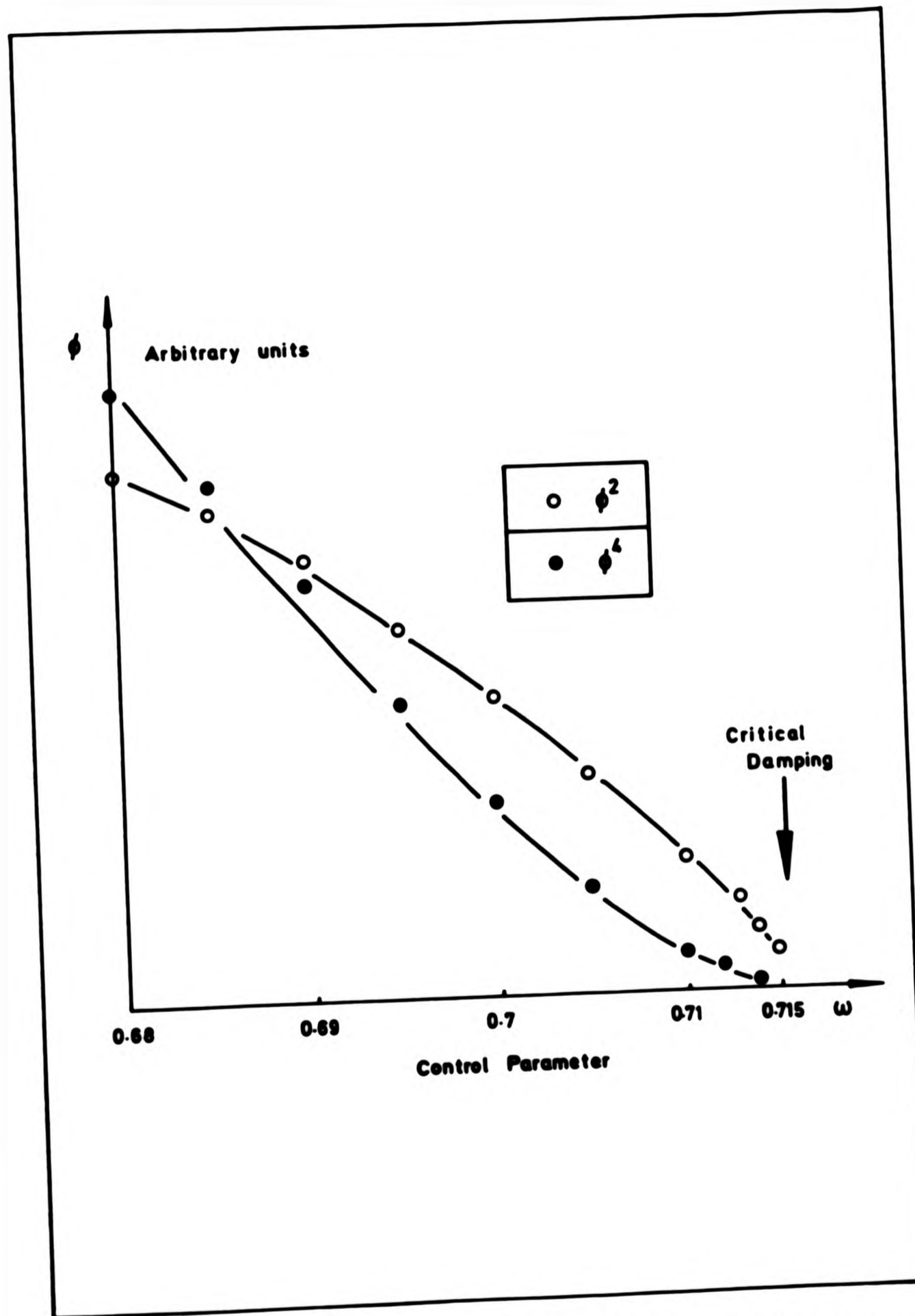


Figure 4.4 Prediction of critical damping as a function of frequency.

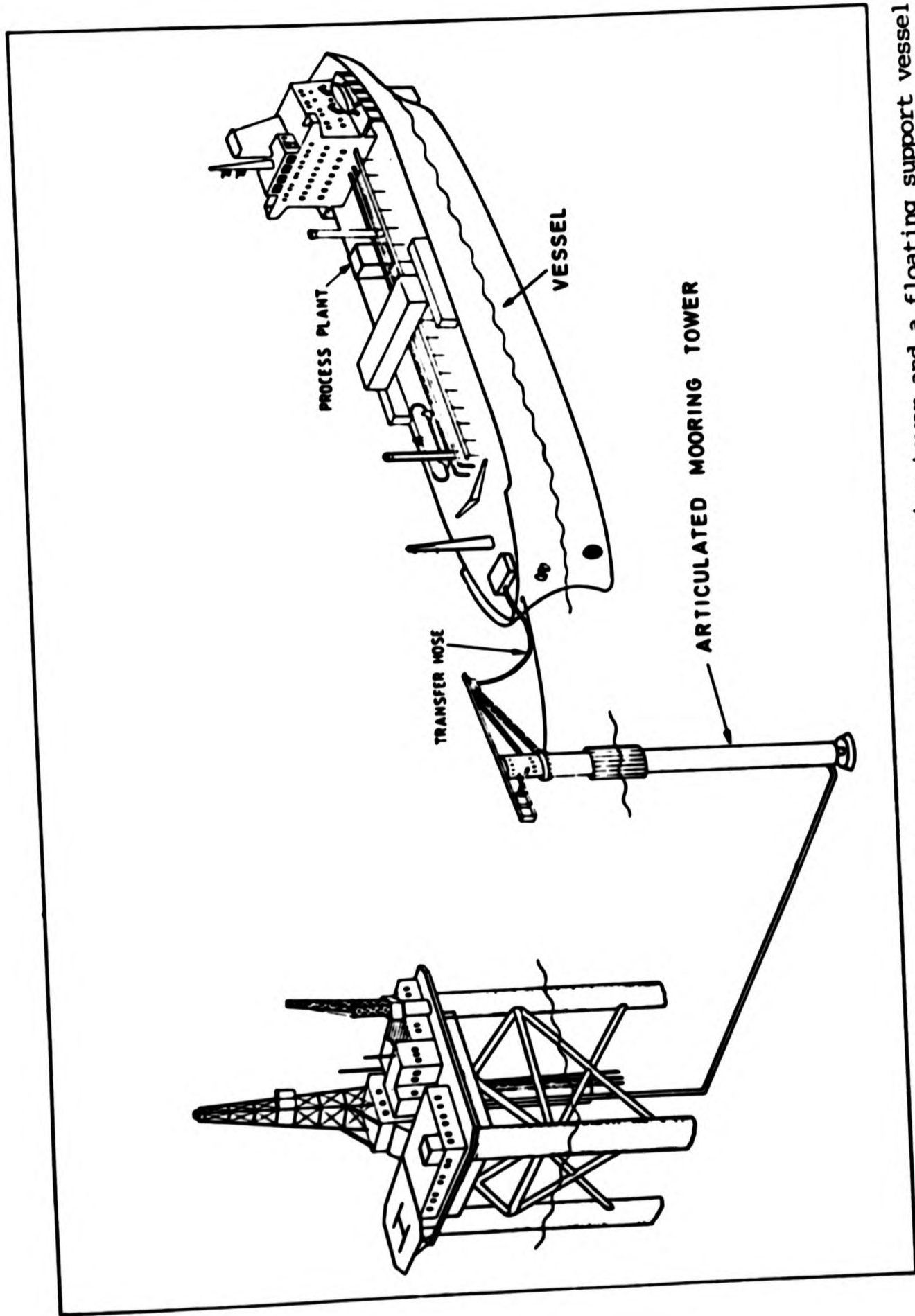


Figure 4.5 Schematic diagram of an articulated mooring tower and a floating support vessel.

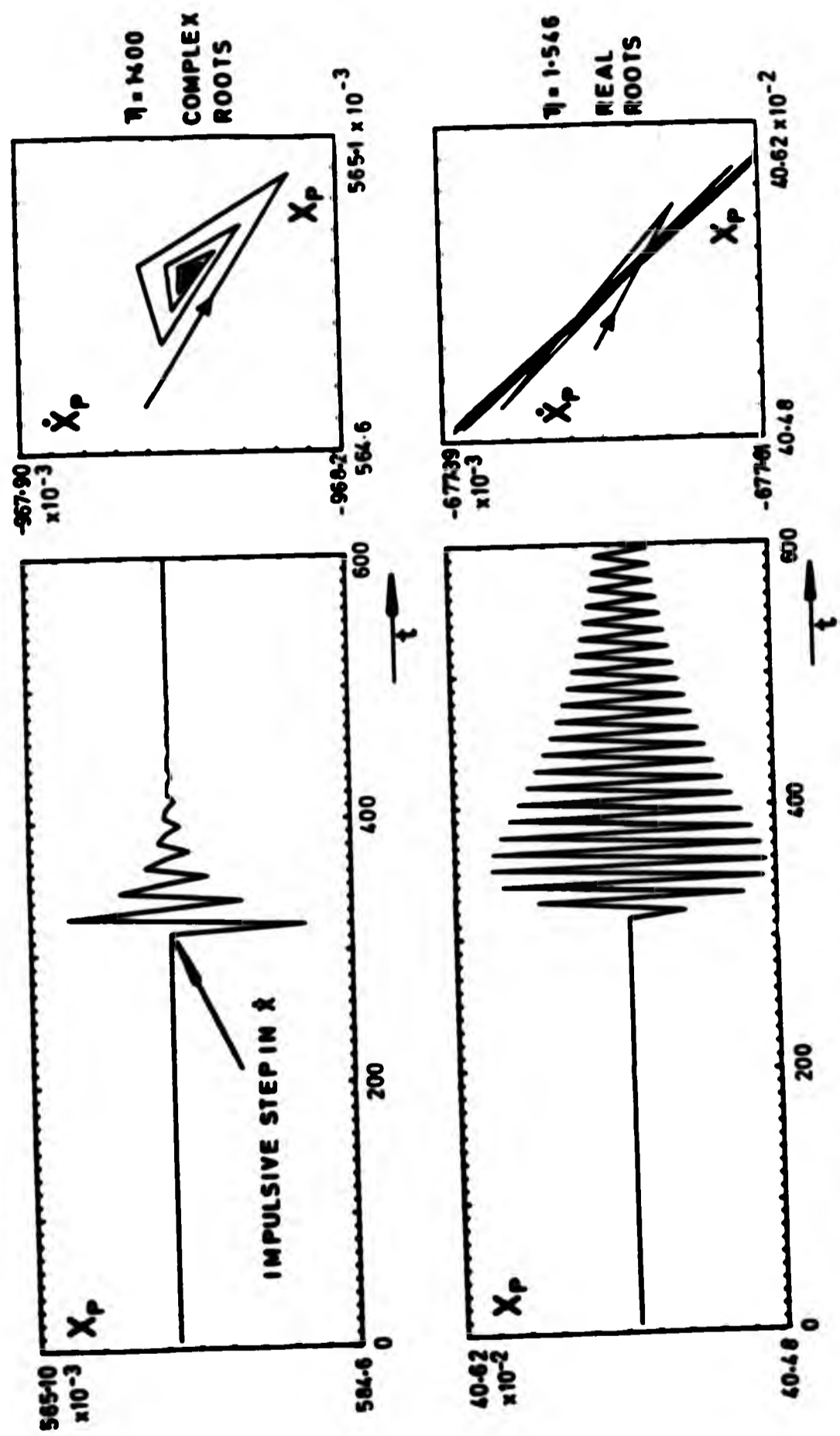


Figure 4.6 Two typical time histories and their associated Poincaré maps just prior to a flip bifurcation.

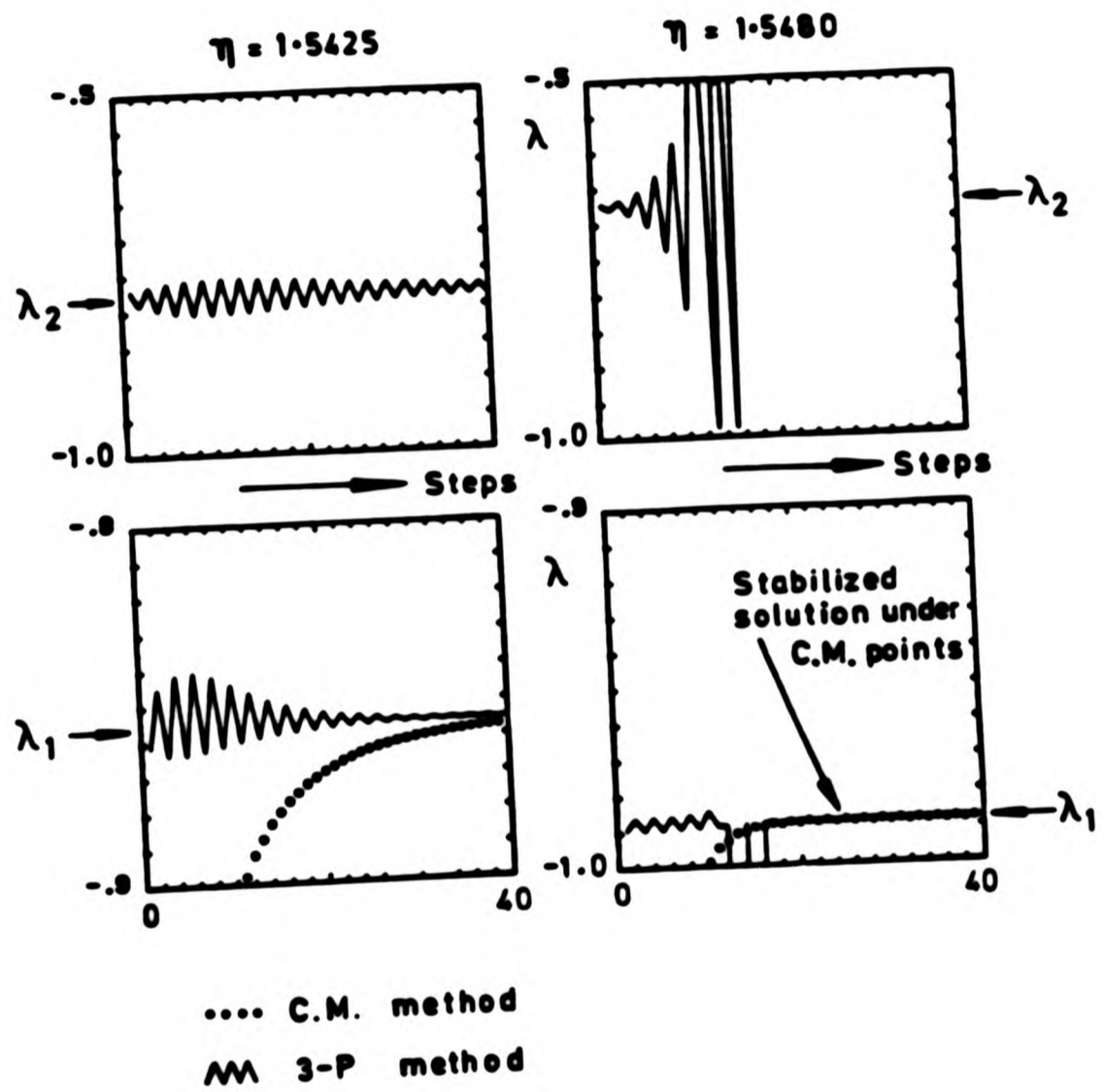
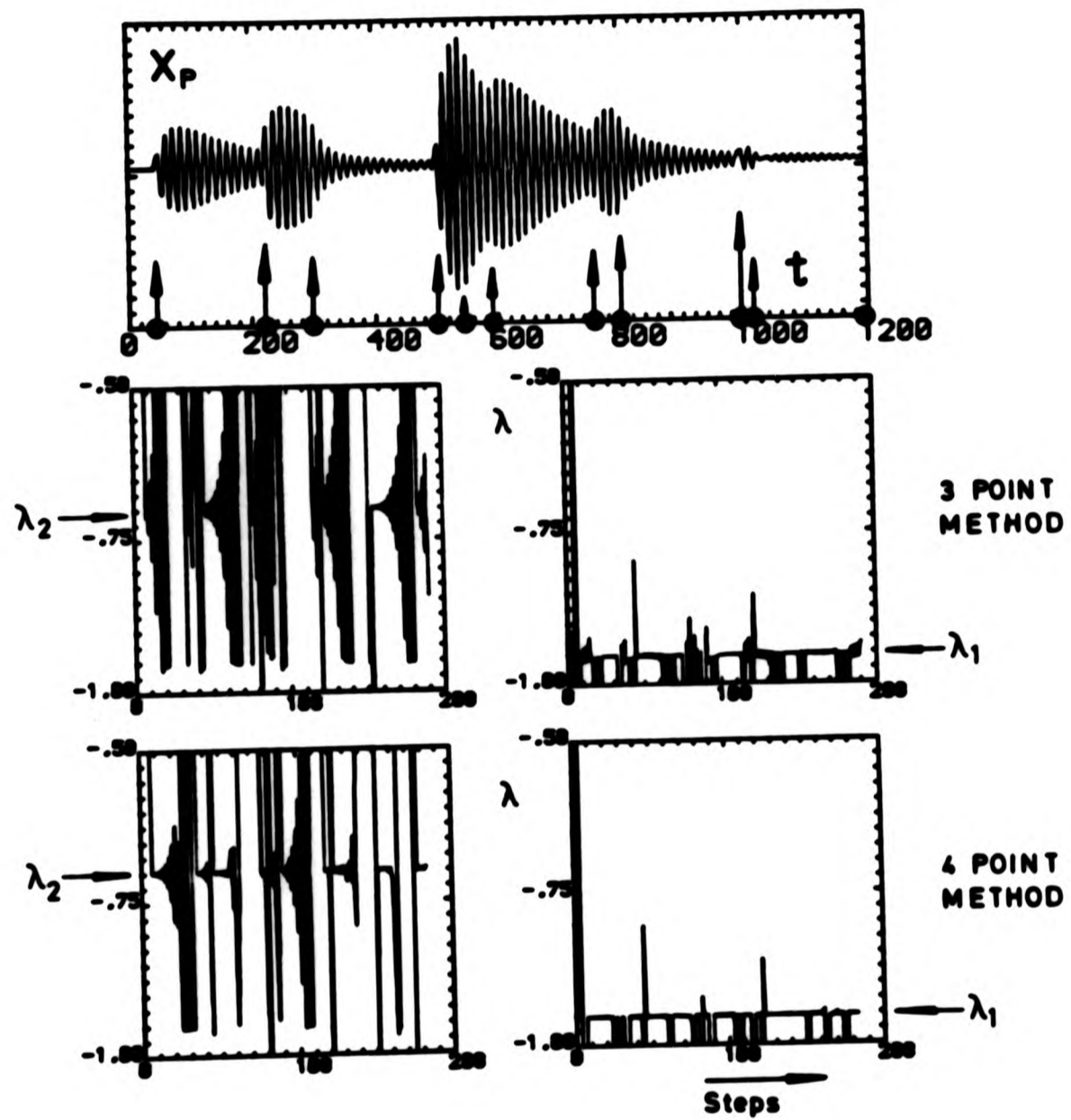


Figure 4.7 Estimation of the eigenvalues using the three-point and Centre Manifold methods at two control parameter values.

RANDOM LOADING for $\eta = 1.546$



Impulses random in magnitude and timing
 Displayed magnitudes are purely schematic

Figure 4.8 Estimation of eigenvalues close to the flip bifurcation under the action of random impulses.

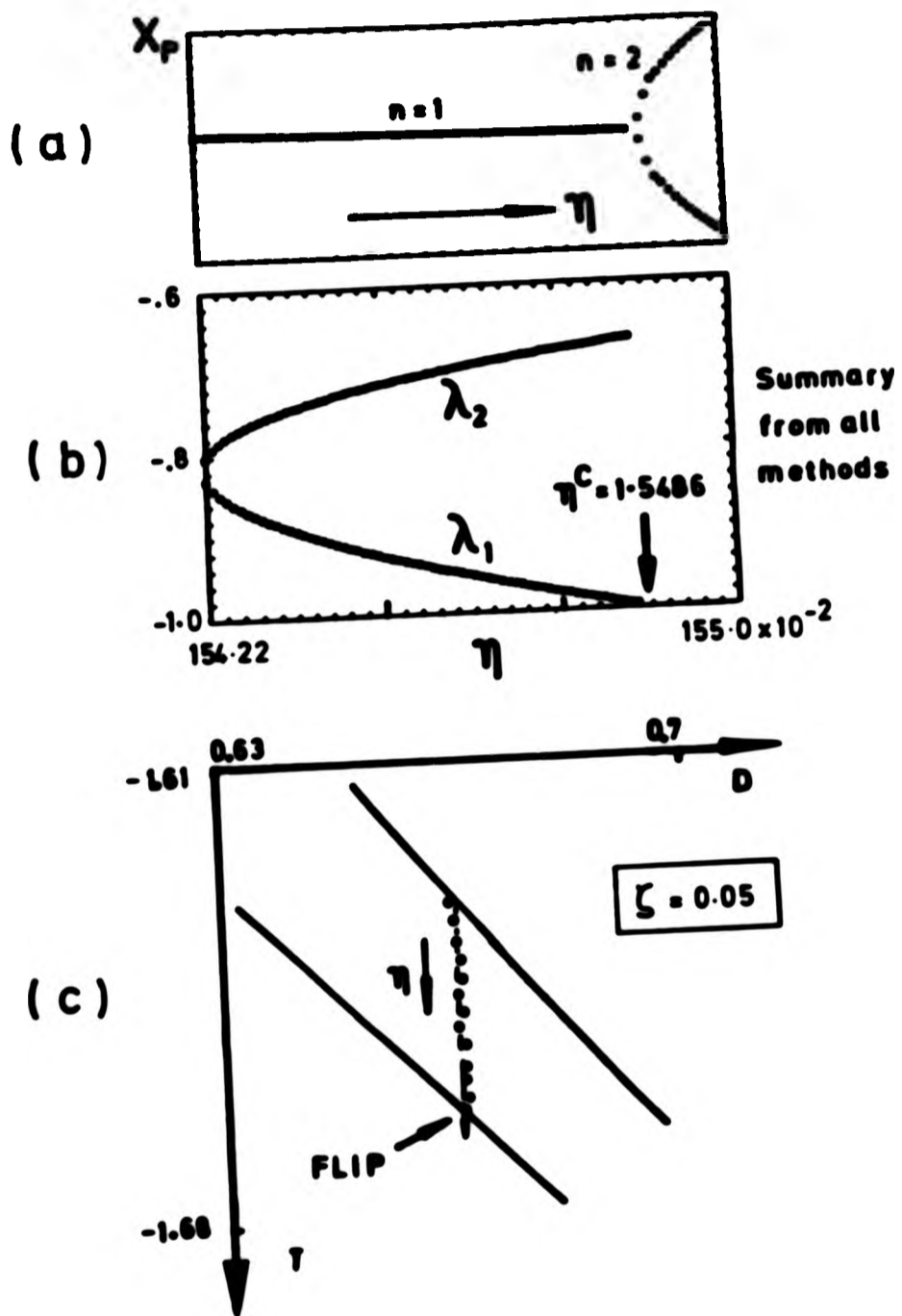


Figure 4.9 Summary of methods for tracking
 (a) bifurcation in the equilibrium path
 (b) movement of eigenvalues
 (c) movement in the (T, D) plane.

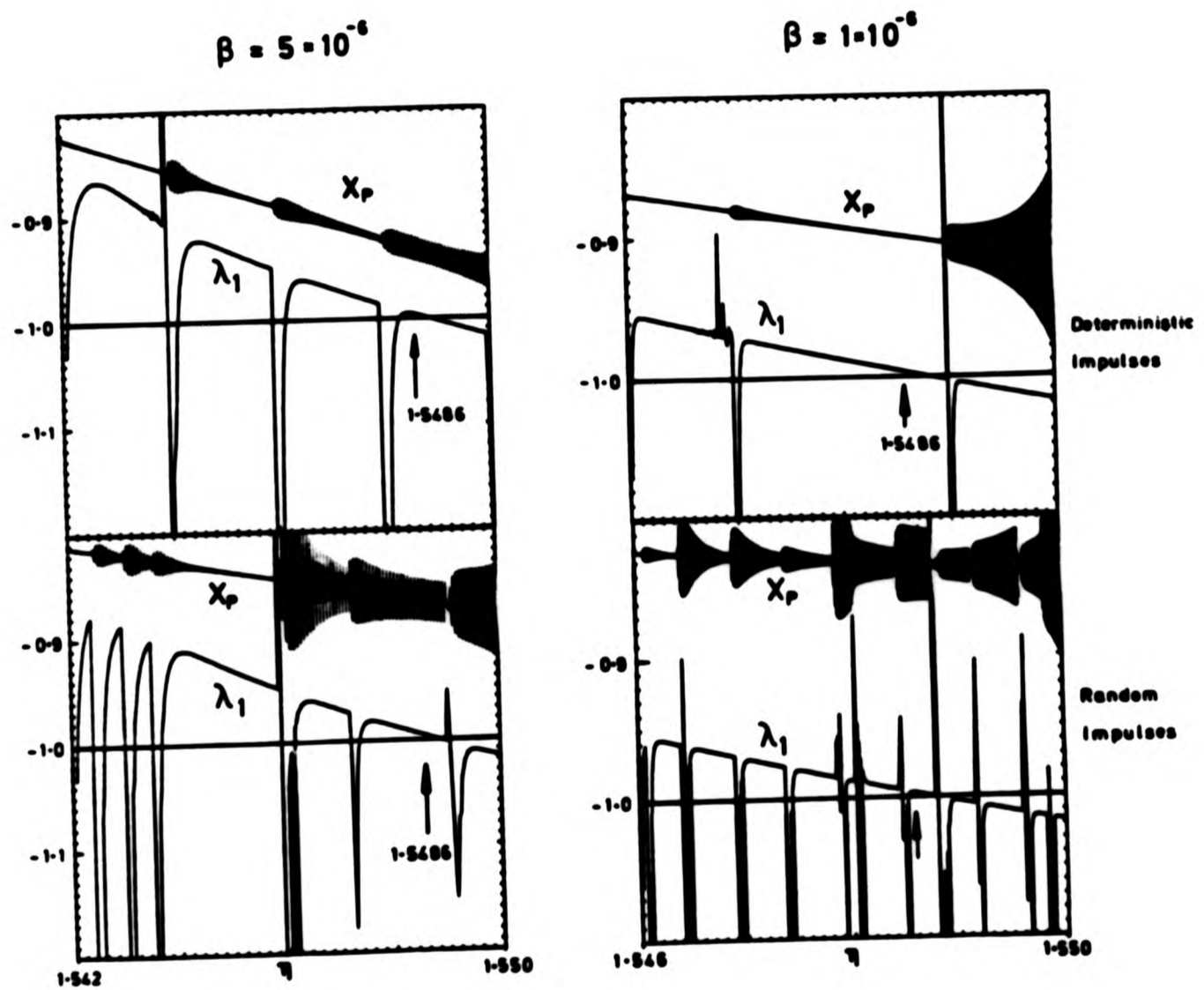


Figure 4.10 Estimation of the critical eigenvalue for an evolving system with two rates of evolution under the action of both deterministic and random impulses.

CHAPTER III.5

THE CHAOTIC MOTIONS OF A SHIP LEADING TO CAPSIZE

The work that shall be reported in this chapter represents some ongoing research that the author is engaged in. Starting from a simple model we shall see that the underlying dynamics can be extremely complicated and it is merely the authors aim to introduce here some of the concepts currently at the forefront of nonlinear dynamics research.

III.5.1 Introduction

In the previous chapter an equation was used to model the roll motion of a ship and this was studied for increasing values of the forcing frequency as a cyclic fold in the response was approached which resulted in capsizing. The main motivation for the work that shall be reported in this chapter arises from the bifurcations occurring in the same model but for decreasing values of the forcing frequency on the other side of the resonance peak. In their experimental studies Wright and Marshfield (1980) found that when the frequency of forcing was approximately $\omega = 0.9$ a subharmonic resonance of the vessel was visible which also unaccountably led to capsizing. Figure 5.1 (taken from Wright and Marshfield) shows the region

in question on the response curve and also an experimental time history of the ship together with the corresponding waveform of the excitation. A point to note is that although the wave was designed to be regular it does contain sufficient fluctuations to make the experiment realistic which also adds weight to justify the numerical/computational type of studies advocated here. A study of the model was undertaken by Virgin (1986) in which he numerically integrated the equation in the region of the flip to subharmonic resonance and included here as figure 5.2 is a diagram taken from his paper. The point A on the response curve corresponds to the point at which the linear eigenvalues coalesce, i.e critical damping, while the point C is where one of the eigenvalues becomes negative (real) producing the flip bifurcation. Also shown on this figure are some sample traces of time histories as the flip is approached. We note that in fact the response undergoes a further flip to an $n=4$ solution and for values of ω just less than this value of the second flip the ship capsizes. A closer investigation of this region was made by Virgin in which he found that the response in fact goes through a complete Feigenbaum period doubling sequence terminating in a chaotic attractor.

The question that naturally springs to mind is "Does the ship capsize due to these chaotic motions?".

Before we attempt to answer this question we review some of the basic concepts of the model and study a local quadratic approximation to the restoring force and comparisons

are also made with the Duffing oscillator as studied by Ueda (1980,1986), Guckenheimer and Holmes (1983), Stewart (1986) and others.

III.5.2 Local Mathematical Models of Ship Roll

An equation of the form

$$m\ddot{x} + b\dot{x} + GZ = f\sin\omega t \quad (5.1)$$

is often used to model the roll motions of a ship or barge in beam seas [Robinson and Stoddart (1986), Cardo et al. (1984)], where x is a measure of the roll angle. The mass of the vessel is here assumed to be a constant which includes the added mass in roll, b is an equivalent linear damping coefficient, and GZ is the restoring force providing the stiffness of the system; both the latter two coefficients being evaluated either experimentally or semi-empirically [Rawson and Tupper (1983)]. In an ideal situation the GZ will be a symmetrical function of roll angle but in reality a vessel is usually biased in some way so that it has a propensity to capsize in a particular favoured direction. This is accounted for in the model by a bias term B such that $GZ = B + g(x)$, which could in fact be due to a shifted or unevenly distributed cargo, ice on the deck, environmental loading or perhaps damage.

The governing potential energy (V) of the system, found by

integrating the stiffness function, for typical biased and unbiased systems are schematically drawn in figure 5.3. In this figure a stable equilibrium point is visualised by a ball shown blacked in resting in a 'potential well', while a white ball resting on a 'potential hill' depicts an unstable point. Also shown in this figure is the (x, \dot{x}) phase portrait of the undamped unforced counterpart of this system. Using this diagrammatic situation the capsize of the vessel can be thought of as the ball being forced by the external force to oscillate inside the potential well in such a manner that at some time the motion surpasses the unstable position and diverges to infinity. (Note that in fact the ball can pass the unstable position and yet not capsize since the force can bring the system back to the potential well).

To examine the precise mechanism of capsize in more detail we shall model the biased system of the ship roll by a local quadratic approximation to the GZ curve, not least of all because of computational expedience.

After a suitable rescaling of the time and roll angle we focus our attention on the simplified equation

$$\ddot{x} + b\dot{x} + x - x^2 = f \sin \omega t, \quad (5.2)$$

which we shall refer to as the single potential well model. The behaviour of this model without forcing for both the undamped and lightly damped cases are sketched out in the diagrams of

figure 5.4(a); the region shown as shaded in the lower diagram indicates the region in the (x, \dot{x}) phase plane for which motions flow onto the equilibrium point as time evolves, i.e. the domain of attraction. As can be seen from this diagram it is precisely the invariant curve which forms the inset to the saddle point which delineates the regions of attraction and escape. This latter fact proves very useful when trying to evaluate the domains of attraction for various coexisting periodic attractors in nonlinear dynamics by first locating the saddle point and then running time backwards to precisely locate this inset.

Similarities were noted between equation (5.2) and a Duffing type of equation, namely

$$\ddot{x} + b\dot{x} - x + x^3 = f\sin\omega t \quad (5.3)$$

as used by Holmes (1979) and others to model the motions of a pendulum, this equation forms a useful comparison to the results that shall follow but could equally be taken as a local approximation in some way. The GZ curve, being locally cubic, leads to an energy surface which has a double potential well as shown in the figure 5.4(b) and consequently we shall refer to this model as the double potential well model; also drawn in this figure are the unforced damped and undamped counterparts of the system. The domain of attraction for the right hand equilibrium state is marked as shaded in the lower diagram and we see that this domain now has a more complex structure that of the single well with bands of attracting regions spiralling

round as we move away from the fixed point. This indicates the sensitivity of initial conditions associated with nonlinear problems. A further point to note is that the double well model has the considerable computational advantage that at no time does the trajectory escape to infinity, escape here being associated with the escape from a particular well; however there is the added complication that motions can occur that straddle both wells.

If we now consider either of these systems to be excited by a small amount of external force then the fixed point becomes a harmonic $n=1$ periodic solution and the saddle point becomes a small saddle cycle, as schematically illustrated in the top diagrams of figure 5.5. The dynamical behaviour of the system is now examined by considering Poincaré sections in the usual manner and so the phase portraits in figure 5.5 are now that of a map and not of a flow; we note though that because of the need for continuity for arbitrarily small forcing the qualitative structure of the phase portrait of the map must be the same as that of the flow. Once again the inset to the saddle (cycle) separates the shaded regions of attraction and is drawn here with a heavier line. The outset, being of less physical significance, is not fully explored in this diagram. Shown in this figure by a dotted line are the small amplitude periodic solutions of the flow and the point which characterises them as such in the Poincaré phase plane. It should be remembered that if the system were given a start, for instance on the inset to the saddle, any subsequent motion is now not that of a flow but

a map, so that a point would step into the saddle in this case along the continuous line drawn with decreasing advancement of distance as the saddle were approached.

III.5.3 Chaotic Capsize

Returning now to the original capsize problem for any given values of the coefficients and variables that describe the motion the ship may or may not capsize. For the purpose of this study it was decided to fix the level of damping at $b=0.1$ and with $m=1$ increase the level of forcing for various fixed frequencies with f a function of time, i.e. evolving, modelling a changing sea-state. This type of approach has the added advantage that as f is increased the ship at some stage must capsize, the main questions being "at what level of forcing does the capsize occur?" and "what mechanism of bifurcation is this phenomenon?".

Early investigations of using this evolving technique to reflect the long term behaviour of the system are shown in figure 5.6 (Note the change in notation with the damping now being given by $\beta=0.1$, $m=1$ and the forcing amplitude is now F and not f as before). For early values of the forcing frequency near $\omega=0.8$ the escape, given when $x=1$ following the rescaling, appears to be caused by a sudden jump in the response of the system. When $\omega > 0.83$ this jump phenomenon, similar to a cyclic fold, does not lead to the capsize of the vessel but instead the response restabilises at a higher amplitude (cf. the response of

a driven beam in chapter II.5), the jump in latter runs being less severe. In each case the response would appear to be slowly increasing in amplitude but it is not this steady increase that causes the eventual capsize, instead a new sudden phenomenon occurs. The appearance of this new unforeseen event is more alarming since there is no apparent indication of its impending intervention such that predictions of capsize based only on the slowly increasing amplitude would considerably overestimate the time (in terms of increasing F) to capsize.

The regime of irregular response immediately prior to the escape was examined in more detail by sampling the response and following the path of fixed points, corresponding to the periodic solution, in the phase plane as the forcing was increased. Some typical examples of the traces are shown in figure 5.7 where the displacement of the Poincaré points is plotted against F (note that this displacement need not necessarily correspond to the maximum amplitude of the response). From these diagrams it is clear that the irregular response of the time history just prior to escape is in fact due to the equilibrium path undergoing a cascade of period doubling (flip) bifurcations which is a well known route to chaotic motions. In the diagrams we also see that for certain values of the forcing frequency the equilibrium path has a fold; for example in the top diagram of figure 5.7 when $\omega = 0.8$ after which point there is no local attractor and so the trajectory diverges (as found in the time history of figure 5.6). If a careful search is made of the phase plane then it is possible to

locate, at lower values of F , a coexisting periodic state that also period doubles, that is the fold point has now extended past the region of period doubling. The particular case when $\omega = 0.85$ has been studied in further detail such that the unstable path can also be located, figure 5.8, from which it is clear that any indepth study of the bifurcations of this type of system must also include routines to follow unstable paths and locate saddle points and their insets.

To verify that the period doubling sequence was complete resulting in chaotic motions the scenario is included here as figure 5.9. This drawing was in fact terminated at $F = 0.109$ since this was the lowest value at which escape had never been seen to occur. This diagram, which is only one half of the period doubling sequence, is similar in structure to that of the Hénon [Hénon (1976)] and logistic [May (1976)] maps including windows of periodic motion. A feature of these maps called a chaotic explosion is also apparent where a chaotic attractor suddenly increases in size (or decreases). This phenomenon, termed an interior crisis by Grebogi et al. (1983), can be seen within the periodic windows (and to the right) and is caused when an unstable path from the original periodic motion collides with a small internal chaotic attractor, the explosion results in a larger chaotic attractor.

A point to note here is that inside these periodic windows if we imagine F to be decreasing then the motion changes from being peiodic to chaotic, this is called an intermittency

explosion and is a further route to chaos. Unfortunately this event is not particularly clear on this figure since the scale is necessarily small, the interested reader is advised to consult the paper to appear by the author [Thompson et al.] or the paper of Grebogi et al. (1983) for similar behaviour for a map.

It is not clear at this stage of research whether the chaotic explosion near $F=0.10875$ could be explained by the ideas of an internal crisis a la Grebogi since the explosion occurs outside the bounds of the original attractor. A further event, termed an exterior crisis by Grebogi, is one which leads to a sudden end of the chaotic attractor of a map caused by the interaction between the chaotic attractor with either an unstable saddle point or its inset. This type of chaotic bifurcation in which the sudden destruction of a chaotic attractor leaves no local attractor is more commonly termed a blue sky catastrophe [see Thompson and Stewart (1986)]. It is clearly this type of bifurcation that leads to the capsizing of the ship but the fact that at the end of the period doubling sequence there is an infinite number of unstable paths adds to the complexity of locating the precise mechanism of escape for this particular equation.

The only readily available test for truly chaotic motion is to plot the chaotic attractor; this being done in figure 5.10 where we see the two bands of the attractor. As the phase angle at which the Poincaré section is taken is varied these bands

fold over and mix (the folding can just be viewed in this diagram), and it is precisely this mixing and folding of the attractor that causes the sensitivity to initial conditions that is identified with chaos. This particular figure also illustrates another problem encountered, namely that of chaotic transients. After a blue sky catastrophe the attractor no longer exists formally. Nevertheless typical trajectories initialised in the region previously occupied by the chaotic attractor appear to move about chaotically in this region but after a finite time the orbit leaves and then rapidly escapes to infinity. The time that such a transient stays within the region varies so that it is difficult to determine whether a particular trajectory would not escape if the machine were left to run for a longer period. Bearing in mind that for a certain system the reverse process might be significant, using these chaotic transients it is desirable to predict at what point the chaotic attractor will appear. A brief comparison has been made with the work of Grebogi et al. (1983) in scaling these chaotic transients and some success has been achieved in a posteriori predicting the critical value when chaotic motions become stable but this work will not be reported here.

The main question that remains to be answered is by what mechanism does the blue sky catastrophe occur. If we look at the generic bifurcations as tabled by Thompson and Stewart (1986), figure 5.11, we note as a matter of interest the way in which a periodic flow can bifurcate so that no attractor exists through

a saddle cycle connection, see figure 5.12 taken from the book of Thompson and Stewart [also see Stewart and Thompson (1986)]. The counterpart of this dangerous bifurcation for a map would be when a saddle point (representing a saddle cycle) collides with a stable node (representing a periodic solution). If we look back to figure 5.8 it is precisely this bifurcation that occurs at the fold point of the equilibrium path where this saddle node collision results in no local attractor.

To determine the reasons for the blue sky event at the end of the chaotic attractor a sensible first approach is to check whether the global saddle, S , or its inset touches the attractor. Little theoretical information is available regarding the path or route taken by the inset to the saddle but some knowledge can be gained by applying the so called Melnikov method [Melnikov (1963)]. In simple terms Melnikov's Method provides an analytic expression for the parameter values at which homoclinic tangency occurs, i.e. when the outset and the inset of the saddle first touch. If the parameter values are varied still further a homoclinic tangle ensues for which Melnikov showed that the inset and the outset must now intersect one another an infinite number of times, schematically illustrated in figure 5.13.

The appendix to this chapter contains a brief account of the method of Melnikov as well as the details of the application of the method to the single well model and also included in the appendix is a scaling of the double potential well model.

The critical value of the forcing calculated by the Melnikov method is given by the relationship

$$F_c = \frac{0.1 \sinh(\pi \omega)}{5 \pi \omega^2} \quad (5.5)$$

With $\omega=1$ this yields $F_c=0.0735$ which compares favourably with the computational evidence of figure 5.14 which, run as it is at $F=0.074$, must be just after the homoclinic tangency has occurred. The shaded region in this diagram depicts the area of the phase plane that leads to escape.

From a computational point of view the inset to a saddle in a map is harder to locate than the inset of flow. In a flow, given an initial condition on a saddle point a trajectory will trace out the inset if time is run backwards. However in a map an initial start steps along the continuous curve representing the inset, these steps may be large with no indication of the path inbetween points. The only way to get a pseudo-continuous picture of the inset is to consider a number of initial conditions using the so called ladder method; this ladder method is a systematic way of subdividing a section of the inset into 'rungs' and iterating each rung or start backwards in time. By a careful choice of the number of rungs in each section an almost continuous line can be achieved. This method is diagrammatically illustrated in figure 5.15 where the points (Poincaré points) P_0, P_1, P_2, \dots and Q_0, Q_1, Q_2, \dots are marked along the inset and outset respectively. P_0 and Q_0 are chosen to be close to the

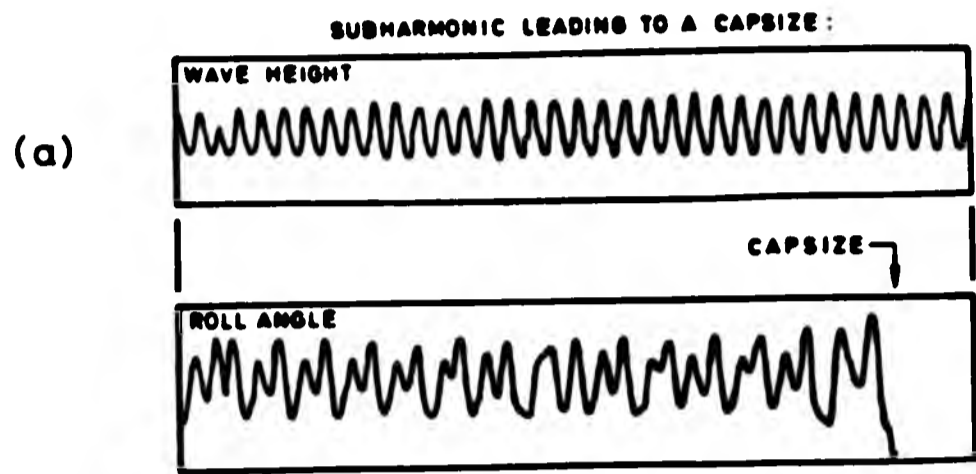
saddle point S with the sections corresponding to an iteration of the map being marked B_0, B_1, \dots on the inset and A_0, A_1, \dots along the outset.

Thus we are now in a position to track the path of the inset to see if it touches the chaotic attractor. The occurrence of a homoclinic tangle complicates the story since the inset and outset now cross each other an infinite number of times. The area trapped between any two such crossings becomes stretched out to form thin 'whiskers' which curl round following the original path of the inset in such a way that the rungs of the ladder can be separated by large distances. The presence of these whiskers mean that the catchment region of the chaotic attractor becomes fractal in nature [see the paper to be published by the author, Thompson, Bishop and Leung]. Figure 5.16 shows some of the complexity of the situation; the shaded region corresponds to the area of the phase plane that leads to escape, exemplified by the sequence $\alpha_1, \alpha_2, \dots$ etc. while the points β_1, β_2, \dots etc. lead to the chaotic attractor. As can be seen from this figure the inset does indeed pass close to the chaotic attractor, a close-up study of which is shown in the top right hand corner.

A summary of the values at which the various bifurcations occur is given here as figure 5.17. The folding of the equilibrium path is characterised by the curves A and B whilst the first and second period doublings occur at C and D with final escape at E. The curve marked M is the value of the

forcing at which the Melnikov method predicts a homoclinic tangency which gives no information about the eventual escape. As the frequency drops to about 0.8 all the curves approach one another and in fact the Melnikov curve can lie above the escape curve schematically illustrated in figure 5.18. This implies that it is also possible to have a chaotic attractor which has a smooth basin boundary [see also Moon and Li (1985)].

It would appear then that from our results it is possible for a chaotic attractor to exist with either a smooth or fractal basin boundary (the basin of attraction) but that the escape is independent of this event associated with a homoclinic tangle. Whether indeed it is the touching of the attractor by the inset from the global saddle or in fact the intervention of the inset of a more local saddle which sees the end of the attractor is as yet unresolved and will form the basis of further research.



(b)

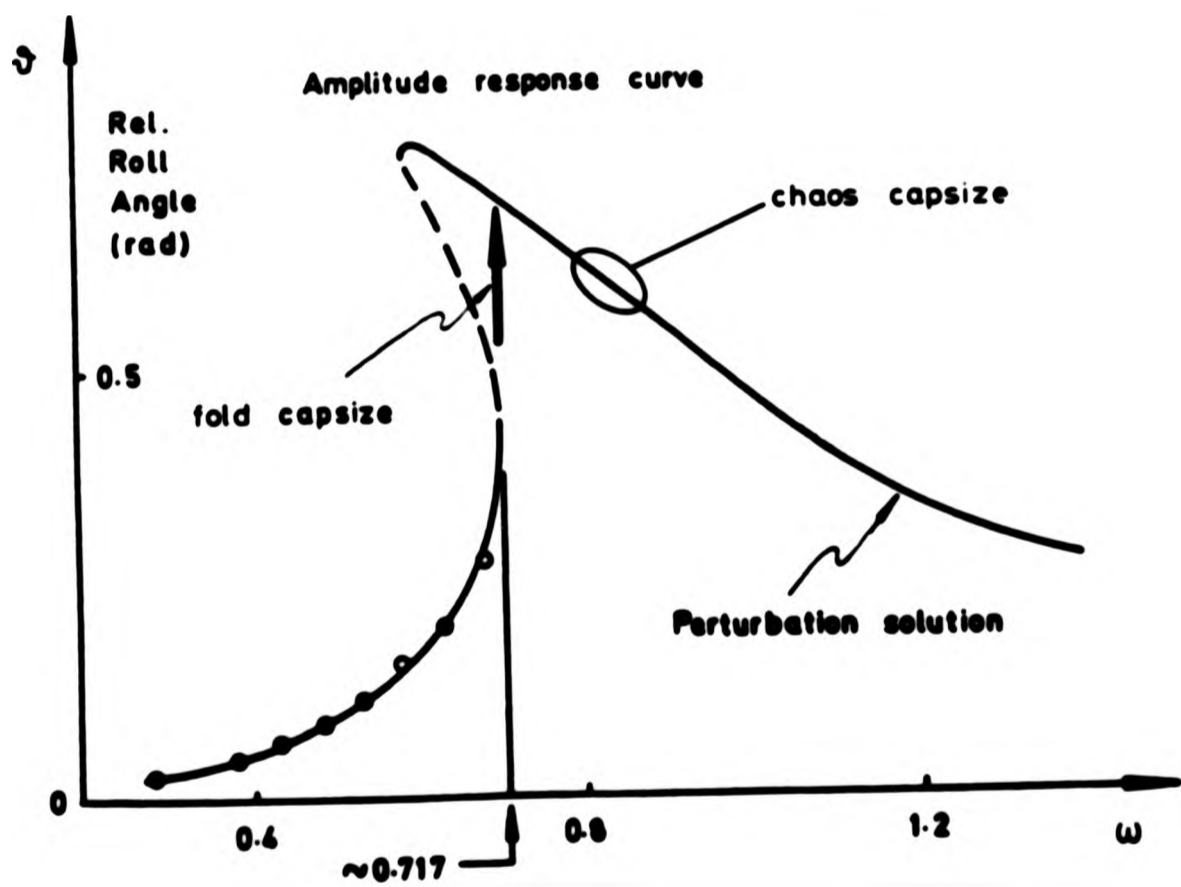


Figure 5.1 (a) Waveform and time history of subharmonic motion leading to capsizes
 (b) Resonance response curve and region of chaotic capsizes.

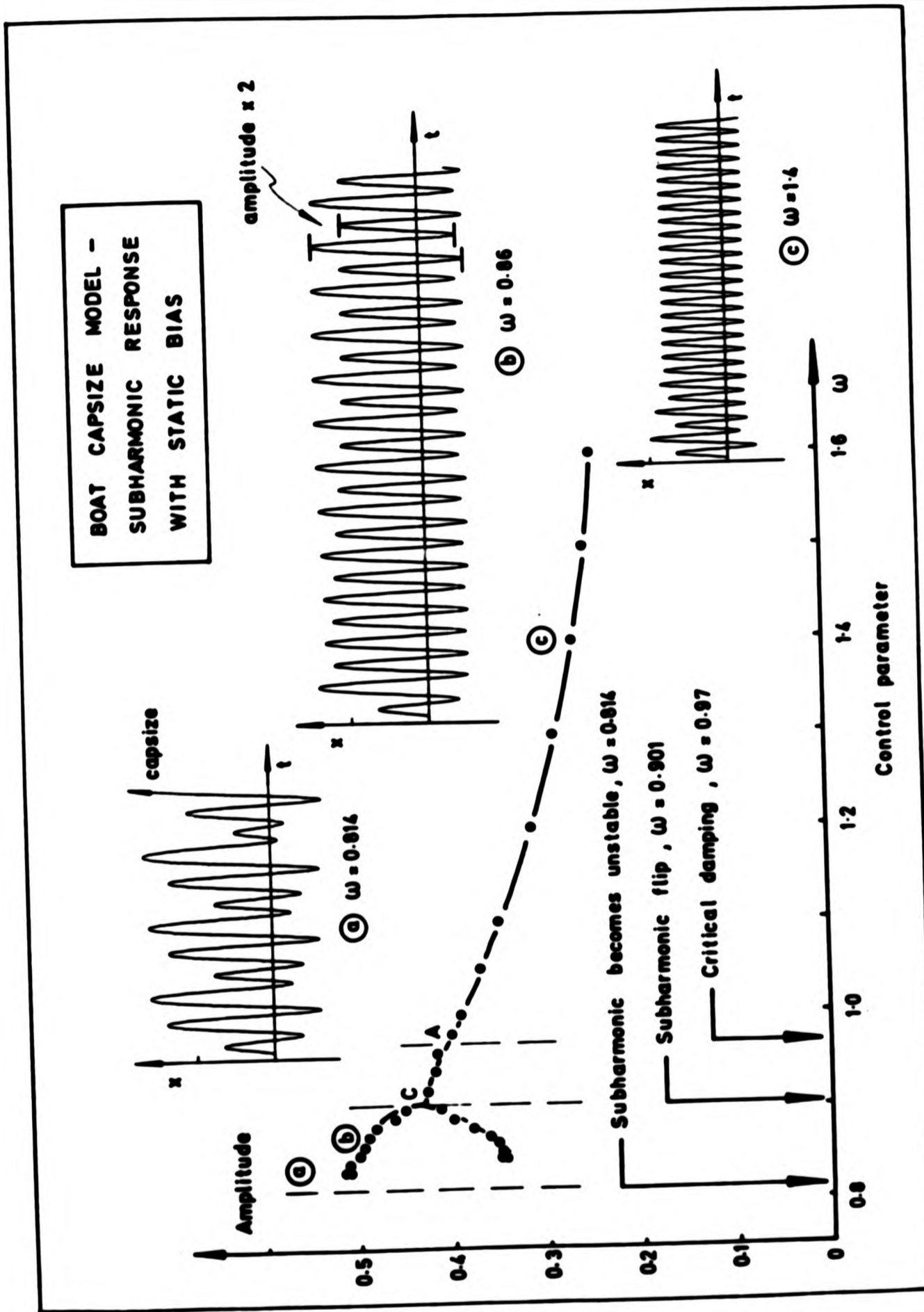


Figure 5.2 Subharmonic motion leading to capsizing in the roll response of a ship [Virgin (1986)].

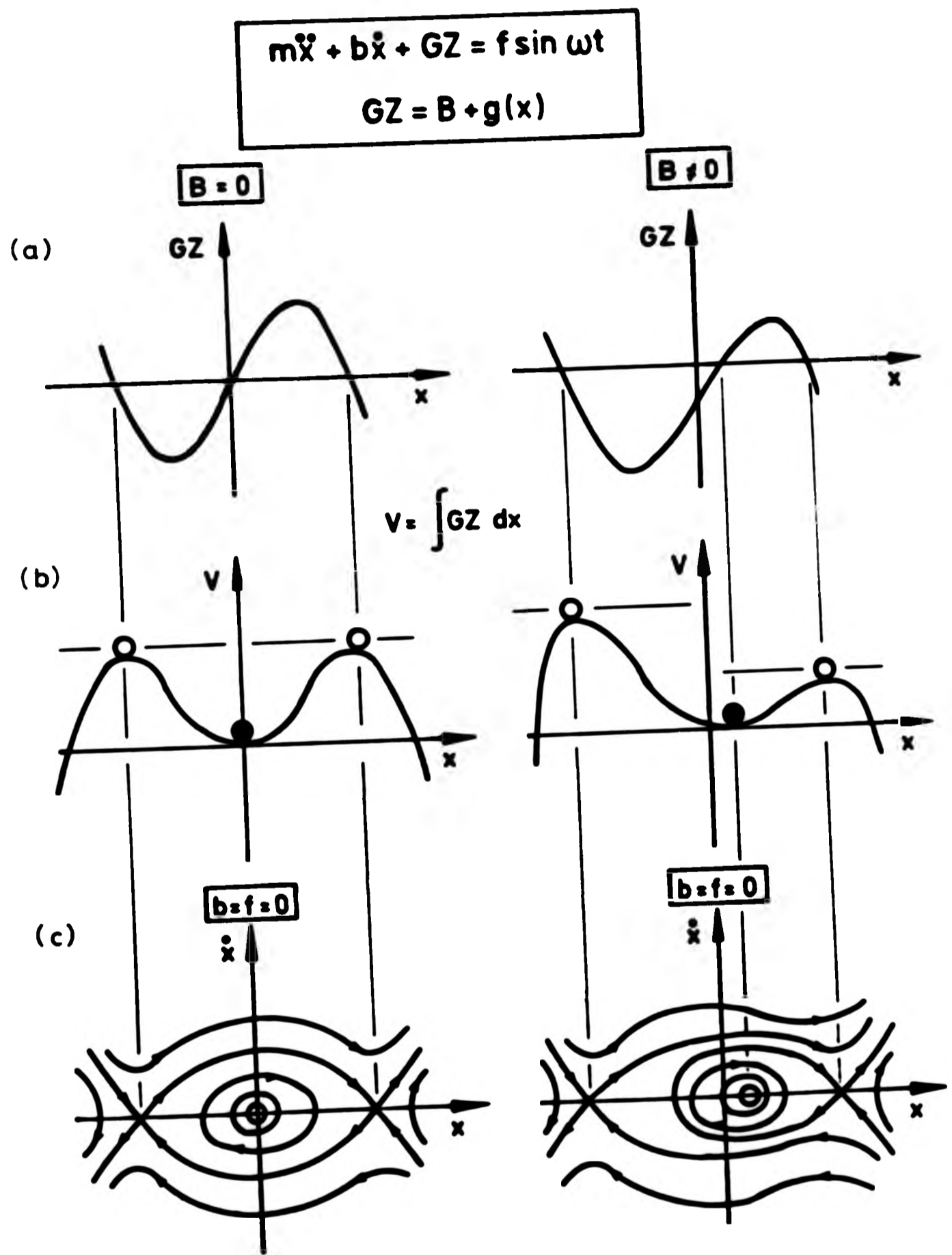
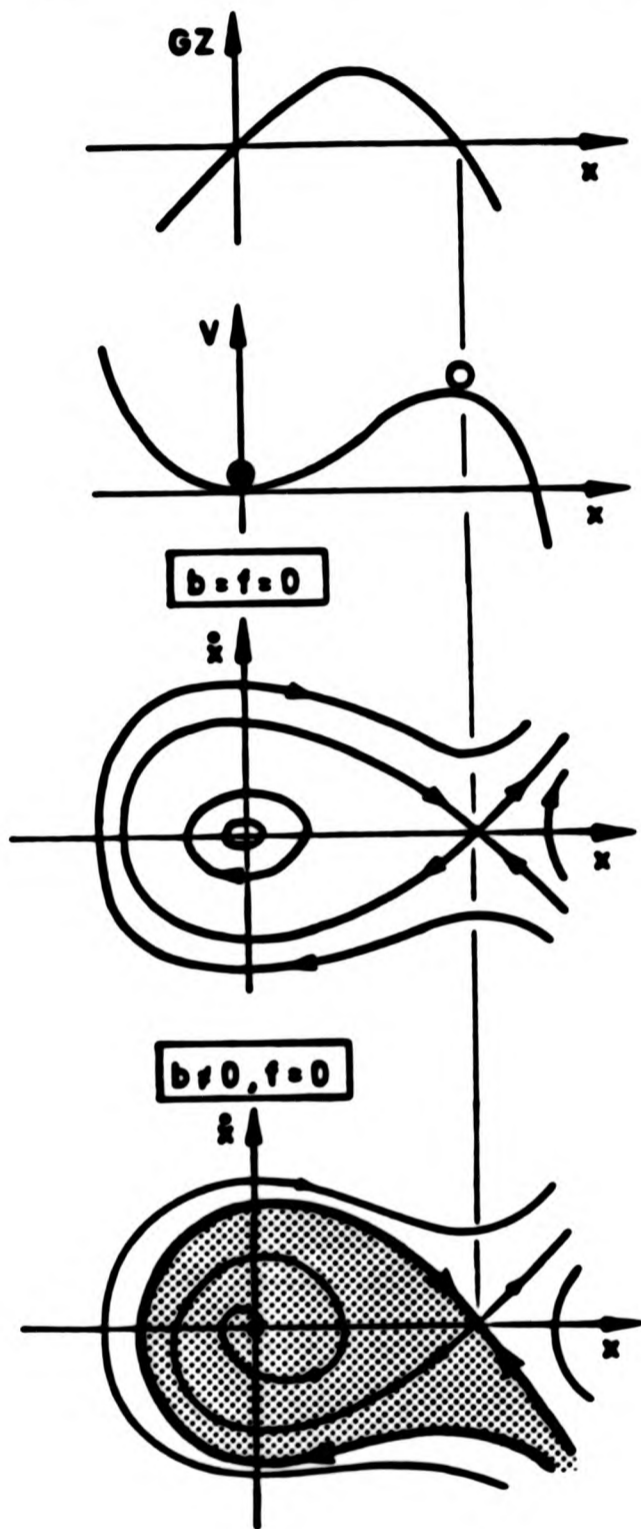


Figure 5.3 (a) Typical restoring force curves (GZ) for unbiased and biased systems
 (b) corresponding governing potential energy function (V)
 (c) undamped unforced phase portraits.

(a)

$$\gamma + b\dot{x} + x - x^2 = f \sin \omega t$$



(b)

$$\gamma + b\dot{x} - x + x^3 = f \sin \omega t$$

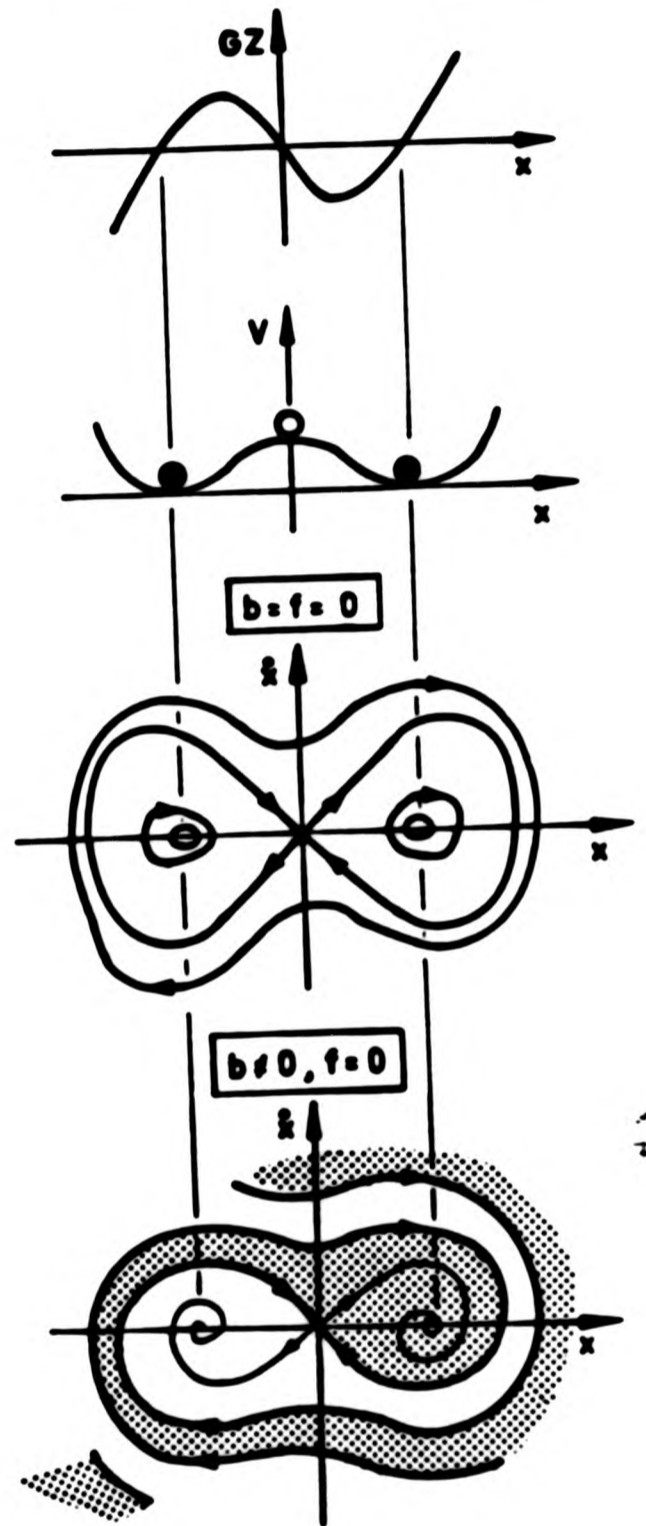
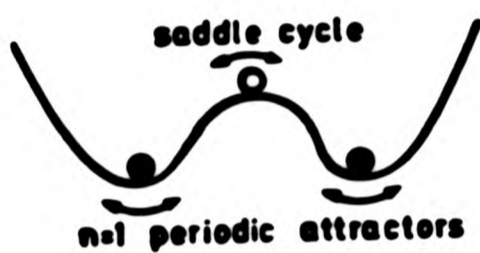


Figure 5.4 Damped and undamped forms of the unforced (a) single well model and (b) double well model.

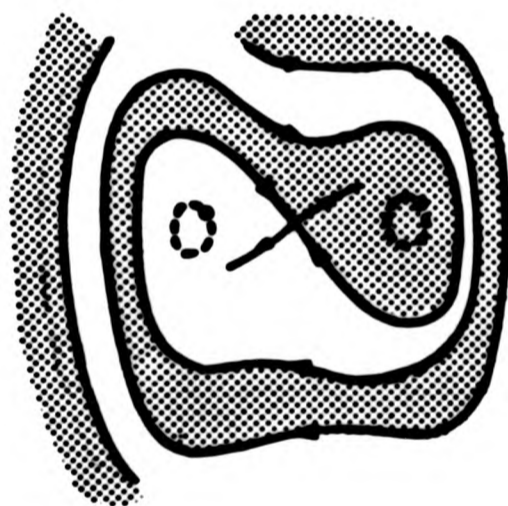
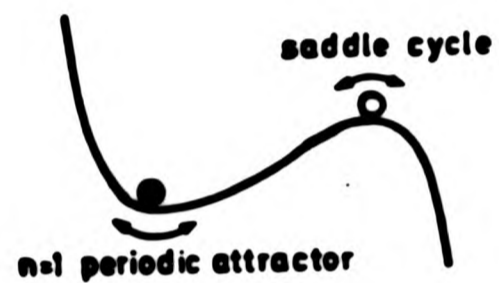
$$\ddot{x} + b\dot{x} - x + x^3 = f \sin \omega t$$

f small



$$\ddot{x} + b\dot{x} + x - x^2 = f \sin \omega t$$

f small



MAP

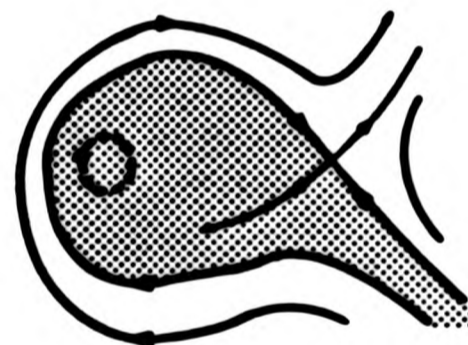


Figure 5.5 Schematic visualisation of the single and double well models and computed phase portraits.

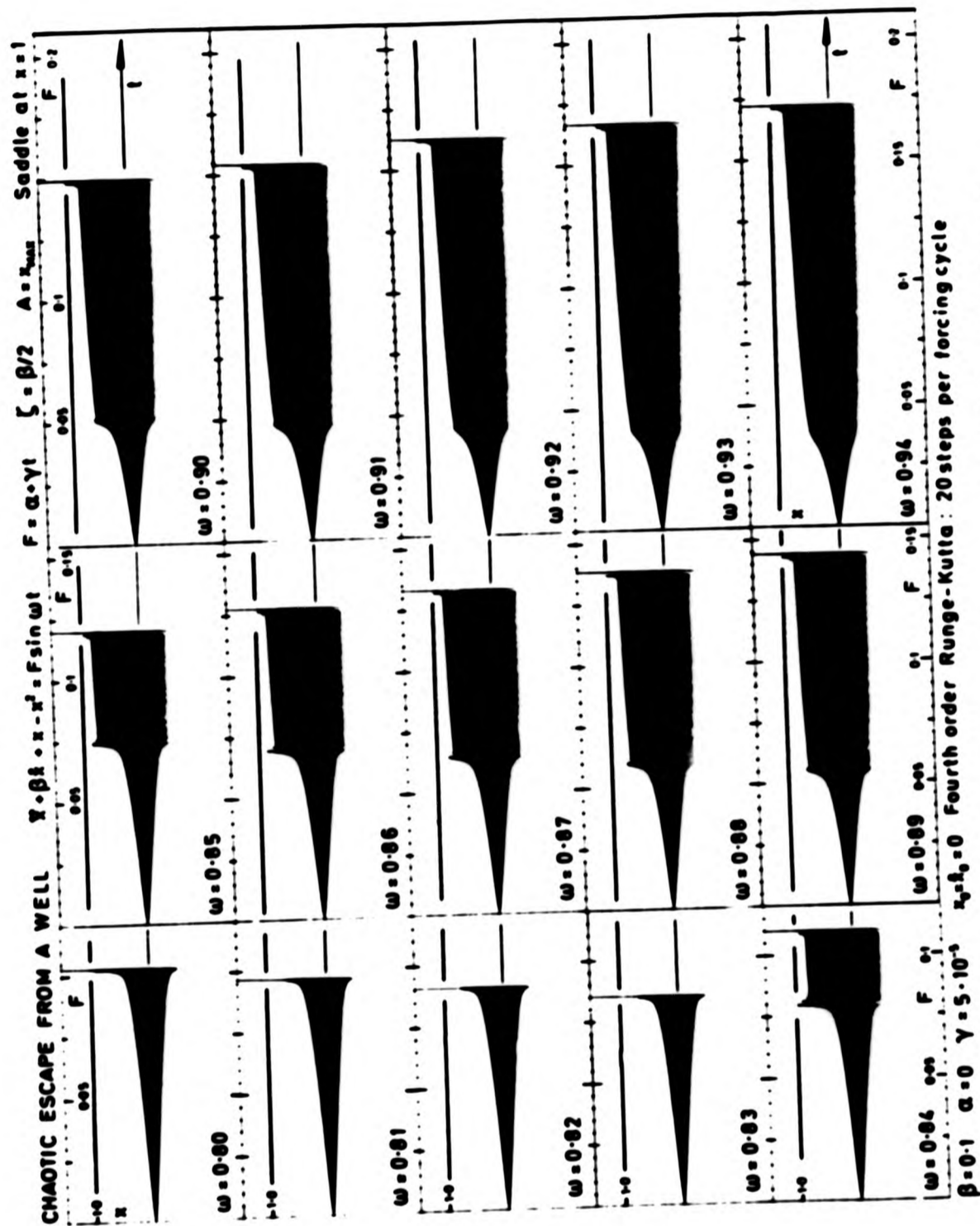
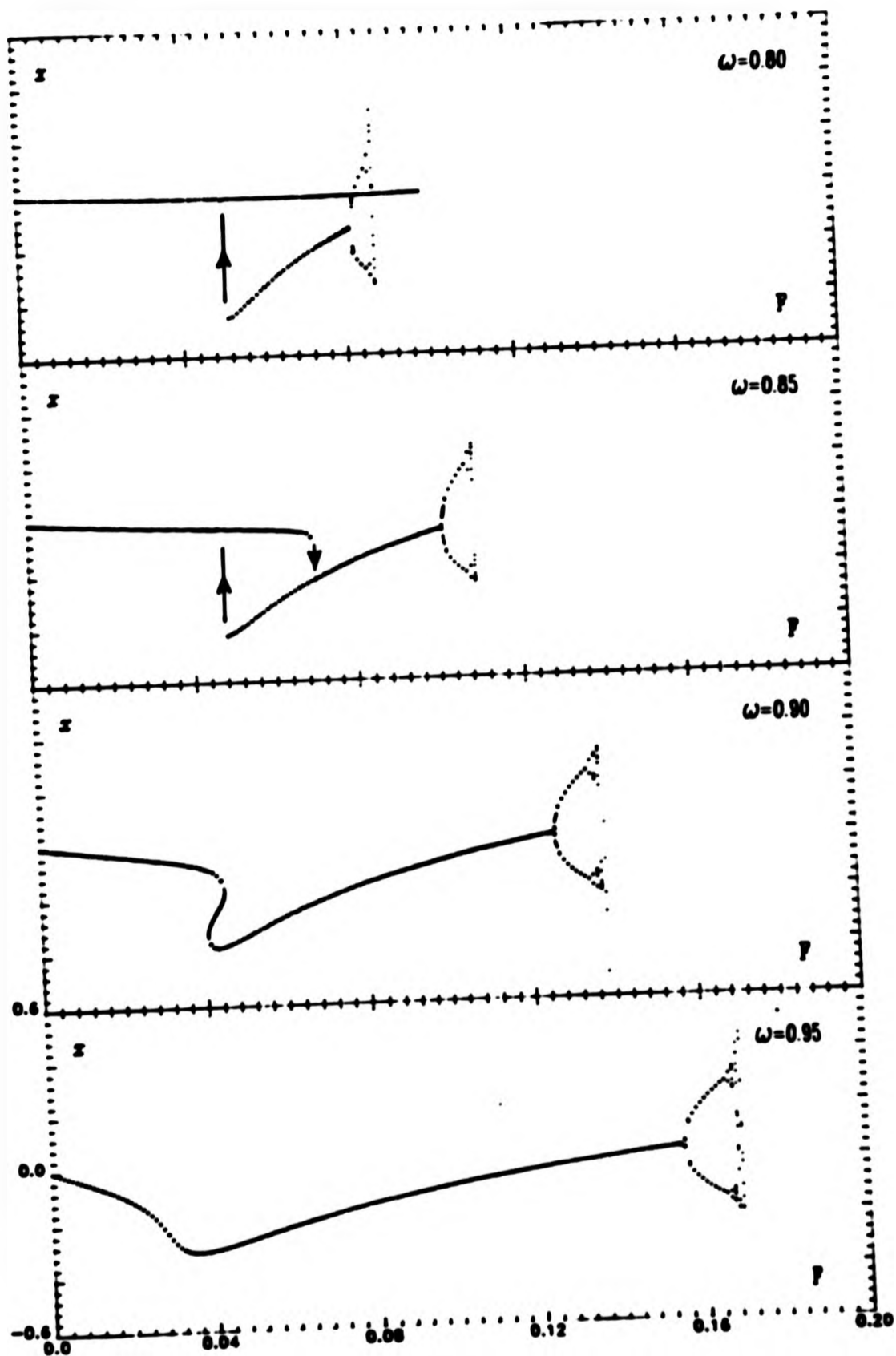


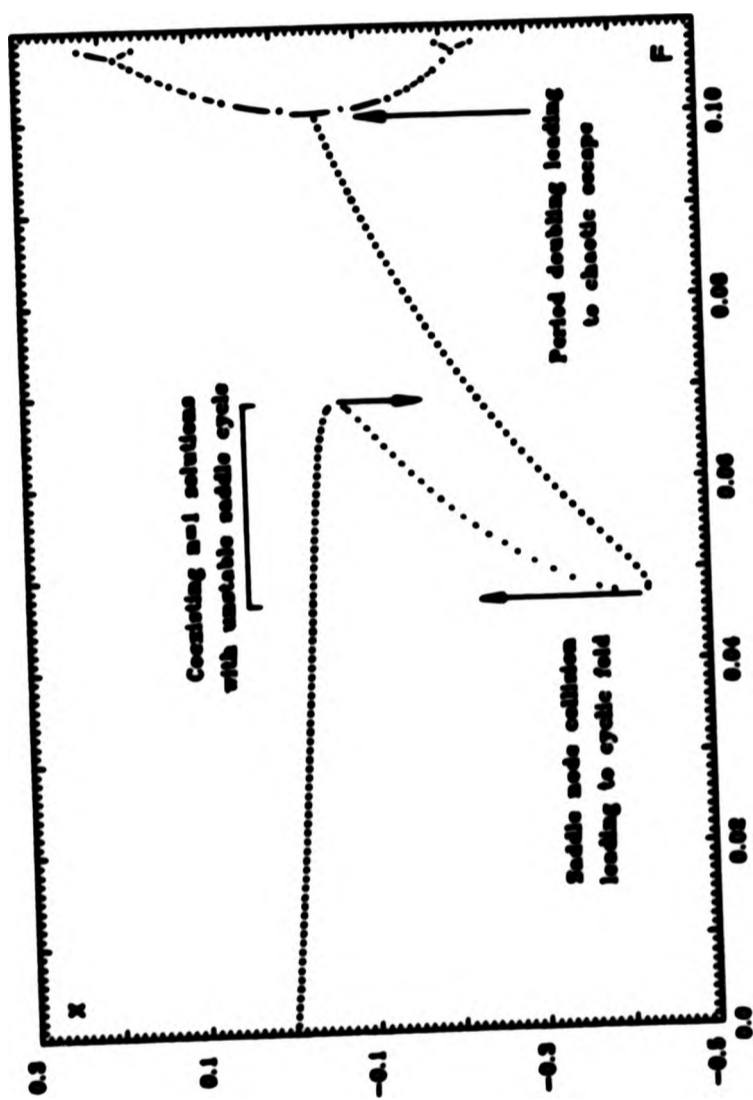
Figure 5.6 Time histories of escape from a potential well for an evolving system.



CHAOTIC ESCAPE FROM A WELL ($\beta=0.1, \Delta F=0.001$)

Figure 5.7 Displacement of Poincaré points plotted against level of forcing (F) at various values of the forcing frequency.

POINCARÉ RESPONSE DIAGRAM OF ESCAPE EQUATION



$$\ddot{x} + \beta \dot{x} + x - x^2 = F \sin \omega t$$

$$\beta = 0.1 \quad \omega = 0.95 \quad \Delta F = 0.001$$

CHAOTIC ESCAPE FROM A POTENTIAL WELL

Figure 5.8 Study of unstable equilibrium path.

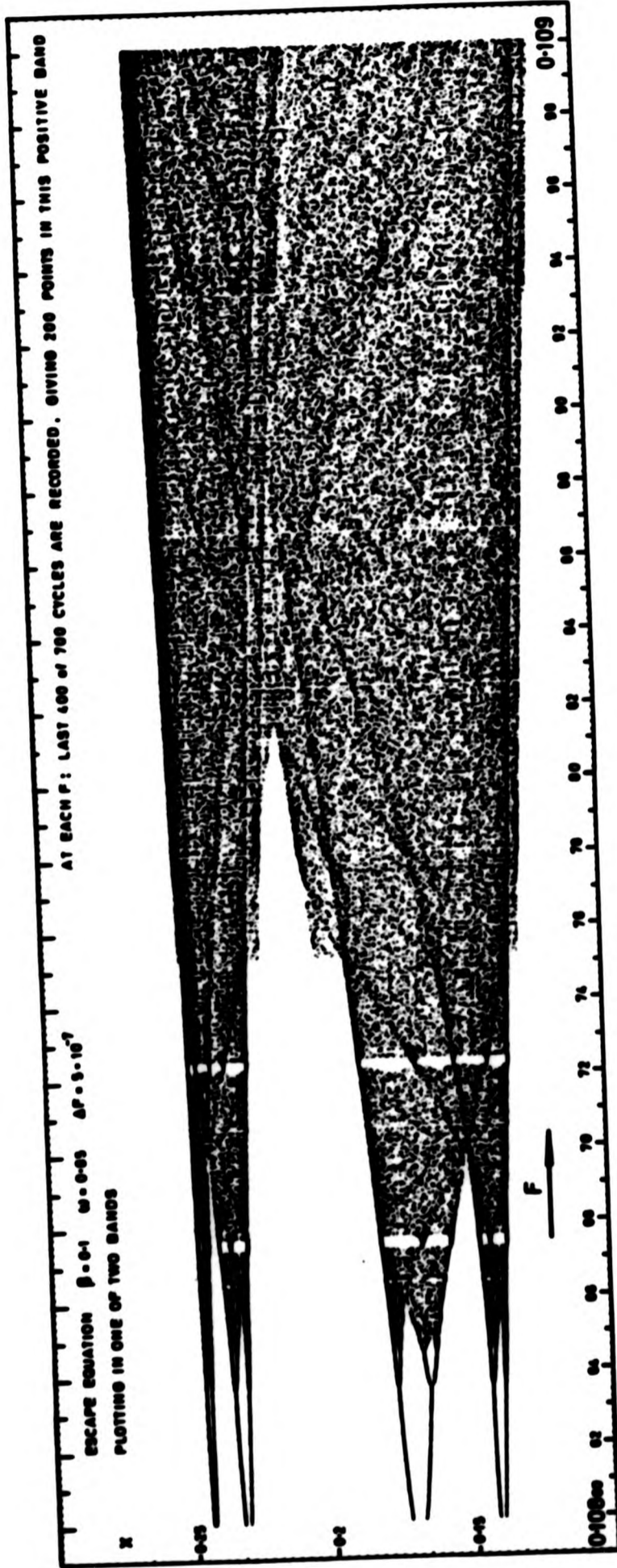


Figure 5.9 Period doubling sequence showing one half of the two band attractor.

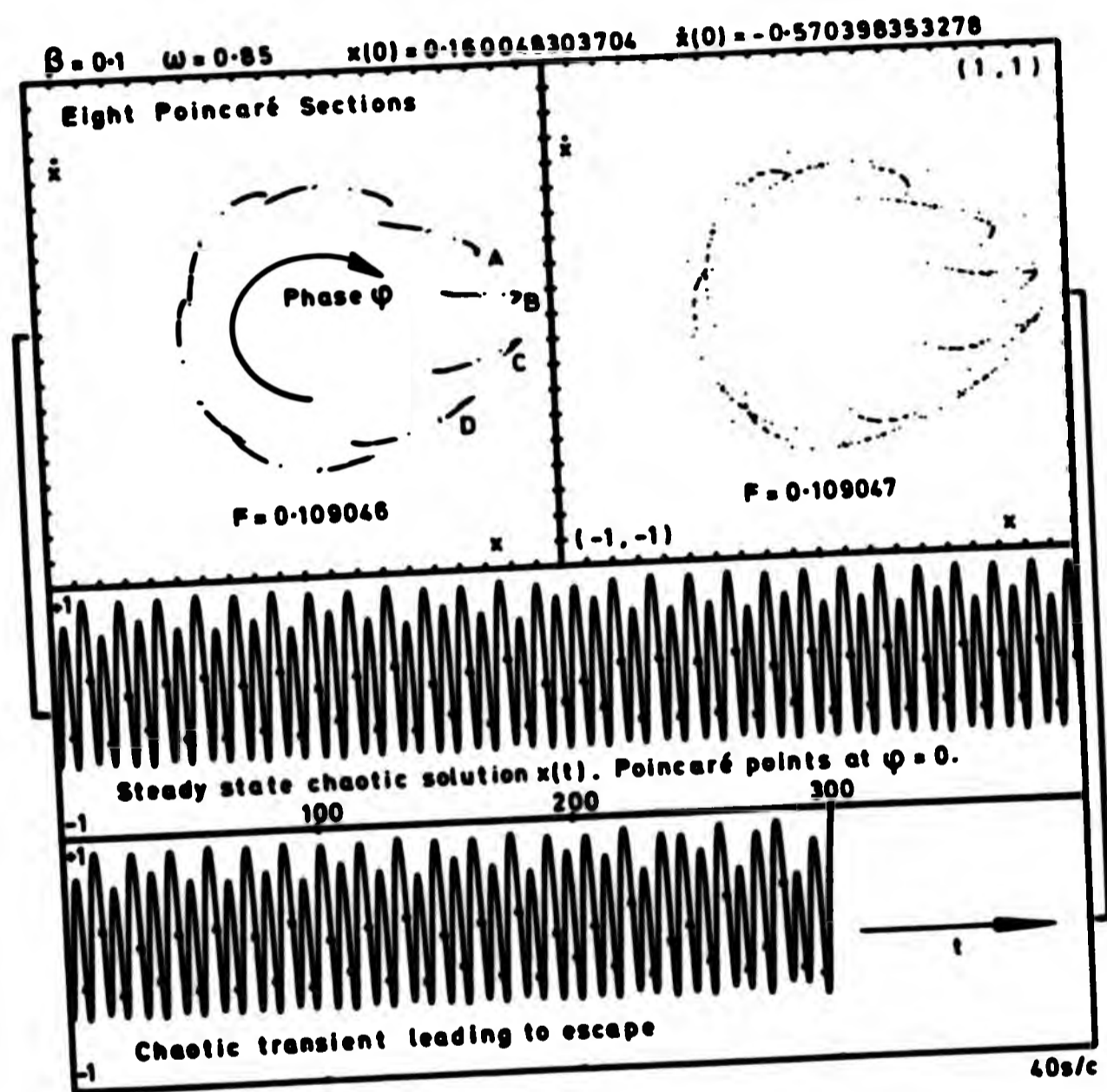


Figure 5.10 The chaotic attractor sampled at different phase angles, a steady state chaotic solution and a chaotic transient.

ATTRACTOR DIMENSION BEFORE THE BIFURCATION		ATTRACTOR DIMENSION AFTER THE BIFURCATION				
SEVERITY	0 POINT	1 CYCLE	2 TORUS	3 CHAOTIC	∞ NO ATTRACTOR	
0 POINT	(Stable-symmetric) (Asymmetric)	Super-crit. Hopf ^a FLOW EXPLOSION ^b		?	FOLD SUB-CRIT. HOPF (UNSTABLE-SYMMETRIC)	
1 CYCLE		Super-crit. FLIP	Super-crit. Neimark MAP EXPLOSION	(Flip cascade) INTERMITTENCY EXPLOSION	CYCLIC FOLD SUB-CRIT. FLIP SUB-CRIT. NEIMARK SADDLE CONNECTION ^c	
2 TORUS						
3 CHAOTIC				CHAOTIC EXPLOSION	CHAOTIC BLUE-SKY CATASTROPHE	




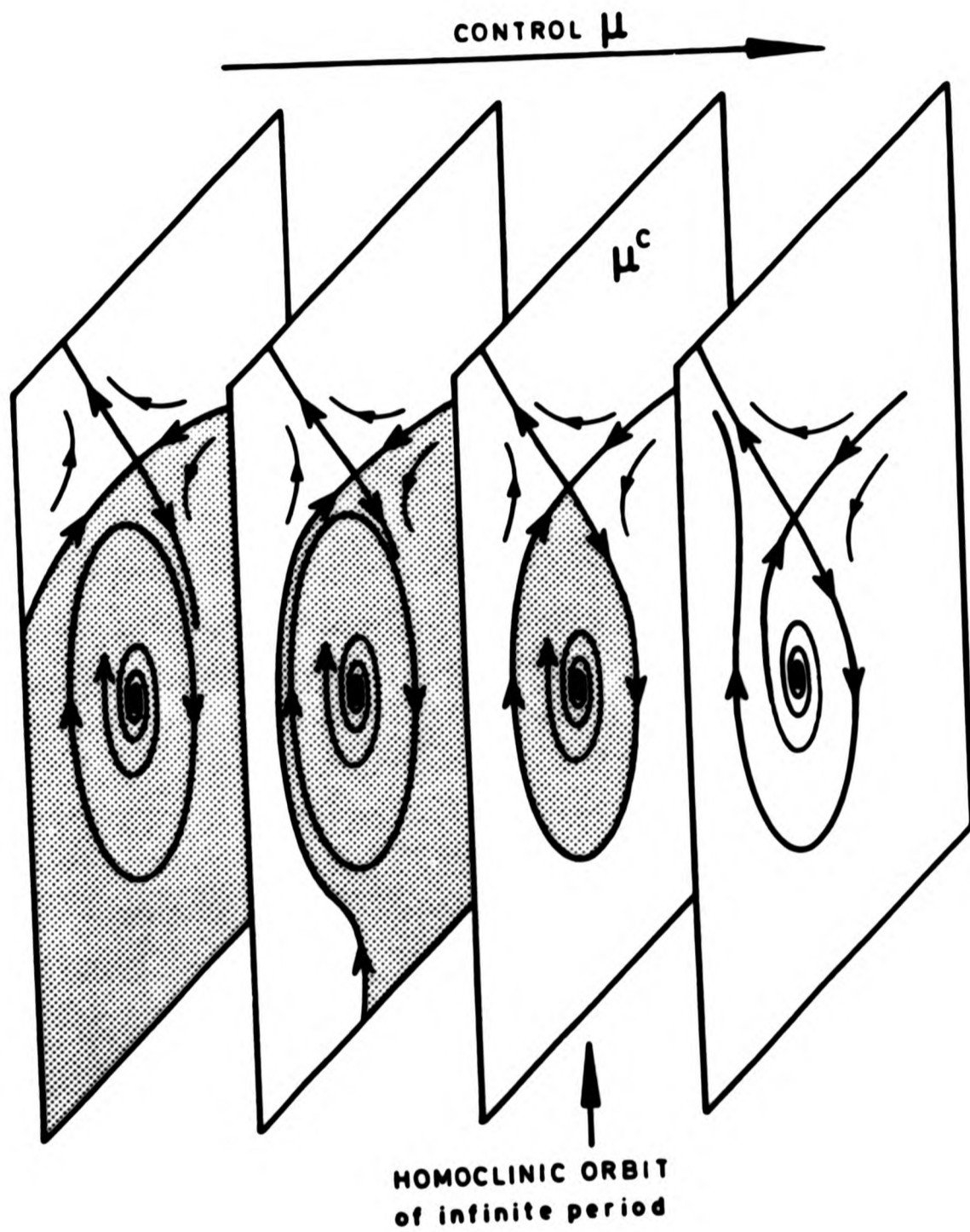
Terminology:		
Subtle i.e. Continuous (lower case) Safe	CATASTROPHIC i.e. DISCONTINUOUS (UPPER CASE) EXPLOSIVE	DANGEROUS
		

Figure 5.11 Classification table of bifurcations [Thompson and Stewart (1986)].



**A SADDLE CONNECTION (BLUE SKY)
CATASTROPHE**

Figure 5.12 Bifurcation of a flow that leaves no local attractor.

HOMOCLINIC TANGLE

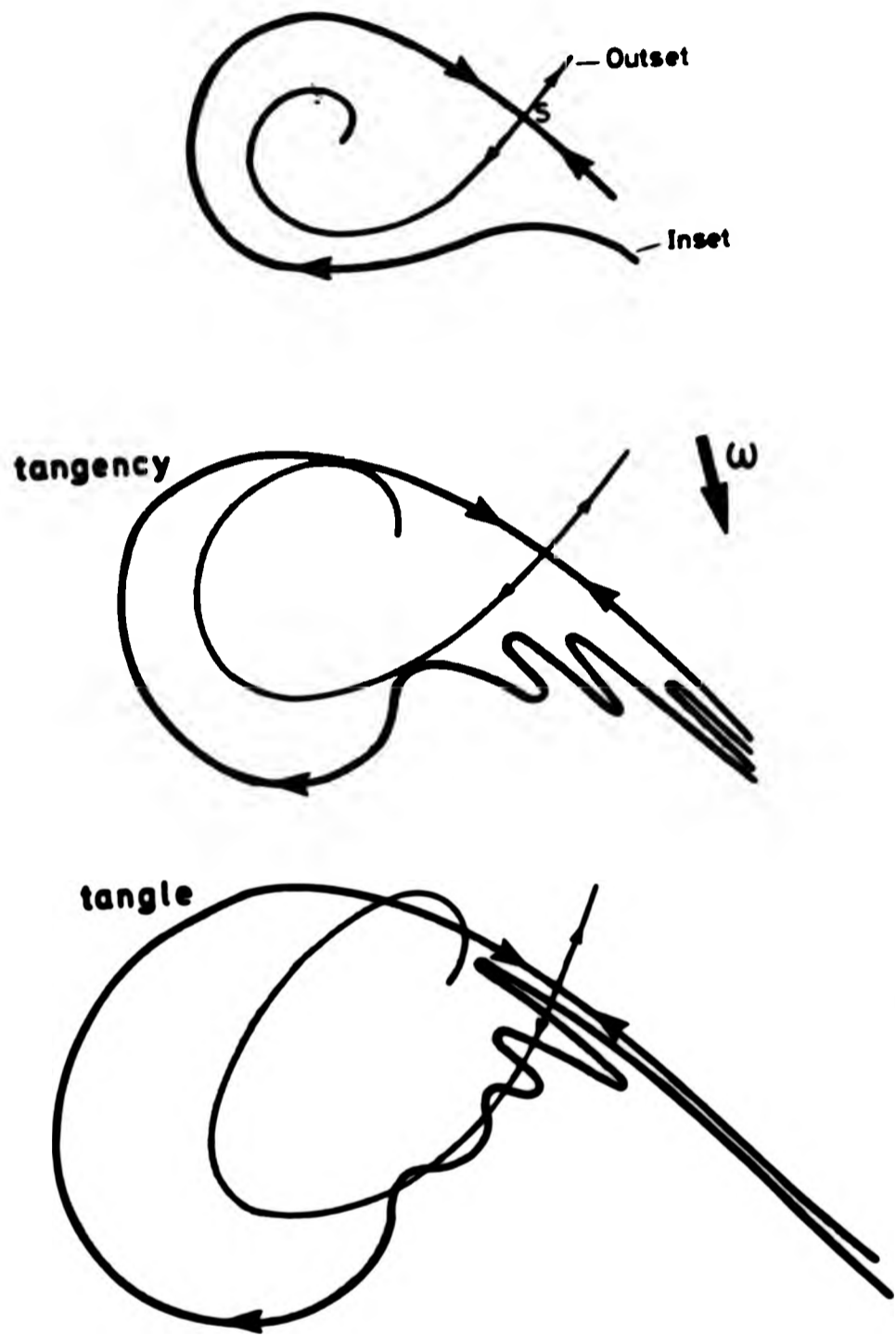
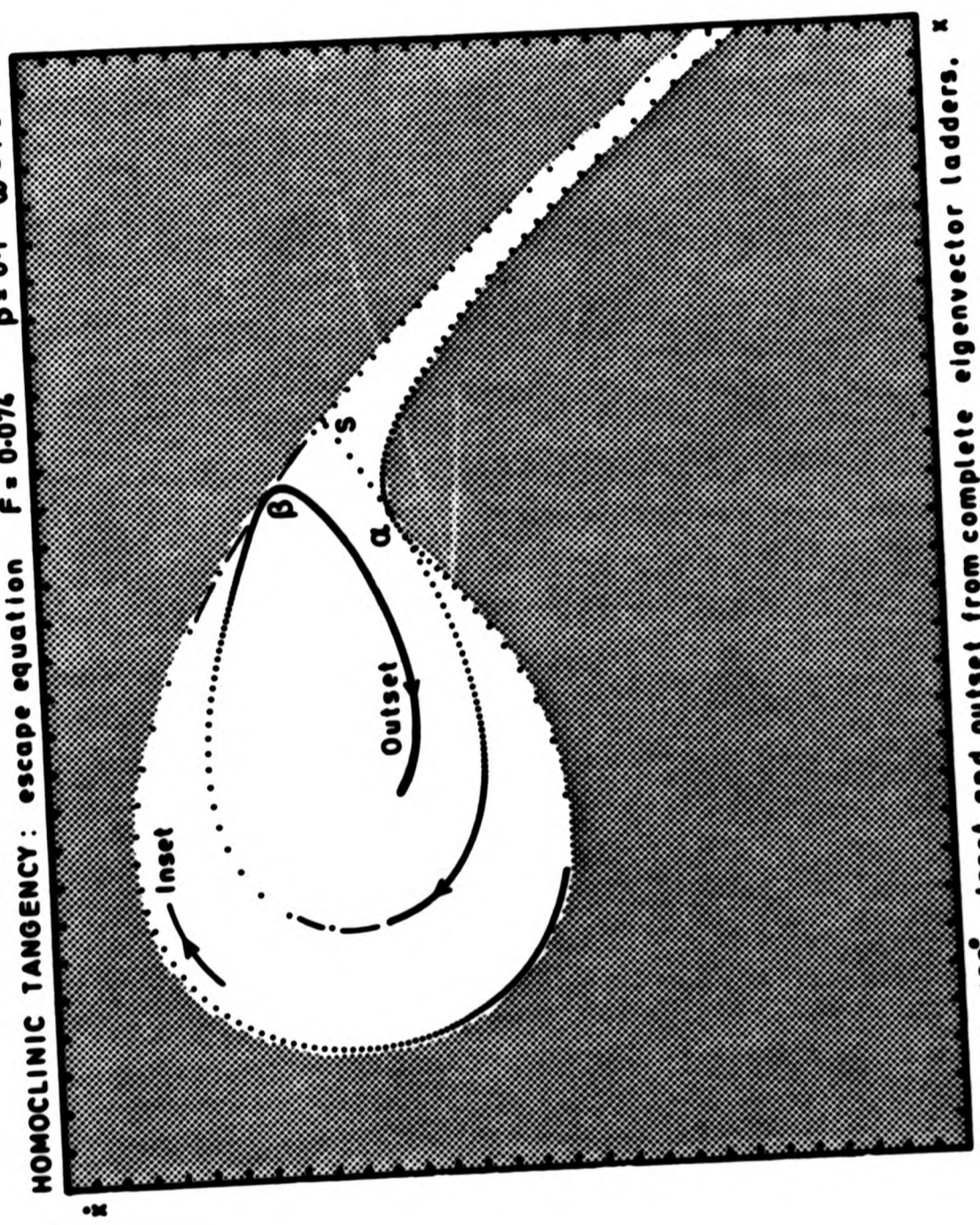


Figure 5.13 Schematic diagram of a homoclinic tangle.

HOMOCLINIC TANGENCY: escape equation $F = 0.074$ $\beta = 0.1$ $\omega = 1.0$



Phase $\varphi = 180^\circ$. Inset and outset from complete eigenvector ladders. $-1 < x < 2$: $-2 < z < 1$.

Figure 5.14 Computed homoclinic tangency.

Ladder Method

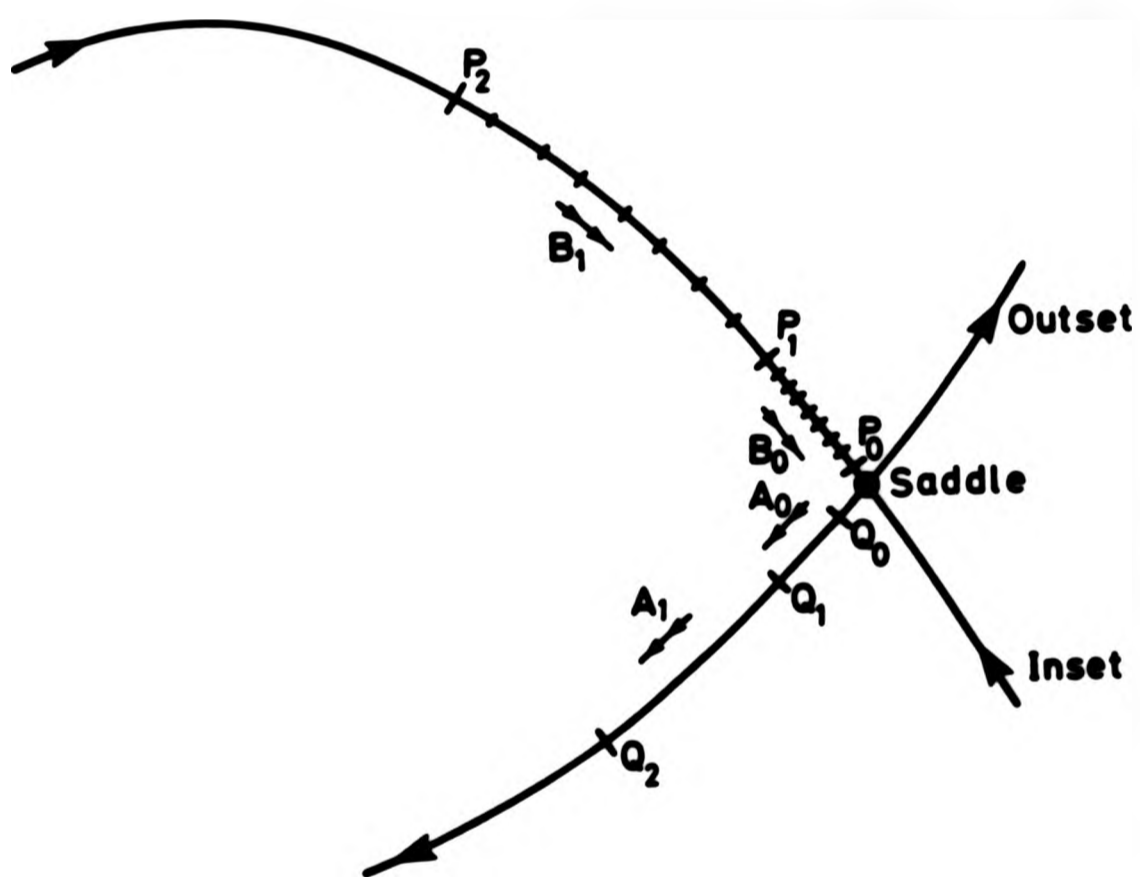


Figure 5.15 Schematic illustration of the ladder method.

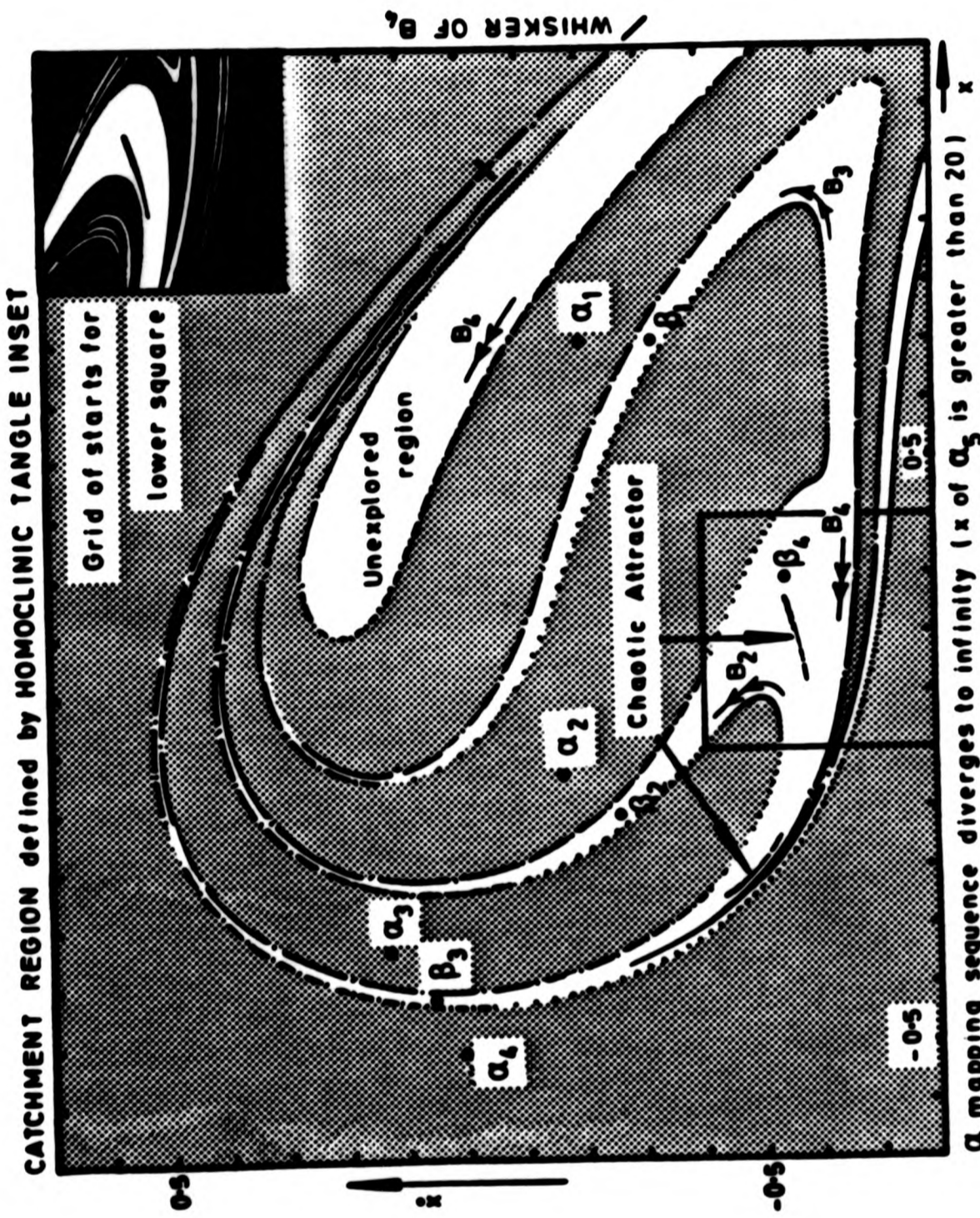


Figure 5.16 Homoclinic tangle close to the extinction of the α mapping sequence diverges to infinity (x of α_5 is greater than 20) β mapping sequence converges to the chaotic attractor

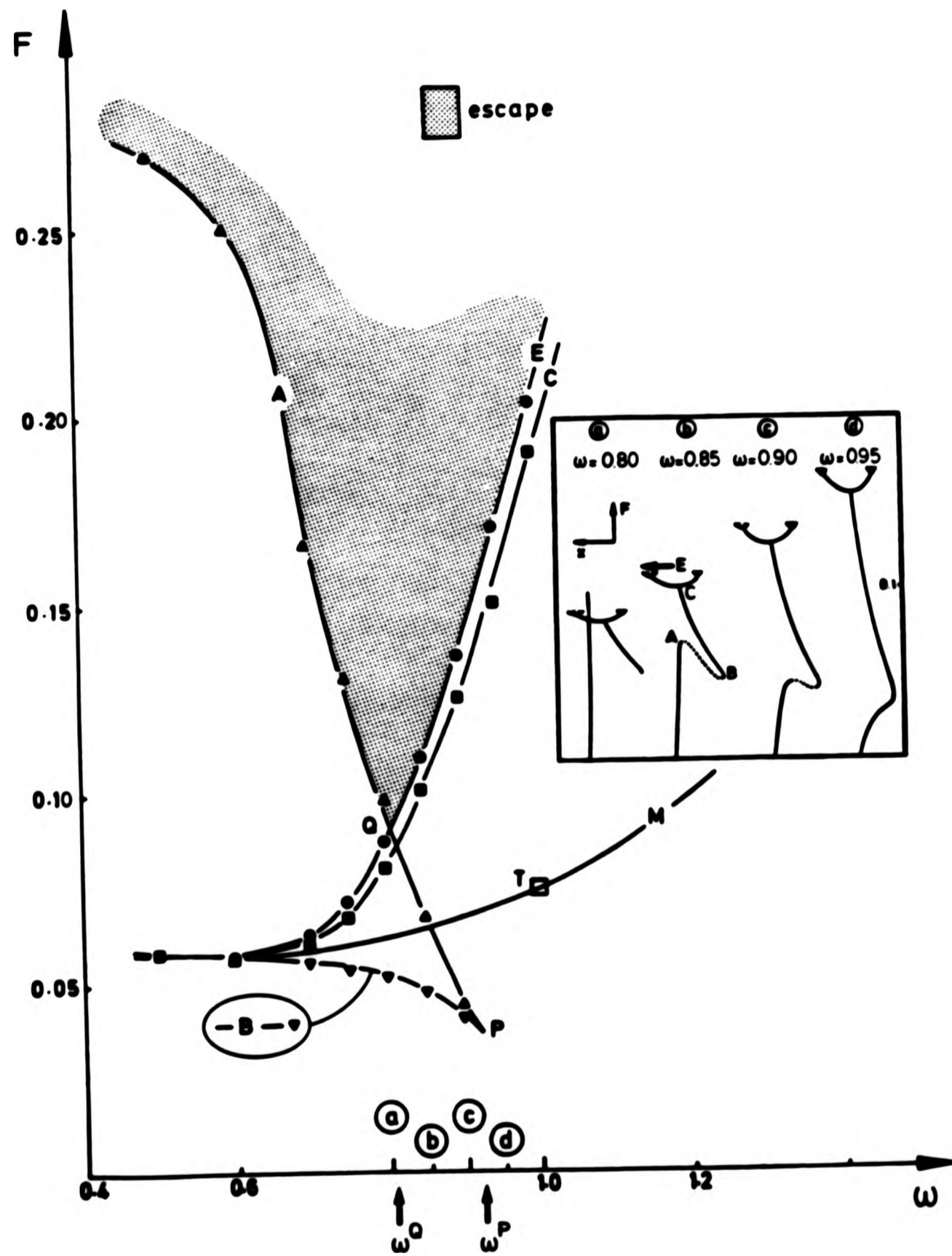


Figure 5.17 Bifurcation diagram.

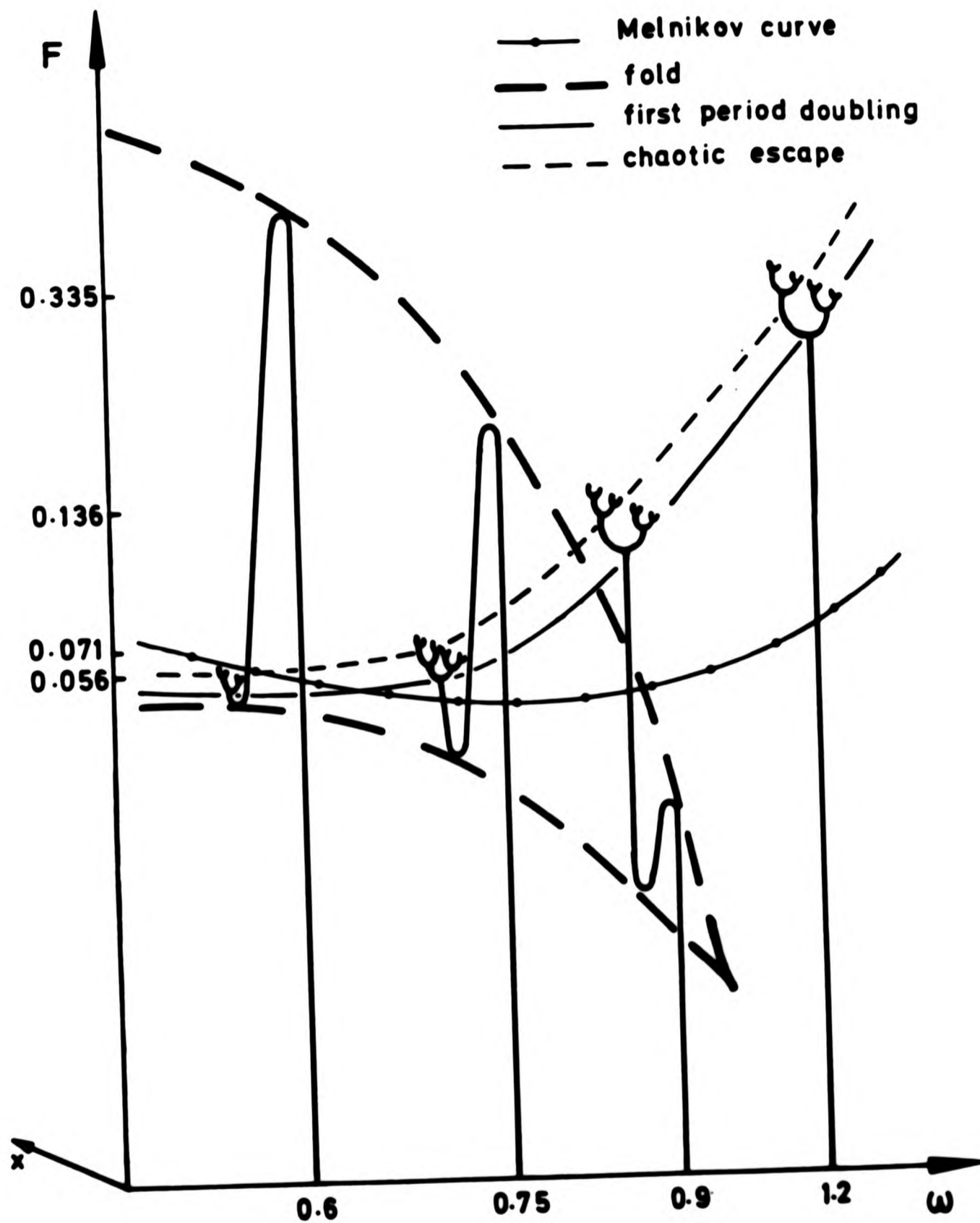


Figure 5.18 Schematic diagrams of equilibrium paths in relation to the Melnikov curve.

CHAPTER III.6

COMPLEX MOTIONS OF A MOORED SEMI-SUBMERSIBLE PLATFORM

To act as a summary of the methods developed for investigating and predicting the cyclic fold (saddle node) and the flip instabilities, both codimension one bifurcations, a study of the possible steady state motions of a moored semi-submersible platform has been carried out. This study, as well as pointing out some of the complexities of nonlinear systems, illustrates how these methods might be applied to any dynamic study of a compliant system.

III.6.1 Introduction

As offshore developments necessarily move into deeper waters the use of fixed steel jacket production platforms becomes uneconomic when the amount of stiffening required to provide for adequate structural stability and fatigue life is taken into account. Concrete gravity structures were originally designed for heavy payloads in shallow waters and are not considered to be well suited for deep water, or temporary, production, consequently much current offshore design is directed towards floating facilities. Catenary moored semi-submersibles are a relatively new and innovative feature in

the field of deep water platforms or transportable production support facilities in the offshore industry [Chou et al. (1983), Rainey (1978)]. The effect of the mooring chains renders the dynamic response of these compliant structures highly nonlinear. So much so, in fact, that traditionally adopted analytical approaches based on assumptions of near-linearity are often inadequate if extreme responses are to be predicted with any certainty. therefore, the role of nonlinear dynamics is a fundamental prerequisite to the understanding of the large amplitude motions [Cash and Rainey (1980), Robinson and Stoddart (1986)].

The growth of research interest into nonlinear dynamics in the field of applied mathematics has been spectacular in recent years [Lighthill (1986)] although it is only comparatively recently that the important qualitative insight afforded by dynamical systems theory has been applied by engineers to current practical industrial or engineering problems [Guckenheimer and Holmes (1983), Thompson (1982)].

As a starting point in the modelling process a dynamical system is often described by a governing equation of motion [Nayfeh and Mook (1979), Patel (1983)]. While there is a relatively complete analytical theory for linear ordinary differential equations, most nonlinear systems cannot be solved in a closed form. Recourse to direct time simulation is perhaps the most useful approach towards a solution and will be adopted throughout this work. In the past direct time domain simulation

have been limited by the expense of computer time but fast, efficient computers are becoming increasingly available so that numerical integration can be used as the main thrust of analysis rather than one or two isolated simulations to verify an approximate method [Cardo et al. (1984), Wright and Marshfield (1980) and Nayfeh and Khdeir (1986)].

For ease of presentation some assumptions and simplifications are necessarily made. Firstly, deterministic forcing is considered modelling a regular sea; random processes will form the basis of later (chapter III.7) and future work. Secondly, the added mass and damping coefficients and the value of the fluid loading are taken as being amplitude and frequency independent, with the justification that there will be a limited interaction between the structure and the free surface [Patel and Walker (1983)]. Finally, only a single degree of freedom will be considered, namely uncoupled surge motions. For large amplitude oscillations it is likely that these modelling assumptions may be violated, however, without these simplifications a study of the variations of all the parameters would be extremely lengthy [cf. Ueda's examination of a two parameter system (1980) see also chapter II.1)]. Nonetheless the design engineer should be aware of the hidden complexities of nonlinear systems when performing time domain simulations.

Despite these restrictions the underlying nonlinearity of the system and the light effective damping results in a variety of complex phenomena including competing steady state solutions,

sensitivity to initial conditions, sudden jumps between resonances incorporating hysteresis loops, and chaotic motions. These features occur in the two cases considered, i.e. leeward lines slack and active, as we shall shortly see.

Due to the assumptions made and the complexity of the behaviour the main emphasis is placed on qualitative behaviour [Thompson and Stewart (1986)]. In other words, even for the relatively simple system considered in this paper, these complex motions are likely to be encountered in a similar form for more sophisticated models and therefore in the actual response of a semi-submersible.

III.6.2 Mathematical Modelling

(a) The underlying equation of motion

The schematic diagram of a moored semi-submersible in figure 6.1 illustrates the system to be modelled considering unidirectional waves. Thus it is possible to focus attention on the single degree of freedom surge motion (X) under the influence of a constant wind or current loading (L), described by the differential equation

$$m\ddot{X} + b\dot{X} + F(X) = L + F_0 \sin \omega t, \quad (6.1)$$

where a dot denotes differentiation with respect to time (t), m

and b are mass and damping coefficients, $F(X)$ is a nonlinear function representing the restoring force and the right hand side of equation (6.1) represents a regular sea with wave force F_0 , frequency ω and period $T=2\pi/\omega$.

The value of the coefficients assumed here to be were obtained by realistic approximations from a recent Case Study [see Dynamics of Compliant Structures (1985)]; a static offset is incorporated into the system simulating the effect of a constant wind force or current loading. The common procedure of slackening off the leeward catenary lines in an attempt to reduce loads changes the form of $F(X)$ and simulations run with both the lee lines active and slack will be considered and the following work aims to explore the response of this system to typical regular waves.

(b) Numerical time simulation

It is a relatively simple matter to integrate a nonlinear ordinary differential equation on a digital computer. A popular scheme is the Runge-Kutta method which has proved to give satisfactory results in a wide range of applications [see the note in chapter III.1].

In making a parametric study of a dynamical system it is necessary to assess the role played by each factor on the resulting behaviour. Such a task can be daunting even for a

relatively simple model [Ueda (1980)]. In this work the mass, damping and stiffness characteristics as well as the wave force are held constant at realistic values and the wave period is chosen as the control parameter. Therefore, the subsequent computations relate to values of the wave period in the region of practical 'design wave' expectations.

Using numerical time integration there are no restrictions to nearly linear systems or small parameters common to many approximate techniques such as the perturbation method. Also, an evolving sea-state and random influences can be handled by this method [Bishop et al. (1986)].

(c) Instabilities and bifurcations

A major concern for an engineer is being able to predict any sudden change in the behaviour of a system that might occur due to a slowly evolving sea-state. It is important to know under what conditions a steady state will lose its stability by jumping to another remote steady state, bifurcating into a different order of subharmonic motion, or even capsizing as seen in chapter III.5.

The dynamical systems theory of differential equations offers guidance to the expected forms of bifurcations under the operation of a control parameter. In fact there are only three

local generic bifurcations in which a periodic dynamical system can lose its stability for one parameter systems [Stewart and Thompson (1986)] and the manifestation of approaching instability has been observed in transient motion and found to be useful for prediction purposes [Bishop and Franciosi]. Also a further justification for using a low order system is that the significant behaviour of large dynamical systems, particularly those approaching instability, is topologically governed by the qualitative behaviour of an attractor of low dimension.

III.6.3 The Leeward Lines Slack Case

(a) Stiffness curve representation and linearization

We start by considering the case of a semi-submersible moored by catenary chains where the leeward mooring lines have been slackened off to reduce tensions [Bishop and Virgin (1987)]. The stiffness characteristics of this system are shown in figure 6.2(a), indicating the comparison between real data (shown by dots) and the corresponding curve fit. An exponential form for this restoring force was adopted to give the required zero stiffness at large negative displacements. It is more convenient to study local oscillations with displacements x about a static offset or equilibrium position X_L , in which case the restoring force may be represented by

$$F(X) = F(X_L + x) \quad (6.3)$$

$$F(x) = L + f(x) , \quad (6.4)$$

where

$$f(x) = L(e^{cx} - 1) . \quad (6.5)$$

The coefficients of the curve fit are given by

$$L = 400g \exp(cX_L) \quad (6.6)$$

since 400g KN is the known load at zero displacement, where $g=9.81 \text{ m/s}^2$ and $c=0.1$.

Although a variety of static offsets can be examined, for the purpose of this study X_L shall be taken to be 6 metres for both the active and slack cases.

Placing the restoring force relationship into the equation of motion gives

$$m\ddot{x} + b\dot{x} + f(x) = F_0 \sin \omega t . \quad (6.7)$$

The mass (m) of the structure under consideration, including added mass, is 45011×10^3 Kg with a damping coefficient (b) of 383 KN/(m/s). The damping used in the model is linear and although this provides a good approximation within a given speed range the essentially quadratic nature of typical damping mechanisms might come into play for larger amplitude/period

ratios. For computational convenience the forcing term F_0 is taken to be constant at 15000 KN corresponding to an 8 metre wave but could readily be incorporated in the following computational analysis as a variable, more realistically modelling the wave force variations according to typical data see figure 6.3.

Expanding the exponential and subsequent linearization of the equation (6.5) yields

$$L(e^{cx} - 1) = Lcx + O(x^2) \quad (6.8)$$

and inserting the relevant coefficients leads to

$$f(x) \sim 715 x \quad (6.9)$$

which gives a natural linearised frequency for the offset of 6 metres as

$$\omega_n = \sqrt{Lc/m} = 0.126 \text{ rad/s} \quad (6.10)$$

and a linearised natural period of

$$T_n = 2\pi/0.126 = 49.85 \text{ seconds} \quad (6.11)$$

The natural periods of the semi-submersible for a range of offset values is shown in figure 6.4.

To measure the range of validity of this linearization the natural period of oscillation of equation (6.7) was computed with no damping or forcing and the deviation from equation (6.11) is illustrated in the lower diagram of figure 6.5. This diagram also shows the potential energy function (V) on which the system can be thought to be oscillating in, obtained by integrating the stiffness function. It can be seen that the natural period is considerably lengthened for large amplitude nonlinear free oscillations.

An analytical expression for the amplitude of the linearised system is the standard result from vibration theory [Thomson (1981) also see chapter II.3] and this may be later compared with the nonlinear amplitudes obtained from numerical integration in the next section.

(b) Competing steady states

The wave period T is used as the control parameter so that a large number of simulations are computed and the resulting final steady state amplitudes obtained, as shown in figure 6.6, for values of T between 10 and 30 seconds. The design wave periods are within this range and for the semi-submersible under consideration are therefore about 25%-50% of the linearised natural period of the system.

The amplitudes shown in figure 6.6 represent the final

motion of a system started from a particular initial condition. Which steady state motion acts as an attractor to the transient trajectory depends on the catchment region for a given value of the wave period. For example, for a wave period of 18 seconds the phase portraits in figure 6.7 show that the system may undergo three different steady state oscillations depending on these initial conditions. Also shown in this diagram are the corresponding time series. A steady state path corresponding to a stable periodic solution may suddenly appear or disappear in the control-amplitude space, or it may bifurcate into a higher order subharmonic by means of the familiar period doubling characteristic of nonlinear dynamics, e.g. the onset of this feature is visible when at $T=22$ seconds the $n=1$ solution loses its stability. This phenomenon will be studied in more detail in the next section. The loss of stability of an attractor was introduced earlier, a more detailed example of these mechanisms will be given in the leeward lines active case. Also shown in figure 6.4 is the linearised amplitude indicating the unexpected and potentially dangerous appearance of large amplitude motions. It should be borne in mind that there may be further attractors present other than those reported here.

(c) Period doubling and chaos

A cascade of period doubling bifurcations will normally lead to a chaotic response under the gradual variation of the

control parameter. The onset of each new bifurcation occurs at a progressively smaller variation in the control parameter until the response can be termed chaotic.

A scenario of period doubling steady states as Poincaré maps is shown in figure 6.8. These pictures are obtained by letting the system settle down after a considerable number of forcing cycles after which sufficient points are plotted to characterise the steady state. For the given wave periods in figure 6.8 bifurcations leading to subharmonics of order 96 are shown, indicating the extremely complex nature of the motion. A plot of the displacement of the Poincaré points against the control parameter in figure 6.9 clearly shows the cascade of period doubling bifurcations. The amplitude of these bifurcating subharmonic resonances relate to the $n=3$ response arm in figure 6.6. It should be noted here that x_p will not in general correspond to the maximum amplitude of the oscillation and that the bifurcations of the arm with positive displacements are so small as to not be visible on the scale drawn.

The result, previously explained in part II, that the ratio of successive distances between bifurcations during a period doubling cascade tends to a universal number was only proved for maps but it is useful to construct these ratios for the cascade under consideration here. If we denote the value of the wave period at which the bifurcation to a subharmonic of order n occurs by T_n then from the investigations reported here we find that

$$\begin{aligned}
 T_1 &= 22.38 \quad , \quad T_2 = 23.59 \quad , \quad T_3 = 23.828 \\
 T_4 &= 23.8695 \quad , \quad T_5 = 23.879 \quad , \quad T_6 = 23.88105 \quad . \quad (6.12)
 \end{aligned}$$

These values produce the following Feigenbaum ratios

$$\delta_i = (T_{i+1} - T_i) / (T_{i+2} - T_{i+1}) \quad , \quad (6.13)$$

as follows

$$\delta_1 = \quad , \quad \delta_2 = 5.735 \quad , \quad \delta_3 = 4.368 \quad , \quad \delta_4 = 4.634$$

remembering that the universal Feigenbaum number is given by $\delta_\infty = 4.6692$.

A close up view of the approach to chaos is shown in figure 6.10 in which the folding of the attractor can just be seen in the bottom right hand diagram. A useful identification of this type of behaviour is obtained by sampling the attractor at different phases of the forcing. A detailed analysis of the chaotic dynamics inevitably involves many aspects of advanced mathematical concepts which will form the basis of further work but suffice it to say here that the subsequent motion of the platform will be highly complex and almost certain to create problems if found to occur in reality.

III.6.4 The Leeward Lines Active Case

(a) Equation of motion

A similar computational study has been carried out when the mooring chains on the leeward side were considered to be active during all motions. The equation describing local departures from an offset of 6 metres is once again given by the equation (6.7) with the same coefficients as before except that the restoring force, seen in figure 6.2(b), can now be represented by a cubic polynomial. The coefficients of this expression were obtained by fitting the data in a least squares sense and found to be such that

$$f(x) = 880.84x + 32.27x^2 + 1.899x^3 . \quad (6.14)$$

By considering a linear approximation the natural frequency and period can be calculated to yield

$$\omega_n = 0.14 \text{ rad/s} , \quad (6.15)$$

and

$$T_n = 44.9 \text{ seconds} . \quad (6.16)$$

The damping factor is

$$\zeta = b / (2m\omega_n) = 0.03 , \quad (6.17)$$

which is relatively small and therefore transient motion will take some time to decay. However, a close approximation to the position of the steady state in the phase plane is given by the steady state of a close by control value so that transients can be minimised to some extent.

(b) Competing steady states

The maximum amplitudes of steady state motions are shown in figure 6.11 where again multiple steady state oscillations for a fixed wave period are the rule not the exception. This amplitude response diagram is more symmetrical than for the lee lines slack case in figure 6.6 as expected but a small asymmetry in wave form is due to the static offset of the semi-submersible. Again interlocking spirals in the domains of attraction of (x, \dot{x}) are encountered although they are not computed here.

The linear steady state can be seen as a small amplitude harmonic ($n=1$) response. However, some unexpected behaviour occurs between $T=18$ and $T=22$ seconds with the appearance of a hysteresis loop. The actual mechanism of the instability will be described in the next section but it is clear that there will be finite jumps between these stable periodic attractors, including jumps to the extremely large amplitude motion which would be catastrophic.

The type of behaviour is complicated by these jumps between harmonic and subharmonic solutions although only the maximum positive and negative amplitudes of the wave form are shown in figure 6.11. The use of a linear solution gives only the small amplitude motion as indicated so that the limitations of linearisation are apparent and it can be seen that even a small deviation from linearity can have a dramatic effect on the dynamic response of the system.

(c) The loss of stability

The incipient loss of stability of a dynamical system is manifested in the transient response. For a one parameter system, such as ours, there are only three distinct ways in which cyclic behaviour can become unstable generically. Dynamical systems theory tells us that these are the fold (saddle-node), flip and Neimark bifurcations, and are characterised by one or more of the eigenvalues, of the underlying linear map, passing through the unit circle in the complex plane and increasing in modulus. Analytically this type of stability theory includes Floquet theory but the numerical procedures described in this work, particularly Poincaré mapping techniques, can be used to obtain useful information about the stability of a dynamical system.

The instabilities introduced in section 6.2 can be observed in the jump behaviour of the semi-submersible as viewed in the steady state response diagram of figure 6.11. These jumps may be more clearly seen in the displacement-control or velocity-control planes. This is shown in figure 6.12 where both x_p and \dot{x}_p versus T are plotted which may be viewed as a three dimensional control space with displacement and velocity at right angles to each other.

As with the lee lines slack case, a stable solution may jump suddenly to a new attractor or bifurcate into a higher order subharmonic in a more subtle fashion. Referring to figure 6.12 and gradually increasing the wave period from $T=12$ seconds, a small amplitude harmonic solution remains stable until about $T=21$ seconds when a jump to an $n=2$ subharmonic oscillation occurs. This subharmonic then restabilises onto the $n=1$ fundamental solution at about $T=24$ seconds until another jump at $T=30$ seconds leads to a large $n=1$ amplitude oscillation. A return journey would simply follow this large amplitude motion and gradually increase in magnitude until a large jump back down to the fundamental solution at $T=13$ seconds occurs. Alternatively following a small amplitude at $T=30$ seconds and decreasing the wave period would lead to a subharmonic flip bifurcation followed by a jump onto the $n=1$ harmonic at about $T=19$ seconds. Therefore not only are the initial conditions crucial to the final steady state motion but also one must know whether the forcing period is gradually increasing or decreasing.

Now considering in more detail the instability phenomena associated with the response of the semi-submersible for wave periods between 18 and 24 seconds and small amplitude oscillations. The displacement of the Poincaré points characterising this type of behaviour are shown in figure 6.13. The type of instability phenomenon can be evaluated by considering the eigenvalues of linear transient motion close to the steady state as described by Bishop et al. (1986).

To represent the Poincaré points of a transient motion we let

$$\begin{aligned} x_p(k) &= x(t_0 + kT) \\ y_p(k) &= \dot{x}(t_0 + kT) \end{aligned} \quad (6.18)$$

or in the vector form

$$z_k = [x_p(k), y_p(k)] \quad (6.19)$$

Then if we let $A(\lambda)$ be a 2x2 matrix of constant coefficients with eigenvalues λ , we may approximate the nonlinear Poincaré map determining the relationship between successive points by a linear map

$$z_{k+1} = A(\lambda)z_k, \quad k=0,1,2,\dots \quad (6.20)$$

The requirement for stability is that

$$|\lambda| < 1, \quad (6.21)$$

but suffice to say here that the fold and the flip bifurcation are characterised by a single real eigenvalue crossing the stability boundary through +1 and -1 respectively.

By applying this technique to monitor transient responses as the wave period is reduced to just below 24 seconds from the right hand diagram of figure 6.13 it can be seen that the subharmonic response, subsequently evident as T is decreased further, is due to a supercritical flip bifurcation. Perhaps more worrying for the design engineer is the presence of a subcritical flip bifurcation in the control phase space at around 21 seconds. This bifurcation is again determined by an eigenvalue passing through -1 as illustrated in the lower diagram of figure 6.13.

To determine the stability of the subharmonic motion along the $n=2$ path we must consider alternate points of the Poincaré map,

$$z_{k+2} = A(\lambda)z_{k+1} = A^2(\lambda)z_k. \quad (6.22)$$

Hence the stability is governed by the position in the complex plane of eigenvalues of $A^2(\lambda)$, i.e. λ^2 . From the left hand diagram of figure 6.13 we see that as the wave period is reduced below 19 seconds the corresponding eigenvalues along the $n=2$

path approach +1 indicating that the reason for the sudden end of the $n=2$ attractor is due to a cyclic fold bifurcation.

The unstable paths, only one of which is shown in figure 6.13 as a dotted line, may be geometrically quite complex and a complete understanding of any model behaviour would necessarily include a knowledge of these unstable paths and domains of attraction.

III.6.5 Conclusions

This discussion has illustrated that extreme care must be taken when modelling a dynamical system with nonlinear ordinary differential equations. Such nonlinear systems exhibit a variety of complex phenomena including chaotic motions and sudden jumps between steady states. If the mathematical model used in this study adequately describes reality then these responses may be expected in practice. In the case of the moored semi-submersible, nonlinearities are dominant so that methods of linear analysis are severely limited. Some analytical tools have predicted the existence and stability of subharmonic oscillations, notably the describing function method [Mees (1981,1983)] usually though with certain restrictions.

Often, direct time domain simulation is used as a check of perturbation or power spectra techniques but sensitivity to initial conditions with coexisting steady state solutions means

that interpretation of these results may be difficult. In some cases the linear theory would underestimate the maximum surge amplitude by a factor of 20. Obviously this would be a serious situation concerning operating conditions and fatigue of mooring chains etc..

The model used in this chapter is a relatively simple one considering, as it does, only deterministic forcing with the most dangerous nonlinear phenomena occurring at long periods. Of particular interest are the presence of sudden jumps which give no real warning of incipient instability of the motion. The variety of complex features exhibited by this model are stimulated by the light effective damping in the system.

Dynamical systems theory is used as a conceptual framework for qualitatively analysing the vast amount of computer generated data. Using this as a guide the typical instabilities and bifurcations of a system can be studied and, to a certain extent, predicted. For more complex models the utilisation of dynamical systems theory is essential if any kind of insight into nonlinear dynamical behaviour is to be achieved.

Improvements to the model would inevitably incorporate a more accurate wave loading representation, including a stochastic sea-state, added mass and damping coefficients as a function of wave frequency, and a multi-degree of freedom approach to study the effect of coupling on say heave, roll and sway. A complete attempt at modelling all of these factors is

daunting but it has been the aim of this chapter to illustrate the complexity of a theoretical mathematical model of a dynamical system simulating the surge motions of a catenary chain moored semi-submersible, to indicate that great care should be taken when carrying out direct time domain simulations of any system with nonlinearities.

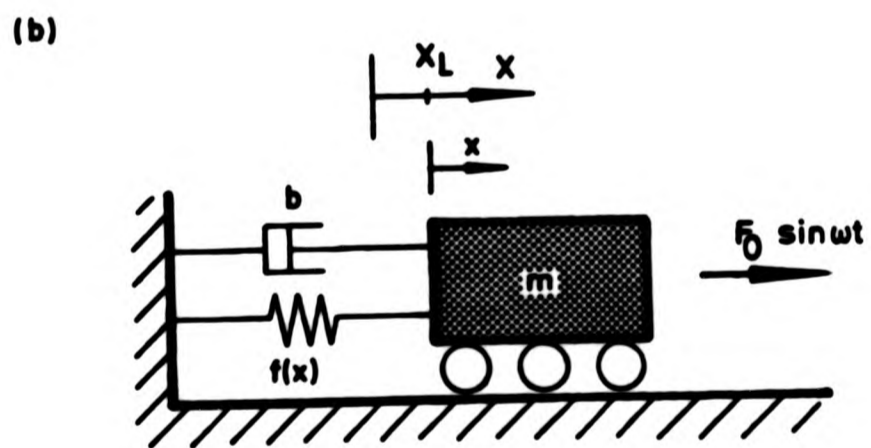
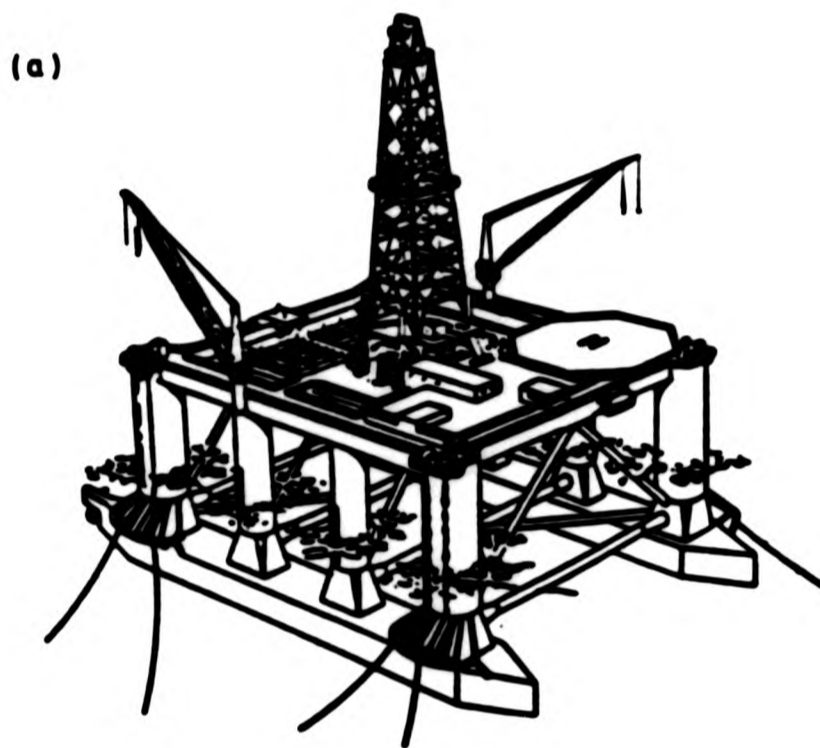


Figure 6.1 Schematic diagram of (a) a moored semi-submersible and (b) its corresponding mechanical model.

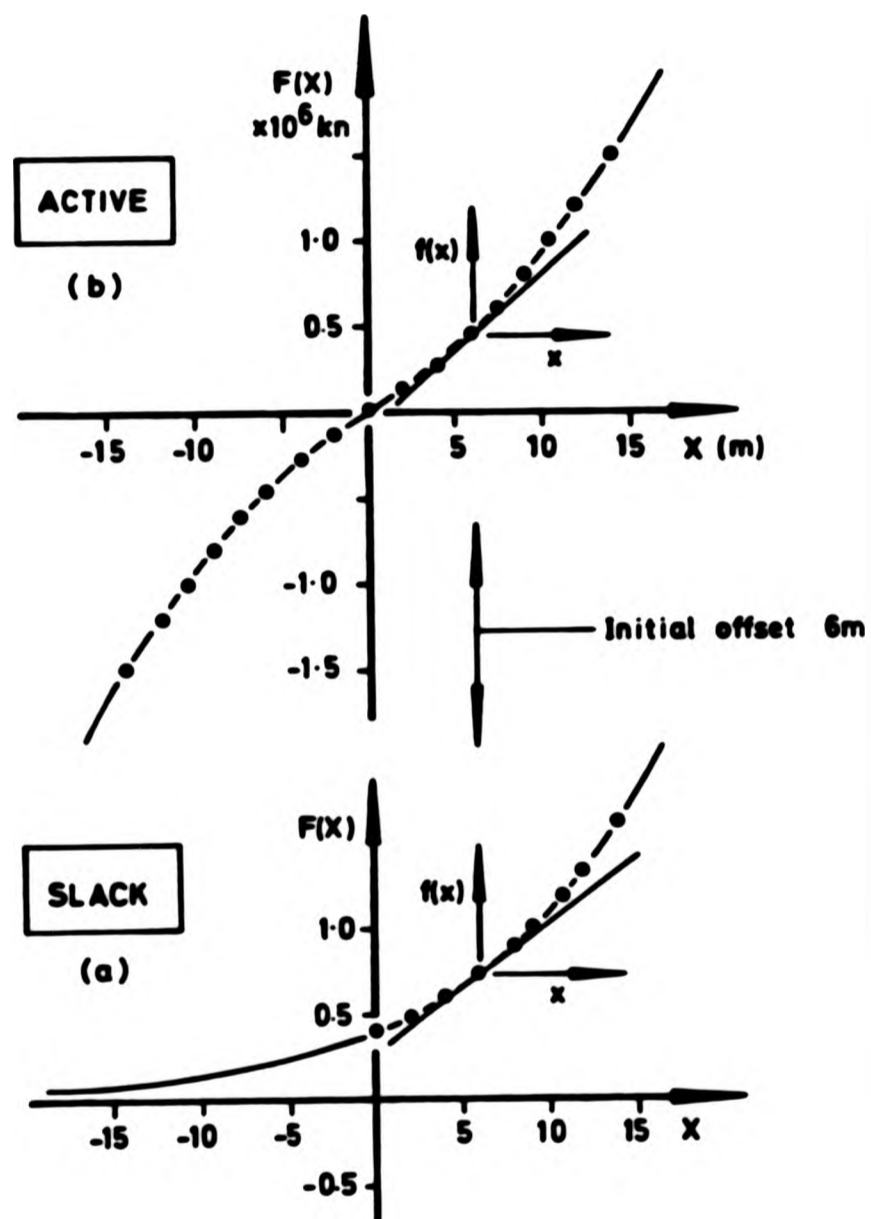


Figure 6.2 Restoring force curves comparing experimental data with a curve fit and displaying linearisation and local axes for a given offset for (a) lee lines slack and (b) lee lines active.

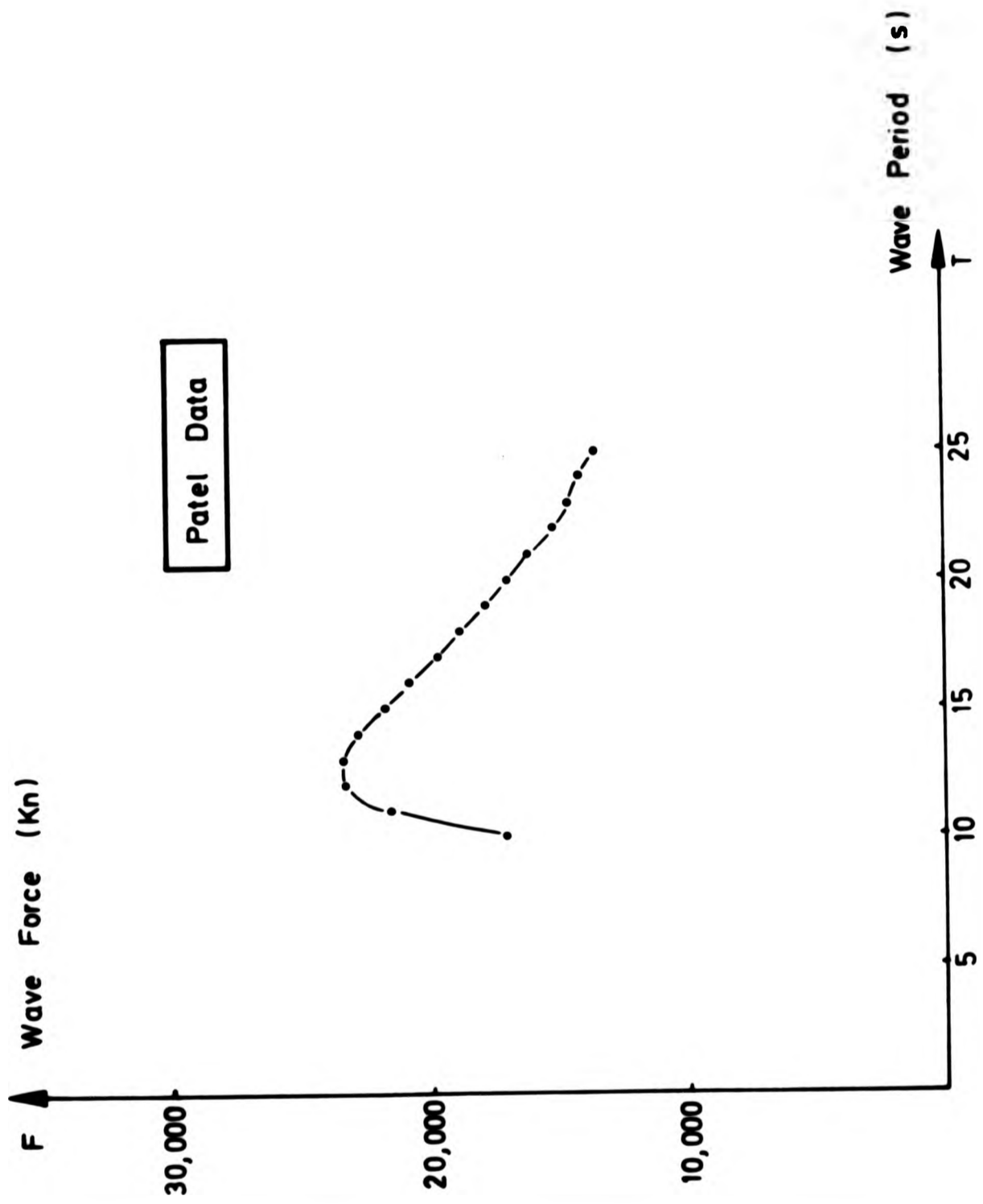


Figure 6.3 Wave force variations.

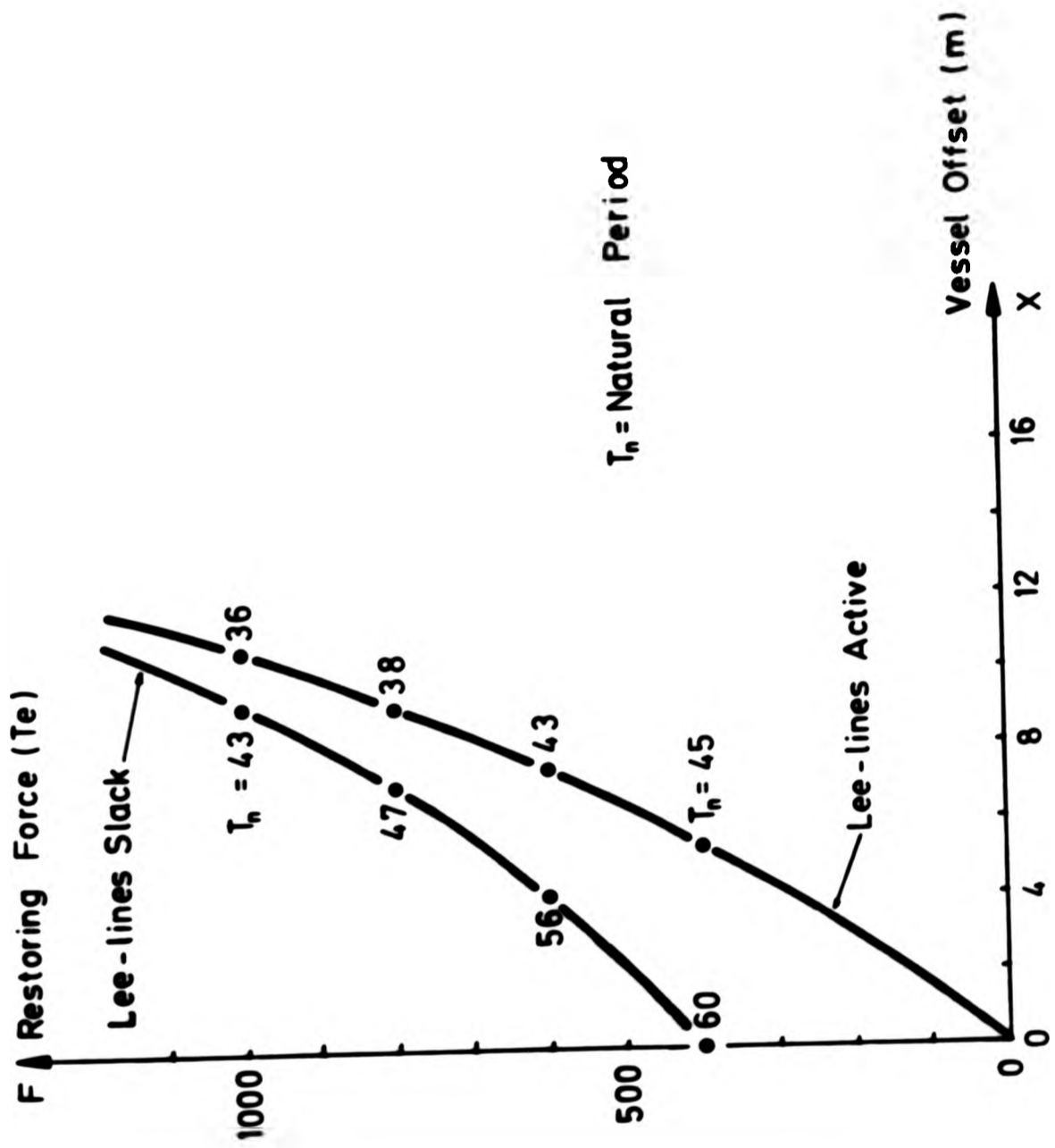
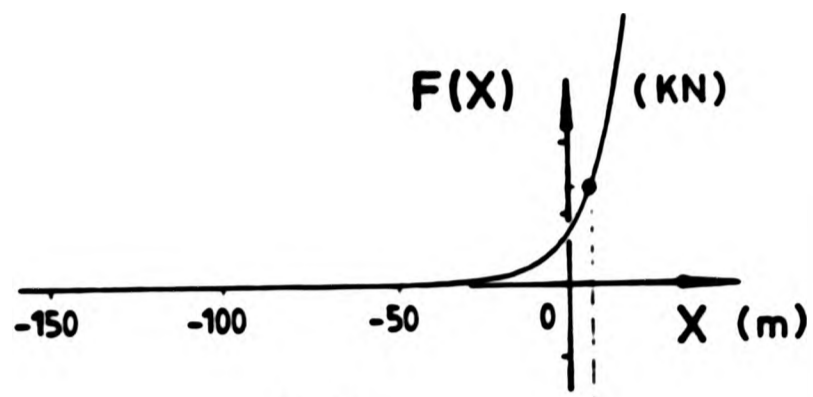
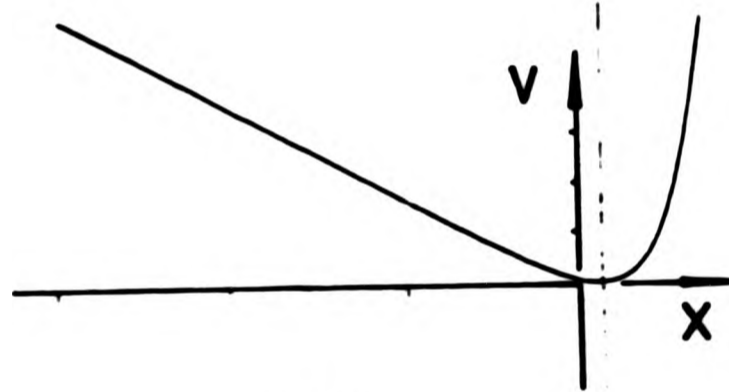


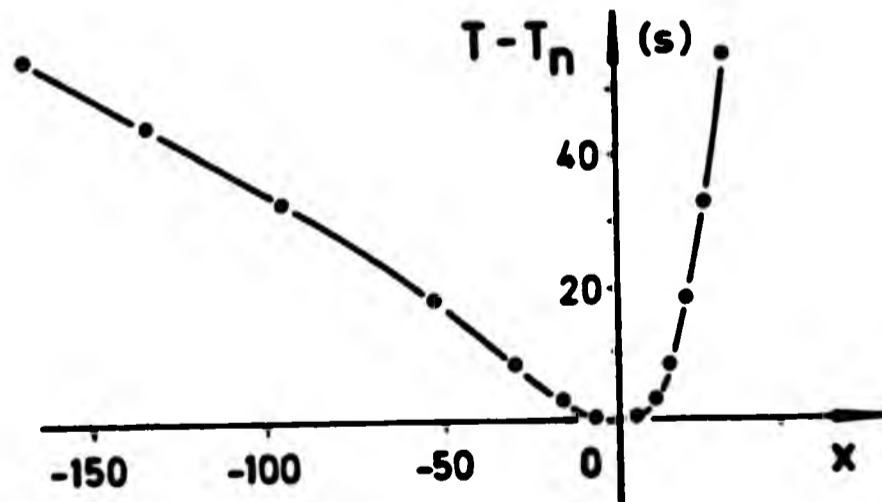
Figure 6.4 Natural periods of a semi-submersible.



(a)



(b)



(c)

Figure 6.5 (a) Restoring force, (b) potential energy and (c) the increase in natural period plotted against displacement (lee lines slack).

SLACK

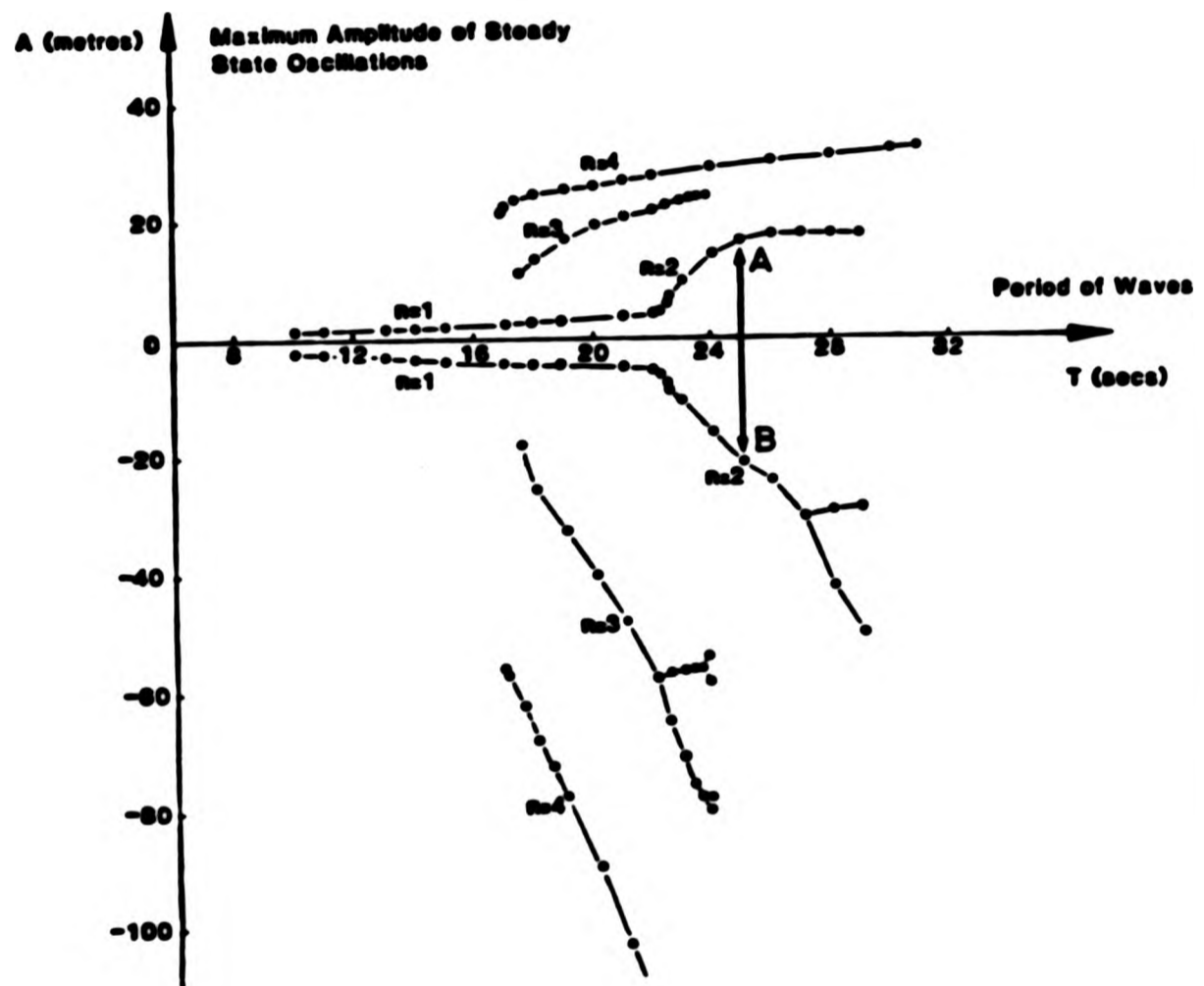


Figure 6.6 Maximum amplitude of steady state oscillations as a function of wave period.

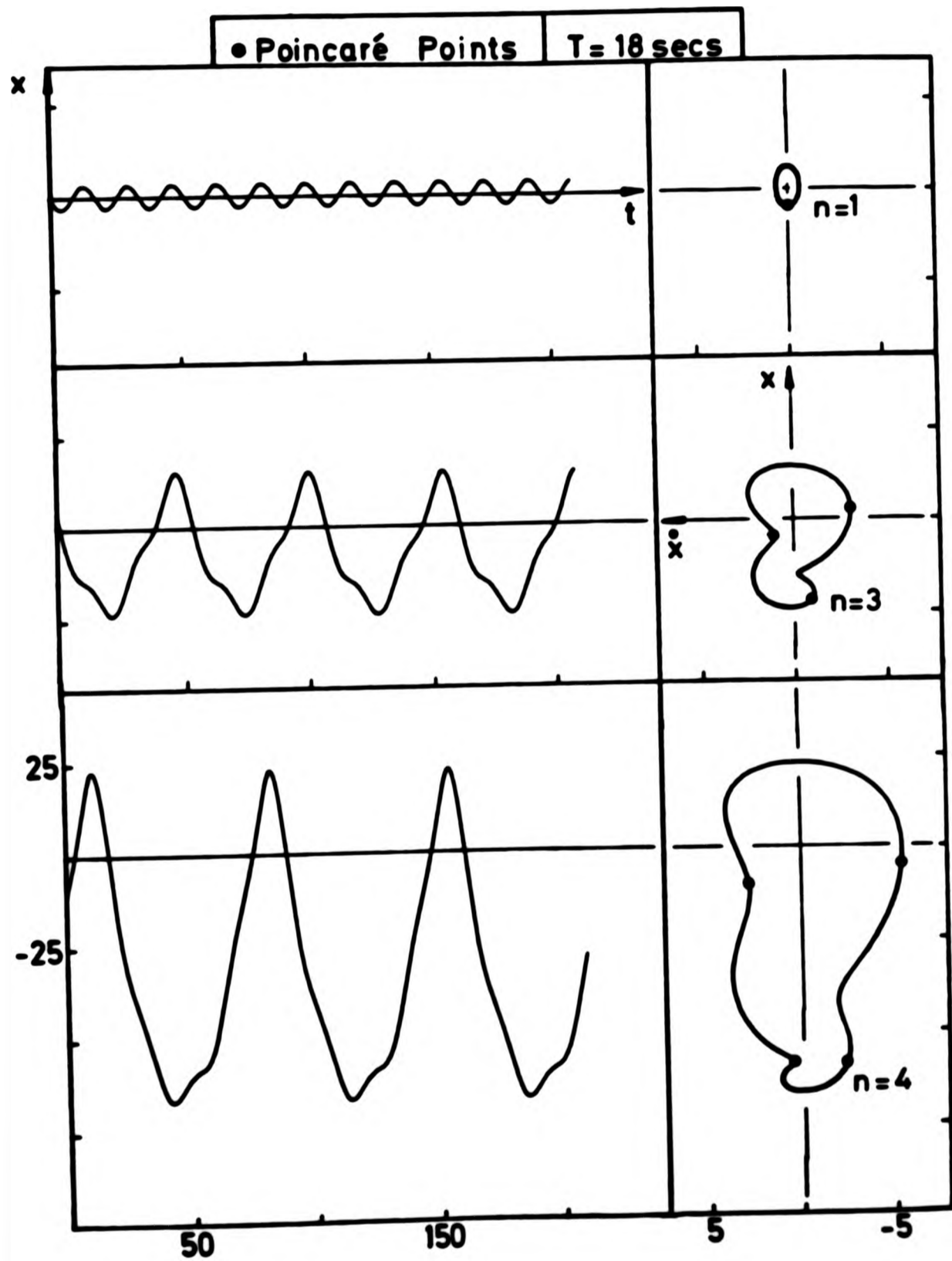


Figure 6.7 Three coexisting steady state motions shown as time series and phase portraits for $T=18$ seconds.

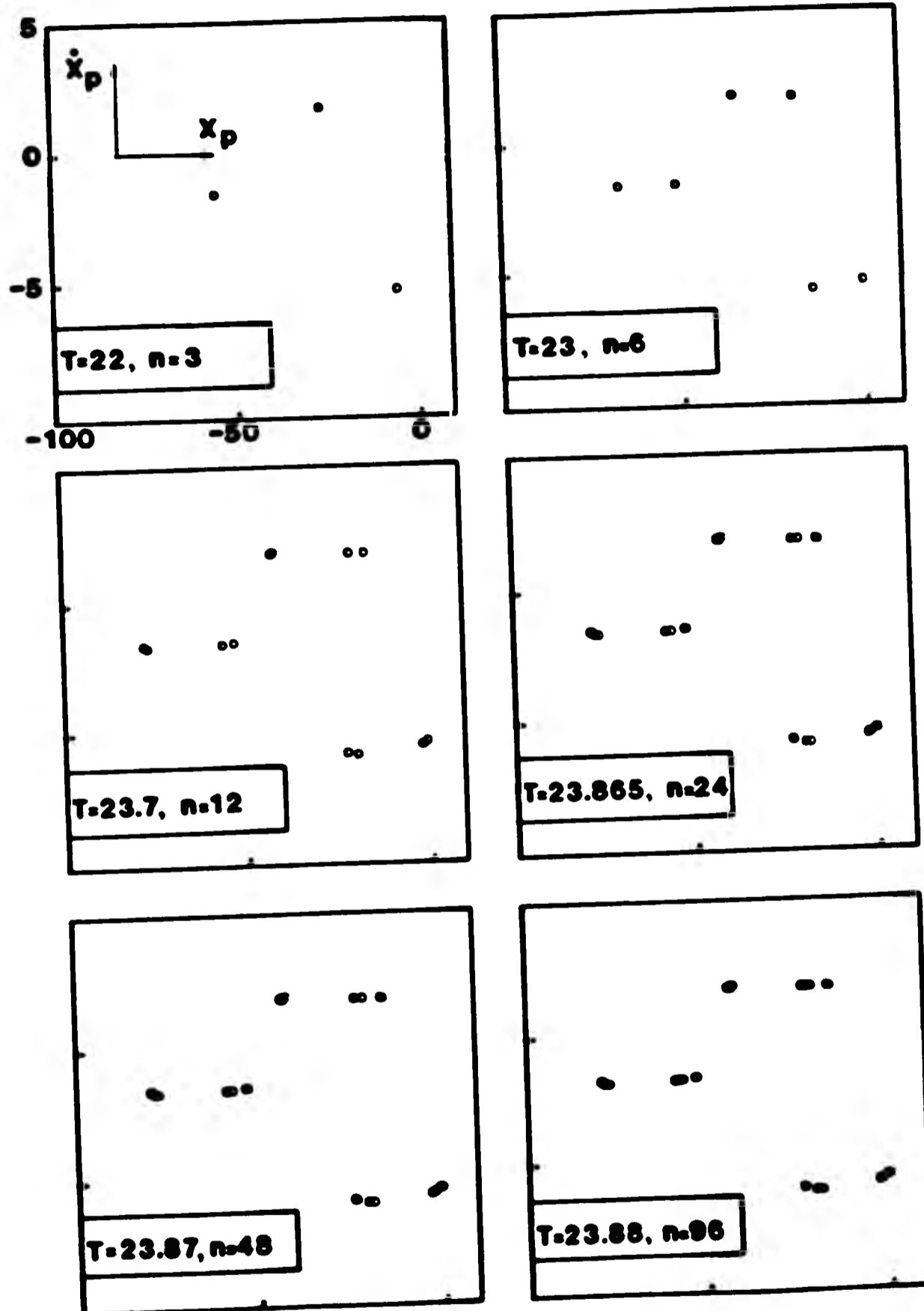


Figure 6.8 Poincaré points through a succession of period doubling bifurcations.

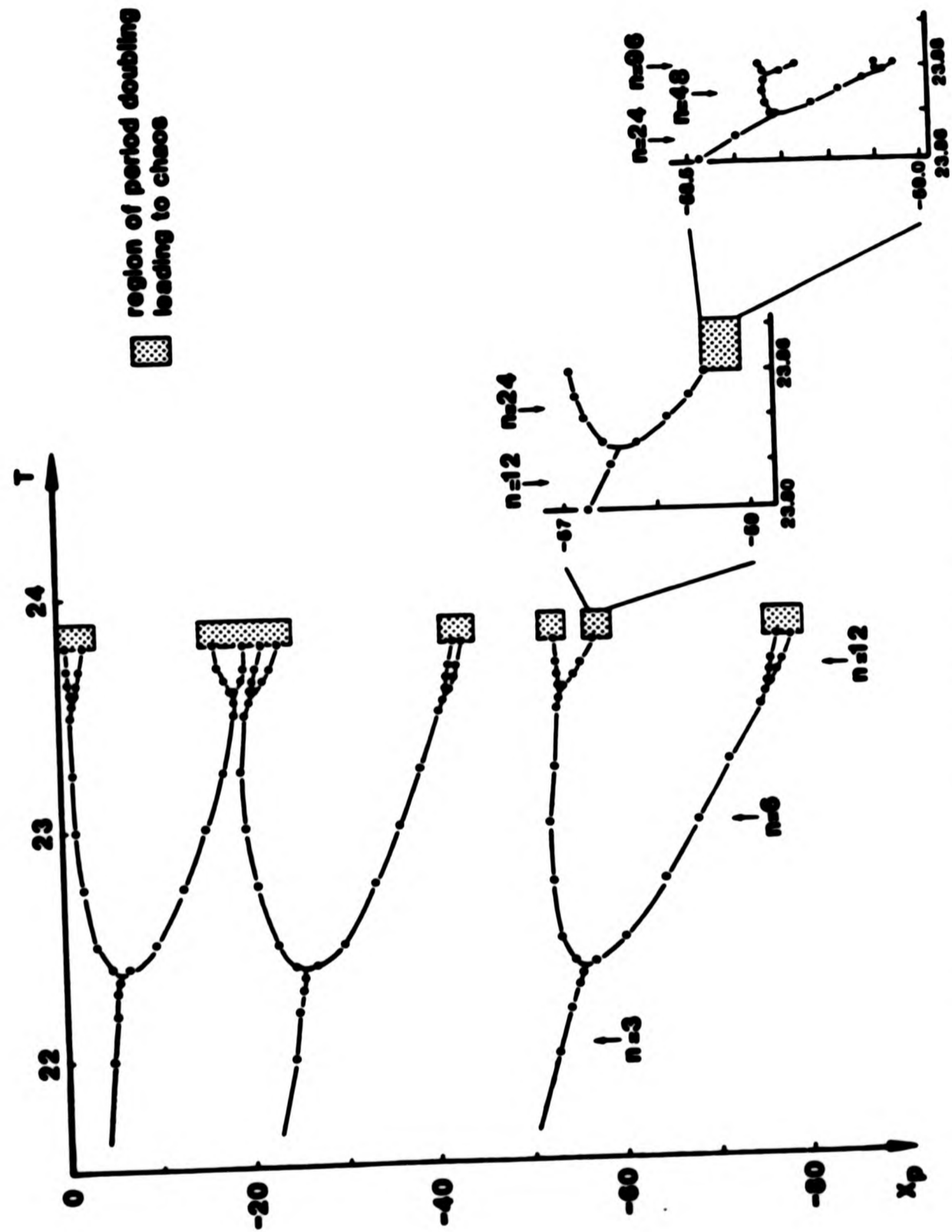


Figure 6.9 A scenario of period doubling bifurcations leading to chaos.

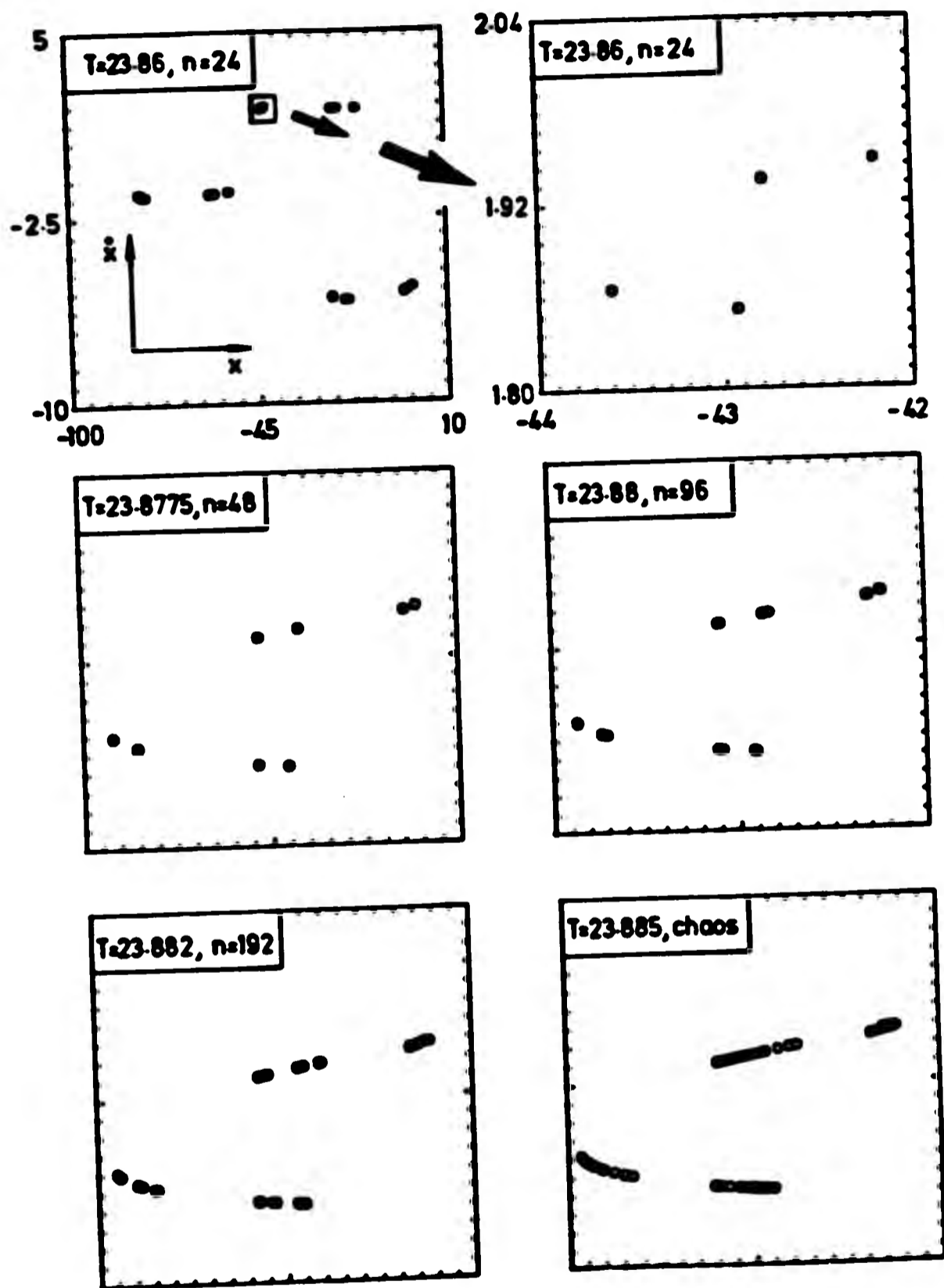


Figure 6.10 A closer look at higher order subharmonics and the chaotic attractor.

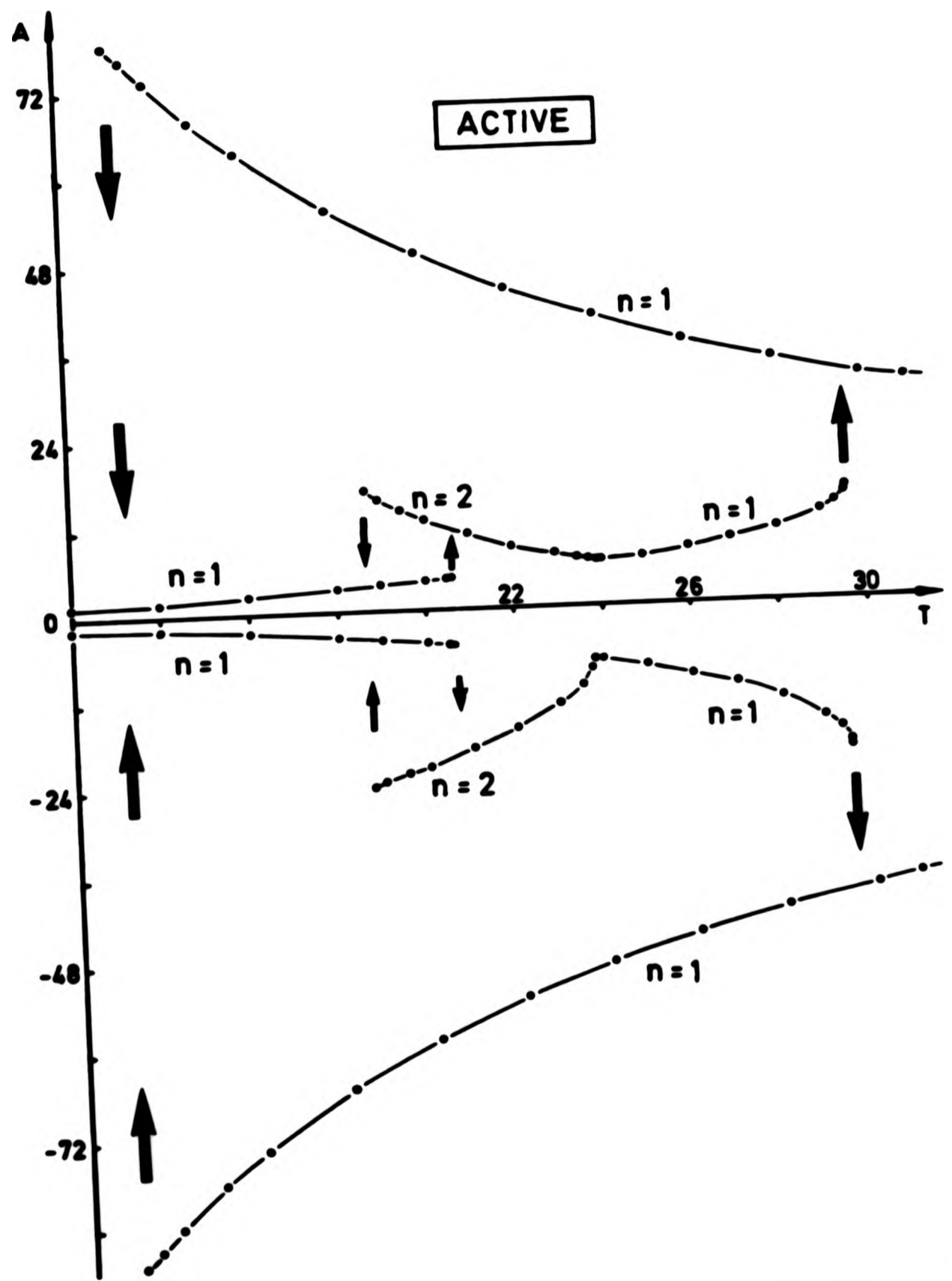


Figure 6.11 Maximum amplitude of steady state oscillations as a function of wave period for lee lines active.

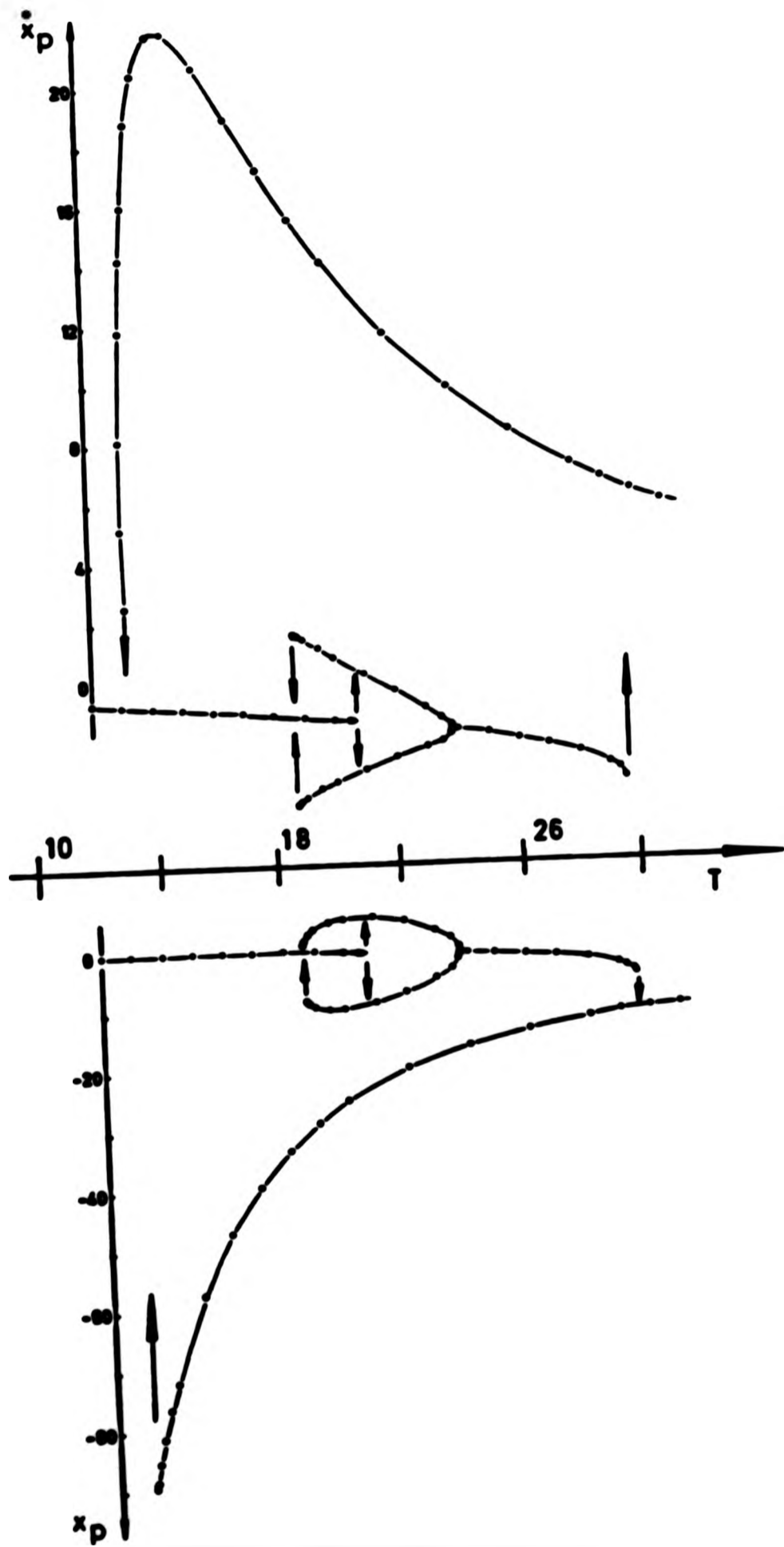


Figure 6.12 Poincaré points plotted against wave period indicating jumps to remote states.

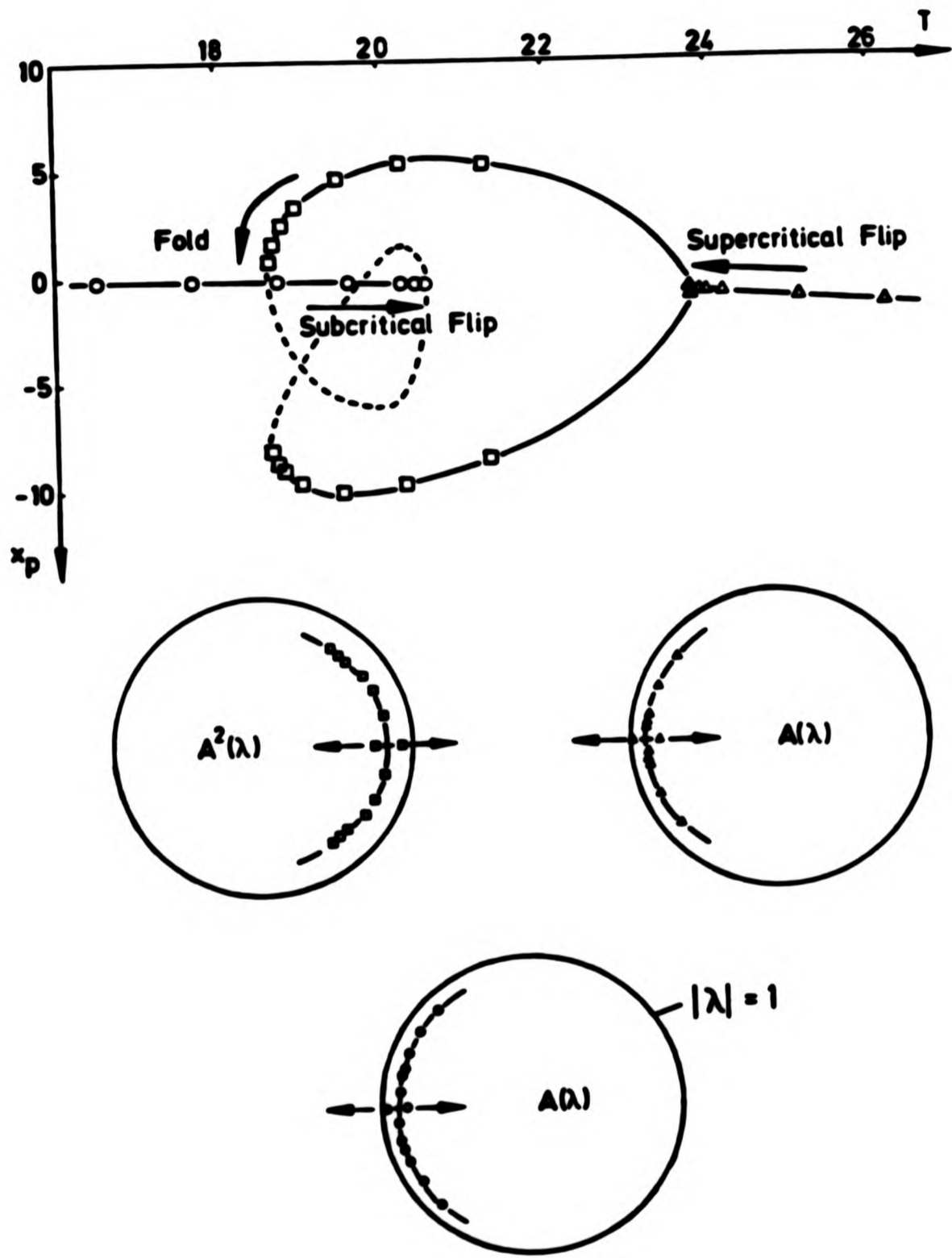


Figure 6.13 A detailed view of the bifurcations and the eigenvalue movement.

CHAPTER III.7

SUBHARMONIC MOTIONS OF NONLINEAR MARINE STRUCTURES

SUBJECTED TO RANDOM FORCING

III.7.1 Introduction

Some important types of offshore structures contain significant nonlinearities or time varying coefficients in their equations of motion [Jefferys]. Well known examples include tension leg platforms, free hanging risers, single point moorings, ships moored against fenders and vessels constrained by stiffened moorings. When such nonlinear systems are subjected to deterministic wave excitation, time domain mathematical models of these structures can display a variety of subharmonic and even chaotic motions whose amplitudes may be dangerously large. In an attempt to see if these nonlinear characteristics and associated instabilities are merely an artifact of the deterministic excitation a study has been made of a known system with increasing amounts of random forcing to determine the robustness of subharmonic resonances. In some situations where regular forcing is prevalent, nonlinear behaviour is unavoidable but the discussion included in this chapter indicates that large amplitude subharmonic motions decrease rapidly in the presence of random excitation and are thus unlikely to cause significant

problems in a random sea-state. Nevertheless, since at some time the forcing waves are likely to be predominantly of one frequency, subharmonic motions should not be flippantly disregarded.

III.7.2 A Pilot Study of the Bilinear Oscillator

The bilinear oscillator has been successfully used to model the behaviour of a compliant offshore facility under the influence of slackening mooring lines with regular, deterministic forcing waves [see Thompson et al. (1984)]. If the mooring lines become slack during dynamic motions the stiffness of the system undergoes a discontinuity which may lead to potentially dangerous oscillations. Subharmonic resonances have been shown to coexist with stable small amplitude fundamental solutions, the observed response depending only upon the initial conditions imparted to the system.

In previous models investigated in this thesis (besides the work monitoring slam loads) it has always assumed that a steady train of ocean waves excite the structure, however in the present chapter we wish to note the effect on the response of the facility when an element of random forcing is considered to be superimposed on top of the usual regular forcing.

The bilinear oscillator in nondimensionalised form is given

by the equation

$$\eta^2 \ddot{X} + 2\zeta\eta \dot{X} + kX = f(t) , \quad (7.1)$$

where η is the frequency ratio, ζ the damping factor and k a stiffness function which undergoes a discontinuity at the origin. The dot represents a differentiation with respect to time t , and the forcing function $f(t)$, modelling the action of the waves, will, in three different ways, be taken to be a random perturbation from a deterministic sinusoidal input. We shall then consider the effect of these approximate models of a changing sea-state on the qualitative behaviour of the system.

III.7.3 Types of Randomness

(a) Method 1: White Noise

The first approach is to add to the sinusoidal input a random function which can be thought of as white noise. Thus

$$f(t) = A(\sin\omega t + \epsilon_1 w(t)) , \quad (7.2)$$

where $w(t)$ produces a small random number whenever $f(t)$ is called during the numerical integration with standard deviation ϵ_1 . Accordingly a power spectrum analysis of the frequencies visible in the input would be a delta function at the forcing frequency with a steady component at all other

frequencies. We expect this method to be well behaved (i.e. continuous) and robust, with predictable perturbations from the deterministic solutions.

(b) Method 2: Frequency Wander

In an attempt to model a quasi-regular but changing sea-state we consider, as an input, a function which has a fundamental frequency which is itself a random function of time

$$f(t) = A \sin(\omega_r t) , \quad (7.4)$$

where the frequency is allowed to wander within the band width

$$\omega(1-e_2) < \omega_r < \omega(1+e_2) \quad (7.5)$$

It is clear that the frequency should not change dramatically between each time step of the numerical integration and so the randomness is merely enforced after a predefined time difference, namely 2π [also see Webster and Trundell (1981)]. Since the frequency of the forcing is itself changing, the question arises "Where do we take our Poincaré sections to be?". To answer this question we follow the natural extension of Poincaré's ideas and sample the time history whenever the input crosses the $x=0$ axis moving in an upwards direction. Of course the Poincaré points themselves will not now settle down but instead occupy a 'Poincaré region', it thus being necessary

to investigate the power spectrum of the output for confirmation of the presence of a subharmonic motion.

(c) Method 3: Bandwidth Spread

The third idealisation of a random perturbation considers the waves not to be made up of a single fundamental frequency but instead to consist of an odd number of frequencies which fit in a prescribed band width, d . As a consequence we take frequency spikes at FFT frequencies that fit into a single time period and then

$$f(t) = \sum_{i=1}^n A_i \sin \omega_i t, \quad (7.6)$$

The resulting power spectrum of the input now has a narrow band width, the constants A_i in this pilot study are taken to be unity. It is envisaged that this approach will have the most effect on the response of the system.

It should be noted here that we are not trying to model the power spectrum of real North sea wave data, since over a long time period this contains a wide range of frequencies, but rather to consider the situation that often occurs in reality where the waves can be seen to have a predominant forcing frequency, i.e. a narrow band spectrum.

Although the spectra of the signals from methods 2 and 3

are very similar a nonlinear system will respond to them very differently. The response of a linear system to an input is the sum of the responses to its separate components; a nonlinear system responds to the time series of the input 'directly' and superposition is not possible. The signals from the first two methods displays a non-Gaussian probability distribution; whereas the third approaches the Gaussian distribution as the number of sinusoidal components is increased. The third signal is, though, the least like a sine wave and so we might expect this method to have greatest effect on the nonlinear phenomena.

III.7.4 Numerical Studies

For the purpose of this pilot study we shall limit our task by considering an exploration of the bilinear oscillator with specific values of the defining coefficients such that for deterministic forcing we know that the solution exhibits either an $n=1$ or $n=4$ solution, depending on the starting conditions, see figure 7.1. Thus, in the first instance following the work of Thompson et al. (1984) we focus our attention on the departure of the solution from the $n=4$ solution indicated by the movement of the four Poincaré points. This is achieved by using the coefficients $\alpha = 10$, $\zeta = 0.1$ and $\eta = 3.95$ and in which case the stiffness k , given by

$$k = \begin{cases} (1 + \sqrt{\alpha})^2 / (4\alpha\eta^2) & \text{for } X > 0 \\ (1 - \sqrt{\alpha})^2 / (4\eta^2) & \text{for } X < 0 \end{cases} , \quad (7.7)$$

can be evaluated.

It can be seen from figures 7.2,7.3 and 7.4 that for an increasing amount of randomness the numerical solution's ability to recognise the $n=4$ subharmonic diminishes. This is especially true for method 3, where by looking at the placement of the Poincaré points alone, there seems to be little semblance of the subharmonic solution present. To verify its appearance it is necessary to look at a power spectrum analysis of the output signal, see the lower right hand diagrams of figures 7.5, 7.6 and 7.7. If a graph of the amplitude of the fourth order subharmonic resonance is plotted against the degree of randomness, as the latter is increased, then it is seen that the amplitude initially decreases rapidly. This is true for each of the three methods, as seen in the last three figures, but none the less some component of the subharmonic resonance still remains.

III.7.5 Conclusions

This pilot study indicates that, although much of the large amplitude subharmonic solutions of an offshore structure as modelled by the bilinear oscillator are severely decreased by the introduction of a certain amount of randomness on top of a deterministic forcing, the qualitative nature of the

nonlinear phenomena still remains. Clearly, bearing in mind the cost of possible damage repair, a thorough investigation of this type of 'random' forcing approach to the nonlinear behaviour is warranted in the future.

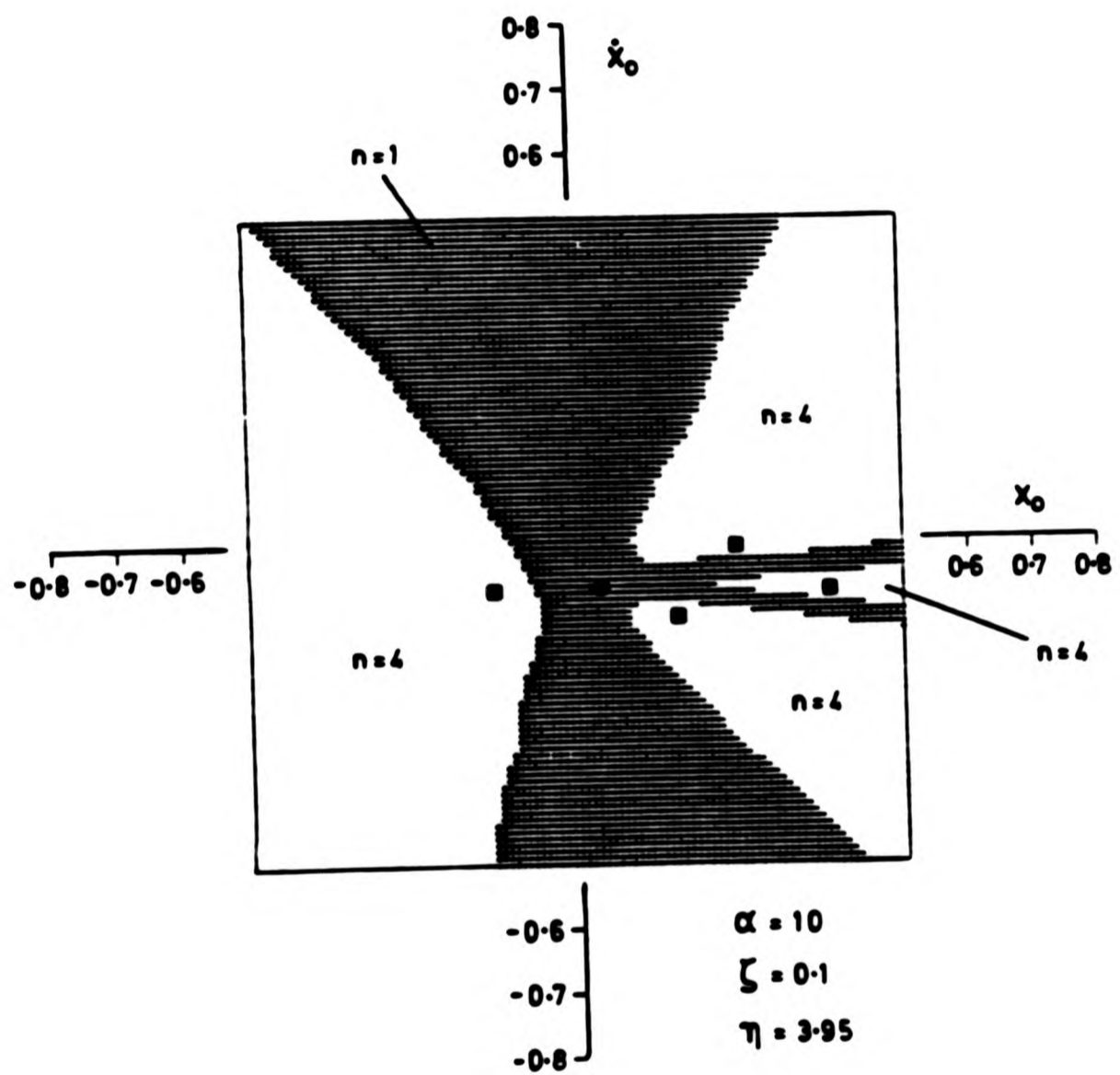


Figure 7.1 Domains of attraction for the $n=1$ and $n=4$ periodic solutions of the bilinear oscillator [Thompson et al. (1984)].

White noise

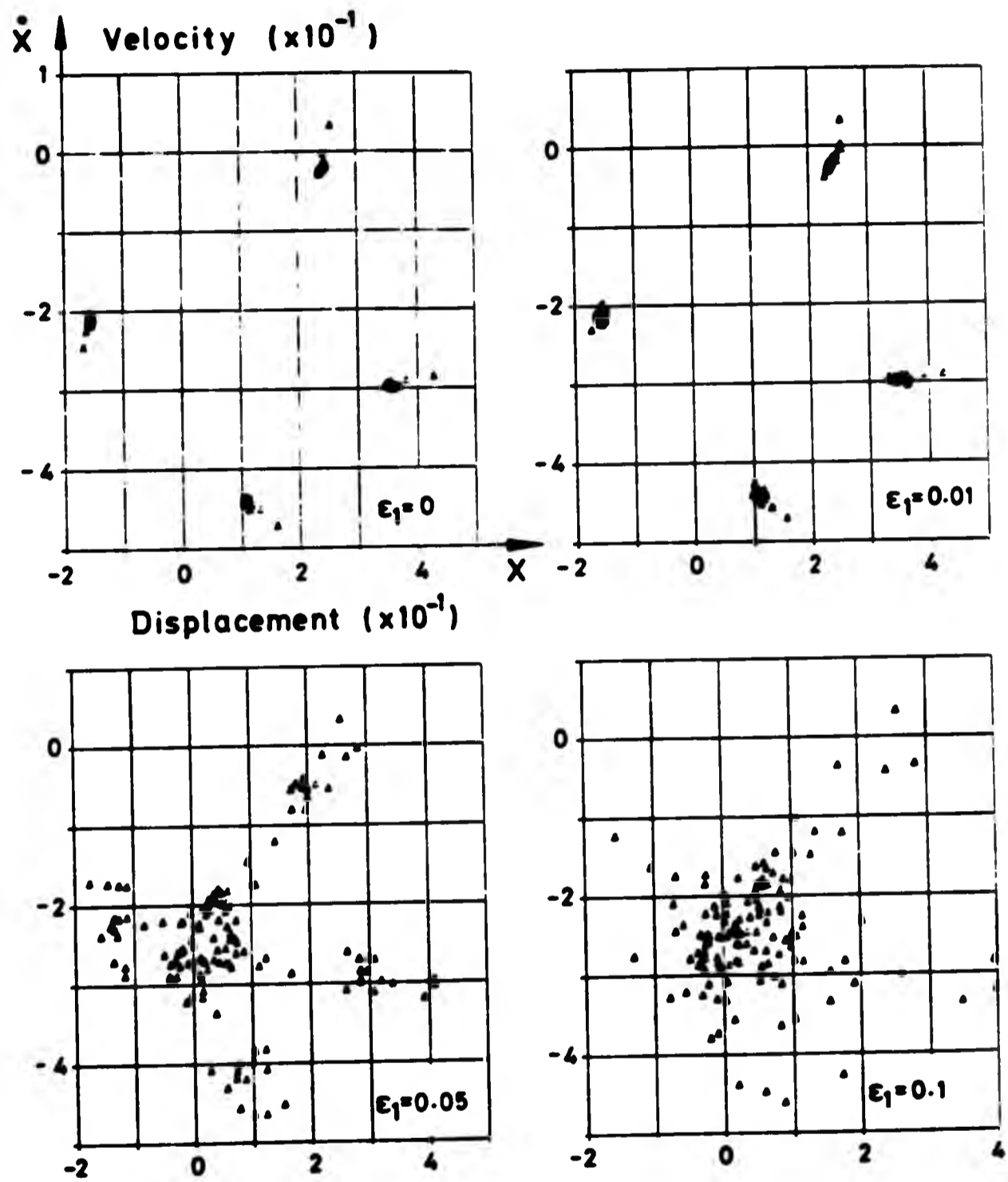


Figure 7.2 Poincaré regions of the $n=4$ solution for increasing amount of white noise.

Frequency wander

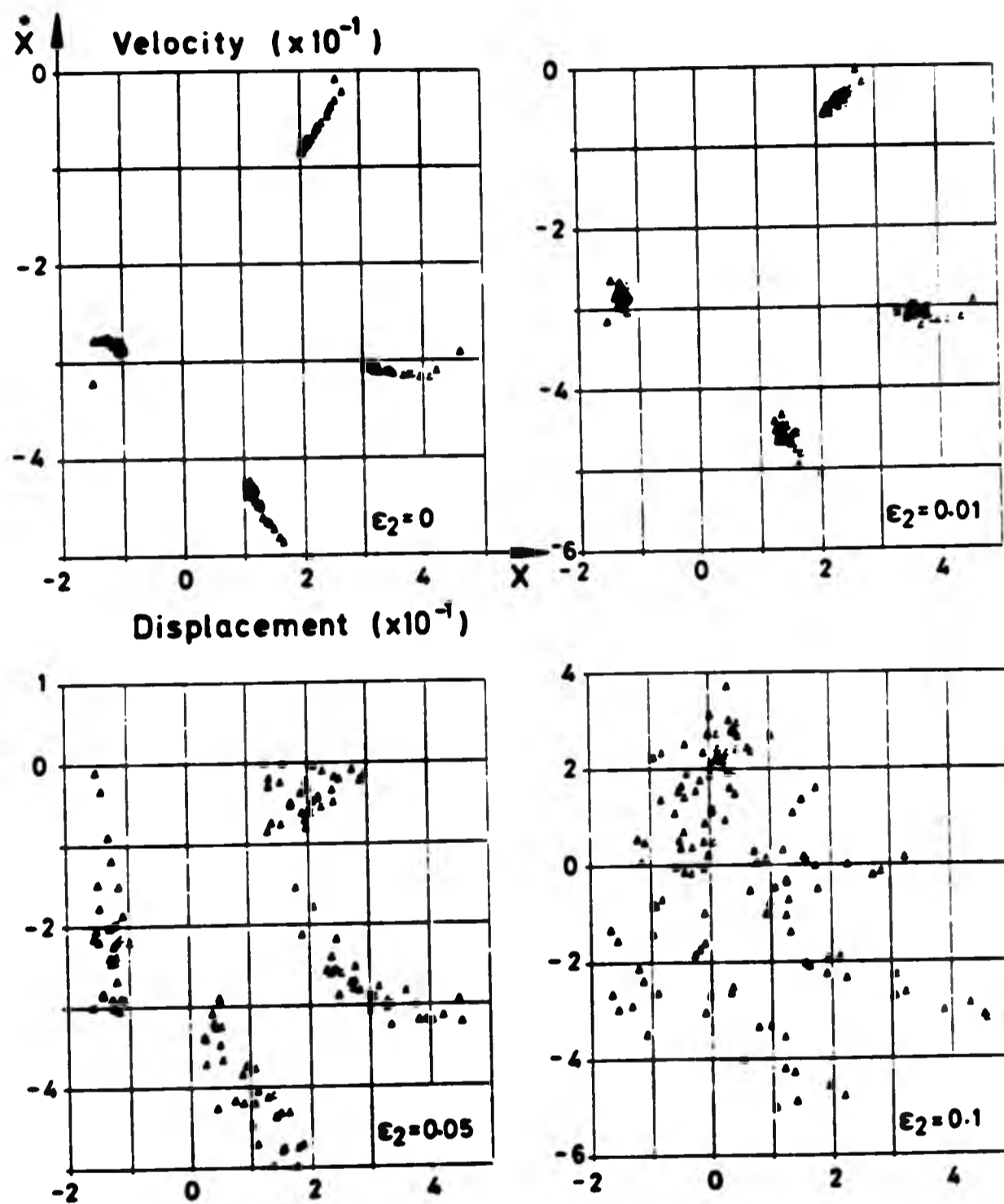


Figure 7.3 Poincaré regions of the $n=4$ solution for increasing amounts of frequency wander.

Bandwidth spread

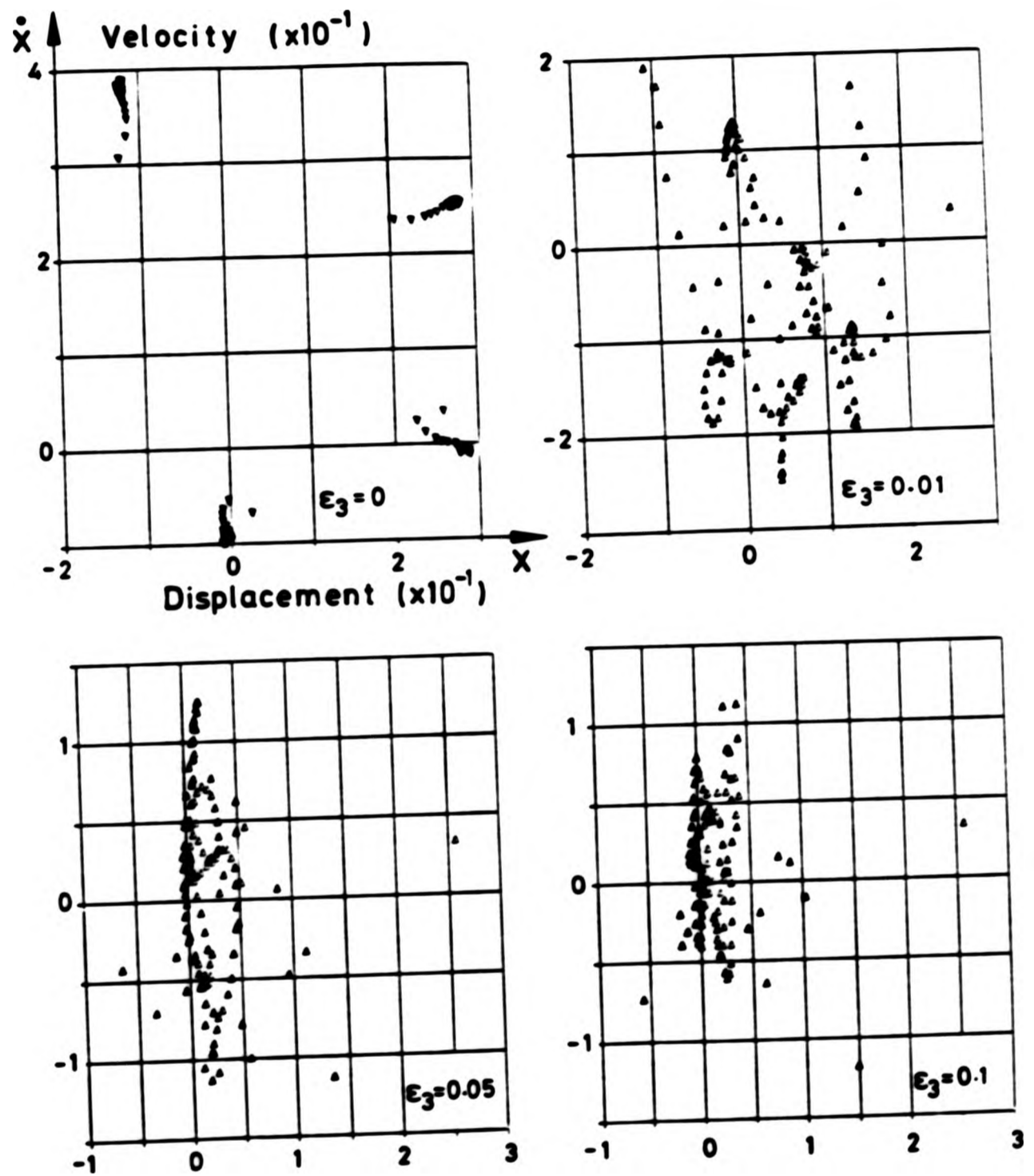


Figure 7.4 Poincaré regions of the $n=4$ solution for increasing amounts of bandwidth spread.

White noise effect on Bilinear oscillator

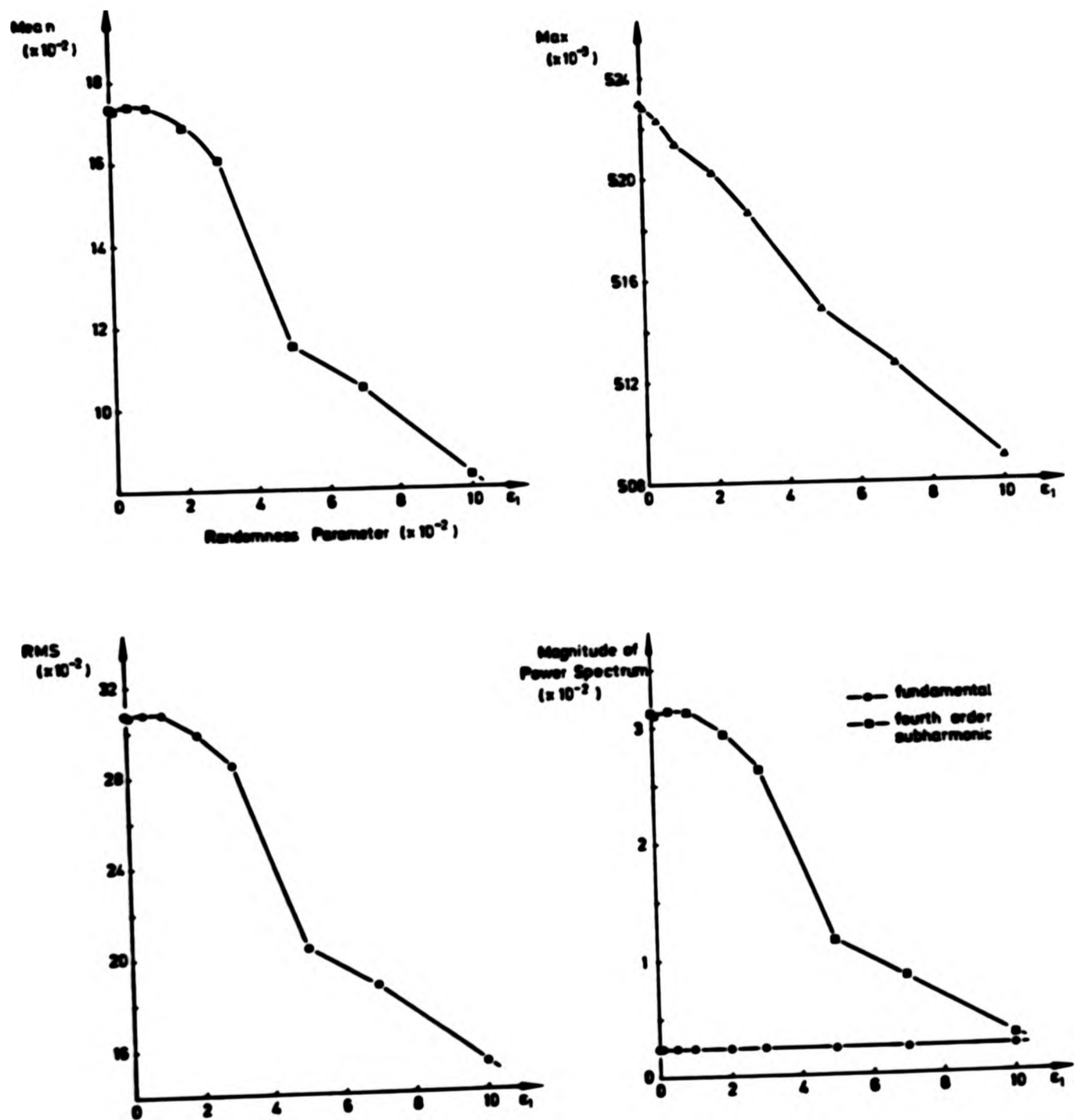


Figure 7.5 The effect of white noise on the mean, max, RMS and magnitude of the power spectrum of the output.

Frequency wander effect on Bilinear oscillator

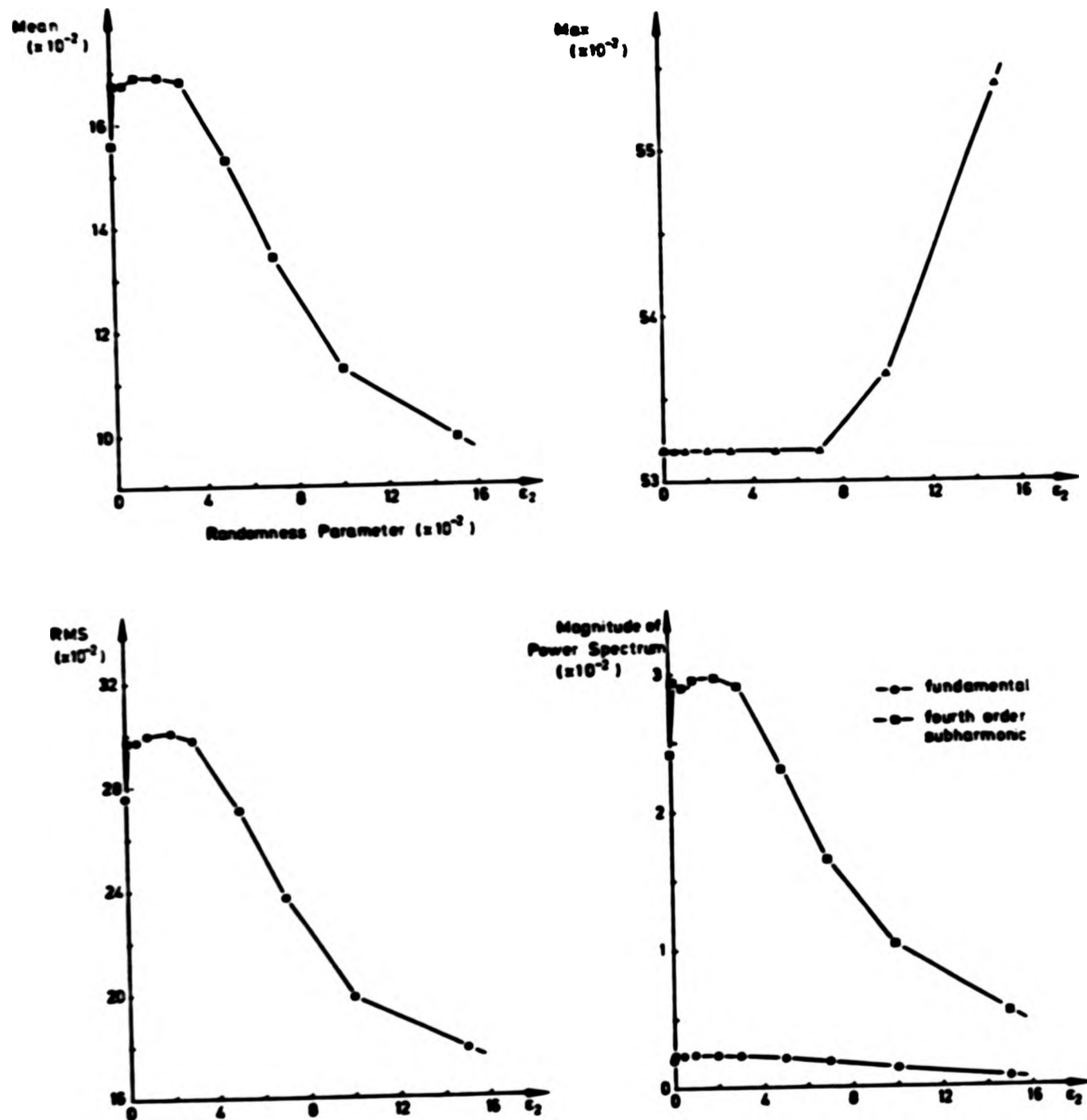


Figure 7.6 The effect of frequency wander on the mean, max, RMS and the magnitude of the power spectrum of the output.

Bandwidth spread effect on Bilinear oscillator

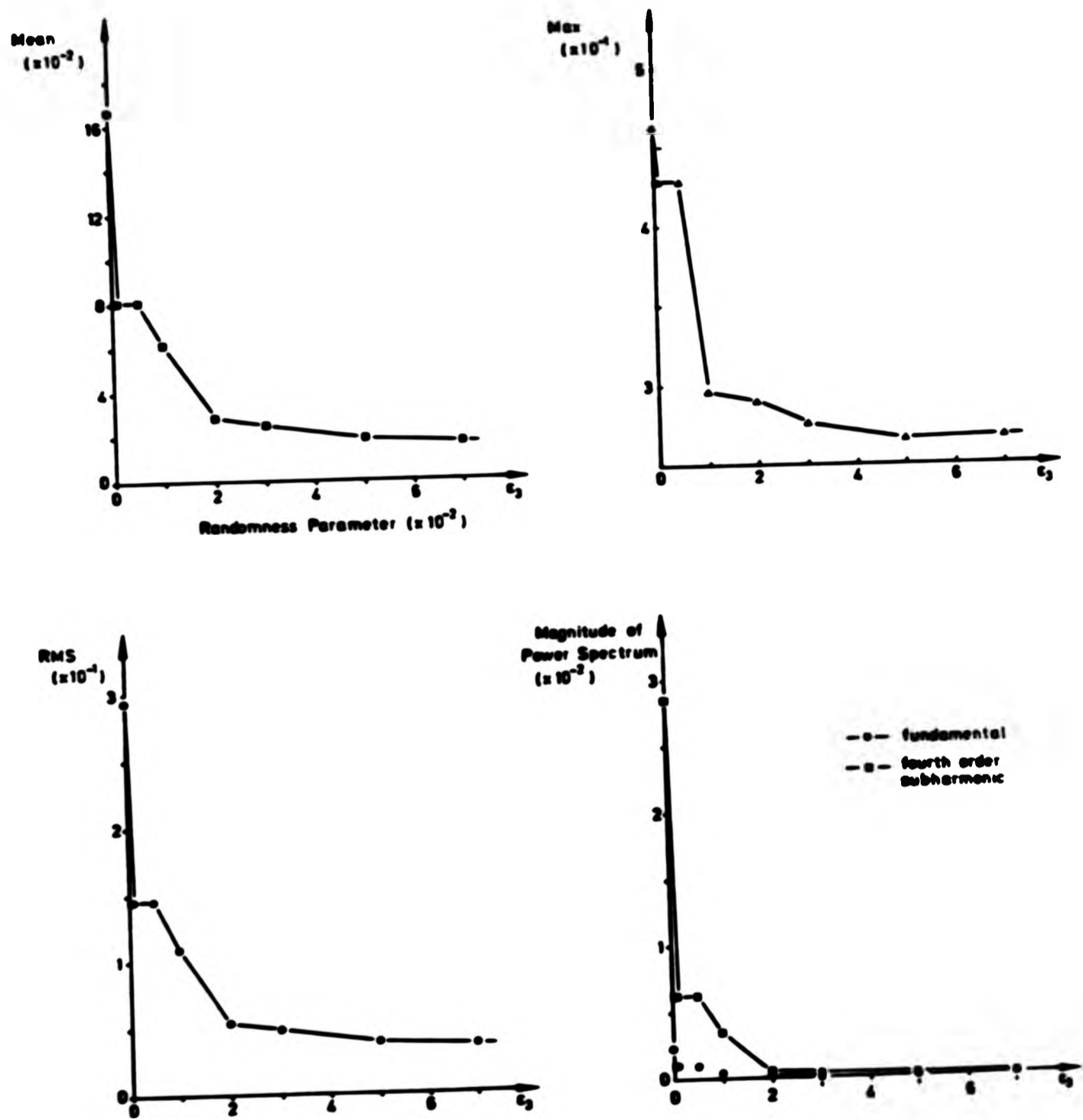


Figure 7.7 The effect of bandwidth spread on the mean, max, RMS and magnitude of the power spectrum of the output.

REFERENCES (PART I)

Akin, J.E., and Pardue, R.M. (1976). Element resequencing for frontal solutions, chapter 42 in MAFELAP 1975 edited by J.R.Whiteman, Academic Press: London

Bank, R.A., and Dupont, T. (1978). An optimal order process for solving elliptic finite element equations, Department of Mathematics, University of Chicago.

Barker, V.A.(ed.) (1977). Sparse Matrix Techniques, Copenhagen 1976. Lecture Notes in Mathematics, Springer Verlag: Berlin.

Batchelor, G.K. (1967). An Introduction to Fluid Dynamics. Cambridge University Press: Cambridge.

Bathe, K.J., and Wilson, E.L. (1976). Numerical Methods in Finite Element Analysis. Prentice Hall: Englewood Cliffs, New Jersey.

Bishop, S.R. (1982). An introduction to the finite element method for solving differential equations, Technical Reports PNL-NA-33/34/35, Department of Mathematics, Polytechnic of North London.

Bishop, S.R. (1983a). Curve fitting, Technical Report PNL-NA-36, Mathematics Department, Polytechnic of North London.

Bishop, S.R. (1983b). Graph 8: A program for curve fitting using piecewise rational quadratic interpolants, Technical Report PNL-NA-37, Mathematics Department, Polytechnic of North London.

Bishop, S.R. (1984a). Graph 8: User guide, Technical Report PNL-NA-38, Mathematics Department, Polytechnic of North London.

Bishop, S.R. (1984b). Approximate integration of a function defined only by a set of data, Technical Report PNL-NA-39, Mathematics Department, Polytechnic of North London.

Brandt, A. (1977). Multi-level adaptive solutions to boundary value problems, *Math. Comp.* 31, p.333-390.

Collins, R.J. (1973). Band width reduction by automatic numbering, *Int. J. Num. Meth. Eng.*, vol.6, p.345-356.

Cuthill, E., and Mckee, J. (1969). Reducing the bandwidth of sparse symmetric matrices, *ACM proceedings of the 24th National Conference*, p.157-172.

Darwin, C.G. (1953). Note on hydrodynamics, *Proc. Cambridge Phil. Soc.*, vol. 49, p.342.

- Davies, A.J. (1980). The Finite Element Method: A First Approach. Clarendon Press: Oxford.
- Detra, R.W. (1953). The secondary flow in curved pipes, Mitt. Inst. Aerodynamik, E.T.H., Zurich, No.20.
- Dyer, G.F. (1979). Mathematical methods for aerodynamic design of turbomachinery blade cascades for high subsonic and transonic flow, Ph.D. thesis, Mathematics Department, Polytechnic of North London.
- Eichenberger, H.P. (1953). Secondary flow within a bend, Journal of Maths and Physics, vol. 32, p.34.
- Frost, D.H. (1976). Computational aspects of the aerodynamic design of vaneless deflector nozzles, M.Phil. thesis, Mathematics Department, Polytechnic of North London.
- Gradsteyn, I.S., and Ryzhik, I.M. (1980). Table of Integrals, Series, and Products. Academic Press: Orlando.
- Gregory, J.A., and Delbourgo, R. (1981). Piecewise rational quadratic interpolation to monotonic data, Technical Report TR/12/81, Brunel University, Uxbridge.
- Hawthorne, W.R. (1965). Engineering aspects, chapter 1 in

Research Frontiers in Fluid Dynamics, edited by Seeger, R.J., and Temple, G., John Wiley: London.

Hinton, E., and Owen, D.R.J. (1977). Finite Element Programming. Academic Press: London.

Irons, B.M. (1970). A frontal solution program for finite element analysis, Int. J. Num. Meth. Eng., vol. 2, p.5-32.

Lighthill, M.J. (1956). Drift, Journal of Fluid Dynamics, vol.1 p.31.

Mikhlin, S.G. (1964). Variation Methods in Mathematical Physics. Pergamon Press: Oxford.

Payne, D. (1969). Contributions to the theoretical aerodynamics of turbomachinery blade rows, Ph.D. thesis, University of London.

Southwell, R.V. (1946). Relaxation Methods in Theoretical Physics. Clarendon Press: Oxford.

Squire, H.B., and Winter, K.G. (1951). The secondary flow in a cascade of airfoils in a non-uniform stream, Journal of Aeronautical Sciences, vol. 18, No.4, p.271.

Zienkiewicz, O.C. (1977). The Finite Element Method. McGraw Hill: London.

REFERENCES (PART II and PART III)

Abraham, R.H., and Marsden, J.E. (1978). Foundations of Mechanics. Benjamin/Cummings: Reading, MA.

Abraham, R.H., and Robbin, J. (1967). Transversal Mappings and Flows. Benjamin: Reading, MA.

Abraham, R.H., and Shaw, C.D. (1982). Dynamics: The Geometry of Behaviour, Part One, Periodic Behaviour. Aerial Press: Santa Cruz, CA.

Abraham, R.H., and Shaw, C.D. (1982). Dynamics: The Geometry of Behaviour, Part Two, Chaotic Behaviour. Aerial Press: Santa Cruz, CA.

Abraham, R.H., and Shaw, C.D. (1982). Dynamics: The Geometry of Behaviour, Part Three, Global Behaviour. Aerial Press: Santa Cruz, CA.

Abraham, R.H., and Stewart, H.B. (1986). A chaotic blue sky catastrophe in forced relaxation oscillations. Physica 21D, p.394-400.

Andereck, C.D., Dickman, R., and Swinney, H.L. (1983). New flows

in a circular Couette system with co-rotating cylinders.
Phys. Fluids, 26, p.1395-1401.

Andronov, A.A., and Pontryagin, L. (1937). Systemes Grossiers.
Dokl. Adad. Nauk. SSSR, 14, p.247-251.

Arnold, V.I. (1983). Geometrical Methods in the Theory of
Ordinary Differential Equations. Springer-Verlag:New York,
Heidelberg, and Berlin.

Aronson, D.G., Chory, M.A., Hall, G.R., and McGeehee, R.P.
(1982). Bifurcations from an invariant circle for two-
parameter families of maps of the plane: a computer
assisted study. Commun. Math. Phys., 83, p.303-354.

Birkhoff, G.D. (1927). Dynamical Systems. American Mathematical
Society: Providence, RI.

Bishop, S.R., and Franciosi, C.. The use of rotation numbers to
predict the incipient folding of a periodic orbit.
To appear in App. Math. Modelling.

Bishop, S.R., Leung, L.M., and Virgin, L.n. (1986). Predicting
incipient jumps to resonance of compliant marine
structures in an evolving sea-state. 5th Int. Symp.
Offshore Mechanics and Arctic Engineering, ASME, III, p.
179-185. Also to appear in revised form in Trans ASME.

Bishop, S.R., and Virgin, L.N.. The onset of chaotic motions of a moored semi-submersible. To be presented at 6th Int. Symp. Offshore Mechanics and Arctic Engineering, ASME, Houston, March 1987.

Braun, M. (1983). Differential Equations and their Applications. 3rd Edition, Springer-Verlag: New York, Heidelberg and Berlin.

Cardo, A., Francescutto, A., and Nabergoj, R. (1984). Nonlinear rolling response in a regular sea. Int. Shipbuilding Progress, 31, p.204-208.

Carr, J. (1981). Applications of Centre Manifold Theory. Springer-Verlag: New York, Heidelberg and Berlin

Cash, D.G.F., and Rainey, R.C.T. (1980). Design rules for the avoidance of subharmonic oscillations in large floating offshore structures. Atkins R & D Ltd.

Chou, F.S.F., Ghosh, S., and Huang, E.W. (1983). Conceptual design process of a tension leg platform. Trans. SNAME, 91, p.275-305.

Cvitanović, P. (ed) (1984). Universality in Chaos. Adam Hilger: Bristol.

Dowell, E.H. (1975). Aeroelasticity in Plates and Shells. Noordhoff: Leyden.

Dynamics of Compliant Structures: Cohesive Programme 1983-1985,
Final Report. SERC Marine Technology Directorate.

Feigenbaum, M.J. (1983). Universal behaviour in nonlinear
systems. *Physica*, 7D, p.16-39.

Flashner, H., and Hsu, C.S. (1983). A study of nonlinear
periodic systems via point mapping methods. *Int. J. Numer.
Meth. Eng.*, 19, p.185-215.

Frisch, U. (1980). Fully developed turbulence and intermittency.
In *Nonlinear Dynamics*, by R.H.G. Helleman (ed.), New York
Academy of Sciences: New York, p.359-367.

Golubitsky, M., and Schaeffer, D. (1985). *Singularity and Groups
in Bifurcation Theory*. Springer-Verlag: New York.

Gorman, K., Reith, L.A., and Swinney, H.L. (1980). Modulation
patterns, multiple frequencies, and other phenomena in
circular Couette flow. In *Nonlinear Dynamics*, R.H.G.
Helleman (ed.). New York Academy of Sciences: New York,
p.10-21.

Gradsteyn, I.S., and Ryzhik, I.M. (1980). *Table of Integrals,
Series, and Products*. Academic Press: Orlando.

Grebowi, C., Ott, E., and Yorke, J.A. (1983). Crises, sudden changes in chaotic attractors, and transient chaos. *Physica*, 7D, p.181-200.

Guckenheimer, J., and Holmes, P. (1983). *Nonlinear Oscillations, Dynamical Systems, and Bifurcations of Vector Fields*. Springer-Verlag: New York, Heidelberg, and Berlin.

Hartman, P. (1964). *Ordinary Differential Equations*. Wiley: New York.

Hayashi, C. (1964). *Nonlinear Oscillations in Physical Systems*. McGraw-Hill: New York.

Helleman, R.H.G. (editor) (1980). *Nonlinear Dynamics* (Annals of the New York Academy of Sciences, vol 357). New York Academy of Sciences: New York.

Hénon, M. (1976). A two dimensional mapping with a strange attractor. *Commun. Math. Phys.*, 50, p.69-77.

Hirsch, M.W., and Smale, S. (1974). *Differential Equations, Dynamical Systems, and Linear Algebra*. Academic Press: New York.

Holden, A.V. (editor) (1986). *Chaos*. Manchester University Press: Manchester.

- Holmes, P.J. (1979). A nonlinear oscillator with a strange attractor. *Phil. Trans. Roy. Soc. Lond. A*, 292, p.419-448.
- Hopf, E. (1942). Abzweigung einer periodischen Lösung von einer stationären Lösung eines Differentialsystems. *Ber. Math.-Phys. Klasse Sachs. Akad. Wiss. Leipzig*, 94, p.1-22. English translation in Marsden and McCracken (1976).
- Hunt, G.W. (1986). Hidden (a)symmetries of elastic and plastic bifurcation. *App. Mech. Rev.*, 39, No.8, p.1165-1186.
- Iooss, G., and Joseph, D.D. (1977). Bifurcation and stability of nT -periodic solutions branching from T -periodic solutions at points of resonance. *Arch. Rat. Mech. Anal.*, 66, p.135-172.
- Iooss, G., and Joseph, D.D. (1980). *Elementary Stability and Bifurcation Theory*. Springer-Verlag: New York.
- Jefferys, E.R.. Nonlinear marine structures with random inputs. To be presented at 6th Int. Symp. Offshore Mechanics and Arctic Engineering, ASME, Houston, March 1987.
- Jordan, D.W., and Smith, P. (1977). *Nonlinear Ordinary Differential Equations*. Oxford University Press: Oxford.
- Kadanoff, L.P. (1983). Roads to chaos. *Phys. Today*, 36, No.12 (December), p.46-53.

Kubiecek, M., and Marek, M. (1983). Computational Methods in Bifurcation Theory and Dissipative Structures. Springer-Verlag: New York.

Langewis, C. (1986). Offshore outlook. 5th Int. Symp. Offshore Mechanics and Arctic Engineering, ASME.

Lighthill, M.J. (1986). The recently recognized failure of predictability in Newtonian dynamics. Proc. R. Soc. Lond. A, 407, p.35-50.

Lloyds Registry of Shipping.

Lorenz, E.N. (1963). Deterministic nonperiodic flow. J. Atmos. Sci., 20, p.130-141.

Lorenz, E.N. (1964). The problem of deducing the climate from the governing equations. Tellus, 16, p.1-11.

Luenberger, D.G. (1979). Introduction to Dynamic Systems: Theory Models, and Applications. Wiley: New York.

Lyapunov, A.M. (1949). Probleme General de la Stabilite du Mouvement (Annals of Mathematical Studies, vol. 17). Princeton University Press: Princeton, NJ.

Marsden, J.E., and McCracken, M. (1976). The Hopf Bifurcation

and its Applications. Springer-Verlag: New York, Heidelberg, and Berlin.

Marshfield, W.B. (1978). AMTE(H) NMI Capsize experiments, series 2, AMTE(H) R78052.

May, R.M. (1976). Simple mathematical models with very complicated dynamics. *Nature*, 261, p.459-467.

Mees, A.I. (1973). Periodic wave forces in nonlinear systems. *Int. J. Control*, 18, No.6, p.1169-1188.

Mees, A.I. (1981). *Dynamics of Feedback Systems*. Wiley: Chichester.

Melnikov, V.K. (1963). On the stability of the center for time periodic perturbations. *Trans. Moscow. Math. Soc.*, 12, p.1-57.

Minorsky, N. (1962). *Nonlinear Oscillations*. Van Nostrand: Princeton, NJ.

Moon, F.C.. *Experiments in Chaotic Vibrations*. To be published by Wiley: New York.

Moon, F.C. and Li, G.-X. (1985). Fractal basin boundaries and homoclinic orbits for periodic motion in a two-well potential. *Phy. Rev. Lett.*, 55, p.1439-1442.

Nayfeh, A.H., and Khdeir, A.A. (1986). Nonlinear rolling of ships in regular beam seas. *Int. Shipbuilding Progress*, 33, p.40-49.

Nayfeh, A.H., and Mook, D.T. (1979). *Nonlinear Oscillations*. Wiley: New York.

Neimark, J. (1959). Some cases of periodic motions depending on parameters. *Dokl. Akad. Nauk. SSSR*, 129, p.736-739.

Newland, D.E. (1984). *Introduction to Random Vibrations and Spectral Analysis*. Longman: Harlow.

Patel, M.H. (1983). On the wave induced motion response of semi-submersibles. *Trans. RINA*, 125, p.221-228.

Patel, M.H., and Walker, S. (1983). On the hydrostatics of floating bodies with articulated appendages. *Trans. RINA*, 125, p.229-236.

Pippard, A.B. (1985). *Response and Stability: An Introduction to the Physical Theory*. Cambridge University Press.

Poincaré, H. (1899). *Les Methods Nouvelles de la Mecanique Celeste*, Vols. 1-3. Gauthier-Villars: Paris.

Poston, T., and Stewart, I. (1978). *Catastrophe Theory and Its Applications*. Pitman: London.

Price, W.G., and Bishop, R.E.D. (1974). Probabalistic Theory of Ship Dynamics. Chapman and Hall: London.

Rainey, R.C.T. (1978). The dynamics of tethered platforms. Trans. RINA, 120, p.59-80.

Rawson, K.J., and Tupper, E.C. (1983). Basic Ship Theory. Longman: London.

Roberts, J.B. (1986). Response of an oscillator with non-linear damping and a softening spring to non-white random excitation. Probabilistic Eng. Mech., 1, p.40-48.

Robinson, R.W., and Stoddart, A.W. (1986). An engineering assessment of the role of non-linearities in transportation barge roll response. Paper No.8, Spring Meeting, RINA, to be published in Trans. RINA.

Ruelle, D., and Takens, F. (1971). On the nature of turbulence. Commun. Math. Phys., 20, p.167-192; 23, p.343-344.

Saaty, T.L. (1967). Modern Nonlinear Equations. Dover: New York.

Sacker, R.J. (1964). On Invariant Surfaces and Bifurcations of Periodic Solutions of Ordinary Differential Equations. IMM-NYU, 333, New York University: New York.

Stewart, H.B. (1986). Hysteresis and chaos in forced oscillations. Presented at the Conference on Qualitative Methods for the Analysis of Nonlinear Dynamics, Henniker, New Hampshire, June 1986. To be published by SIAM, editors Salam, F., and Levi, M..

Stewart, H.B., and Thompson, J.M.T. (1986). Towards a classification of generic bifurcations in dissipative dynamical systems. *Dynamics and Stability of Systems*, 1, p.87-96.

Stoker, J.J. (1950). *Nonlinear Vibrations*. Wiley: New York.

Swinney, H.L. (1983). Observations of order and chaos in nonlinear systems. *Physica*, 7D, p.3-15.

Thom, R. (1975). *Structural Stability and Morphogenesis*. W.A.Benjamin: Reading, MA.

Thompson, J.M.T. (1982). *Instabilities and Catastrophes in Science and Engineering*. Wiley: Chichester.

Thompson, J.M.T. (1983). Complex dynamics of compliant offshore structures. *Proc. Roy. Soc. Lond. A*, 387, p.407-427.

Thompson, J.M.T., Bishop, S.R., and Leung, L.M.. Fractal basin boundaries and chaotic bifurcations prior to escape from a potential well. Submitted for publication in *Phys. Lett.*

Thompson, J.M.T., Bokaian, A.R., and Ghaifari, R. (1984). Subharmonic and chaotic motions of compliant offshore structures and articulated mooring towers. ASME J. Energy Resources Tech., 106, p.191-198.

Thompson, J.M.T., and Lunn, T.S. (1981). Resonance-sensitivity in dynamic Hopf bifurcations under fluid loading. App. Math. Modelling, 5, p.143-150.

Thompson, J.M.T., and Stewart, H.B. (1984). Folding and mixing in the Birkhoff-Shaw chaotic attractor. Phys. Lett., 103A, p.229-231.

Thompson, J.M.T., and Stewart, H.B. (1986). Nonlinear Dynamics and Chaos. Wiley: Chichester.

Thompson, J.M.T., and Virgin, L.N. (1986). Predicting a jump to resonance using transient maps and beats. Int. J. Nonlinear Mech.. To appear.

Thomson, W.T. (1981). Theory of Vibration With Applications. Prentice-Hall: Englewood Cliffs, NJ.

Ueda, Y. (1979). Randomly transitional phenomena in the system governed by Duffing's equation. J.Stat. Phys., 20, p.181-196.

Ueda, Y. (1980). Steady motions exhibited by Duffing's equation: a picture book of regular and chaotic motions. In New

Approaches to Nonlinear Problems in Dynamics, P.J.Holmes (ed.), p.311-322. SIAM: Philadelphia.

Ueda, Y., Nakajima, H., Hikiyara, T., and Stewart, H.B. (1986). Forced two-well potential Duffing's oscillator. Presented at the Conference on Qualitative Methods for the Analysis of Nonlinear Dynamics, Henniker, New Hampshire, June 1986. To be published by SIAM, editors Salam, F., and Levi, M..

Vidal, C., Roux, J.-C., Bachelart, S., and Rossi, A. (1980). Experimental study of the transition to turbulence in the Belousov-Zhabotinskii reaction. In Nonlinear Dynamics, R.H.G.Helleman (ed.), p.377-396. New York Academy of Sciences: New York.

Virgin, L.N.. Parametric studies of the dynamic evolution through a fold. J. Sound Vibration. To be published.

Virgin, L.N. (1986). The nonlinear rolling response of a vessel including chaotic motions leading to capsize in regular seas. To appear in Applied Ocean Research.

Virgin, L.N., and Bishop, S.R.. Complex motions of a moored semi-submersible. Submitted to Ocean Engineering.

Webster, W.C., and Trundell, R.W. (1981). Statistical description of local motions of a ship in waves. Proc. Berkeley Conf. on Directional Wave Spectra Applications, ASCE, NY.

Wright, J.H.G., and Marshfield, W.B. (1980). Ship roll response and capsize behaviour in beam seas. Trans RINA, 122, p.129-148.

Zeeman, E.C. (1977). Catastrophe Theory: Selected Papers 1972-1977. Addison Wesley: Reading MA.

APPENDIX

MELNIKOV'S METHOD

CHAPTER III.5 APPENDIX

MELNIKOV'S METHOD

III.5A.1 Theory

Melnikov's method was first developed by the Russian mathematician Melnikov (1963) and has more recently been detailed by Guckenheimer and Holmes (1983). The method has several areas of application but we shall restrict our attention here to the determination of a homoclinic tangency, i.e. when the inset and the outset (the stable and unstable manifolds in the terminology of Guckenheimer and Holmes) of a hyperbolic saddle point collide as was illustrated in figure III.5.13. If we consider the method as described by Guckenheimer and Holmes then we discuss the Poincaré map of the time periodic nonautonomous system

$$\begin{aligned}\dot{x} &= f_1(x,y) + \epsilon g_1(x,y,t) \\ \dot{y} &= f_2(x,y) + \epsilon g_2(x,y,t) ,\end{aligned}\tag{5A.1}$$

where the functions g_1 and g_2 are periodic with period T , ϵ is a small parameter and the functions f_1 and f_2 are such that if $\epsilon = 0$ the system is Hamiltonian. However for ease of notation if we define the vector quantities

$$\dot{X} = \begin{bmatrix} \dot{x} \\ \dot{y} \end{bmatrix}, \quad f = \begin{bmatrix} f_1 \\ f_2 \end{bmatrix}, \quad g = \begin{bmatrix} g_1 \\ g_2 \end{bmatrix}, \quad (5A.2)$$

so that the system is now given by

$$\dot{X} = f(X) + \epsilon g(X,t). \quad (5A.3)$$

It is also convenient at this point to define the wedge product \wedge by

$$f \wedge g = f_1 g_2 - f_2 g_1. \quad (5A.4)$$

Now for the unperturbed flow, i.e. with $\epsilon=0$, we assume that the system has a homoclinic orbit $q^0(t)$ to a hyperbolic saddle point S_0 , see figure 5A.1. The interior of this homoclinic orbit is filled with a continuous family of curves, $q^\alpha(t): \alpha \in (-1,0)$, with periods T_α such that T_α tends to infinity as α tends to zero. Note that the period of these orbits need not necessarily coincide with the period of the forcing T , say.

As is usual in such systems it is possible to construct the Poincaré map $P_\epsilon^{t_0}$, where the phase portrait of the suspended autonomous flow is sampled on the section Σ^{t_0} at multiples of the forcing period T . The time at which this section is taken is varied and consequently appears in various stages of the analysis. Under these conditions, and because of the need for continuity from the flow case, the unperturbed Poincaré map $P_0^{t_0}$

will possess a hyperbolic saddle point S_0 . This structure will be highly degenerate under a perturbation ϵ and will yield either transverse homoclinic orbits or no homoclinic points at all. The existence of a unique hyperbolic saddle point $S_\epsilon^{t_0}$ (the position of which will depend on the section time t_0) and the relationship between the unperturbed stable and unstable manifolds and the corresponding perturbed manifolds depend on the parameter ϵ being sufficiently small [see lemmas 5.1 and 5.2 of Guckenheimer and Holmes (1983)].

The separation of the inset and the outset of the perturbed system on the section $\Sigma_\epsilon^{t_0}$ at the point $q^0(t=0)$ is defined by

$$d(t_0) = q_\epsilon^u(t_0) - q_\epsilon^s(t_0) \quad (5A.5)$$

as illustrated in figure 5A.2. The points $q_\epsilon^u(t_0)$ and $q_\epsilon^s(t_0)$ are the points on the unstable and stable manifolds closest to the saddle $S_\epsilon^{t_0}$ (along the manifolds) which also lies on the normal

$$f^\perp(q^0(0)) = \begin{bmatrix} -f_1(q^0(0)) \\ f_2(q^0(0)) \end{bmatrix}. \quad (5A.6)$$

Theorem

Defining the Melnikov function $M(t_0)$ as

$$M(t_0) = \int_{-\infty}^{\infty} f(q^0(t-t_0)) \wedge g(q^0(t-t_0), t) dt \quad (5A.7)$$

then if $M(t_0)$ has simple zeros, and is independent of ϵ (sufficiently small) the inset and outset intersect transversely. If $M(t_0)$ has no zeros then the manifolds do not intersect.

The proof is based on the evaluation of two integrals around the unperturbed homoclinic orbit from which it is possible to show that

$$d(t_0) = \epsilon M(t_0) / |f(q^0(0))| + O(\epsilon^2) . \quad (5A.8)$$

Now provided that $M(t_0)$ is independent of ϵ the higher terms of this expansion will be dominated by the first term and since $|f(q^0(0))| = O(1)$ then $M(t_0)$ gives a good estimate of the separation of the manifolds at $q^0(0)$ on the section $\Sigma_\epsilon^{t_0}$. As the time that this section is taken is varied if $M(t_0)$ oscillates about zero then $q_\epsilon^u(t_0)$ and $q_\epsilon^s(t_0)$ must change their orientation with respect to the normal f^\perp . Furthermore if this kind of oscillation occurs then there must be a time $t_0 = \tau$ say when $q_\epsilon^u(\tau) = q_\epsilon^s(\tau)$ and we have a homoclinic point, but since all the Poincaré maps are equivalent the unstable and stable manifolds W^u and W^s must intersect for all t_0 , $0 < t_0 < T$, i.e. no matter where we choose the Poincaré section there will be a homoclinic point and the manifolds must cross an infinite number of times. Conversely if $M(t_0)$ has no zeros then the manifolds do

not intersect as $q_{\epsilon}^u(t_0)$ and $q_{\epsilon}^s(t_0)$ retain the same orientation.

$M(t_0)$ is in fact periodic in t_0 with period T and so effectively what the method is doing is standing at the fixed point $q^0(0)$ on a moving cross section and watching the perturbed manifolds oscillate as t_0 varies between 0 and T .

III.5A.2 Applications of the Melnikov Method

As an example of the use of the Melnikov method we shall consider the calculation of the Melnikov function for the single potential well system equation III.5.2 considered in chapter III.5 which can equivalently be described by the system

$$\begin{aligned}\dot{x} &= y \\ \dot{y} &= -x + x^2 + F \sin \omega t - \beta y.\end{aligned}\tag{5A.9}$$

To meet with the necessity for a small parameter ϵ we introduce the change of variables $F = \epsilon F'$ and $\beta = \epsilon \beta'$ so that the system (5A.9) becomes

$$\begin{aligned}\dot{x} &= y \\ \dot{y} &= -x + x^2 + \epsilon (F' \sin \omega t - \beta' y).\end{aligned}\tag{5A.10}$$

Before the Melnikov function can be evaluated the solution along the unperturbed homoclinic orbit has to be found, and with

this aim we first examine the fixed points of the unperturbed system, namely

$$\ddot{x} + x - x^2 = 0 . \quad (5A.11)$$

the fixed points of which are at $x=y=0$ and $x=1, y=0$, the former corresponding to a centre while the latter is an unstable saddle point (obtained by a linear stability analysis). The Hamiltonian function is

$$H = y^2/2 + x^2/2 - x^3/3 , \quad (5A.12)$$

so that at the saddle $H=1/6$. The curve $H=1/6$ forms a homoclinic orbit enclosing the centre at $(0,0)$ and by integrating the Hamiltonian the solution of the differential equation along this orbit is given by

$$x^\circ(t) = 1 - 3/(1+\cosh t) \quad (5A.13)$$

and

$$y^\circ(t) = 3\sinh t / (1+\cosh t)^2 . \quad (5A.14)$$

It is possible here to make a comparison with the double potential well model introduced in chapter III.5, for which there is already an abundance of literature available, by virtue of scaling the height of the potential barrier or hill so as to match that of the single well (i.e. $H=1/6$).

All that remains to be done is to calculate the Melnikov function and here we note that since the component $g_1=0$, then with the change of variable $t=t+t_0$, the function reduces to

$$M_B(t_0) = \int_{-\infty}^{\infty} y^0(t) (F' \sin \omega(t+t_0) - \beta' y^0(t)) dt. \quad (5A.15)$$

Substitution of the solution $y^0(t)$ into this expression yields

$$M_B(t_0) = 3F' I_1 - 9 \beta' I_2, \quad (5A.16)$$

where

$$I_1 = \int_{-\infty}^{\infty} \frac{\sinh t \sin \omega(t+t_0) dt}{(1+\cosh t)^2} \quad (5A.17)$$

and

$$I_2 = \int_{-\infty}^{\infty} \frac{\sinh^2 t dt}{(1+\cosh t)^4}. \quad (5A.18)$$

The evaluation of the second of these integrals is lengthy but straightforward [see Gradstein and Ryzhik (1980)] and can be found to be equal to $2/15$. The first of these integrals requires an application of the method of residues; by the use of the change of variables $z=t/2$ the integral is transformed into the integral

$$I_1 = \text{Imag } e^{i\omega t_0} \int_{-\infty}^{\infty} \frac{\sinh z e^{i2\omega z}}{\cosh^3 z} dz . \quad (5A.19)$$

If we now consider instead a contour integral which is from $-R$ to $+R$ along the real axis and a semi-circular arc of radius R then as R tends to infinity this complex contour approximates the limits of the integral I_1 . The poles of the integrand which lie within this contour are when $\cosh z = 0$, i.e. when

$$z = (2n+1)\pi i/2 ; n=0,1,2,\dots . \quad (5A.20)$$

Then expanding $\sinh z$ and $\cosh z$ about these poles it is possible to find the sum of the residues so that applying the residue theorem gives

$$I_1 = \text{Imag } e^{i\omega t_0} 2\pi i 2\omega^2 \sum_{n=0}^{\infty} e^{\omega(2n+1)\pi} . \quad (5A.21)$$

The series is a geometric progression which may be summed to yield

$$I_1 = -2\pi\omega^2 \cos\omega t_0 / \sinh(\pi\omega) , \quad (5A.22)$$

whereupon the Melnikov function becomes

$$M(t_0) = -6F'\pi\omega^2 \cos\omega t_0 / \sinh(\pi\omega) - \beta'6/5 . \quad (5A.23)$$

Transverse homoclinic intersections can thus only occur when $M(t_0)$ has zeros, i.e. when

$$\cos \omega t_0 = - \beta' \sinh(\pi \omega) / (5F' \pi \omega^2) . \quad (5A.24)$$

Since in the studies detailed in chapter III.5 we held the damping constant at 0.1 we see that the stable and unstable manifolds intersect when

$$F_B = 0.1 \sinh(\pi \omega) / (5 \pi \omega^2) . \quad (5A.25)$$

If we enforce the scaling necessary for the potential barrier of the two well problem to be the same height as that of the single then the corresponding result [see Guckenheimer and Holmes (1983)] is when

$$F_H = 0.4 \sqrt{2} \cosh(\pi \omega \sqrt{6/4}) / (9 \pi \omega) . \quad (5A.26)$$

The bifurcation diagram of figure 5A.3 shows both these curves but once again there appears to be no real information that can be retrieved from this Melnikov curve regarding the eventual escape of the system to infinity.

In conclusion it should be said that the particulars of the application of the method of Melnikov to the local equation used for the purpose of this investigation is reasonably straightforward but needs to be included here since it may prove after all to play a vital role in the final outcome of the system, and since not previously reported needed to be calculated and set down for the records. Furthermore since

there is already a weight of information is available regarding the double potential well problem it is natural to suppose that the reader may wish to make certain comparisons and therefore, despite the fact that it is an entirely different problem, the discussions are included here for completeness.

Unperturbed Homoclinic Orbit

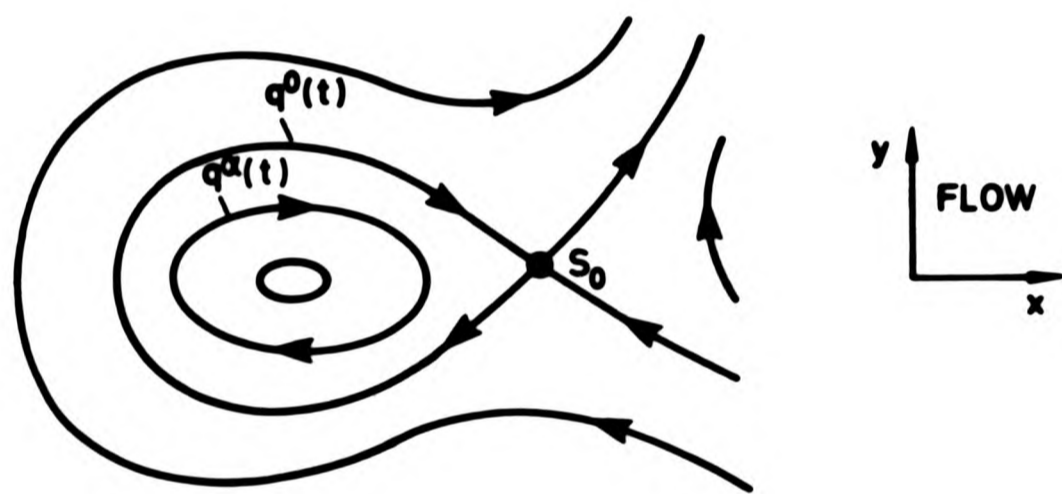


Figure 5A.1 Unperturbed homoclinic orbit.

Perturbed Manifolds and Distance Function

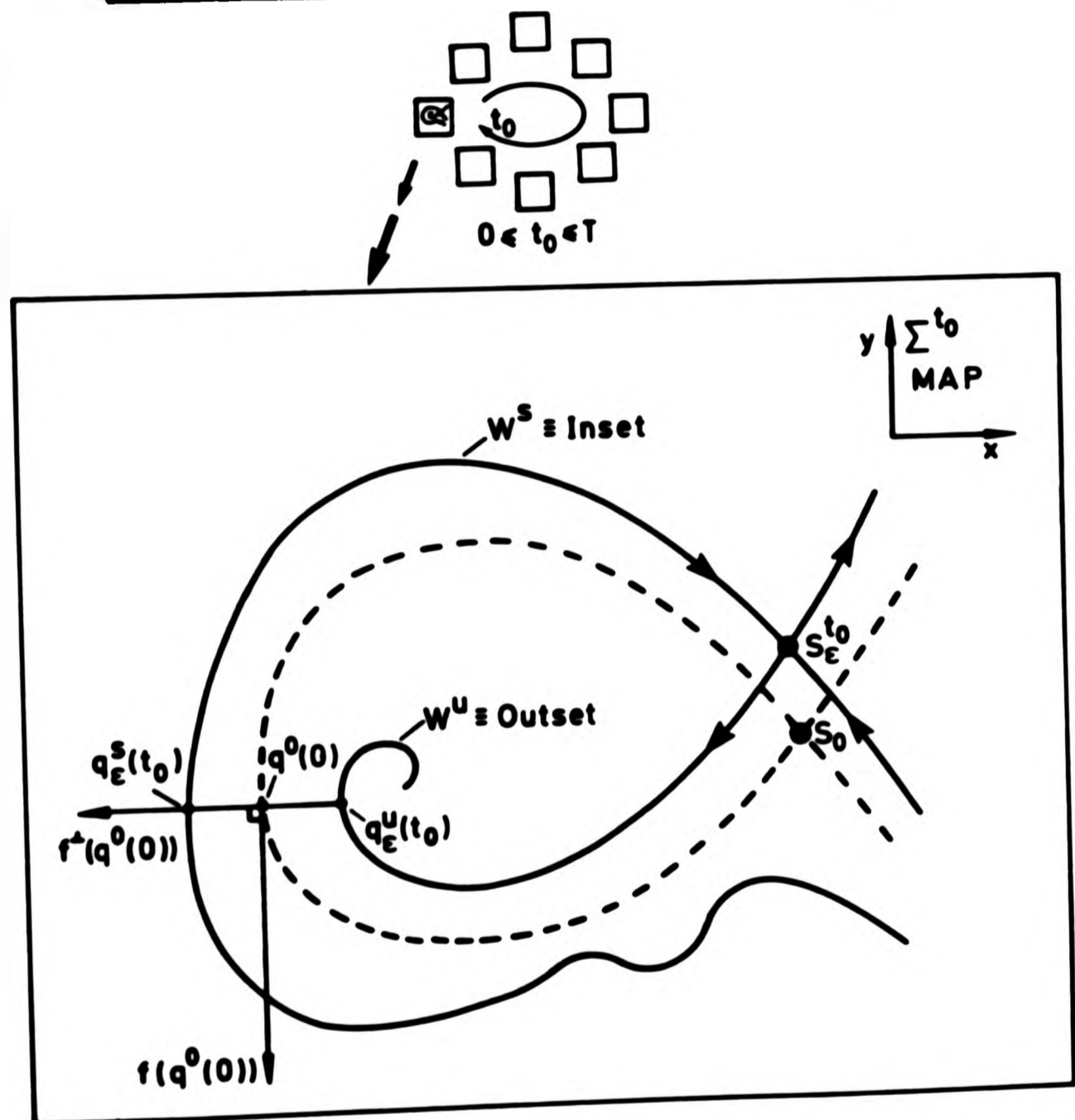


Figure 5A.2 Definition of distance function separating the inset and the outset from the perturbed saddle point.

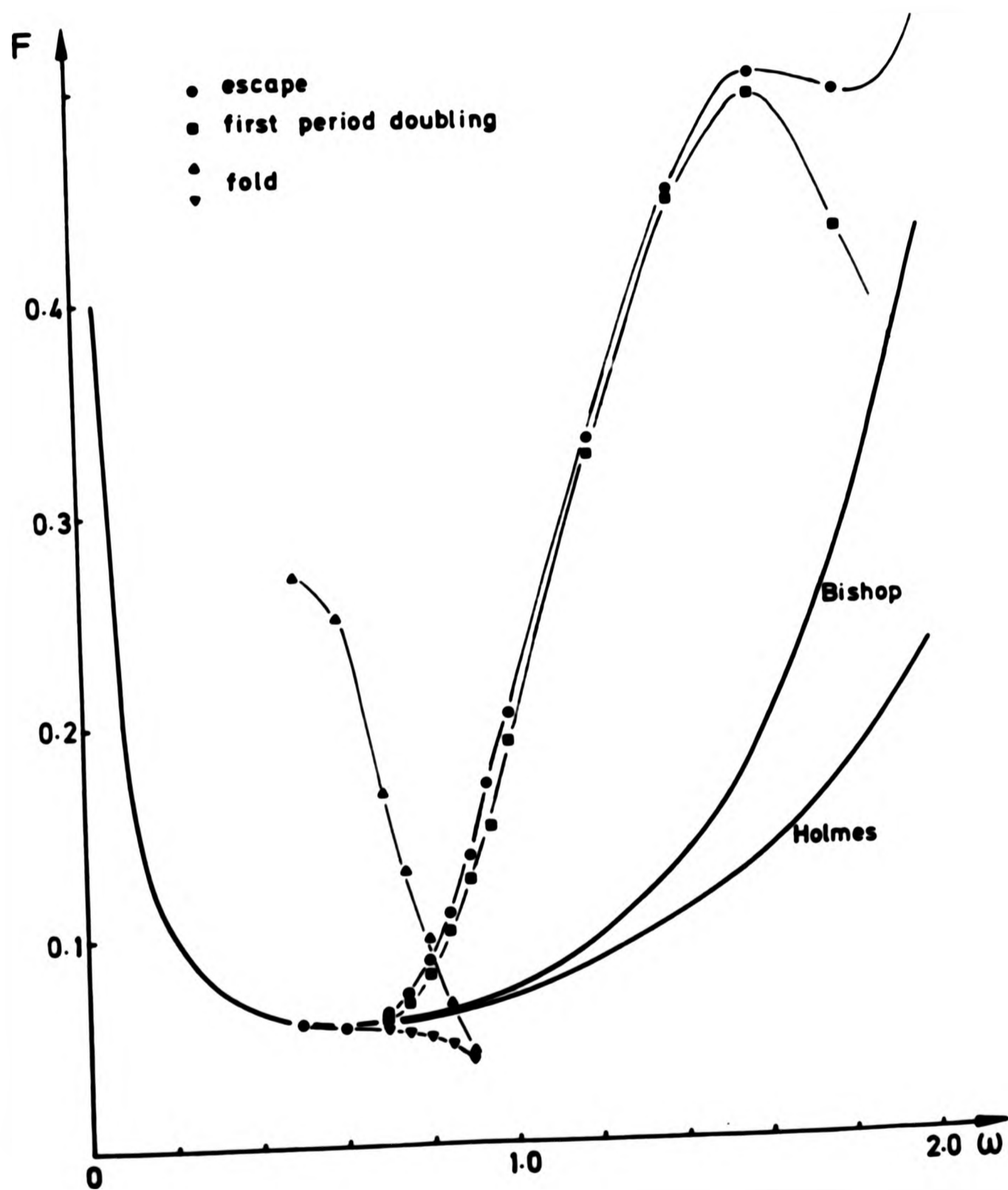


Figure 5A.3 Bifurcation diagram of forcing amplitude versus frequency. Included is the Melnikov curve due to the author and the scaled curve due to Holmes [Guckenheimer and Holmes (1983)].

Attention is drawn to the fact that the copyright of this thesis rests with its author.

This copy of the thesis has been supplied on condition that anyone who consults it is understood to recognise that its copyright rests with its author and that no quotation from the thesis and no information derived from it may be published without the author's prior written consent.

2

D7 3375'87

END